Volume 08
Issue 01
June 2026

IJASST

International Journal of
Applied Sciences and Smart Technologies

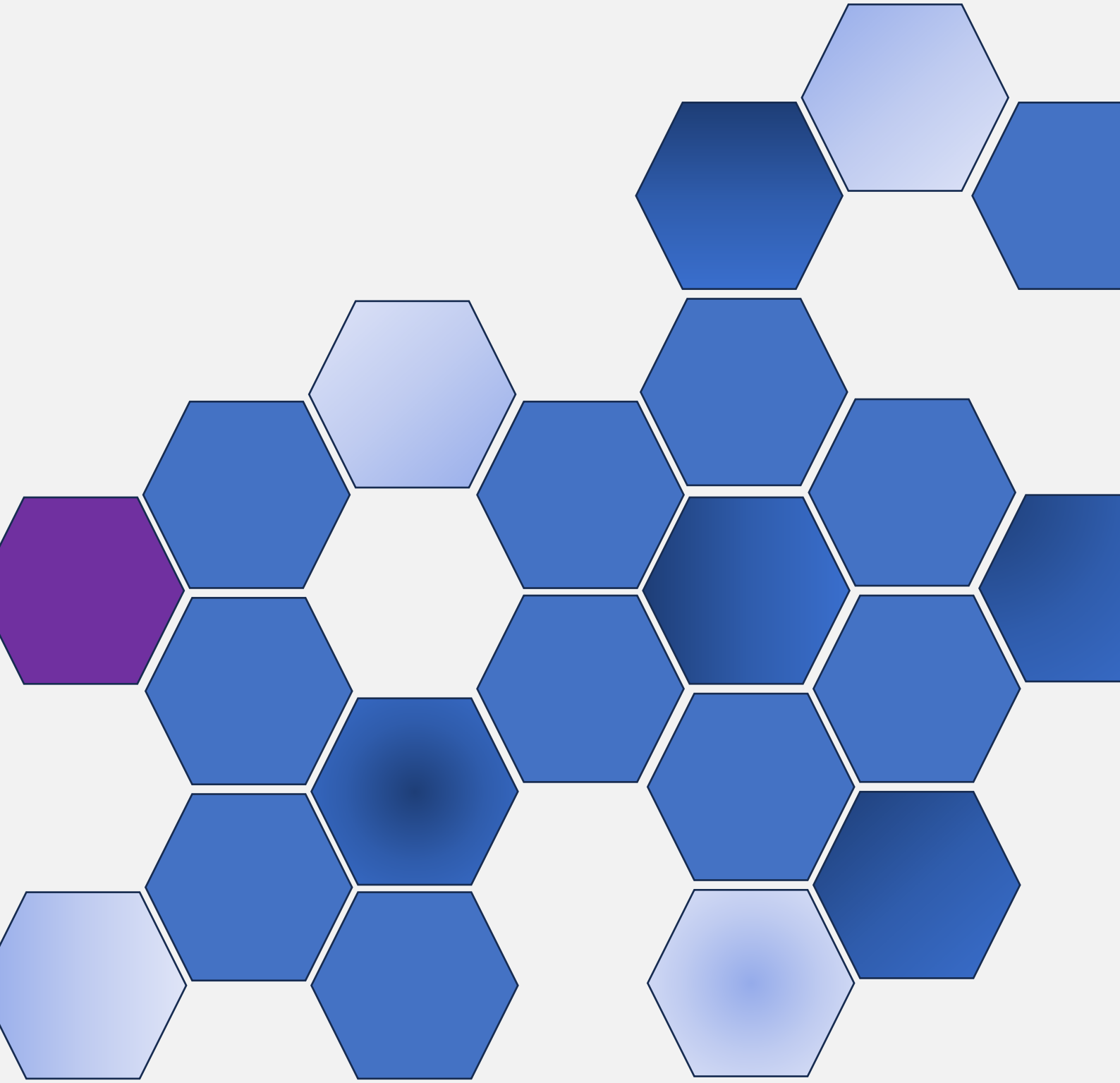

Faculty of Science and Technology
Universitas Sanata Dharma

IJASST
International Journal of
Applied Sciences and Smart Technologies
p-ISSN 2655-8564, e-ISSN 2685-943, 2026

Volume 08
Issue 01

CONTENTS

IJASST
International Journal of
Applied Sciences and Smart Technologies
p-ISSN 2655-8564, e-ISSN 2685-943, 2025

Volume 08
Issue 01

IJASST
International Journal of
Applied Sciences and Smart Technologies
p-ISSN 2655-8564, e-ISSN 2685-943

EDITORIAL BOARD

Contact us
International Journal of Applied Sciences and Smart Technologies
Faculty of Science and Technology
Universitas Sanata Dharma
Kampus III Paingan, Maguwoharjo, Depok, Sleman
Yogyakarta, 55282
Phone : +62 274883037 ext. 523110, 52320
Fax : +62 272886529
Email : editorial.ijasst@usd.ac.id
Website : http://e-journal.usd.ac.id/index.php/IJASST

IJASST is an open-access peer-reviewed journal that mediates the dissemination of research and studies conducted by academicians, researchers, and practitioners in science, engineering, and technology.

IJASST
International Journal of
Applied Sciences and Smart Technologies
p-ISSN 2655-8564, e-ISSN 2685-943

PREFACE

Dear readers, we are delighted to serve you Volume 08, Issue 01 of *International Journal of Applied Sciences and Smart Technologies* (IJASST), which is managed and published by the Faculty of Science and Technology, Universitas Sanata Dharma. IJASST is an open-access peer-reviewed journal that mediates the dissemination of research and studies conducted by academicians, researchers, and practitioners in science, engineering, and technology. Its scope also includes basic sciences which relate to technology, such as applied mathematics, physics, and chemistry.

In this edition, we have sixteen papers authored by researchers from Indonesia, Bangladesh, India, Malaysia, and Africa. Submitted papers are reviewed fairly using the open journal system (OJS) of IJASST. After the review process, accepted papers of the journal are publicly available for free at the website of IJASST. For future issues, we are looking forward to your contributions to IJASST.

Dr. I Made Wicaksana Ekaputra
Editor in Chief
IJASST

IJASST International Journal of Applied Sciences and Smart Technologies
p-ISSN 2655-8564, e-ISSN 2685-943, pp. 1-8, 2026
Volume 08
Issue 01

A Simulation-Based Approach To Spiral Pump Design

Hengky Luntungan[1*], Stenly Tangkuman [1], Benny L. Maluegha[1]

[1]*Mechanical Engineering Department, Sam Ratulangi University,*
Jl. Kampus Unsrat, Bahu, 95115, Indonesia
[*]*Corresponding Author: hengky_luntungan@unsrat.ac.id*

(Received 24-11-2025; Revised 10-04-2026; Accepted 13-04-2026)

Abstract

The consistent availability of irrigation water in agricultural areas remains a challenge to this day, due to the fact that rivers are always located at a lower elevation than farmland. As an alternative solution, a spiral pump has been introduced that operates solely using the kinetic energy of river water flow, unlike conventional water pumps that always require electricity or fossil fuels. This study aims to develop a simulation-based spiral pump design by integrating findings from previous analyses regarding fluid flow behavior and water wheel performance. Accordingly, using SolidWorks software, a comprehensive geometric model of the spiral pump was created, consisting of a 1.2-meter-diameter undershot water wheel, an eight-coil spiral hose with a 2-inch diameter, and a support frame. Through static structural simulation, it was also determined that a hydraulic force of 72.63 N and a torque of 32.68 Nm act on the water wheel, with the shaft withstanding a force of 174.06 N. The von Mises stress on the shaft is 3.746×10^6 N/m², while on the blades it is 1.711×10^7 N/m²; these stress values are well below the yield strength of A36 steel for the shaft and aluminum alloy for the blades. Thus, based on CFD-based flow rate analysis, hydraulic head evaluation, and structural validation, this study has produced an integrated design that ensures operational efficiency and structural safety. This spiral pump design can be developed into a prototype for field application as a cost-effective renewable energy solution.

Keywords: Spiral Pump, Renewable Energy, Water Wheel, Water Supply, Simulation And Design

1 Introduction

Water has a significant impact on agricultural productivity. This is particularly evident in rural areas that rely heavily on river water for irrigation. The situation is further complicated by the fact that rivers are generally located in low-lying areas and are often quite far from farmland. Under such conditions, farmers use mechanical pumps powered

by electricity or fossil fuels. However, the operational costs are often prohibitively high, leading to significantly increased production costs [1].

Spiral pumps, as a renewable energy technology, can provide a solution to irrigation system issues on agricultural land. First introduced by H. A. Wirtz in 1746, the spiral pump is a water pumping technology that operates without an external power source. Rediscovered and refined by Peter Morgan, the spiral pump harnesses the kinetic energy of flowing water to lift water from a water source to agricultural fields, making it particularly well-suited for agricultural environments in remote areas [2]. Spiral pumps feature a simple mechanism, low maintenance requirements, and high reliability, making them an effective solution for irrigation in rural areas.

The performance of a spiral pump depends heavily on two main components: the impeller and the spiral hose. Previous research has shown that impeller parameters such as diameter, blade angle, and flow velocity directly influence the mechanical power transmitted to the spiral pump [1][3]. On the other hand, the fluid flow velocity within the hose largely determines the discharge rate and head that can be achieved, as verified through computational fluid dynamics (CFD) simulations [4][5]. These fundamental principles form the basis of a multi-year research project conducted from 2023 to 2025.

In the 2023 study, CFD simulations identified the relationship between hose diameter and flow performance. Furthermore, the 2024 study analyzed the power characteristics and head of an undershot-type water wheel based on flow velocities measured in the field. Based on these findings, the 2025 study focused on the design of a comprehensive spiral pump system using CAD modeling and structural simulation. This design integrates validated parameters from the previous two years to produce a safe, manufacturable pump prototype suitable for agricultural applications.

2 Theoretical Background

The wetted cross-sectional area represents the portion of the blade or paddle surface of the water wheel that is directly exposed to or immersed in the flowing water [6][7]. For d as the water depth on the wheel and w as the width of the wheel, the wetted cross-sectional area (A) can be calculated using the following equation.

$$A = d.w \quad (1)$$

On the water wheel, a force is generated due to the impact of flowing water [7][8]. For a water velocity V, wetted cross-sectional area A, and fluid density ρ, the resulting force Facting on the water wheel can be calculated using the following equation.

$$F = ½\, \rho\, A\, V^2 \quad (2)$$

Subsequently, a torque is generated on the shaft as a result of this force [9]. For the resulting force $F$and the water wheel radius r, the torque Tcan be calculated using the following equation

$$T = F.r \quad (3)$$

The output power of a spiral pump refers to the amount of mechanical or hydraulic power delivered by the pump as it transfers water from a lower elevation to a higher one [10][11]. The power generated is also directly proportional to the density (ρ), gravitational acceleration (g), water discharge (Q), and pump head (H), which can be formulated as follows.

$$P_{out} = \rho.\, g.\, Q.\, H \quad (4)$$

3 Method

The design process begins with integrating CFD-based discharge outputs and hydraulic head analysis from the previous researches. SolidWorks software was used to create precise parametric models of all components, thereby ensuring dimensional accuracy for the subsequent fabrication process. The structural simulations in this study included mesh generation, determination of loading conditions, stress analysis, and deformation evaluation based on the properties of A36 steel and aluminum alloys. The boundary conditions in this study include hydraulic forces, torsional loads, the effects of gravity, and structural constraints. Thus, a comprehensive approach has been taken to ensure the manufacturability and reliability of the spiral pump design.

4 Application and Results

4.1 Integration of Previous Findings

The key performance parameters of the spiral pump were derived from the results of previous studies. Computational analyses from prior research on fluid flow within the spiral hose indicated that the optimal hose diameter is 2 inches to achieve a maximum flow rate of 0.00183 m^3/s. Furthermore, based on a previous evaluation of the waterwheel's performance, it was found that the spiral pump system can operate effectively up to a height of 5 meters, which generally meets the needs of small-scale agricultural irrigation. Ultimately, based on these two findings, the dimensional and mechanical parameters for developing a suitable spiral pump design have been determined.

4.2 Structural Simulation Results

To ensure the mechanical reliability of the spiral pump system under operational loads, a structural simulation was conducted. The loads acting on the system consist of a thrust force of 72.63 N acting on the impeller blades, which results in a torque of 32.68 Nm transmitted to the impeller shaft. In addition, the shaft also bears a gravitational load from other components of 174.06 N. Simulation results show that the von Mises stress on the shaft is 3.746×10^6 N/m^2, a value well below the yield strength of A36 steel, which is 6.204×10^8 N/m^2. On the other hand, the von Mises stress on the water turbine blades is 1.711×10^7 N/m^2, which is also below the yield strength of the aluminum alloy material. Fig. 1 displays the distribution of von Mises stress occurring on the shaft. This indicates that the stress levels remain below the material's failure limit. Thus, these results confirm a safe design for the spiral pump.

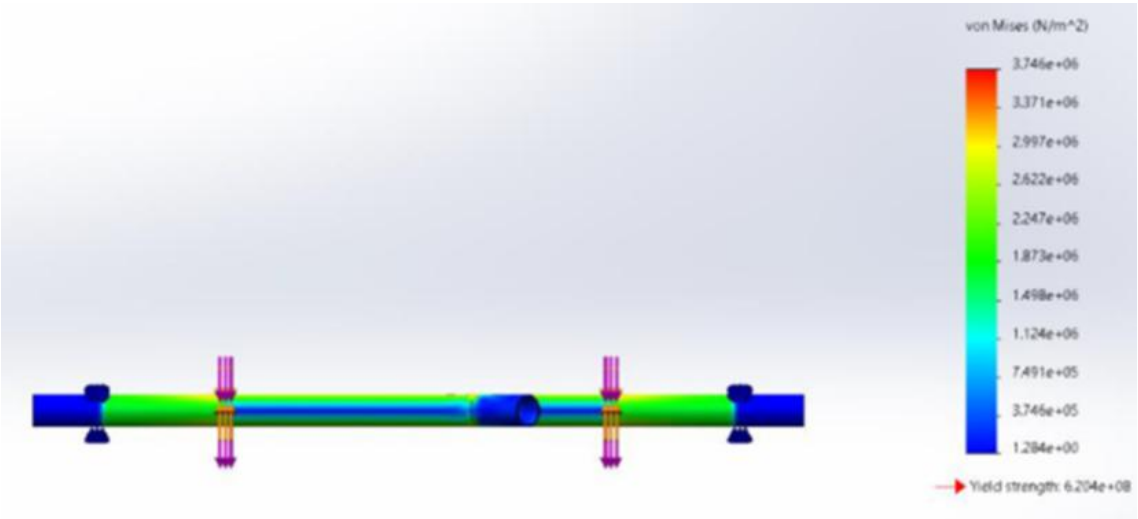

Figure 1. Results of the shaft stress simulation

4.3 Overall Integration

In this study, a CAD model was developed consisting of a water wheel with a diameter of 1.2 meters and a width of 0.6 meters, along with an optimal configuration of a 2-inch-diameter spiral hose with eight coils. The shaft was designed with an outer diameter of 50.8 mm and is made of ASTM A36 steel. The wall thickness and shaft length are 8 mm and 1200 mm, respectively, to ensure adequate stiffness and strength. On the other hand, an aluminum alloy is used for the water impeller blades, with lengths, widths, and thicknesses of 60 mm, 30 mm, and 1.5 mm, respectively, ensuring structural durability and reducing polar inertia. Fig. 2 shows the spiral pump with its complete geometric design, including key dimensions and component configurations, which will serve as the basis for structural evaluation.

The combination of the results of the previous analyses and the structural evaluation has formed an integrated design framework based on simulation. Based on the flow analysis, the appropriate pipe size has been determined; based on the hydraulic performance analysis, the achievable head can be estimated; and based on the structural simulation, the mechanical safety and overall design durability of the spiral pump can be confirmed. Ultimately, this spiral pump design is viable and ready to proceed to prototype fabrication and further testing.

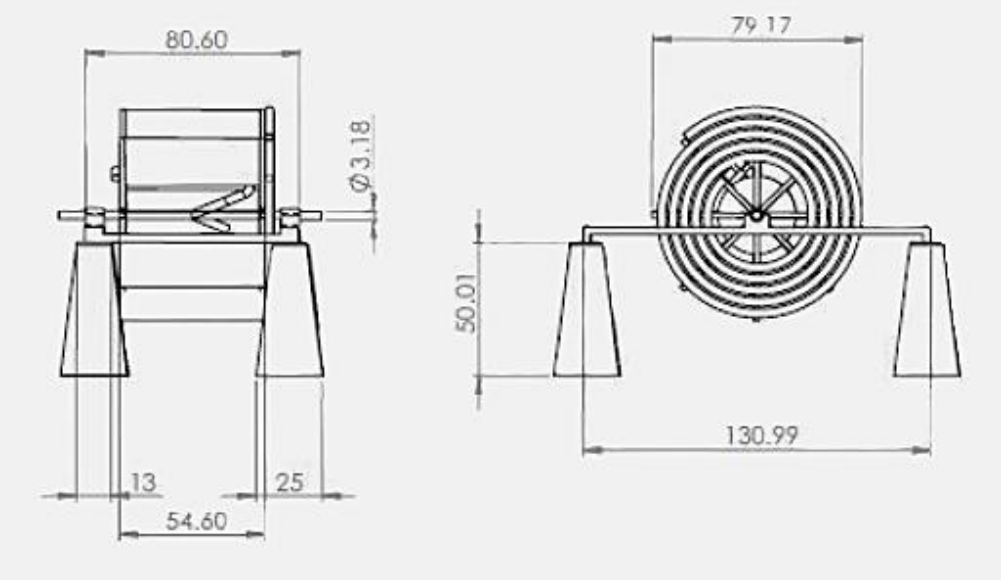

Figure 2. The spiral pump design

5 Conclusions

The success of the spiral pump design in this study was achieved thanks to insights gained from previous research phases. Furthermore, the structural simulations conducted in this study have confirmed that the shaft, impeller, and other critical components are within safe strength limits when subjected to the anticipated loads. Therefore, the finalized spiral pump design is structurally robust, functionally feasible, and ready for prototype fabrication and subsequent field testing.

Acknowledgements

This research was funded by Sam Ratulangi University in 2025 through a basic research scheme (RDUU-K2).

References

[1] Luntungan Hengky, Stenly Tangkuman, dan I Nyoman Gede, 2023. Analysis of Spiral Pump Discharge Based on Simulation of Fluid Flow In Hoses. *International*

Journal of Applied Sciences and Smart Technologies, Volume 5, Issue 2, pages 355–364.

[2] Peter Tailer, *The Spiral Pump A High Lift Slow Turning Pump*, 1986, https://lurkertech.com/water/pump/tailer/

[3] Luntungan Hengky, Stenly Tangkuman, dan I Nyoman Gede, 2024. Analysis of Spiral Pump Head Based on Water Wheel Parameters. *International Journal of Applied Sciences and Smart Technologies*, Volume 7, Issue 01, pages 159–168.

[4] Kumar Fanesh, J. Sinha, Kamalkant, et al, Design and Development of a Spiral Tube Water Wheel Pumping System: A Review*, AgricultureAssociation of Textile Chemical and Critical Reviews Journal*, 2023, 217 – 222.

[5] Patel Priyankkumar R., et al, Design Of Spiral Tube Agriculture Water Wheel Pump. *International Journal Of Applied Research In Science And Engineering*, 2017, pp.560-565.

[6] Satish H. Patil et al, A Review Paper on Spiral Tube Water Wheel Pump, *International Journal of Advance Research in Science and Engineering*, Vol. 6 Issue. 08, 2017, pp 1123-1125.

[7] Mukhtar Anas and Gatut Rubiono, Spiral Pumping Wheel Turbine Application Concept for Irrigation with Different Altitudes, *Gandrung: Jurnal Pengadian Kepada Masyarakat*, Vol. 3, No.2, 2022, pp.626-632.

[8] R. Eko, Agung Fauzi Hanafi, I. G. N. A. Satria Prasetya D.Y., and Enggar Priyadi, Design And Manufacture Of Undershot Waterwheel As A Spiral Pump Driven For Agricultural Irrigation, *SJMEkinematika*, vol. 8, no. 1, pp. 13-24, Jun. 2023.

[9] Diaz Eddisney, Carlos Trinchet and Javier Vargas, Design and Simulation of a Spiral Hydraulic Pump Based on Multi-Objective Optimization, *ARPN Journal of Engineering and Applied Sciences*, Vol.15, No.5, 2020, pp. 657-663.

[10] Kumar Fanesh, Jitendra Sinha and Kamalkant, Development and Testing of a Spiral Type Water Wheel Pumping System, *Internasional Journal of Current Microbiology and Applied Sciences*, Vol. 9, No. 5, 2020, pp. 3061-3069.

[11] Lee Man Djun, J.Y.Chan, J.Ling and P.S.Lee, Design and Development of Zero Electricity Water Pump for Rural Development, *Universal Journal of Mechanical Engineering*, Vol.7, No.6, 2019, pp. 441-449.

IJASST
International Journal of
Applied Sciences and Smart Technologies
p-ISSN 2655-8564, e-ISSN 2685-943, pp. 9-28, 2026

Volume 08
Issue 01

The Influence of Printing Parameter Variations on the Dimensional Accuracy of 3D Nylon Carbon FDM Prints Using the Grey-Taguchi Method

Gilang Argya Dyaksa[1], Felix Krisna Aji Nugraha[2*], Heryoga Winarbawa[1], Kristian Ismartaya[3], Robertus Bellarmino Radya Ananda[1], Hadrianus Felin Saputra[1]

[1]*Faculty of Science & Technology,Sanata Dharma University, Paingan Maguwoharjo Depok SlemanYogyakarta, 55282, Indonesia*
[2]*Faculty of Vocational Mechatronics Engineering, Sanata Dharma Paingan Maguwoharjo Depok Sleman Yogyakarta, 55282, Indonesia*
[3] *Faculty of Architecture and Design, Universitas Kristen Duta Wacana, Kotabaru, Yogyakarta, 55224, Indonesia*
[*]*Corresponding Author: felix@usd.ac.id*

(Received 31-10-2025; Revised 02-03-2026; Accepted 12-03-2026)

Abstract

The dimensional accuracy of the printed specimen in the process of forming a workpiece with carbon fiber material using the Creality K1 Max printer machine requires a combination of parameters in the printing process. The printing type using Fused Deposition Modeling (FDM) is a very popular type of printing process, in this process the filament of the raw material is heated to form the desired product. Nylon carbon was chosen because it has high strength and heat resistance, so it is quite potential for various types of applications. Dimensional accuracy is a major problem in the printing process using 3D printing, especially if the printed product will be assembled either in a mechanical system or a non-mechanical system. The results of the dimensional accuracy of the object printing process are greatly influenced by the selection of parameters used in the printing process. The printing parameter optimization process uses the Grey-Taguchi method, this method was chosen because this method combines multi-dimensional workpieces according to product quality. The specimen or workpiece uses the ASTM D638 standard. Dimensions are 165 length, 13 neck, 19 width, and 7 mm thick. Deviation or dimensional accuracy is based on the largest GRG value in the parameter composition. The research results obtained the following printing parameter factors: a layer thickness of 0.2 mm, a nozzle temperature of 280°C, and a printing speed of 60 mm/s, also layer thickness is the most influence parameter that increasing the dimensional accuracy.

Keywords: FDM; nylon carbon; dimensional accuracy; optimization; grey Taguchi

1 Introduction

The development of three-dimensional printing technology, also know as 3D printing, has brought significant changes in various fields including manufacturing, medicine, and automotive. Among these technologies, Fused Deposition Modeling (FDM) is a highly popular 3D printing technology due to its ease of use and relatively low cost in producing prototypes and functional components [1]. As FDM technology continues to evolve, the types of printable materials have also become more diverse, one of which is nylon carbon. Nylon carbon possesses high mechanical strength and is resistant to heat. Regardless of the raw material used, the quality of 3D prints heavily depends on printing parameters such as nozzle temperature, print speed, and layer thickness [2]. Variations in these parameters determine the mechanical properties and dimensional accuracy of the final product, which are two crucial aspects from an industrial application perspective [3], [4].

Previous research has shown that material made from nylon carbon has a great potential in 3D printing applications. Nylon carbon is lightweight material yet offers high strength [5]. Research on FDM parameter optimization is mostly limited to materials such as PLA and ABS. Studies on nylon carbon materials are still scarce. Findings indicate that nylon filament reinforced with carbon fiber has good potential for structural applications due to its stiffness and heat resistance, however it is affected by variations in printing parameters such as layer thickness and extrusion rate [6]. Another study showed a significant influence of parameters such as layer thickness and infill density on dimensional accuracy in PLA material, where a layer thickness of 0.2 mm resulted in the lowest dimensional deviation of ±0.15 mm [7]. Investigation the flexural strength of carbon-reinforced nylon composites produced using 3D printing technology. The targeted parameters were the effects of infill density and layer thickness on mechanical performance [8]. The results showed that a 100% infill density could withstand a maximum load of 127 N, while a 50% infill density could withstand a maximum load of

76.7 N. Study about the effect of increasing fill density on the tensile strength and elongation of carbon fiber filament materials [9]. The test specimens were produced using 3D printing with nylon carbon fiber and PLA carbon fiber filaments, both with a diameter of 1.75 mm. The specimens were experimentally tested using a Universal Testing Machine. Based on the experimental results, nylon carbon fiber filament showed elongation ranging from 16.970% to 26.681% and tensile strength between 19.244 MPa and 23.899 MPa, while PLA carbon fiber filament showed elongation ranging from 7.673% to 15.546% and tensile strength between 18.580 MPa and 24.552 MPa. It can be concluded that the fill density parameter affects the elongation and tensile strength of the material, and thus can be used as a setting parameter in 3D printing. With various results from studies that have been conducted, nylon carbon filament has the potential to be a reliable filament to be used in functional applications that require high strength, and this material also has the potential to be an alternative material for several types of metals and thermoset polymers because it has characteristics lightweight structure and mechanical capabilities [10].

Therefore, this study aims to analyze the influence of variations in FDM printing process parameters on the dimensional accuracy of specimens made of Nylon Carbon using 3 main parameters, namely layer thickness, nozzle temperature, and printing speed. The results of the experiment will be analyzed using the Grey-Taguchi method to obtain the optimal combination of parameters for dimensional accuracy. The Grey-Taguchi method is used to identify the optimal parameter combinations to produce products with the best performance. The results of this study are expected to contribute to academics and practitioners in the use of nylon carbon material as an alternative material intended for functional components which of course have high precision.

2 Material and Methods

The workpiece specimen follows the ASTM D638 standard. The 3D model of the specimen was created using CAD software. The printed specimen design dimensions are shown in the Fig. 1. The use of the ASTM D638 specimen in this study is because this study continues to tensile testing in the next study, but before tensile test, dimensional

accuracy is performed. The material used in this study is the latest eSUN 3D Filament: ePA Nylon Carbon Fiber Filament. The material specifications are shown in the following Table 1.

This study identifies the influence of printing parameters on the dimensional accuracy and tensile strength of nylon carbon filament specimens. The research varies three key parameters namely layer thickness (LT), nozzle temperature (NT), and printing speed (PS). The level selection of the three parameters is based on the recommendation of printing parameters based on the technical data sheet (TDS) which can be accessed through esun3d.com.

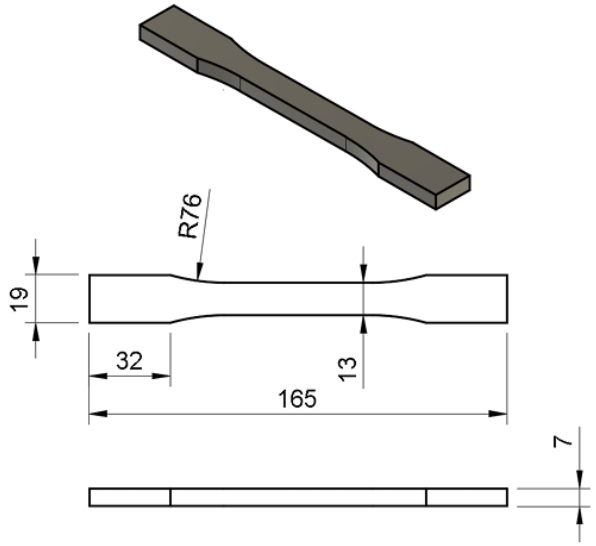

Figure 1. ASTM D638 Specimen

Table 1. Material Specifications eSUN ePA-CF

Filament diameter	1.75 mm
Extruder Temperatur	260 – 300 ^{0}C
Density	1.24 g/cm^3
Printing speed	40 -100 mm/s
Tensile Strength	140 Mpa
Elongation at Break	10.61 %

We can see in Fig. 2, which is a list of recommended printing parameters for ePA-CF or nylon carbon materials for the 3D printing process. Extruder temperature or commonly called nozzle temperature is in the range of 260 ºC - 300 ºC, while the printing speed is in the range of 40 – 100 mm/s. The layer thickness value is in range 0.1-0.2 mm, this value is commonly used for printing in fused deposition modeling machine. Therefore, the value in TDS is the basis for selecting the level of each parameter in this study.

Layer thickness is set at three levels: 0.1 mm, 0.16 mm, and 0.2 mm. Smaller layer thicknesses are expected to enhance interlayer bonding strength. Second, the nozzle temperature i.e., the temperature at the nozzle used to extrude the filament is varied at 260 °C, 280 °C, and 300 °C. Lastly, the printing speed defined as the movement speed of the nozzle during the printing process—is adjusted to three levels: 60 mm/s, 80 mm/s, and 100 mm/s. Higher printing speeds can accelerate the printing process but may reduce surface quality. The tabulation of printing parameter variations is shown in the following Table 2.

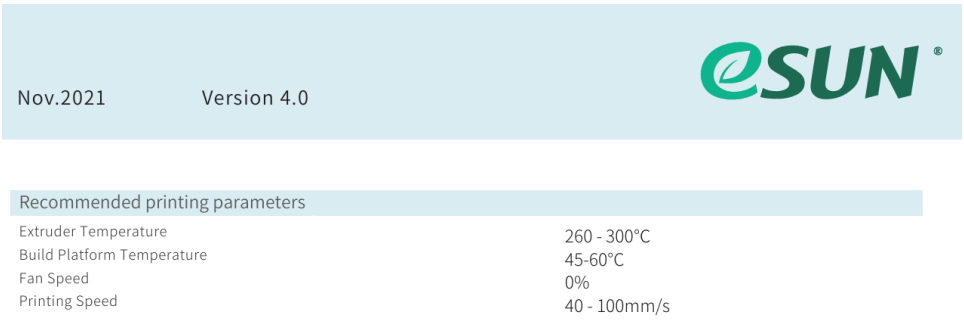

Figure 2. eSun ePA-CF TDS [11].

Table 2. Printing Parameter Variations

Parameter	1	2	3
Layer thickness (mm)	0.1	0.16	0.2
Nozzle temperature (^{O}C)	260	280	300
Printing speed (mm/s)	60	80	100

The specimens will be printed using the Creality K1 Max machine with a print size of 300 x 300 x 300 mm. Dual Gear Direct Drive Extruder Type with maximum nozzle temperature 300 ºC. The scenario of combining three printing parameters, each with three levels, for the specimen printing process was carried out using the full factorial method with an L_{27} Orthogonal Array (OA), as shown in the table 3

Table 3. Combination Printing Parameter

Run No.	PARAMETER		
	Layer thickness	Nozzle temperature	Printing speed
1	0.2	260	80
2	0.2	300	80
3	0.2	280	80
4	0.2	300	100
5	0.2	260	60
6	0.2	280	60
7	0.16	300	100
8	0.16	300	60
9	0.16	300	80
10	0.2	300	60
11	0.16	280	100
12	0.2	280	100
13	0.16	260	80
14	0.1	260	60
15	0.16	260	100
16	0.1	300	100
17	0.1	280	100
18	0.1	280	80
19	0.16	260	60
20	0.16	280	80
21	0.16	280	60
22	0.1	300	60
23	0.1	260	100
24	0.1	260	80
25	0.1	300	80
26	0.1	280	60
27	0.2	260	100

Dimensional accuracy tests will be performed using specimens that have been printed according to Figure 1. The dimensions measured are 4, namely length 165 mm, width 19 mm, neck 13 mm, and thickness 7 mm. Dimensional measurements of the specimen were carried out using an Insize digital caliper 1108-200 (8”/200 mm), with a measuring range of 0–200 mm and an accuracy of 0.01 mm.

As we can see in Fig. 3, it is the position of the printed specimen on the bed machine. Each size represents the direction of each axis on the machine. Length 165 mm represents the direction on the x-axis, the width is 19 mm and the neck is 13 mm represents the direction on the Y-axis, and the thickness of 7 mm represents the direction of the Z-axis. The measurement process is conducted after all specimens have been printed and the specimens have reached room temperature. Each dimension is measured at least three times per specimen, then the average value of the dimension is obtained. These results were then analyzed using Taguchi analysis, to obtain the S/N ratio value. These values are used to: 1) identify factors that significantly affect responses; 2) identify the combination of parameters that produce the most optimal responses; and 3) the value of the S/N ratio is a variable used in the calculation of multi-responses optimization using Grey Relational Analysis (GRA).

The Taguchi method is a statistical method that is commonly used to improve the quality of a product, optimize performance by varying the factors that affect the output [12]. In this study, we want to determine the effect of varied printing parameters on the dimensional accuracy of 3D printing results using nylon carbon material.

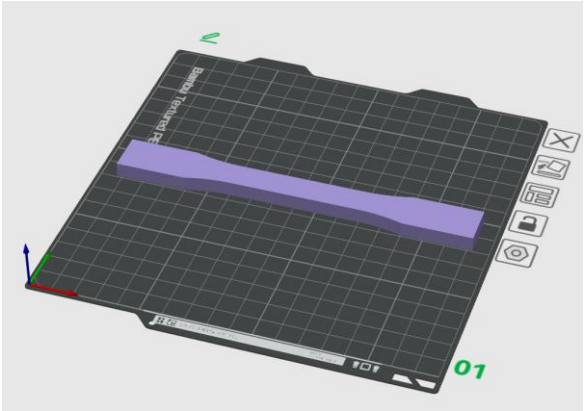

Figure 3. Specimen print position.

The output of the analysis is at least to know what parameters have the most influence on dimensional accuracy, as well as to find out the combination of printing parameters that produce the most optimal dimensional accuracy. The signal-to-noise (S/N) ratio was computed using the "smaller-the-better" criterion, since the objective of this study was to minimize dimensional deviation.

GRA will also be carried out which is an analysis method to measure the level of connectivity between factors [13]. This method is commonly used in the Taguchi method to optimize responses, especially if the trend in the S/N ratio is different for each factor studied, also the limitations of the Taguchi method are cannot optimize several responses simultaneously [14], [15].

The first step in GRA method is to normalize the S/N Ratio value from each test result. The normalization value is calculated using equation 1, which is intended for the Small is Better criterion [15]. Sequentially, max $y_j(q)$ and min $y_j(q)$ are the largest and smallest values of $y_j(q)$ values studied.

$$y_{ij} = \frac{\max y_j - y_i}{\max y_j - \min y_j} \tag{1}$$

The next step is to calculate Deviation Sequence value, which involves finding the absolute difference between value of 1 and the previous normalized S/N Ratio data [15]. The deviation sequence calculation uses equation 2.

$$\Delta_{0ij} = y_{0j} - y_{ij} \tag{2}$$

which:

Δ_{0ij} : sequence deviation value in the experiment i and response j

y_{0j} : maximum value of normalized S/N Ratio (value 1)

y_{ij} : normalized value of S/N Ratio in experiment i and response j

After deviation sequence value is obtained, Grey Relational Coefficient (GRC) and Grey Relational Grade (GRG) values are calculated. GRC is calculated using equation 3, while GRG is the average of all-four GRC values for each response [14] (the importance level of each response is same). The distinguishing coefficient value uses 0.5, in accordance with the values commonly used in previous studies.

$$GRC\ y_{ij} = \frac{\Delta_{min} + \zeta.\Delta_{max}}{\Delta_{0ij} + \zeta.\Delta_{max}} \tag{3}$$

which:

Δ_{min} : minimum value of deviation sequence,

Δ_{max} : maximum value of deviation sequence,

ζ : distinguish coefficient, generally has a value of 0.5.

GRG value are then processed in non-weighted GRG value calculation to identify factors that influence all responses and confirm the best parameters based on the GRG values at each factor level [14].

3 Results and Discussions

The specimens that have been printed using all combination parameters are shown in Fig. 4. The specimens were examined using a dial-caliper to obtain the actual dimension of length, width, neck-width, and thickness (responses) data of each specimen. Each specimen was measured three times for each response, and the average value was recorded as the actual measurement data. Dimensional deviation was obtained by subtracting the nominal dimension value (the size in the design drawing) from the measured value. A smaller deviation value indicates better results, as it indicates a higher level of accuracy in the 3D printing process. The next step is to conduct a Taguchi analysis using the Small is better criterion. This criterion was chosen based on the research objective, which was to achieve the smallest dimensional deviation. The analysis yielded

the S/N Ratio value, which is displayed along with the measurement results in Table 4 below.

Figure 4. 3D printed speciment

Table 4. Specimen measurement results and S/N Ratio

Run No.	Average measurement on dimensions				S/N Ratio value			
	length 165	width 19	neck 13	thickness 7	length 165	width 19	neck 13	thickness 7
1	165.02	19.27	13.26	7.16	-44.350	-25.925	-22.795	-17.5218
2	165.18	19.38	13.38	7.05	-44.359	-25.946	-22.803	-16.9761
3	165.13	19.35	13.32	7.07	-44.356	-25.940	-22.792	-17.0469
4	165.27	19.60	13.60	7.19	-44.364	-25.937	-22.794	-17.0048
5	165.26	19.57	13.57	7.19	-44.363	-25.937	-22.789	-17.0211
6	165.30	19.53	13.50	7.18	-44.365	-25.944	-22.803	-17.1063
7	165.59	19.78	13.80	7.52	-44.380	-25.945	-22.799	-17.1292
8	165.62	19.81	13.79	7.10	-44.382	-25.921	-22.774	-17.1493
9	165.56	19.77	13.78	7.48	-44.379	-25.946	-22.817	-17.055
10	165.32	19.51	13.51	7.02	-44.366	-25.948	-22.802	-17.0088
11	165.14	19.44	13.46	7.07	-44.356	-25.901	-22.751	-17.1386
12	165.12	19.45	13.43	7.11	-44.355	-25.942	-22.807	-17.0374
13	165.51	19.73	13.73	7.19	-44.376	-25.846	-22.667	-17.1319
14	165.36	19.57	13.57	7.17	-44.368	-25.696	-22.450	-17.101
15	165.36	19.59	13.62	7.19	-44.368	-25.831	-22.650	-17.1373
16	165.71	19.82	13.79	7.12	-44.387	-25.815	-22.598	-17.0007
17	165.68	19.83	13.81	7.17	-44.385	-25.805	-22.614	-16.9212
18	165.67	19.82	13.82	7.11	-44.385	-25.771	-22.581	-16.9911
19	165.17	19.53	13.49	7.08	-44.358	-25.814	-22.608	-17.1198
20	165.07	19.41	13.43	7.10	-44.353	-25.831	-22.650	-17.109
21	165.20	19.52	13.50	7.15	-44.360	-25.839	-22.683	-17.1399

22	165.62	19.83	13.80	7.19	-44.382	-25.760	-22.561	-17.0279
23	165.52	19.77	13.76	7.20	-44.377	-25.747	-22.528	-16.9624
24	165.65	19.83	13.83	7.12	-44.383	-25.732	-22.487	-16.9829
25	165.75	19.83	13.81	7.06	-44.389	-25.808	-22.609	-17.0834
26	165.72	19.81	13.80	7.08	-44.387	-25.780	-22.560	-17.0387
27	165.75	19.84	13.81	7.09	-44.388	-25.920	-22.782	-17.4742

The results of Taguchi analysis show that the model formed for Length (165) response has an R^2 value of 0.5534. Thus, the model formed is significantly able to explain 55.34% of overall results obtained. Layer Thickness factor has the largest contribution to Length (165) response, with a p-value of 0.001. Thus, Layer Thickness has an influence on Length (165) response of 44.06%. Evidence of Layer Thickness influence on Length (165) response is shown in Fig. 5. The model formed for Width (19) response has an R^2 value of 0.5711. This model is significantly able to explain 57.11% of overall results obtained. Layer Thickness factor has the largest contribution to Width (19) response, with a p-value of 0.001. Thus, Layer Thickness has an influence on Width (19) response of 44.69%, as shown in Fig. 6.

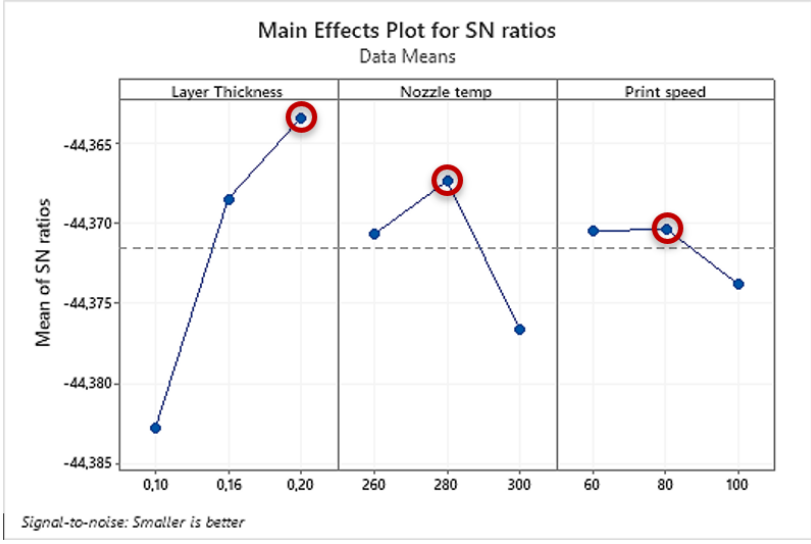

Figure 5. Main effect plot (S/N Ratio) for Length (165) response

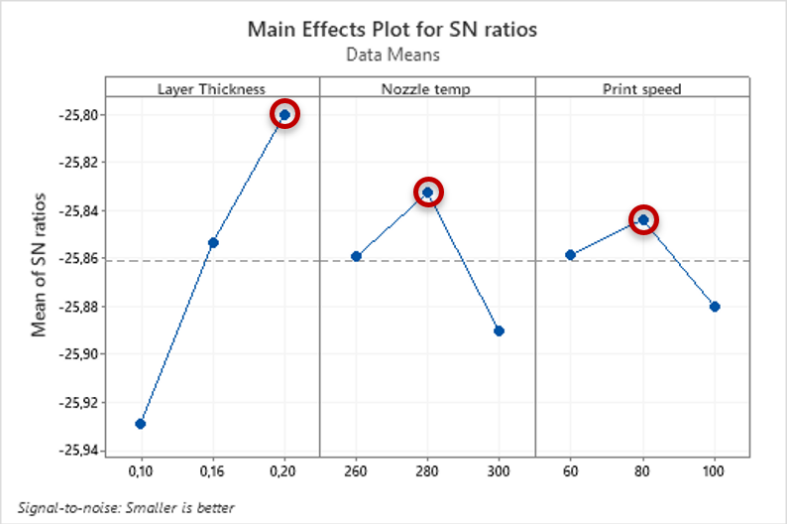

Figure 6. Main effect plot (S/N Ratio) for Width (19) response

For Neck-width (13) response, the formed model has an R^2 value of 0.5817, which means that this model is significantly able to explain 58.17% of overall results obtained. Similar to previous responses, Layer Thickness factor is the most influential factor on this response. In Neck-width (13) response, Layer Thickness factor has an influence of 45.02% with a p-value of 0.001. This large influence is shown in Main Effect Plot for Neck-width (13) response in Figure 7. Meanwhile, the formed model for Thickness (7) response only has an R^2 value of 0.2524 or only explains 25.24% of overall response value obtained. In this model, there is no factor that dominantly influences to Thickness (7) response. This can be seen in Fig. 8, which shows that all factors contribute a relatively balanced influence on Thickness (7) response.

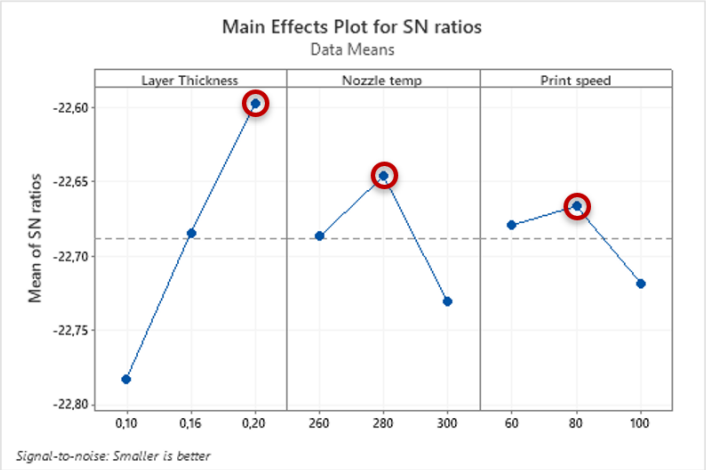

Figure 7. Main effect plot (S/N Ratio) for Neck-width (13) response

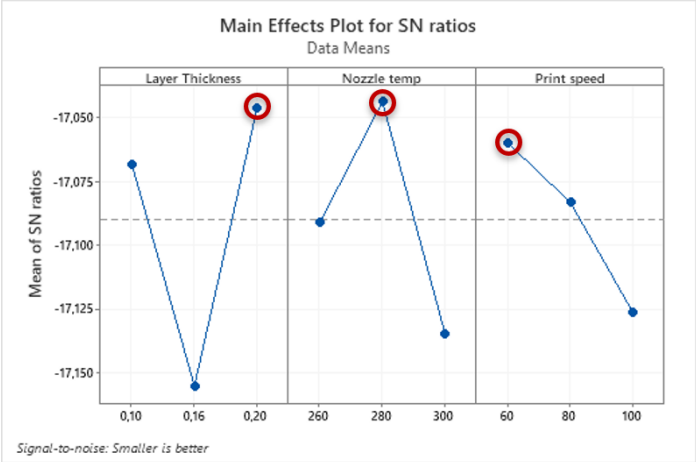

Figure 8. Main effect plot (S/N Ratio) for Thickness (7) response

From all-four Main Effect Plot images above, the best combination of process parameters for each response can also be identified. Length (165), Width (19), and Neck-width (13) responses have the least dimensional deviations in the process parameters of Layer Thickness 0.2 mm, Nozzle Temperature 280°C, dan Printing Speed 80 mm/s. While Thickness (7) response has least dimensional deviations in process parameters Layer Thickness 0.2 mm, Nozzle Temperature 280°C, dan Printing Speed 60 mm/s. The Taguchi method cannot optimize several responses simultaneously [14], so an additional procedure is needed that can optimize all-four responses in a balance.

GRA is implemented to optimize the multi-response Length (165), Width (19), and Neck-width (13), and Thickness (7) simultaneously. GRA begins by calculating the normalization value using equation 1 and deviation sequence using equation 2. The normalization value is calculated using the S/N Ratio value that has been obtained in the previous Taguchi analysis. The results of normalization and deviation sequence calculation are shown in Table 5 below.

Table 5. Normalized value and deviation sequences

Run no.	Normalized value from S/N Ratio				Deviation sequence			
	Length 165	**Width 19**	**Width-neck 13**	**Thick 7**	**Length 165**	**Width 19**	**Width-neck 13**	**Thick 7**
1	0.000	0.000	0.000	0.287	1.00	1.00	1.00	0.71
2	0.220	0.195	0.214	0.062	0.78	0.80	0.79	0.94
3	0.151	0.142	0.107	0.103	0.85	0.86	0.89	0.90
4	0.343	0.582	0.602	0.348	0.66	0.42	0.40	0.65
5	0.329	0.530	0.549	0.348	0.67	0.47	0.45	0.65
6	0.384	0.460	0.426	0.328	0.62	0.54	0.57	0.67
7	0.781	0.896	0.948	1.000	0.22	0.10	0.05	0.00
8	0.822	0.948	0.931	0.165	0.18	0.05	0.07	0.84
9	0.740	0.879	0.914	0.922	0.26	0.12	0.09	0.08
10	0.411	0.425	0.444	0.000	0.59	0.58	0.56	1.00
11	0.165	0.301	0.356	0.103	0.84	0.70	0.64	0.90
12	0.137	0.319	0.303	0.185	0.86	0.68	0.70	0.81
13	0.672	0.809	0.828	0.348	0.33	0.19	0.17	0.65
14	0.466	0.530	0.549	0.307	0.53	0.47	0.45	0.69
15	0.466	0.565	0.636	0.348	0.53	0.44	0.36	0.65
16	0.945	0.965	0.931	0.206	0.05	0.03	0.07	0.79
17	0.904	0.983	0.966	0.307	0.10	0.02	0.03	0.69
18	0.891	0.965	0.983	0.185	0.11	0.03	0.02	0.81
19	0.206	0.460	0.409	0.124	0.79	0.54	0.59	0.88
20	0.069	0.248	0.303	0.165	0.93	0.75	0.70	0.84
21	0.247	0.442	0.426	0.267	0.75	0.56	0.57	0.73
22	0.822	0.983	0.948	0.348	0.18	0.02	0.05	0.65
23	0.685	0.879	0.879	0.368	0.31	0.12	0.12	0.63
24	0.863	0.983	1.000	0.206	0.14	0.02	0.00	0.79
25	1.000	0.983	0.966	0.083	0.00	0.02	0.03	0.92
26	0.959	0.948	0.948	0.124	0.04	0.05	0.05	0.88
27	1.000	1.000	0.966	0.144	0.00	0.00	0.03	0.86

The calculation is continued by calculating the Grey Relational Coefficient (GRC) and Grey Relational Grade (GRG) using equation 3. GRG values are obtained from the average GRC value (all responses) in each treatment parameter. This shows that the weight of the importance of each response is equal or balanced. The results of the GRC and GRG calculations are shown in Table 6.

The results of non-weighted GRG calculation are shown in Table 7. The smallest non-weighted value for each parameter indicates the level that provides Small is Better response characteristic [15]. Delta value indicates the difference between the largest and smallest non-weighted values. A large Delta value indicates that the parameter has a large influence on all four responses, and vice versa.

Table 6. Grey Relational Coefficient and Grey Relational Grade

Run no.	GRC				GRG
	Length 165	**Width 19**	**Width-neck 13**	**Thick 7**	
1	0.33	0.33	0.33	0.41	0.3531
2	0.39	0.38	0.39	0.35	0.3776
3	0.37	0.37	0.36	0.36	0.3640
4	0.43	0.54	0.56	0.43	0.4919
5	0.43	0.52	0.53	0.43	0.4756
6	0.45	0.48	0.47	0.43	0.4552
7	0.70	0.83	0.91	1.00	0.8575
8	0.74	0.91	0.88	0.37	0.7243
9	0.66	0.80	0.85	0.87	0.7954
10	0.46	0.46	0.47	0.33	0.4328
11	0.37	0.42	0.44	0.36	0.3966
12	0.37	0.42	0.42	0.38	0.3970
13	0.60	0.72	0.74	0.43	0.6263
14	0.48	0.52	0.53	0.42	0.4860
15	0.48	0.53	0.58	0.43	0.5079
16	0.90	0.94	0.88	0.39	0.7755
17	0.84	0.97	0.94	0.42	0.7902
18	0.82	0.94	0.97	0.38	0.7757
19	0.39	0.48	0.46	0.36	0.4221
20	0.35	0.40	0.42	0.37	0.3852
21	0.40	0.47	0.47	0.41	0.4357
22	0.74	0.97	0.91	0.43	0.7612
23	0.61	0.80	0.81	0.44	0.6665

24	0.79	0.97	1.00	0.39	0.7845
25	1.00	0.97	0.94	0.35	0.8137
26	0.92	0.91	0.91	0.36	0.7750
27	1.00	1.00	0.94	0.37	0.8261

Table 7. Non-weighted GRG

Level code	Parameter		
	Layer Thickness	Noozle Temp.	Printing Speed
1	0.7365	0.5720	**0.5520***
2	0.5723	**0.5305***	0.5862
3	**0.4637***	0.6700	0.6344
Delta	0.273	0.139	0.082
Rank	**1**	**2**	**3**
Best Parameter	Layer Thickness 0.20 mm, Nozzle Temperature 280°C, Printing Speed 60 mm/s		

Based on optimization results using a combination of Taguchi and GRA, it can be seen that the 3D printing process parameters with optimal and simultaneous response results of Length (165), Width (19), Neck-width (13), and Thickness (7) are: Layer Thickness 0.20 mm, Nozzle Temperature 280°C, and Printing Speed 60 mm/s. Based on GRA calculations, it is also known that the Layer Thickness factor is factor that has the most significant influence on all-four responses, as evidenced by the largest Delta value. This is in line with the results of the ANOVA analysis for each response.

4 Conclusions

This research successfully implemented experiments by utilizing the Taguchi analysis method and optimizing the response of Length (165), Width (19), Neck Width (13), and Thickness (7) simultaneously using the Gray Relational Analysis method. The results of the study showed that the process of printing objects with ASTM D-638 shapes and dimensions, using Creality K1 Max brand 3D printing, with process parameters of 0.2 mm layer thickness, 280°C nozzle temperature, and 60 mm/s printing speed with carbon nylon material is the best printing process parameter that produces the most

optimal dimensional accuracy response. Meanwhile, the layer thickness factor is a factor that contributes significantly to dimensional accuracy.

Acknowledgements

The author would like to thank the Institute for Research and Community Service (LPPM) of Sanata Dharma University for helping in providing research grant funds in accordance with the research program implementation agreement document 016 Penel./LPPM-USD/II/2025, so that the research can be carried out to completion.

Research members have also contributed until the research runs smoothly and is completed. Gilang Argya Dyaksa as the chief researcher responsible for coordinating, monitoring, and evaluating the research, Felix Krisna Aji Nugraha and Heryoga Winarbawa as the preparation of the dimensional accuracy test work procedure, Kristian Ismartaya as the analysis and processing of data from the dimensional accuracy test, also Robertus Bellarmino Radya Ananda and Hadrianus Felin Saputra as the implementer and data collector of the test results.

References

[1] R. B. Kristiawan, F. Imaduddin, D. Ariawan, Ubaidillah, and Z. Arifin, "A review on the fused deposition modeling (FDM) 3D printing: Filament processing, materials, and printing parameters," Jan. 01, 2021, *De Gruyter Open Ltd*. doi: 10.1515/eng-2021-0063.

[2] A. Widyo Nugroho, D. Tohidin, and C. Budiyantoro, "Analisis pengaruh parameter proses terhadap kuat tarik produk 3D Printing dari bahan Polyvinyl Alcohol (PVA)," *Jurnal Program Studi Teknik Mesin UM Metro*, vol. 9, no. 2, pp. 154–161, 2020, Accessed: Jan. 30, 2025. [Online]. Available: http://ojs.ummetro.ac.id/index.php/turbo

[3] Pristiansyah, Hasdiansah, and Sugiyarto, "Optimasi Parameter Proses 3D Printing FDM Terhadap Akurasi Dimensi Menggunakan Filament Eflex," *Jurnal Teknologi Manufaktur*, vol. 11, no. 01, 2019.

[4] H. Bakhtiari, A. Nouri, and M. Tolouei-Rad, "Impact of 3D printing parameters on static and fatigue properties of polylactic acid (PLA) bone scaffolds," *Int. J. Fatigue*, vol. 186, Sep. 2024, doi: 10.1016/j.ijfatigue.2024.108420.

[5] P. K. Thanikonda, J. K. Rao, and D. K. Vaka, "3D Printed Composite Materials: Innovations In Additive Manufacturing And Mechanical Performance," *Educational Administration: Theory and Practice*, 2024, doi: 10.53555/kuey.v30i10.8075.

[6] I. Farina, N. Singh, F. Colangelo, R. Luciano, G. Bonazzi, and F. Fraternali, "High-Performance Nylon-6 Sustainable Filaments for Additive Manufacturing," *Materials*, vol. 12, no. 23, p. 3955, Nov. 2019, doi: 10.3390/ma12233955.

[7] A. Dey and N. Yodo, "A systematic survey of FDM process parameter optimization and their influence on part characteristics," Sep. 01, 2019, *MDPI Multidisciplinary Digital Publishing Institute*. doi: 10.3390/jmmp3030064.

[8] V. Kumar, D. Veeman, M. Vellaisamy, and V. Singh, "Evaluation of flexural strength of 3D-Printed nylon with carbon reinforcement: An experimental validation using ANN," *Polymer (Guildf).*, vol. 316, Jan. 2025, doi: 10.1016/j.polymer.2024.127854.

[9] B. D. Prihadianto, S. Darmo, D. A. Hasan, and D. N. Ananda, "Analisis Kekuatan Tarik dan Regangan Filamen Carbon Fiber Hasil 3D Print dengan Variasi Fill Density," *Infotekmesin*, vol. 14, no. 2, pp. 390–396, Jul. 2023, doi: 10.35970/infotekmesin.v14i2.1936.

[10] I. M. Alarifi, "A performance evaluation study of 3d printed nylon/glass fiber and nylon/carbon fiber composite materials," *Journal of Materials Research and Technology*, vol. 21, pp. 884–892, Nov. 2022, doi: 10.1016/j.jmrt.2022.09.085.

[11] Ltd. Shenzhen Esun Industrial Co., "ePA-CF Technical Data Sheet," 2021, *Esun, Shenzen*. [Online]. Available: www.esun3d.net

[12] M. B. Wicaksono and F. K. A. Nugraha, "Optimization of 3D Printing Parameters Using the Taguchi Method to Improve Dimensional Precision Martinus," *J. Teknol.*, vol. 12, no. 2, pp. 70–75, 2022, doi: 10.35134/jitekin.v12i2.76.

[13] B. L. Jian, C. C. Wang, H. T. Yau, L. W. Wu, and A. H. Tian, "Optimization of lathe cutting parameters using taguchi method and grey relational analysis," *Sensors and Materials*, vol. 32, no. 3, pp. 843–858, 2020, doi: 10.18494/SAM.2020.2674.

[14] K. Ismartaya, B. Bawono, and P. W. Anggoro, "Hardness and Toughness Investigation of ASSAB 705 Steel by Various Tempering Temperatures," *Key Eng. Mater.*, vol. 951, pp. 11–20, 2023, doi: 10.4028/p-qhlFk6.

[15] M. I. Qazi, R. Akhtar, M. Abas, Q. S. Khalid, A. R. Babar, and C. I. Pruncu, "An integrated approach of GRA coupled with principal component analysis for multi-optimization of shielded metal arc welding (SMAW) process," *Materials*, vol. 13, no. 16, 2020, doi: 10.3390/MA13163457.

This page intentionally left blank

IJASST
International Journal of
Applied Sciences and Smart Technologies
p-ISSN 2655-8564, e-ISSN 2685-943, pp. 29-42, 2026

Volume 08
Issue 01

Technical and Cost Barriers in Accessing Smart Educational Technologies in Rural Areas

Nusrat Jahan

Department of Economics, Begum Badrunnessa Govt. Girls College, Dhaka, Bangladesh
Corresponding Author: nusratnitu2002@gmail.com

(Received 09-07-2025; Revised 27-08-2025; Accepted 09-04-2026)

Abstract

This research study explores how data costs and technical issues affect the use of LowDataMode, based on insights from 100 people living in a resource-limited setting. Using chi-square tests and logistic regression, I analyzed how device types, network access, barriers, and platform usability influence LowDataMode use. Results show high data consumption (41%) as the primary barrier, significantly linked to LowDataMode use ($p = 0.023$), with marginal significance in regression ($p = 0.086$). Technical barriers, including lack of affordable devices (28%) and offline learning options (19%), hinder adoption, particularly for shared family device and laptop/desktop users ($p = 0.052$). 3G users (55%) face greater data cost challenges, while Wi-Fi users (15%) rarely need LowDataMode. Higher platform usability was associated with a greater likelihood of skipping LowDataMode ($\beta = 1.48$, $p = 0.008$), suggesting that intuitive, feature-rich apps may encourage more data-intensive activity and thus raise users' data costs. And, non-significant was technical barriers include network stability ($p = 0.315$) and technical problems ($p = 0.545$).

Keywords: Smart Education, Smart Educational Technology, Technical and Cost Barriers

1 Introduction

The integration of smart educational technologies, such as mobile learning platforms, e-reading applications, and virtual classrooms, has revolutionized access to education globally, offering opportunities to bridge educational disparities in underserved regions [1]. In developing countries like Bangladesh, where in 2024 is about 59% of the population resides in rural areas [2], these technologies hold immense potential to enhance educational equity, aligning with Sustainable Development Goal 4 (SDG-4) for inclusive education [3]. However, the adoption of smart educational

technologies in rural contexts is impeded by significant technical and cost-related barriers, including unreliable devices, poor network connectivity, high data costs, and limited digital literacy [4] [5]. These challenges exacerbate the digital divide, limiting the ability of rural populations to leverage digital tools for learning [6] [7]. In Bangladesh, studies have consistently highlighted infrastructural constraints as a primary barrier.

For instance, researchers [5] noted that, inadequate internet connectivity and outdated devices hinder ICT integration in rural classrooms. These researchers [8] emphasized the lack of community-based ICT facilities, such as digital hubs, which limits access to devices and technical support. These findings align with international research, where this researcher [9] reported that students' lack of technical skills and inadequate infrastructure are significant barriers to ICT use in rural schools across developing nations. Another researcher [10] further noted that rural areas globally face challenges like geographic isolation and out-migration of youth, reducing the diffusion of digital technologies. Cost-related barriers are equally critical.

In Bangladesh, Researcher - Hernandez [11] identified high data costs as a major impediment, with rural households spending a significant portion of their income on internet access. Internationally, researchers [12] highlighted that the cost of devices and data plans in rural India creates a financial burden, limiting technology adoption [13].

This study addresses these challenges by investigating the technical and cost barriers impacting the access and use of smart educational technologies in rural Bangladesh.

The research question is, what technical and cost barriers impact the access and use of smart educational technologies in rural areas in Bangladesh? Then I test the null hypothesis (H0): There is no significant impact of technical or cost barriers on the use of smart educational technologies in rural areas, against the alternative hypothesis (H1): Technical and cost barriers significantly affect the use of smart educational technologies in rural areas. Using a structured, closed-ended questionnaire, I was collect primary quantitative data on device reliability, network stability, data cost burden, and platform usability. Descriptive statistics, chi-square tests, and ordinal

logistic regression are employed to analyze relationships and predict the impact of these barriers on technology use.

By providing empirical evidence, this study aims to inform targeted interventions, such as affordable data plans, offline learning modules, and teacher training programs, to enhance digital inclusion. The findings contribute to the discourse on achieving SDG 4 and support Bangladesh's vision of a Smart Bangladesh by 2041 [14]. The paper is structured as follows: Section 2 reviews the literature, Section 3 details the methodology, Section 4 presents results, and Section 5 discusses implications and conclusions.

2 Material and Methods

This study employed a quantitative research approach to investigate the impact of data cost and technical barriers on LowDataMode adoption among users in Darial Union, Bakerganj Upazila, Barishal District, Bangladesh. Participants were surveyed about their demographics, device usage, and network access, barriers to smart educational technology use, platform usability, and perceptions of LowDataMode's role in managing data costs. The survey collected data on age, gender, education, device type, network type, network stability, data cost barriers, content type preferences, technical problems, LowDataMode usage frequency, and suggested improvements for technology access in rural areas.

2.1 Instruments

The primary instrument was a structured survey designed for quantitative analysis of LowDataMode adoption. The survey consisted of closed-ended questions, including yes/no options, Likert scales, and multiple-choice answers to ensure clarity and facilitate statistical analysis. Questions covered: age group (example: 18–24, 25–34), gender (male, female), education level (example: secondary, higher secondary), primary device (smartphone, tablet), device reliability, network type (example: 3G, 4G, Wi-Fi), network stability, impact of poor network quality, data cost as a barrier, content type consuming the most data (example: video-based, interactive apps), LowDataMode usage (regular, occasional, desired but not used, or not needed), platform usability (rated 0–5), frequency of technical problems, biggest technical or

cost-related barrier (example: high data consumption, lack of affordable devices), and key improvements needed for smart educational technology access. A pilot test was conducted with 10 participants to verify the survey's clarity and effectiveness, with no changes made. The survey was administered via Google Forms for accessibility and ease of data collection.

2.2 Data Collection

To Data collection targeted residents of Darial Union, Bakerganj Upazila, Barishal District, Bangladesh, to capture a diverse sample of technology users across ages and educational backgrounds. The Google Form was disseminated online through social media platforms, primarily Messenger, to reach participants. Additionally, I was physically visited the region, engaging with residents to explain the study and provide the Google Form link for participation. For individuals without access to social media or email, I facilitated participation by discussing the survey and ensuring they could respond via the online form. A total of 100 participants provided informed consent through an online Google Form, which mentioned: "Participation in this study is voluntary. No participants are identifiable here. By proceeding with this survey, you consent to participate in this study. Your responses will be kept confidential and will be used solely for research purposes."

2.3 Survey Design

The survey was designed to gather comprehensive data on LowDataMode adoption and its relationship to data cost and technical barriers in rural Bangladesh. Demographic questions (age, gender, education) provided context, as these factors influence technology use. Questions on device type, device reliability, and network type assessed technological infrastructure, while queries on network stability, poor network quality, data-cost barriers, and technical problems identified obstacles to adoption. Participants rated platform usability and LowDataMode usage frequency, using Likert scales and categorical options to quantify perceptions. Additional questions explored the biggest technical or cost-related barrier and the most critical improvement needed to enhance smart educational technology access, offering insights into potential solutions for rural settings. The survey's structure ensured a

broad range of responses to understand how data costs and technical barriers affect LowDataMode adoption.

2.4 Data Analysis

At first, here data was entered into Microsoft Excel using coded values for efficiency and exported as a .CSV file. The dataset was then loaded into JASP (version 0.18.2) for analysis, with coded values converted to string values for analytical clarity. Descriptive statistics summarized central tendencies and variability in demographics, device usage, network access, barriers, platform usability, and LowDataMode usage, providing an overview of usage patterns and perceptions. Chi-square tests examined relationships between categorical variables, such as LowDataMode usage with network type, biggest barriers, or device type, to identify significant associations. A logistic regression model predicted non-adoption of LowDataMode, incorporating predictors like platform usability, high data consumption, network stability, and data cost barriers, technical problems, and device reliability. All analyses were conducted to explore the influence of data costs and technical barriers on LowDataMode adoption. And, the manuscript was prepared using Microsoft Word software.

3 Results and Discussions

Here 100 participants were mostly young: 43% were 25–34, 33% were 18–24, 22% were under 18, and just 2% were 35–44. The group was 68% male and 32% female. Education-wise, 38% had higher secondary schooling, 33% were undergraduates, 16% had secondary education, and 13% were graduates or postgraduates. Smartphones ruled the device scene at 54%, followed by tablets (16%), laptops/desktops (15%), shared family devices (13%), and button-phones (2%). For network access, 55% used 3G, 30% used 4G, and 15% used Wi-Fi. The biggest barrier was high data consumption (41%), followed by lack of affordable devices (28%), lack of offline learning options (19%), and poor network coverage (12%). Most people used video-based content (60%) or interactive apps (39%), with only 1% on text-based content, which makes that data a bit shaky. LowDataMode usage broke down as 19% using it regularly, 37% occasionally, 40% wanting to but not using it, and 4% saying they neither use nor need it.

Fig. 1 shows how people use devices and networks. Smartphones lead with 54 users, followed by tablets (16), laptops/desktops (15), shared family devices (13), and button-phones (2). For networks, 3G is most common (55), then 4G (30), and Wi-Fi (15). This highlights the dominance of mobile devices and 3G in our sample.

Then here Fig. 2 shows that, how LowDataMode usage varies by network type (chi-square = 25.189, df = 6, $p < 0.001$, Cramer's V = 0.355). All 4 people who don't use or need LowDataMode are on Wi-Fi. Meanwhile, 3G users make up most of the other groups: 62.5% (25) of those who want to use it, 54.1% (20) of occasional users, and 52.6% (10) of regular users. 4G is used some, like 36.8% (7) for regular users, but not by the "don't need it" group.

Now, Fig. 3 shows how barriers affect LowDataMode use (chi-square = 19.282, df = 9, p = 0.023, Cramer's V = 0.254). High data consumption, a key data cost issue, dominates for occasional users (62.2%, 23). Potential adopters cite technical barriers: lack of affordable devices (42.5%, 17) and lack of offline learning options (27.5%, 11). The 4 who don't need it split evenly (1 each).

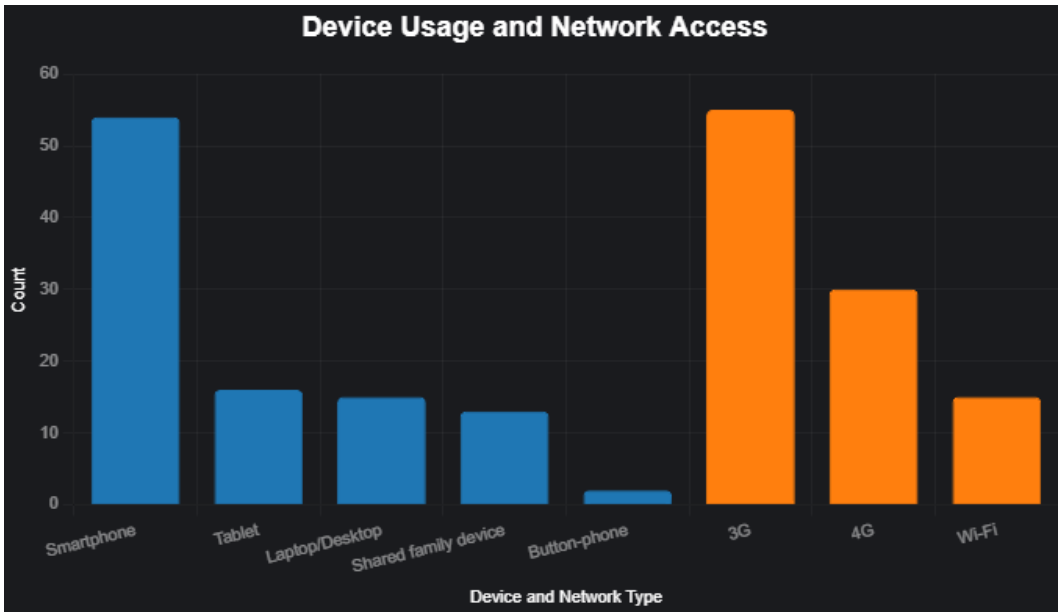

Figure 1. Device Usage and Network Access.

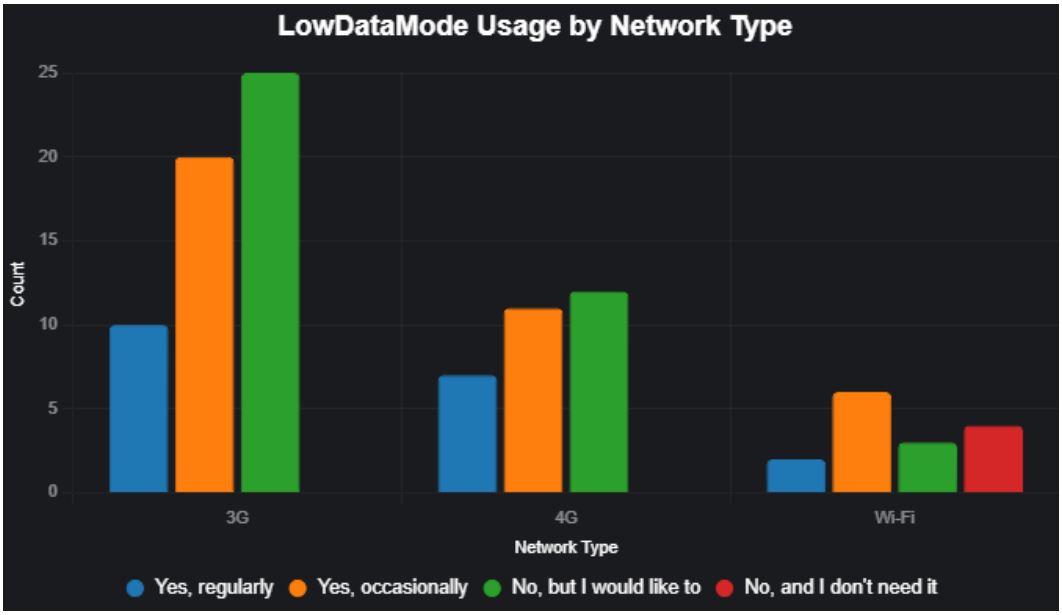

Figure 2. LowDataMode Usage by Network Type.

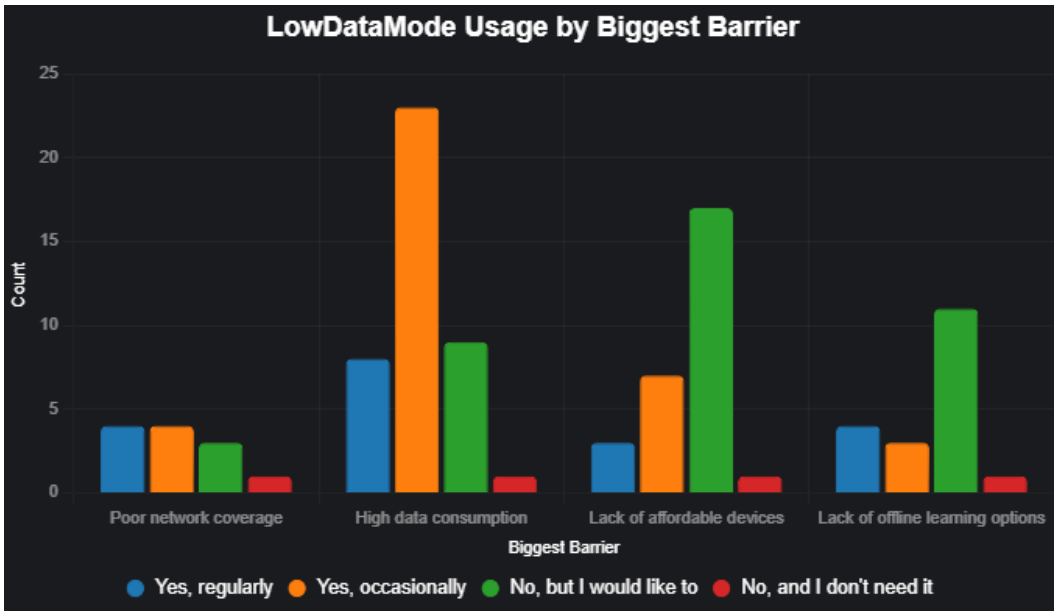

Figure 3. LowDataMode Usage by Biggest Barrier.

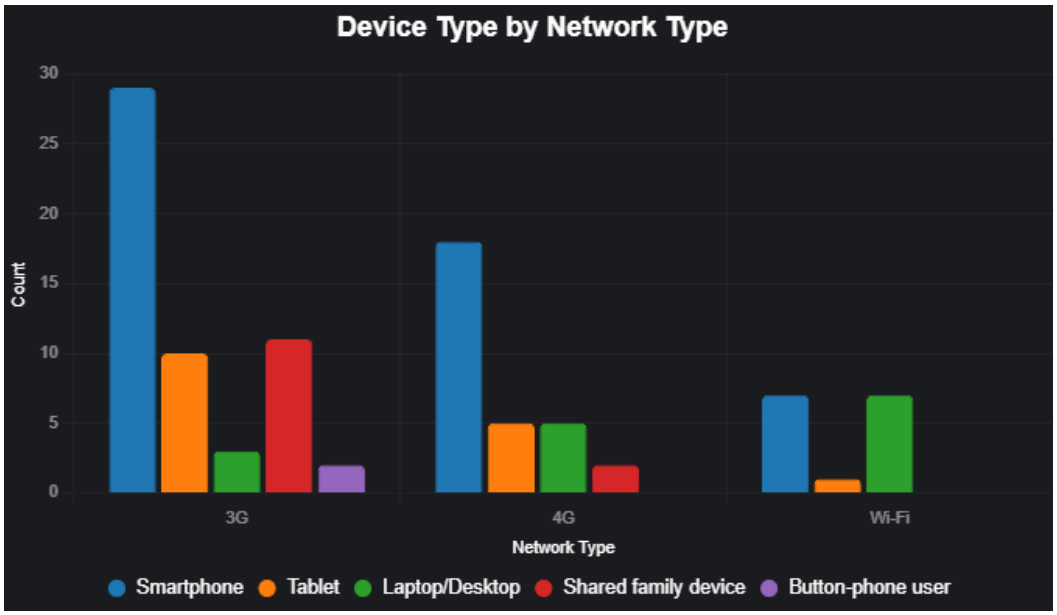

Figure 4. Device Type by Network Type.

Fig. 4 shows device types across network types (chi-square = 21.364, df = 8, p = 0.006, Cramer's V = 0.327). Laptop/desktop users lean toward Wi-Fi (46.7%, 7). Shared family devices (84.6%, 11) and button-phones (100%, 2) stick to 3G. Smartphones (53.7%, 29) and tablets (62.5%, 10) mostly use 3G, with some 4G (33.3%, 31.3%).

Fig. 5 shows how platform usability affects not using LowDataMode ($\beta = 1.477$, SE = 0.556, p = 0.008, 95% CI [0.387, 2.567]). The chance of skipping LowDataMode jumps from 2.47% at usability score 0 to 95.67% at score 5.

Fig. 6 shows p-values for tests and predictors. Blue bars ($p < 0.05$) are significant: LowDataMode vs. NetworkType ($p < 0.001$), BiggestBarrier ($p = 0.023$, includes data cost), User-friendly platform ($p = 0.016$), DeviceType vs. NetworkType ($p = 0.006$), and PlatformUsability ($p = 0.008$). Orange bars ($p < 0.10$) are marginally significant: DeviceType vs. BiggestBarrier ($p = 0.052$, technical barriers), High Data Consumption ($p = 0.086$), Intercept ($p = 0.052$). Red bars (e.g., DataCostBarrier, $p = 0.966$; NetworkBarrier, $p = 0.216$; TechProblems, $p = 0.545$; DeviceReliability, $p = 0.350$) aren't significant.

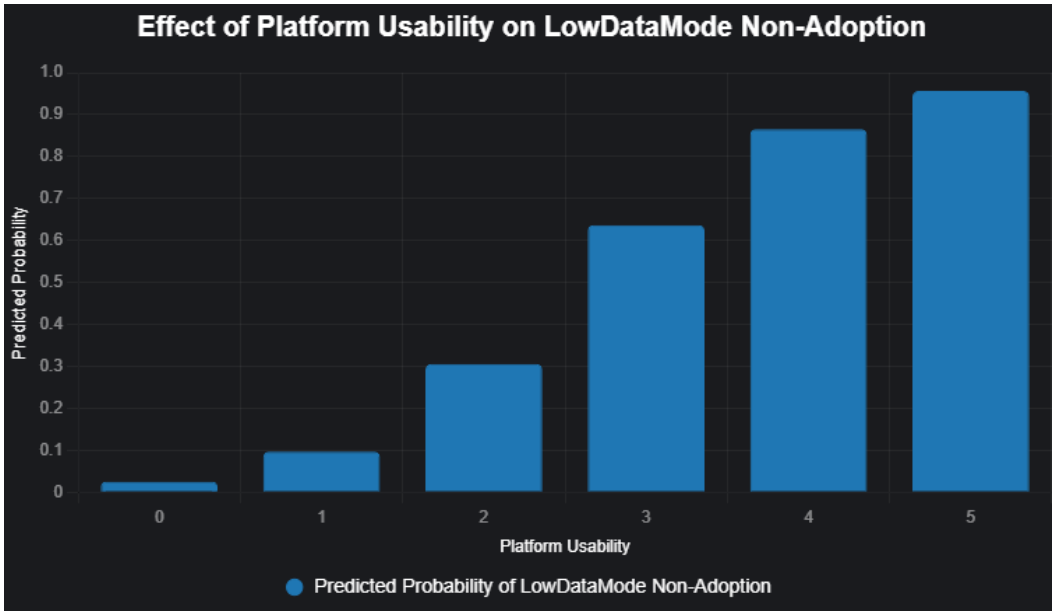

Figure 5. Effect of PlatformUsability on LowDataMode Non-Adoption.

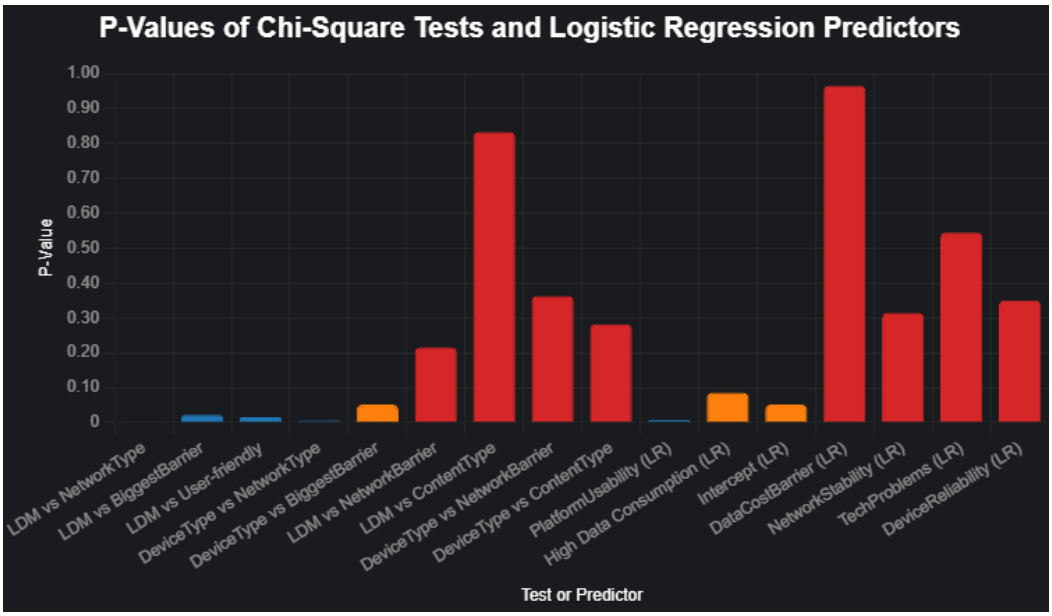

Figure 6. P-Values of Key Tests and Predictors.

Figure 7 shows device types by barriers (chi-square = 20.884, df = 12, p = 0.052, Cramer's V = 0.264). Shared family device users often cite lack of affordable devices (53.8%, 7), a technical barrier. Laptop/desktop users frequently mention lack of offline learning options (46.7%, 7). Smartphones (40.7%, 22) and tablets (37.5%, 6) point to high data consumption, a data cost issue.

Fig. 6 and 7 cover additional findings. LowDataMode showed no significant links with NetworkBarrier (p = 0.216) or ContentType (p = 0.833), nor did DeviceType with NetworkBarrier (p = 0.363) or ContentType (p = 0.282), as shown in Fig. 6's high p-values. Text-based content (1%) made results unreliable. User-friendly platform was likely significant (p = 0.016, Fig. 6), but I lack its data for a detailed figure.

My model (M1) predicted who skips LowDataMode, outperforming the baseline (delta chi-square = 32.873, df = 14, p = 0.003). Fit measures were solid (McFadden = 0.240, Nagelkerke = 0.375, Tjur = 0.292, Cox & Snell = 0.280). Fig. 5 shows PlatformUsability's strong effect (β = 1.477, p = 0.008). Fig. 6 shows High Data Consumption (β = -1.582, p = 0.086) and Intercept (β = -3.681, p = 0.052) as marginally significant, with DataCostBarrier (p = 0.966), NetworkStability (p = 0.315), TechProblems (p = 0.545), and DeviceReliability (p = 0.350) not significant.

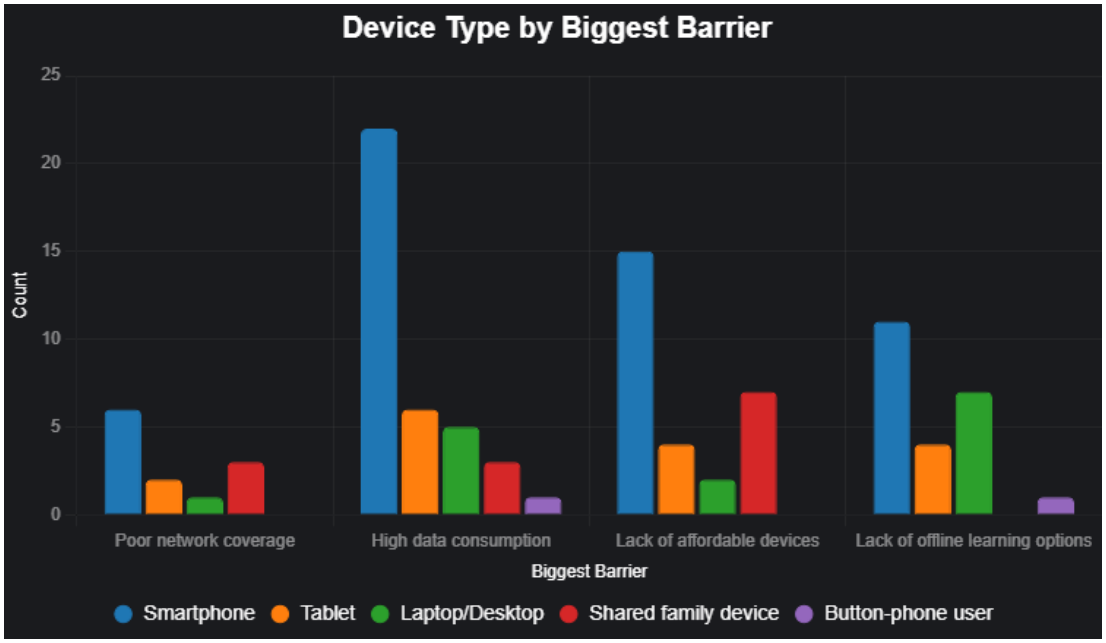

Figure 7. Device Type by Biggest Barrier.

Fig. 3 shows high data consumption (41%) as the top issue, especially for occasional users (62.2%), and Fig. 6 confirms its marginal significance ($p = 0.086$), pushing users toward LowDataMode. Technical barriers, like lack of affordable devices (28%) and offline learning options (19%), affect potential adopters (42.5%, 27.5%, Fig. 3) and vary by device type (Fig. 7, $p = 0.052$), with shared family devices (53.8%) and laptops/desktops (46.7%) highlighting these issues. 3G users (55%, Fig.s 1, 2) face significant data cost challenges, while Wi-Fi users (Fig. 2) don't need LowDataMode due to lower costs. User-friendly platforms (Fig. 5) increase data-heavy content use (60% videos), exacerbating data costs. Fig. 6 confirms significant ($p < 0.05$) and marginally significant ($p < 0.10$) factors. Other technical barriers like NetworkBarrier ($p = 0.216$) and TechProblems ($p = 0.545$) were not significant (Fig. 6). The small sample (100) and sparse text-based content data (1%) limit some findings, and lack user-friendly platform data for a full picture.

4 Conclusion

This research study confirms that high data costs and technical barriers, particularly lack of affordable devices and offline learning options, are major obstacles to LowDataMode adoption. High data consumption drives many to use LowDataMode, especially among 3G users (55%), who face significant cost constraints, while Wi-Fi users rarely need it. Technical barriers disproportionately affect users of shared family devices and laptops/desktops, limiting access to data-efficient platforms. User-friendly platforms, while beneficial, increase data usage, worsening cost issues. These findings shows that many people, about 40% who want to use LowDataMode but simply can't. This really highlights the need for more data-friendly platforms, affordable devices, and offline features to support them.

Acknowledgments

I would like to express my sincere gratitude to my supervisor for his valuable guidance and support throughout this research. I am thankful to the participants from

rural communities who shared their insights. And, I also appreciate my family and peers for their constant encouragement during this research journey.

References

[1] Bates, A.W. (Tony), Teaching in a Digital Age, Open Educational Resources Collection, 2015.

[2] "Rural population (% of total population) - Bangladesh," 2024. [Online]. https://data.worldbank.org/indicator/SP.RUR.TOTL.ZS?end=2024&locations=BD&start=2024.

[3] M. G. V. Bucheli, J. Gómez-Galán, M. L. C. Mesa and L. L. Catalán, "Digital technologies as enablers of universal design for learning: higher education students' perceptions in the context of SDG4," *Discover Sustainability,* 2024.

[4] K. A. Bingimlas, "Barriers to the Successful Integration of ICT in Teaching and Learning Environments: A Review of the Literature," *Eurasia Journal of Mathematics, Science and Technology Education,* pp. 235-245, 2009.

[5] M. S. H. Khan, M. Hasan and C. K. Clement, "Barriers to the Introduction of ICT into Education in Developing Countries: The Example of Bangladesh," *International Journal of Instruction,* 2012.

[6] T. Correa and I. Pavez, "Digital Inclusion in Rural Areas: A Qualitative Exploration of Challenges Faced by People From Isolated Communities," *Journal of Computer-Mediated Communication,* 2015.

[7] M. S. Khalid, "ICT In Education: Secondary Technical Vocationaleducation And Training Institute Centered Diffusion Ofinnovation In Rural Bangladesh," in *Proceedings of INTED2011 Conference*, Valencia, Spain, 2011.

[8] M. A. Islam, K. Mostak and G. Hoq, "Community Internet Access in Rural Areas: A study on Community Information Centres in Bangladesh," *Malaysian Journal of Library and Information Science,* pp. 109-124, 2010.

[9] J. S. Fu, "ICT in education: A critical literature review and its implications," *International Journal of Education and Development using Information and Communication Technology,* pp. 112-125, 2013.

[10] B. Whitacre, R. Gallardo and S. Strover, "Broadband's contribution to economic growth in rural areas: Moving towards a causal relationship," *Telecommunications Policy,* 2014.

[11] K. Hernandez, "Barriers to Digital Services Adoption in Bangladesh," 2019.

[12] S. Fennell, P. Kaur, A. Jhunjhunwala, D. Narayanan, C. Loyola, J. Bedi and Y. Singh, "Examining linkages between Smart Villages and Smart Cities: Learning from rural youth accessing the internet in India," *Telecommunications Policy,* pp. 810-823, 2018.

[13] R. Tamim, R. M. Bernard, E. Borokhovski, P. C. Abrami and R. F. Schmid, "What Forty Years of Research Says About the Impact of Technology on Learning A Second-Order Meta-Analysis and Validation Study," *Review of Educational Research,* 2011.

[14] M. R. Uddin, "The role of the digital economy in Bangladesh's economic - development," *Sustainable Technology and Entrepreneurship,* 2024.

This page intentionally left

IJASST
International Journal of
Applied Sciences and Smart Technologies
p-ISSN 2655-8564, e-ISSN 2685-943, pp. 43-56, 2026

Volume 08
Issue 01

Handling Highly Imbalanced Flood Data Using K-Means Clustering in Skyline Query Dominance Testing

Vega Purwayoga[1*], Zakwan Gusnadi [1], Winda Ayu Anggraini[2]

[1]*Faculty of Engineering, Siliwangi University, Indonesia*
[2]*Faculty of Economics and Business, Siliwangi University, Indonesia*
[*]*Corresponding Author: vega.purwayoga@unsil.ac.id*

(Received 21-09-2025; Revised 30-10-2025; Accepted 16-04-2026)

Abstract

Skyline query is a recommendation algorithm used to select objects based on multi-attribute preferences, but a key challenge is that its results can be highly imbalanced, where only a small number of objects meet the preferred criteria. This imbalance reduces the reliability of spatial decision-making, including in flood vulnerability assessment. This study addresses the issue by applying a modified Sort-Filter Skyline method that considers maximum and minimum attribute preferences during sorting. The skyline output shows a strong class imbalance, with only 18 areas identified as flood-prone compared to 1,574 non-flood-prone areas. To mitigate this, K-Means clustering is used as a refinement step. The Elbow and Gap Statistic methods recommend three clusters as optimal, while the Silhouette method suggests eight. Cluster distribution analysis shows that three clusters produce a more balanced representation, with Scheme 1 and Scheme 3 showing better balance ratios and lower variation than Scheme 2. Thus, clustering into three groups helps achieve a more representative mapping of flood-prone areas.

Keywords: Flood, Imbalanced Data, K-Means Clustering, Skyline Query

1 Introduction

High rainfall intensity, lowland topography, and interregional river flows are key factors that increase vulnerability to flooding. Therefore, flood potential identification plays a crucial role, not only in mapping high-risk areas but also in providing a foundation for disaster mitigation planning, strengthening community resilience, and setting local intervention priorities. By applying data-driven vulnerability analysis, utilizing both tabular sources and information from online news, flood potential mapping can provide a more comprehensive picture of the risks faced while also contributing to global agendas on disaster risk reduction and sustainable development [1].

The search and recommendation of optimal locations for various case studies can be performed using a skyline query [2], [3]. Skyline query works by examining the dominance of each factor associated with an object or location [4], [5]. In the context of disaster management, particularly floods, Skyline Query can be applied to evaluate locations based on multiple attributes such as elevation, rainfall, land slope, and land cover [6], [7]. In data science, the function of a skyline query is to narrow the search space so that the computational time required to identify relevant objects can be optimized [8], [9].

Skyline Query is effective in selecting the most relevant information, ensuring that the recommended results align with predefined preferences. For instance, in the case of flood disasters, a skyline query may recommend areas with the lowest elevation, the highest rainfall, and/or the flattest slope [7]. This dominance testing results in only a small number of areas being labeled as flood-prone compared to those classified as non-flood-prone [10], [11]. Consequently, the recommendations lead to imbalanced data.

Data imbalance, one of the outcomes produced by a skyline query, presents a significant challenge in classification tasks. Ideally, the knowledge derived from data classification should come from a dataset with balanced labels, ensuring that no particular label disproportionately influences the model [12], [13]. The imbalance resulting from skyline queries can be addressed by applying clustering-based rebalancing, in which data is grouped into several clusters according to the number of clusters determined or recommended [14].

One of the most popular and widely used clustering algorithms is K-Means, which partitions data into groups based on their proximity to cluster centers (centroids). K-Means is advantageous due to its high computational efficiency and its ability to handle large-scale datasets [15], [16]. One approach to addressing data imbalance is by determining the appropriate number of clusters in K-Means. Several well-established methods for recommending the optimal number of clusters (K) include the Elbow, Silhouette, Davies-Bouldin Index, and Calinski-Harabasz methods [17]. Study [18] evealed that the two most effective methods for optimizing K are the Elbow and Silhouette approaches, both of which recommended the same K value in the case of disaster data clustering.

Based on the imbalanced data problem generated by the skyline query algorithm, this study proposes a solution to address the issue. The first objective of this research is to apply the skyline query algorithm to recommend flood-prone areas. The second objective is to implement K-Means optimized using the Elbow and Silhouette methods. The data clustered with K-Means will form several new groups according to the number of clusters determined. The level of data balance will then be measured based on the difference in the number of objects within each cluster.

2 Material and Methods

Studi Area and Research Data

The study area in this research covers several regions in Central Java Province, including Batang, Blora, Boyolali, Demak, Grobogan, Jepara, Karanganyar, Kendal, Klaten, Magelang City, Semarang City, Kudus, Magelang, Pati, Rembang, Semarang, Sragen, Sukoharjo, and Temanggung. These regions are identified as frequently experiencing flood events according to data from National Disaster Management Agency (BNPB). This research consists of several stages: data acquisition, dominance testing using the skyline query algorithm, application of K-Means clustering, and visualization of data distribution.

Data Acquisition

Some of the data acquired in this study include administrative boundaries, elevation, land cover, slope, and rainfall. Administrative boundary data were obtained from the Geospatial Information Agency (BIG) and then filtered to select only a number of sample regions. Elevation and slope data were sourced from National Digital Elevation Model (DEMNAS), which are in raster format and therefore required several preprocessing steps to generate appropriate classes and weights. Rainfall data were collected from multiple weather stations located in Central Java Province, with the values from each station interpolated across the entire study area. Another critical dataset for identifying flood-prone areas is land cover, which helps determine land use within the study area. The smaller the proportion of infiltration areas in a region, the higher its flood risk [19].

Data Integration

In the data integration stage, all datasets were standardized into the same coordinate reference system and clipped using the administrative boundaries as the study area reference. Elevation and slope data from DEMNAS were reclassified to form analysis classes with assigned weights. Rainfall data from multiple weather stations were interpolated to produce a continuous rainfall surface. Land cover data were simplified into broader categories relevant to flood assessment. Finally, all processed layers were combined through spatial overlay to form a single integrated dataset for analysis.

Dominance Testing using Skyline Query

This study applies a modified Sort-Filter Skyline (SFS) algorithm. In terms of performance, SFS is faster in recommending an object as part of the skyline set because it performs sorting in advance [20]. The modification introduced in this research involves adjusting the formula when an attribute preference is set to minimum, allowing the recommendation results to better align with the criteria for flood potential. The modification can be seen in line 2 of Algorithm 1.

Algorithm 1. Res-Q

Input: Dataset D
Output: The Set of skyline points of *D*

```
1:  D ← if ("D[ai]= minimum preference") then
2:          1 – normalize D[ai]
3:      else
4:          normalize D[ai]
5:      end if
6:  E(D) ← calculate entropy of D[ai] using (3)
7:  D ← sort dataset by descending D[ai]
8:  S ← data with the highest entropy D
9:  From 1 to D
10:     if ("D is not dominated") then
11:         write (S, D)
12:     else
13:         remove (S, D)
14:     end if
15: end
```

The modification is applied during the normalization process, as normalization directly affects the entropy calculation. Entropy is one of the values used to determine whether an object is more highly recommended or not. When the attribute preference is set to minimum, smaller values should be considered more preferable; therefore, the normalization formula must be inverted. This adjustment appears in line 2 of Algorithm 1, where minimum preference uses reverse normalization. For example, regions with lower elevation are more likely to experience flooding, which represents a minimum preference condition. Conversely, maximum preference is applied when higher values indicate greater flood potential, such as regions with high rainfall intensity, which is processed using the normalization shown in line 3.

Clustering using K-Means Cluster

K-Means works by partitioning data into several groups initialized with a predefined value of K (the number of clusters) [21] [22]. Each cluster contains data with similar characteristics, as similarity is measured using the Euclidean distance formula. In this study, the determination of the optimal number of clusters (K) was carried out using the Elbow, Gap Statistic, and Silhouette methods [23].

Visualization of Data Distribution

The areas belonging to each cluster were visualized in the form of histograms to observe the data distribution within each cluster. Data balance was assessed by measuring the difference in the number of members across the formed clusters. To determine whether the data distribution was balanced or not, the Coefficient of Variation (CV) was employed.

3 Results and Discussions

Data Acquisition

The study area of this research covers several regions in Central Java Province. The regions presented in Fig. 1 are identified as having a high flood potential based on data from National Disaster Management Agency (BNPB).

Figure 1. Study area

Dominance Testing using Skyline Query

The dominance test using the skyline query identified 18 regions as flood-prone, while 1,574 regions were classified as low potential. The imbalance between these two categories is highly significant. The distribution results are visualized in the histogram in Fig. 2, which clearly illustrates the frequency differences between classes.

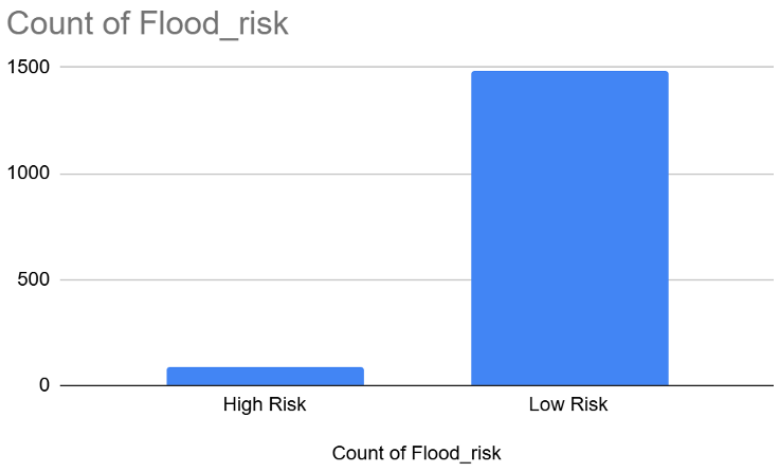

Figure 2. The results of the dominance test

Clustering using K-Means Cluster

The data clustering was carried out under three scenarios, following the approaches used to determine the most optimal value of K. The K recommendations based on the Elbow and Gap Statistic methods are shown in Fig. 1 (a)-(c). Both the Elbow and Gap Statistic methods suggested an optimal K of 3, while the Silhouette method recommended a K value of 8.

The variation in the recommended number of clusters comes from the different principles used by each evaluation method. The Elbow method, shown in Fig. 3(a), identifies K = 3 because the decrease in the sum of squared errors becomes noticeably smaller after that point, meaning additional clusters do not add much explanatory value. The Gap Statistic in Fig. 3(b) also points to K = 3, as this value gives the largest separation between the actual data clustering and the reference distribution, indicating that three clusters capture the most meaningful structure in the dataset. Meanwhile, the Silhouette method in Fig. 3(c) suggests K = 8, as this configuration provides the highest average silhouette score, reflecting clusters that are more compact and clearly separated. The Silhouette method tends to detect finer patterns in the data, which is why it favors a larger number of clusters.

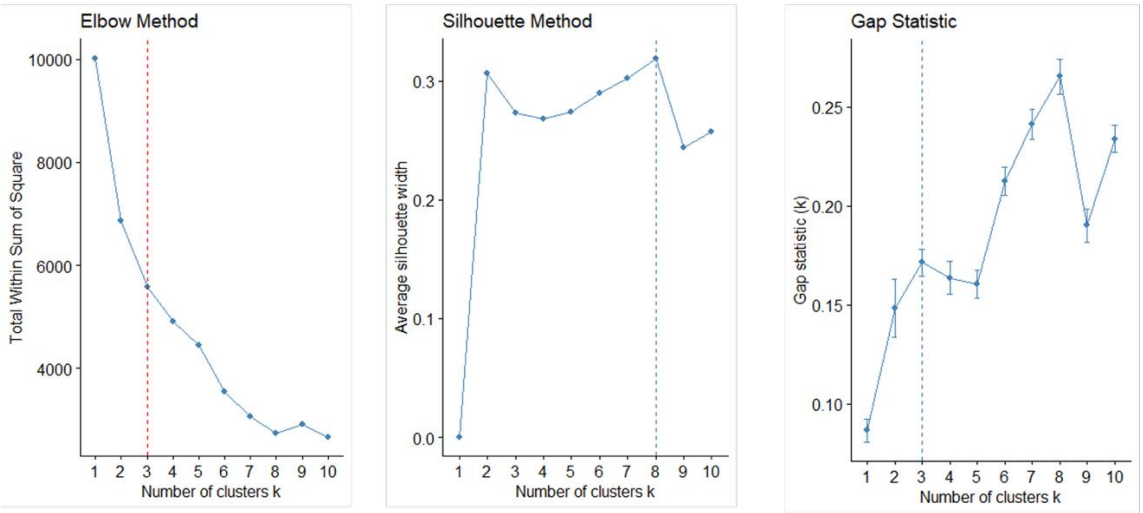

(a) (b) (c)

Figure 3. The recommendation results of the methods are as follows: (a) Elbow; (b) Silhouette; (c) Gap Statistic.

Thus, choosing between K = 3 or K = 8 depends on the analysis objective: whether the study prioritizes broader, more general clustering patterns, or a more detailed clustering that highlights local differences.

Visualization of Data Distribution

The visualization of data distribution is presented in Fig. 2. Fig. 4 (a) shows the distribution when the number of clusters K=3, which corresponds to the recommendation from the Elbow and Gap Statistic methods. Meanwhile, Fig. 4 (b) illustrates the distribution resulting from K-Means clustering with K=8. Each scheme was evaluated to determine the degree of balance in cluster membership using the balance ratio and coefficient of variation (CV), as shown in Table 1.

In general, a balance ratio close to 1 and a low CV value indicate strong clustering performance because the number of members across clusters is relatively even. The results show that Scheme 1 and Scheme 3, which both generate three clusters, have a balance ratio of 1.3 and a CV of 13.9%, reflecting a relatively balanced cluster size distribution with low variation. In contrast, Scheme 2 has a balance ratio of 2.8 and a CV of 34.8%, indicating high variation and a more uneven distribution of cluster members.

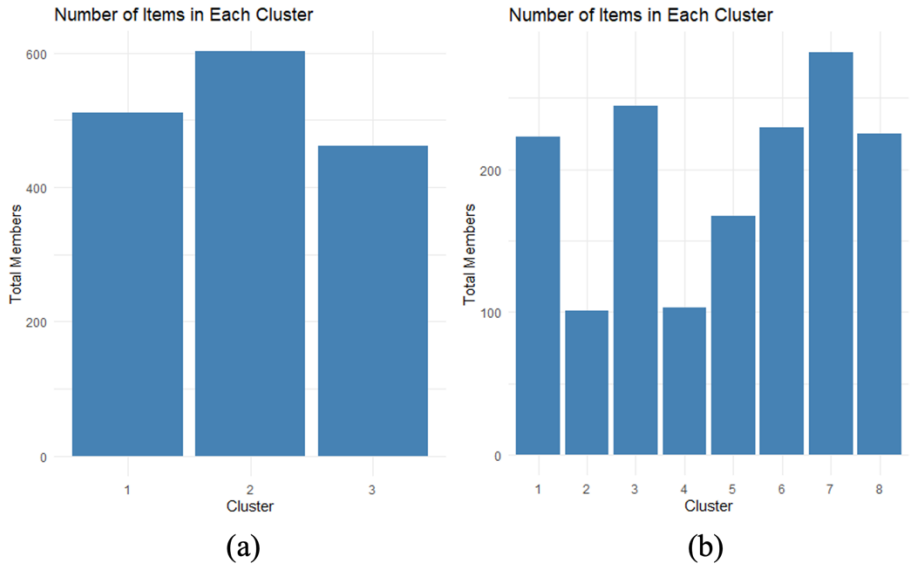

Figure 4. Cluster membership distribution: (a) k=3, (b) k=8

Therefore, Scheme 1 (Elbow) and Scheme 3 (Gap Statistic) demonstrate stronger clustering performance compared to Scheme 2 (Silhouette), which is considered less balanced. The visualization of the clustering results can be seen in Fig. 5.

Table 1. Comparison of balance ratio and coefficient of variation values

Schema	Cluster	Cluster Membership	Balance Ratio	Coefficient of Variation (%)
Schema 1, and Schema 3	C1	501	**1.3**	**13.9**
	C2	602		
	C3	461		
Schema 2	C1	223	**2.8**	**34.8**
	C2	101		
	C3	244		
	C4	103		
	C5	167		
	C6	229		
	C7	282		
	C8	225		

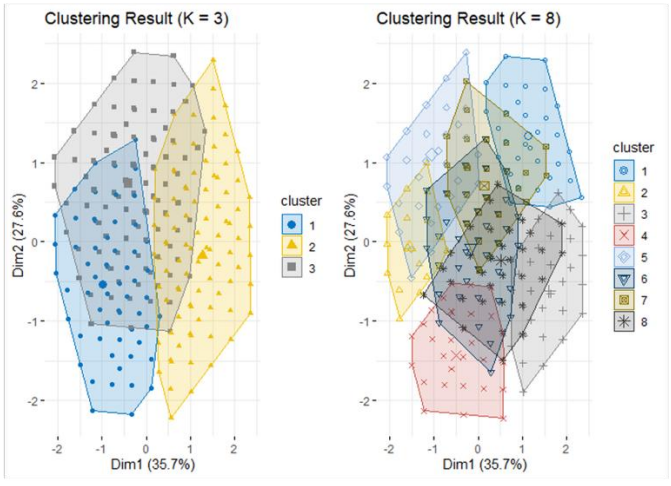

(a) (b)

Figure 5. Clusterring result: (a) k=3, (b) k=8

4 Conclusions

The analysis results indicate a data imbalance generated by the skyline query, with 18 areas identified as flood-prone and 1,574 areas categorized as low-risk. In determining the number of clusters, the Elbow and Gap Statistic methods recommend K=3, while the Silhouette method suggests K=8. The evaluation of cluster membership distribution shows that Schemes 1 and 3 are more balanced compared to Scheme 2. Future research should focus on the relevance of flood classes with spatial and environmental factors. For machine learning applications, it is recommended to apply imbalance handling techniques such as SMOTE or cost-sensitive learning, along with ensemble algorithms, to improve model accuracy in identifying the limited number of flood-prone areas.

Acknowledgements

The authors would like to express their gratitude to the Research and Community Service Institute of Universitas Siliwangi for providing financial support in the 2025 fiscal year, which enabled this research to be successfully conducted. Sincere thanks are also extended to all parties who contributed to the research process and the preparation of this article.

References

[1] B. I. Nasution, F. M. Saputra, R. Kurniawan, A. N. Ridwan, A. Fudholi, and B. Sumargo, "Urban vulnerability to floods investigation in jakarta, Indonesia: A hybrid optimized fuzzy spatial clustering and news media analysis approach," *International Journal of Disaster Risk Reduction*, vol. 83, p. 103407, Dec. 2022, doi: 10.1016/j.ijdrr.2022.103407.

[2] N. T. Lapatta, "Ecotourism Recommendations based on Sentiments Using Skyline Query and Apache-Spark," *Journal of Social Science*, vol. 3, no. 3, pp. 534–546, May 2022, doi: 10.46799/jss.v3i3.333.

[3] V. Purwayoga, S. Yuliyanti, A. Nurkholis, H. Gunawan, S. Sokid, and N. Kartini, "Distribution Model of Personal Protective Equipment (PPE) Using the Spatial Dominance Test and Decision Tree Algorithm," *JOIV : International Journal on Informatics Visualization*, vol. 8, no. 3, p. 1445, Sep. 2024, doi: 10.62527/joiv.8.3.2471.

[4] V. Purwayoga and B. Susanto, "Rekomendasi Daerah Penyalur Tenaga Kesehatan Covid-19 Dengan Menggunakan Skyline Query," *Fountain of Informatics Journal*, vol. 7, no. 1, p. 22, Oct. 2021, doi: 10.21111/fij.v7i1.5720.

[5] V. Purwayoga, "Modified skyline query to measure priority region for personal protective equipment recipient of COVID-19 health workers," *Jurnal Teknologi dan Sistem Komputer*, vol. 9, no. 3, pp. 167–173, Jul. 2021, doi: 10.14710/jtsiskom.2021.14003.

[6] V. Purwayoga, E. N. F. Dewi, and Z. Gusnadi, "B-Shinance: Aplikasi R-Shiny Interaktif untuk Percepatan Visualisasi Daerah Potensi Banjir Berdasarkan Uji Dominasi," *JASIEK (Jurnal Aplikasi Sains, Informasi, Elektronika dan Komputer)*, vol. 5, no. 2, pp. 69–76, Dec. 2023, doi: 10.26905/jasiek.v5i2.11546.

[7] V. Purwayoga and Z. Gusnadi, "Perbandingan Metode Pengukuran Jarak pada Analisis Potensi Banjir Menggunakan Spatial Skyline Query," *Infomatek*, vol. 27, no. 1, pp. 87–94, Jun. 2025, doi: 10.23969/infomatek.v27i1.24149.

[8] M. A. Mohamud *et al.*, "A Systematic Literature Review of Skyline Query Processing Over Data Stream," *IEEE Access*, vol. 11, pp. 72813–72835, 2023, doi: 10.1109/ACCESS.2023.3295117.

[9] R. Amin, "Development of Skyline Query Algorithm for Individual Preference Recommendation in Streaming Data," *Journal of Applied Data Sciences*, vol. 6, no. 2, pp. 1012–1025, May 2025, doi: 10.47738/jads.v6i2.599.

[10] A. Vlachou, C. Doulkeridis, J. B. Rocha-Junior, and K. Nørvåg, "Decisive skyline queries for truly balancing multiple criteria," *Data Knowl Eng*, vol. 147, p. 102206, Sep. 2023, doi: 10.1016/j.datak.2023.102206.

[11] V. Purwayoga, M. Al Husaini, and H. H. Lukmana, "Visualisasi Skyline Query untuk Distribusi Tenaga Kesehatan COVID-19," *Jurnal Teknik Informatika dan Sistem Informasi*, vol. 9, no. 1, Apr. 2023, doi: 10.28932/jutisi.v9i1.5624.

[12] Ainaa Hanis Zuhairi, Fitri Yakub, Mas Omar, Muhammad Sharifuddin, Khamarrul Azahari Razak, and Amrul Faruq, "Imbalanced Flood Forecast Dataset Resampling Using SMOTE-Tomek Link," *Proceedings of International Exchange and Innovation Conference on Engineering & Sciences (IEICES)*, vol. 10, pp. 845–850, Oct. 2024, doi: 10.5109/7323359.

[13] D. Dablain, "DeepSMOTE: Fusing Deep Learning and SMOTE for Imbalanced Data," *IEEE Trans Neural Netw Learn Syst*, 2022, doi: 10.1109/TNNLS.2021.3136503.

[14] J. C. Munguía Mondragón, E. Rendón Lara, R. Alejo Eleuterio, E. E. Granda Gutirrez, and F. Del Razo López, "Density-Based Clustering to Deal with Highly Imbalanced Data in Multi-Class Problems," *Mathematics*, vol. 11, no. 18, p. 4008, Sep. 2023, doi: 10.3390/math11184008.

[15] F. Reviantika, C. N. Harahap, and Y. Azhar, "Analisis Gempa Bumi Pada Pulau Jawa Menggunakan Clustering Algoritma K-Means Analysis Earthquake in Java Island Using Clustering K-Means Algorithm," *Jurnal Dinamika Informatika*, vol. 9, no. 1, 2020, [Online]. Available: https://twitter.com/infobmkg

[16] Michael Kevin Adinata, Ali Mahmudi, and Yosep Agus Pranoto, "Klasterisasi Daerah Rawan Bencana Alam Menggunakan Algoritma K-Means," *Infotek: Jurnal*

Informatika dan Teknologi, vol. 8, no. 1, pp. 250–260, Jan. 2025, doi: 10.29408/jit.v8i1.28196.

[17] I. F. Ashari, E. Dwi Nugroho, R. Baraku, I. Novri Yanda, and R. Liwardana, "Analysis of Elbow, Silhouette, Davies-Bouldin, Calinski-Harabasz, and Rand-Index Evaluation on K-Means Algorithm for Classifying Flood-Affected Areas in Jakarta," *Journal of Applied Informatics and Computing*, vol. 7, no. 1, pp. 89–97, Jul. 2023, doi: 10.30871/jaic.v7i1.4947.

[18] D. Hartama, W. Wanayumini, and I. S. Damanik, "Pengelompokan Algoritma K-Means dan K-Medoid Berdasarkan Lokasi Daerah Rawan Bencana di Indonesia dengan Optimasi Elbow, DBI, dan Silhouette," *Building of Informatics, Technology and Science (BITS)*, vol. 6, no. 2, Sep. 2024, doi: 10.47065/bits.v6i2.5851.

[19] A. Parven *et al.*, "Impacts of disaster and land-use change on food security and adaptation: Evidence from the delta community in Bangladesh," *International Journal of Disaster Risk Reduction*, vol. 78, p. 103119, Aug. 2022, doi: 10.1016/j.ijdrr.2022.103119.

[20] A. Annisa and S. Khairina, "Location Selection Based on Surrounding Facilities in Google Maps using Sort Filter Skyline Algorithm," *Khazanah Informatika : Jurnal Ilmu Komputer dan Informatika*, vol. 7, no. 2, pp. 65–72, Jul. 2021, doi: 10.23917/khif.v7i2.12939.

[21] V. Purwayoga and B. Susanto, "Pengelompokkan Daerah Berdasarkan Ketersediaan Masjid Muhammadiyah Dengan Algoritma K-Means," *Jurnal Teknologi,* vol. 13, no. 1, 2021, doi: 10.24853/jurtek.13.1.75-80.

[22] N. H. Wulandari and V. Purwayoga, "Cluster Change Analysis to Assess the Effectiveness of Speaking Skill Techniques using Machine Learning,"

International Journal of Applied Sciences and Smart Technologies, vol. 7, no. 1, pp. 1–14, Jun. 2025, doi: 10.24071/ijasst.v7i1.9667.

[23] V. Purwayoga, "Optimasi Jumlah Cluster pada Algoritme K-Means untuk Evaluasi Kinerja Dosen," *Jurnal Informatika Universitas Pamulang*, vol. 6, no. 1, p. 118, Mar. 2021, doi: 10.32493/informatika.v6i1.9522.

IJASST
International Journal of
Applied Sciences and Smart Technologies
p-ISSN 2655-8564, e-ISSN 2685-943, pp. 57-80, 2026

Volume 08
Issue 01

Modelling and Analysis of Ziegler-Nichols PID Tuning on Water Tank Control System

Regina Chelinia Erianda Putri[1], Bernadeta Wuri Harini [1*]

[1]*Faculty of Science and Technology, University of Sanata Dharma, Paingan, Maguwoharjo, Depok, Sleman, Yogyakarta, Indonesia*
[*]*Corresponding Author: wuribernard@usd.ac.id*

(Received 09-04-2026; Revised 09-05-2026; Accepted 11-05-2026)

Abstract

In the industrial world, the water level in the tank is often controlled using a PID controller. The main problem in using a PID controller is the problem of tuning the three PID parameters (Proportional gain, Integral gain, and Derivative gain). In this study, the parameter controller tuning is done using the heuristic tuning method that is applied on the water level plant and the Ziegler-Nichols tuning method that is simulated using MATLAB software. The results of both tuning methods will be compared. To simulate the control system, the water level system in the tank is modeled in the form of a first-order plus dead time modified with the Pade approach. Tuning using the Ziegler-Nichols method produced a good response, where the final value of the water level was the same as the set point value (SSE = 0%) with a settling time of 6.18 minutes.

Keywords: Heuristic, Mathematical modelling, Tuning, Water tank, Ziegler-Nichols

1 Introduction

The Proportional-Integral-Derivative (PID) controller is a conventional controller widely used in various industries to automatically control systems. Although many other modern control methods have been developed, such as the Fuzzy Logic controller [1], adaptive controller [2], genetic algorithm controller [3], and a neural network-based controller [4], the PID controller is still widely used because it has proven reliable in controlling the system. A PID controller is a simple, flexible, and effective system [5]. In addition, the Proportional-Integral-Derivative (PID) Controller has good stability and is easy to implement [6].

The PID controller has three control parameters that must be determined. These three parameters are proportional gain (K_p), integral gain (K_i), and differential gain (K_d).

The main difficulty in using a PID controller is determining the values of these three parameters to achieve a stable system quickly and to have the system output (controlled variable) reach the desired value (set point). In practice, these three PID controller parameters are tuned using the Heuristic method (trial and error). This method is widely used in practice because it does not require mathematical equations. The disadvantages of the Heuristic method are that it requires an experienced designer, the process is time-consuming, and there is no guarantee that the correct controller will be obtained [7]. To overcome the weaknesses of this method, the Ziegler-Nichols tuning method was developed [8, 9].

In process control, the three main variables typically controlled are level, temperature, and pressure. For processes that do not require heating, such as water tanks, the primary variable that must be controlled is the water level in the tank. By nature, processes are nonlinear systems. These processes have mathematical models with dead time/time delay. Therefore, these processes can be modeled in the form of First Order plus Dead Time (FOPDT) [10] or First Order plus Time Delay (FOPTD) [11]. Unfortunately, the presence of this dead time/time delay makes it difficult to simulate control systems. Therefore, this dead time/time delay is modified using the Pade approach [13, 14].

In this study, the water level system in the tank will be controlled by a PID controller. The three controller parameters, namely K_p, K_i and K_d, are tuned using a heuristic method. The results of this tuning will be compared with the results of tuning using the Ziegler-Nichols method, simulated using MATLAB software. To simulate this water level control system, the system is modeled in the form of a modified FOPDT using the Padé approach. All simulation results will be analyzed comprehensively and compared with the results of heuristic tuning to provide the most effective control system performance.

2 Literature Review

In general, a control system is used to regulate the output of a system (plant). The control system is correcting the plant output by controlling variables that can affect the

plant. The control system works by comparing the current process value and the desired value (set point).

A. PID

In engineering practice, PID control is one of the most significant control systems and consists of proportional, integral, and differential control. PID is a linear controller that produces control outputs based on system feedback. The input of the PID controller is obtained by calculating the error between the desired value (set point) and the actual value (process variable). The output of this PID controller is shown in the following equation (1) [5].

$$u(t) = K_p e(t) + K_i \int e(t) + K_d \frac{de(t)}{dt} \quad (1)$$

where $u(t)$ is the output of the controller, $e(t)$ is the actual error, while K_p, K_i and K_d are gain of Proportional (K_p), Integral (K_i) and Derivative (K_d). The schematics of the equation are shown in Fig. 1.

These three components have their respective roles. If the Proportional gain (K_p) value is large, it will produce a larger output with the same error. However, proportional reinforcement that is too high can lead to system instability. In contrast, low proportional gain results in smaller outputs for the same fault, making the controller less sensitive. Integral gain (K_i) reduces the time to reach the system endpoint and eliminates some of the steady state errors (SSE).

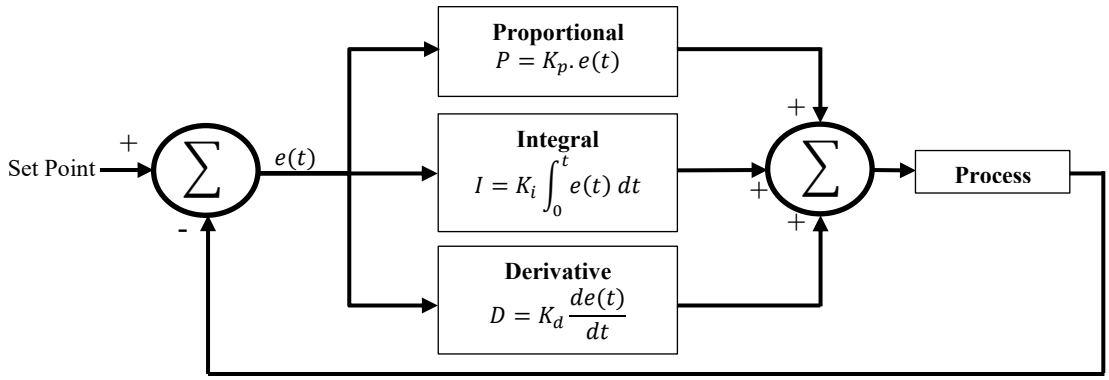

Figure 1. Schematic of PID Controller

However, the higher the integral gain value, the shorter the time for the system to reach the steady state point (T_s). The integral control will accumulate all previous errors. While the Derivative Gain (K_d) is a differential control that improves the setup time and stability of the system [6].

B. Modelling

If the model is unknown, experiments are carried out on the system. The First-Order Plus Time Delay (FOPTD) or the First-Order Plus Dead Time (FOPDT) is one of the methods used for system modeling [8]. The FOPDT model is often used because it provides a good balance in explaining the process's behavior. The FOPDT model is the right choice for a wide range of higher-level industrial process needs, as simulation is much easier. The FOPDT model has transfer functions as stated in equation (2) [9-11].

$$G_p(s) = \frac{Ke^{-t_0 s}}{\tau s+1} \tag{2}$$

where t_0 is dead time, and τ is the time constant. There are three methods for estimating the dead time and time constant. They are Fit 1, Fit 2, and Fit 3 [12] that are shown in Fig. 2. The value of the dead time and time constant is stated in equations (3) and (4).

$$\tau = \frac{3}{2}(t_2 - t_1) \tag{3}$$

$$t_0 = t_2 - \tau \tag{4}$$

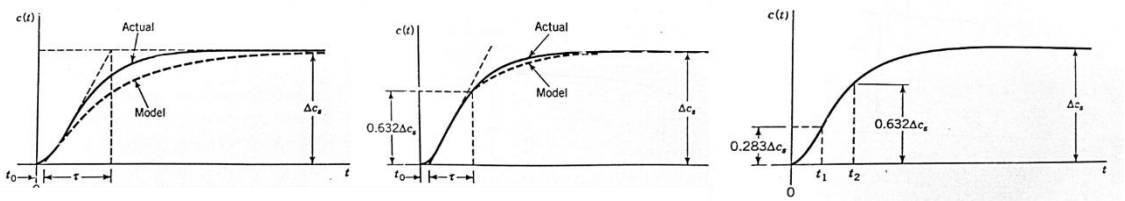

(a) (b) (c)

Figure *2.* FOPDT model parameter by; (a) Fit 1, (b) Fit 2, (c) Fit 3

The FOPDT method still has a delay element. Padé approximation is used to replace the delay element ($e^{t_0 s}$). Padé approximation is a mathematical technique with rational fractions to make it easy to analyze/tune. This model uses controller tuning rules and can be used as a replacement model in computational simulations for optimization purposes [13]. The approximations are shown in equation (5).

$$e^{-t_0 s} = \frac{1-\frac{t_0}{2}s}{1+\frac{t_0}{2}s} \tag{5}$$

Some control system designs require a rational transfer function. Padé's approximation provides a specific type of approximation to dead time in a continuous process system.

C. Ziegler Nichols Methods

Heuristic is the method that has evolved based on practical implementations or simulations [15]. The use of heuristic algorithms allows for automatic search of optimal PID (K_p, K_i, K_d) parameters without the need for an exact model to speed up the tuning process and improve control performance. If the model is unknown, experiments are carried out on the system. As explained in the introduction, the weaknesses of the heuristic method (trial and error) are overcome by using the Ziegler-Nichols tuning method. This method is used to determine in the real-time process control system [14]. The Ziegler-Nichols theorem for each K_p, K_i, K_d is shown in Table 1. Curve response for the Ziegler-Nichols Method is shown in Fig. 3.

Table 1. Ziegler Nichols Theorem

Controller	K_p	T_i	T_d
P	$\left(\frac{\tau}{t_0}\right)$	0	0
PI	$0.9\left(\frac{\tau}{t_0}\right)$	$\frac{t_0}{0.3}$	0
PID	$1.2\left(\frac{\tau}{t_0}\right)$	$2\,t_0$	0.5 L

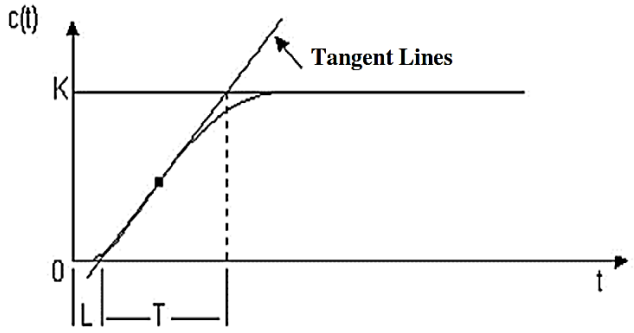

Figure 3. Curve response of the Ziegler-Nichols Method

The values of k, L, and T (where a = kL/T) can be determined through the straightforward estimation presented. By employing the variables L and a, one can derive the conditions of parameters utilizing the Ziegler-Nichols methodology.

3 Material and Methods

Academic studies and research often use water-filling systems to test the structure of control systems. The system used for testing utilizes a tiered water-filling system, with one tank stacked on top of another. The upper tank serves as the control tank, and the lower tank serves as the reservoir. Figs 4(a) and (b) shows the setup and physical structure of the water-filling system used in this experiment.

The system has several parts of the hardware system attached to a plant:

- Water level sensor to measure the height of each tank
- DC pump that supplies water flow to fill a controlled tank system.

Figure 5 shows the controller panel equipped with a switch to activate the controller. The controller is set by changing the position of the selector to adjust the magnitude of the gain P, I, and D as shown in Figs. 6(a) - (c).

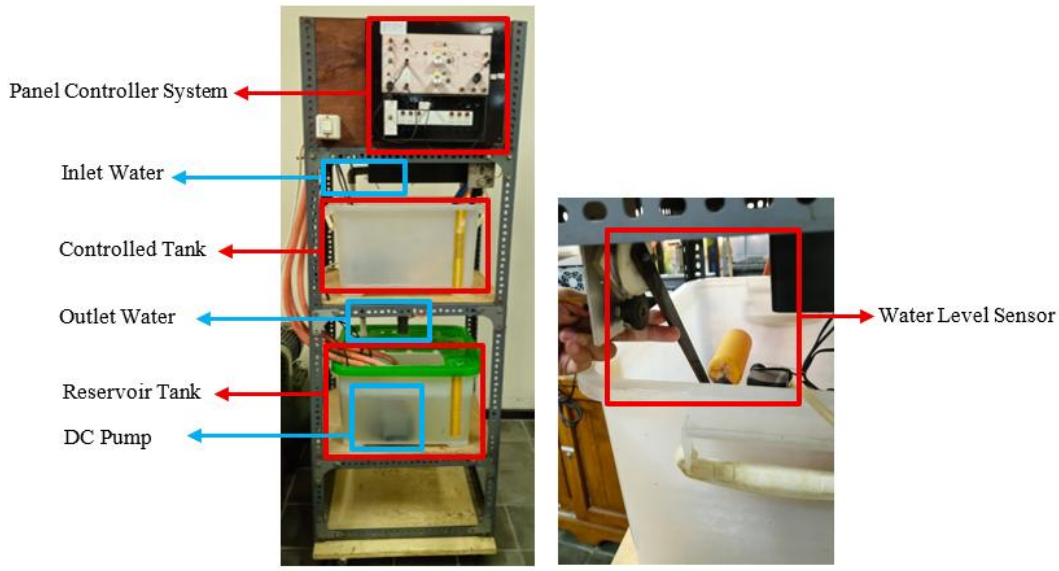

(a) (b)

Figure 4. The water tank; (a) physical arrangement of two tanks, (b) water level sensor

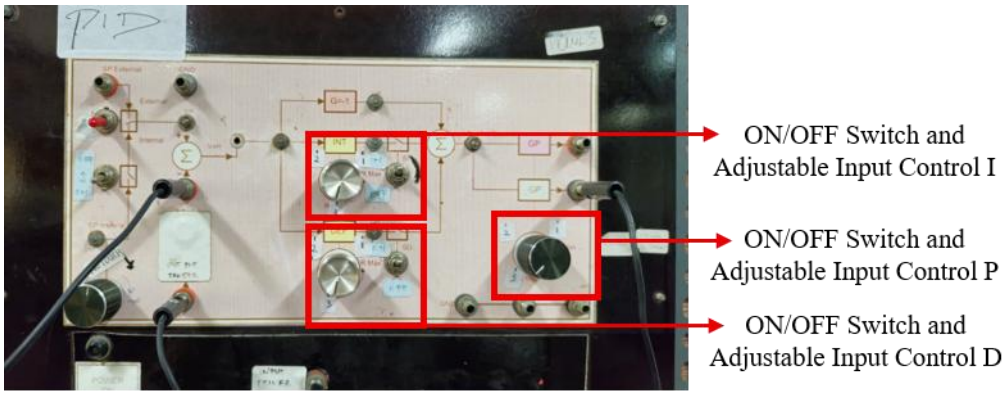

Figure 5. Panel Controller

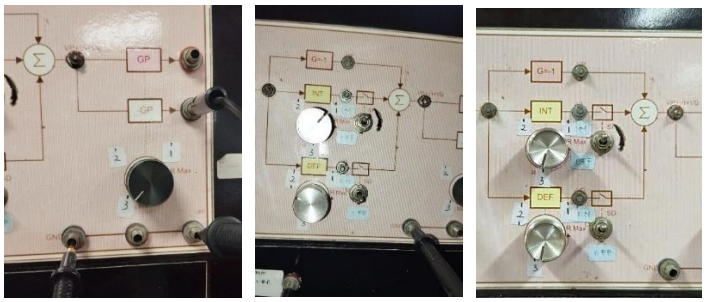

(a) (b) (c)

Figure 6. Parameter controller setting; (a) Gain P in position 3, (b) Gain I in position 1, (c) Gain D in position 3

The research steps are as follows:

1. Collecting water level vs time data to model the plant
   Data collection was carried out using a multimeter and the water level in the control tank.
2. Manual tuning using the Heuristic method
   A. P action only
      a) Eliminate I and D
      b) Give step input, starting from K_p small, then increase it
      c) Find the best response and record the K_p value that provides the best response
   B. I action
      a) Eliminate D
      b) Use the $K_p$value obtained in step A
      c) Give step input, starting from a small K_i, then increase it
      d) Find the best response and record the K_i value that provides the best response
   C. D action
      a) Use the K_p value obtained in step A and the K_i value obtained in step B
      b) Give step input, starting from a small K_d, then increase it
      c) Find the best response and record the K_d value that provides the best response
3. Data collection was carried out using 9 position combinations.
4. Build a plant model
5. Design of PID controller
6. Simulation of water level control system

Heuristic data retrieval is taken as shown in Fig. 7. The set point value used in this study is 11.5 cm.

Figure 7. Data collection at the position P=3 and I=2

4 Results and Discussions

This research focuses on system analysis using a heuristic approach, modelling the system to design optimization of PID control using tuning with the Ziegler-Nichols method. The system used is a system that is not known to have a mathematical model or a Laplace form of the plant.

A. Heuristic Experiment

The results of the heuristic experiment for the P gain tuning of the system are shown in Figs 8(a) - (c). Transient Response with Proportional Controller shown in Table 2. Where $\tau =$ the time constant, T_r = Rise Time, T_s = Settling Time, FV = Final Value, and SSE = Steady State Error. The table shows that with a set point of 11.5 cm, the steady-state error (SSE) in all three experiments was still large, exceeding 17%, even with the K_p value increased. This indicates that using a proportional controller alone is insufficient for this water level control system. Therefore, an integral controller is necessary.

The results of the heuristic experiment for tuning the PI gain of the system are shown in Figs. 9(a) - (c). Transient Response of Plant with Proportional and Integrator (PI) Controller shown in Table 3. C_{max} is the highest value of the plant's response. In these three experiments, stability was not achieved, so the SSE value could not be

calculated. However, when compared with the results of the P controller, the system output value was closer to the Set Point value (11.5 cm). Comparing the three figures, Figure 9(c) appears to have the best response, with the response oscillations decreasing rapidly. This means the system will reach stability more quickly. To achieve greater stability, the PI controller is combined with a derivative controller to form a PID controller.

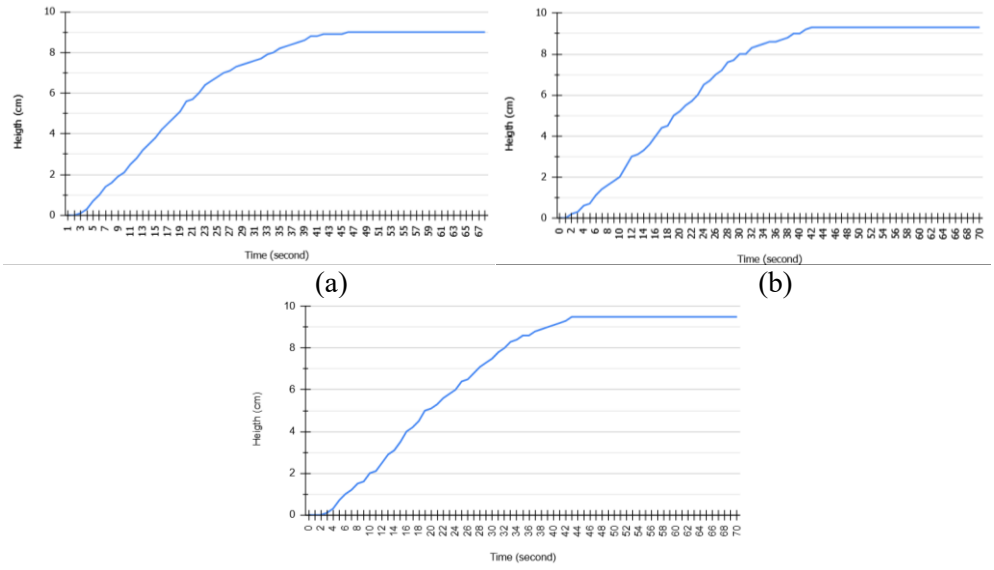

Figure 8. Response with P; (a) Position 2, (b) Position 2.5, (c) Position 3

Table 2. Transient Response with P gain (K_p)

Experiment	Position	K_p	τ (s)	T_r (s)	T_s (s)	FV (cm)	SSE (%)
1	2	6.85	20	62.9	40	9	21.74
2	2.5	8.10	22.8	27.5	40.5	9.3	19.13
3	3	8.31	24	28.5	42	9.5	17.39

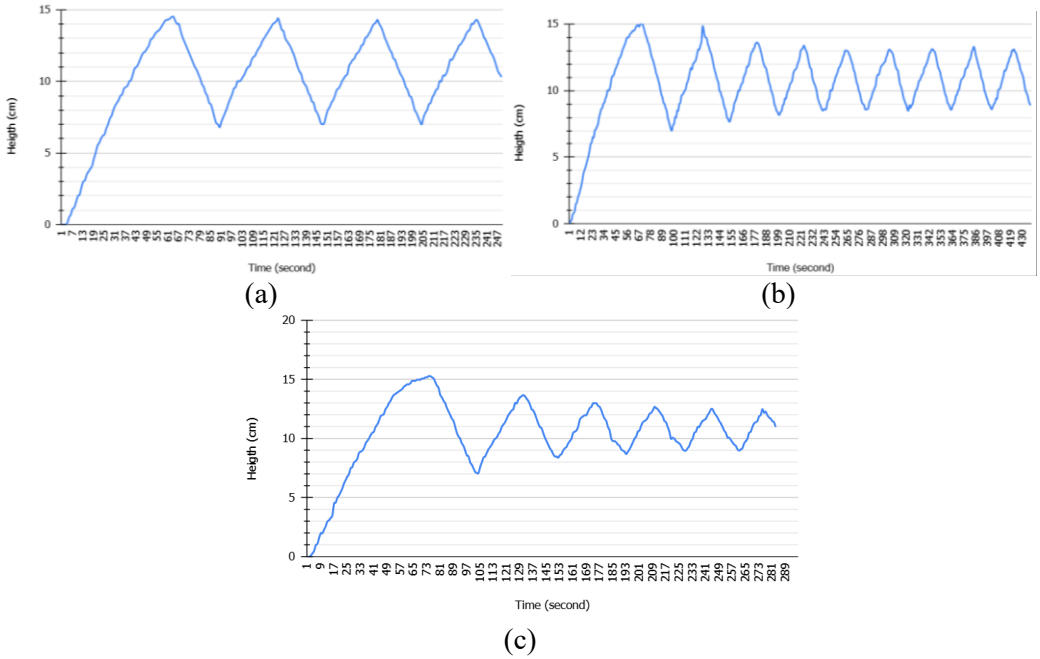

Figure 9. Response with PI; (a) in Position P=3, I=1, (b) in Position P=3, I=2, (c) in Position P=3, I=3

The results of the heuristic experiment for tuning the PID gain to the system are shown in Figure 10(a)(b)(c). Transient Response of Plant with Proportional Integral Derivative (PID) controller shown in Table 4. Figure 10 and Table 4 show that the best response was obtained in the third experiment with settings of K_P=8.31, K_i=4.75, and K_d=2.3. However, the results obtained were not as expected. Therefore, these results will be compared with the simulation results using MATLAB.

Table 3. Transient Response with PI

Experiment	Position		Gain		C_{max}	Tp (s)
	P	I	K_p	K_i		
1	3	1	8.31	9.57	14.5	64
2	3	2	8.31	7.30	15	68
3	3	3	8.31	4.47	15.3	19

Table 4. Transient Response with PID

Experiment	Position			Gain			C_{max}	Tp (s)
	P	I	D	K_p	K_i	K_d		
1	3	3	1	8.31	4.47	0.30	15.3	76
2	3	3	2	8.31	4.47	1.85	15.2	76
3	3	3	3	8.31	4.47	2.30	15.1	76

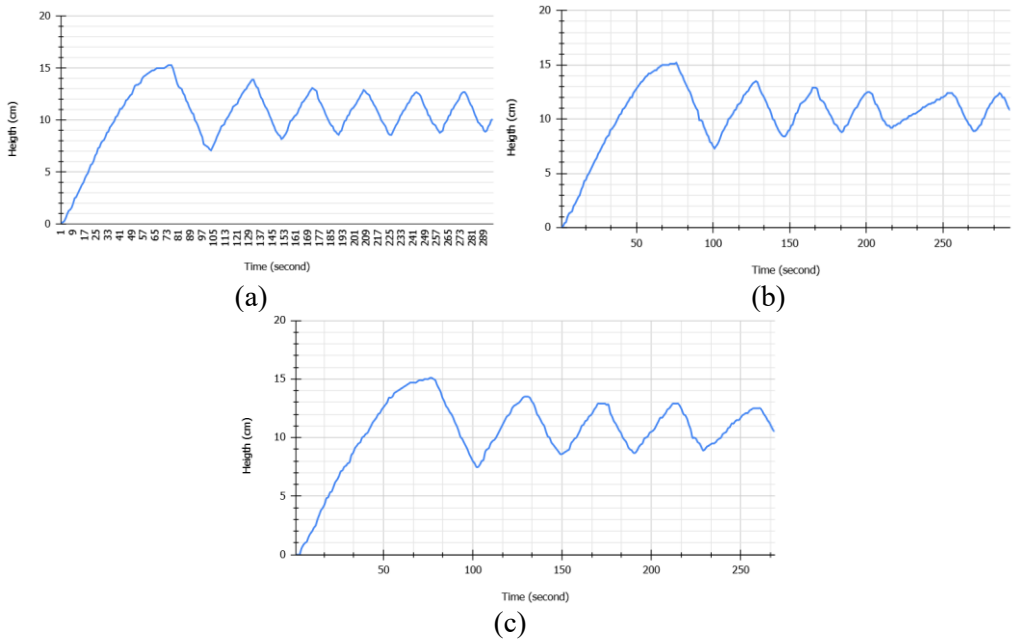

Figure 10. Response with PID in Position; (a) P=3, I=3,D=1, (b) P=3, I=3,D=2, (c) P=3, I=3, D=3

B. Numerical Simulation

i. Modelling

The plant used will be modeled by generating a response output from experimental results. The output of the open-loop system response is shown in Fig. 11. From an open-loop system based on experiment, the mathematical model of gain (K) is obtained, stated in equation (6).

$$K = \frac{\Delta C(s)}{\Delta M(s)} = \frac{13.3\ \text{cm}}{100\%CO} = 0.133\ \frac{\text{cm}}{\%CO} \quad (6)$$

where CO = controller output.

The FOPTD model, as stated in Equation 2, with the Padé approximation as stated in Equation 3, can then be rewritten using Fit 1 (Fig. 12) and Fit 2 (Fig. 13). The data in this model is taken in an open-loop system.

From Fig. 12, the value is obtained $t_0 = 4s$ and $\tau = 39 - 4 = 35s$ so that the FOPDT model is stated in equation (7).

$$G_p(s) = \frac{0.133e^{-4s}}{35s+1} \tag{7}$$

Using Padé approximations, a plant model in Laplace's equation becomes equation (8).

$$G_p(s) = \frac{0.133}{35s+1}\ \frac{1-2s}{1+2s} \tag{8}$$

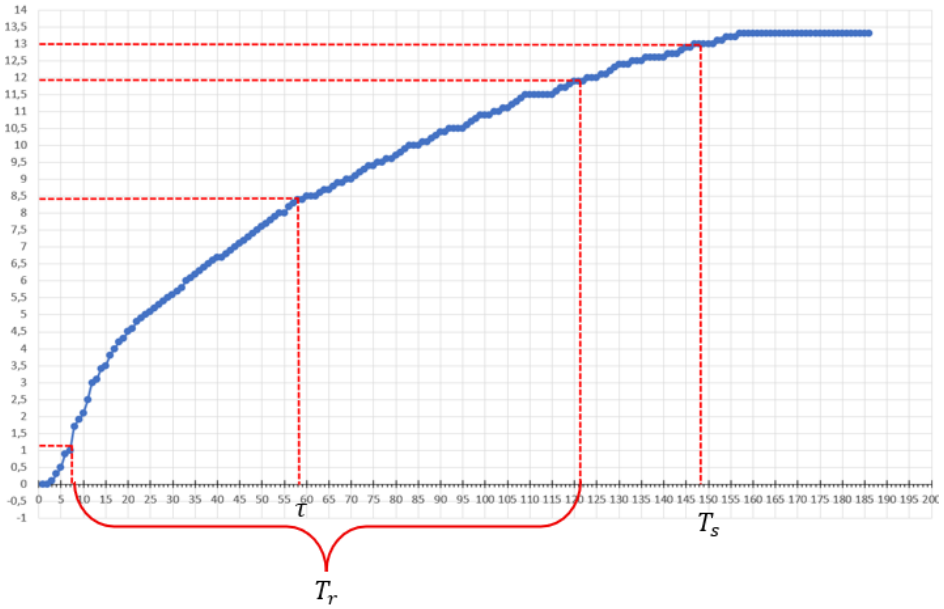

Figure 11. Response Open-loop Model

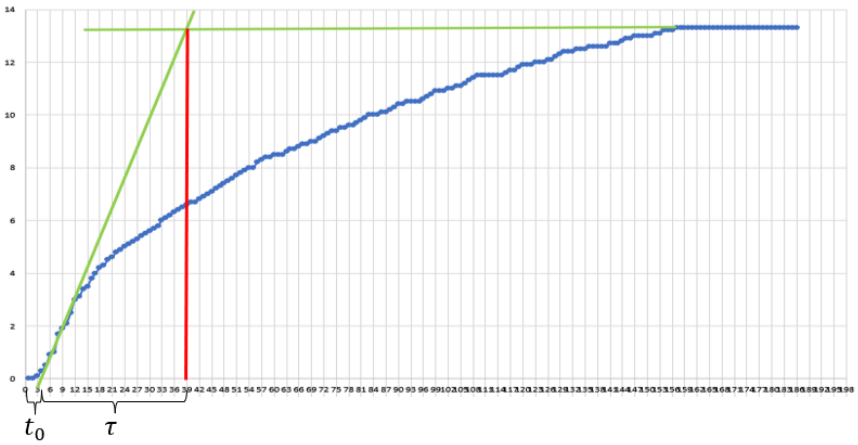

Figure 12. Open Loop Model using Fit 1

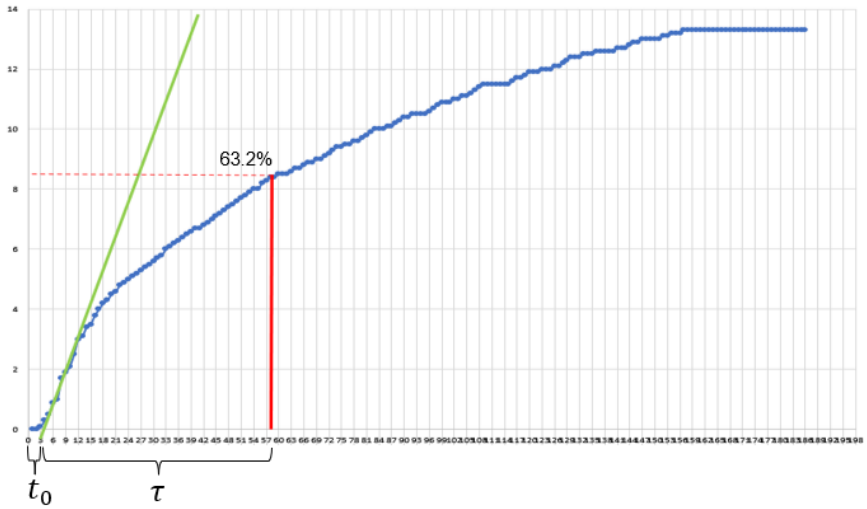

Figure 13. Open Loop Model using Fit 2

From Fig. 13, the value $t_0 = 4s$ and $\tau = 58 - 4 = 54s$ are obtained, so that the Laplace equation on the plant is stated in equation (9)

$$G_p(s) = \frac{0.133e^{-4s}}{54s+1} \tag{9}$$

Using Padé approximations, the plant equation in the Laplace model becomes equation (10).

$$G_p(s) = \frac{0.133}{54s+1} \frac{1-2s}{1+2s} \quad (10)$$

In the fit 3 modeling, t_1=15 seconds and t_2=58 seconds were obtained, which resulted in a negative dead time value, so the fit 3 modeling was not used.

For model comparison, the K value on the Fit 1 and Fit 2 models is multiplied by 100 to get the same Final Value as the actual value. The results of the simulation can be seen in Figs. 14(a) and (b). A comparison of the response characteristics between the model and the actual value is shown in Table 5. Considering that the settling time in the Fit 1 model is close to the actual value, the Fit 1 model is used in the next calculation.

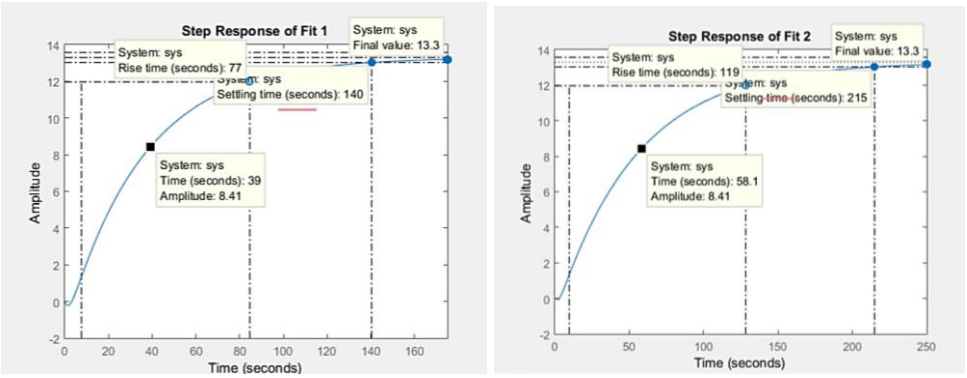

(a) (b)

Figure 24. Simulation Result of the Modelling using; (a) Fit 1, (b) Fit 2

Table 5. Comparison Fit 1 and Fit 2

Parameter	Plant	Fit 1 Model	Fit 2 Model	Unit
Final Values	13.3	13.3	13.3	cm
Rise Time	114.8	77	119	second
Settling Time	147	140	215	second
Time Constant	58	39	58.1	second

ii. Controller Tuning using Ziegler-Nichols Method

Based on the Ziegler-Nichols rule, it produces the number of tuning results as shown in Table 6. In the table, 3 types of controllers are designed. They are Proportional (P), Proportional Integral (PI), and Proportional Integral Derivative (PID) controllers.

The amount of the controller gain will be used as a gain recommendation in the system. From the combination of gains, we will see the response of each gain in the system that has been modeled.

Proportional Controller (P Controller)

From Table 6, it can be obtained that $K_P = 8.75$. The block diagram of the system and the magnitude of the K_P gain are shown in Figure 15, and Figure 16 is the Transient Response of the system.

The model in Laplace's for the block diagram (Figure 15) is shown in equation (11).

$$\frac{C(s)}{R(s)} = \frac{8.75 \frac{0.133}{35s+1}\frac{1-2s}{1+2s}}{1+8.75 \frac{0.133}{35s+1}\frac{1-2s}{1+2s}} = \frac{-2.3275s+1.16375}{70s^2+34.6725s+2.16375} \quad (11)$$

The results of the simulation of the Laplace equation above are shown in Fig. 16.

Table 6. Controller Tuning using Ziegler-Nichols

Controller	K_p	T_i	T_d
P	8.75	-	-
PI	7.875	13.32	-
PID	10.5	8	2

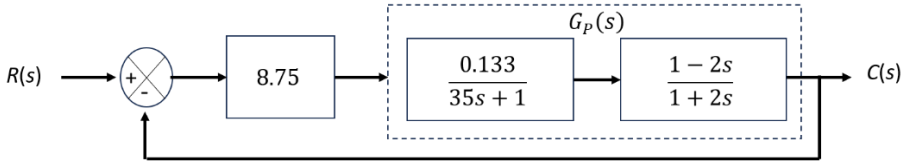

Figure 35. Ziegler-Nichols Tuning Block Diagram with $K_p = 8.75$

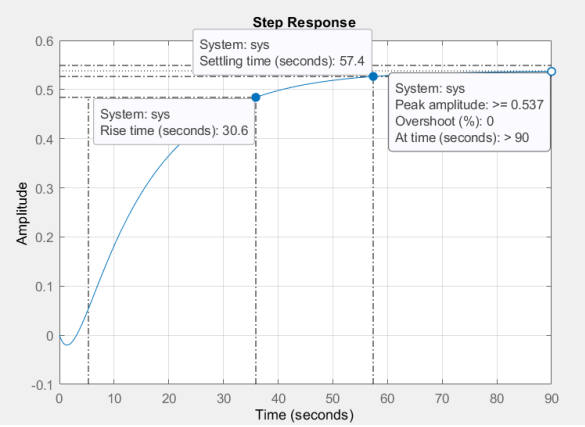

Figure 46. Response Transient using a Proportional controller only with K_p = 8.75

Proportional-Integral Controller (PI Controller)

From the table, it can be obtained that $K_p = 7.875,\ T_i = 13.32s$. The value of Ki is shown in equation (12).

$$K_i = \frac{1}{T_i} = \frac{1}{13.32} = 0.0751 \tag{12}$$

The controller formula uses parallel structure, so the controller transfer function is shown in equation (13).

$$G_c(s) = K_p + \frac{K_i}{s} = 7.875 + \frac{0.0751}{s} = \frac{7.875s+0.0751}{s} \tag{13}$$

The block diagram of the system with the magnitude of the K_p and K_i gain is shown in Fig. 17. The transfer function of the system is stated in equation (14).

$$\frac{C(s)}{R(s)} = \frac{\frac{7.875s+0.0751}{s}\ \frac{0.133}{35s+1}\ \frac{1-2s}{1+2s}}{1+\frac{7.875s+0.0751}{s}\ \frac{0.133}{35s+1}\ \frac{1-2s}{1+2s}} = \frac{-2.0948s^2+1.0274s+0.01}{70s^3+34.9052s^2+2.0274s+0.01} \tag{14}$$

The results of the simulation of the Laplace equation above are shown in Fig. 18.

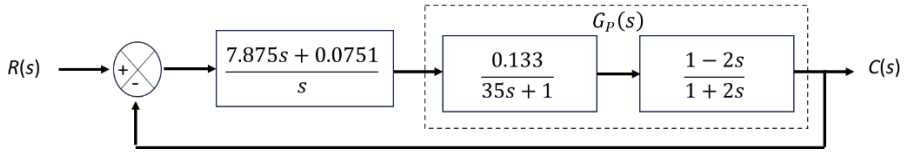

Figure 5. Ziegler-Nichols Tuning Block Diagram with $K_p = 7.875$ *and* $K_i = 0.0751$

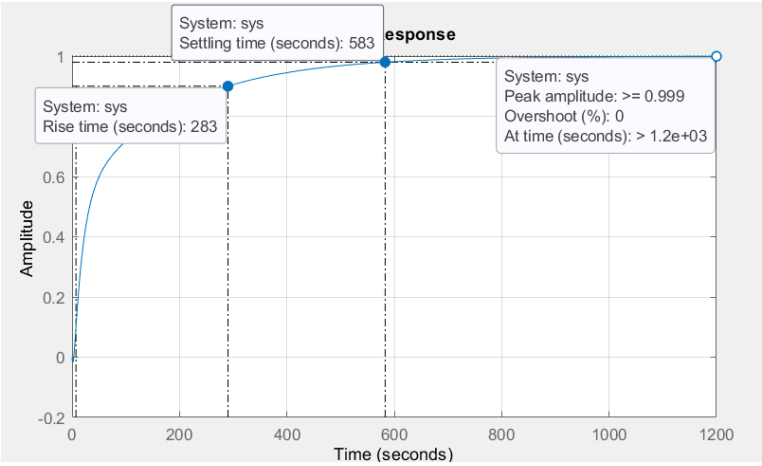

Figure 18. Response Transient using PI controller with K_p = 7.875 and K_i=0.0751

Proportional-Integral-Derivative Controller (PID Controller)

From Table 6, it can be obtained that $K_p = 10.5$, $T_i = 8s$. The values of K_i and K_d are stated in equations (15) and (16).

$$K_i = \frac{1}{T_i} = \frac{1}{8} = 0.125 \quad (15)$$

$$K_d = T_d = 2 \quad (16)$$

The controller formula uses parallel structure, so the controller transfer function is shown in equation (17).

$$G_c(s) = K_p + \frac{K_i}{s} + K_d s = 10.5 + \frac{0.125}{s} + 2s = \frac{2s^2+10.5s+0.125}{s} \quad (17)$$

The block diagram of the system and the magnitude of the K_p, K_i, K_d gains are shown in Fig. 19. The transfer function of the system is stated in equation (18). Fig. 20 shows the Transient Response of the system.

A comparison of these three curves is presented in Fig. 21 and Table 7. This figure and table compare the transient response of the system with P, PI, and PID control mechanisms. All three systems were given step input. In the first simulation, the plant was controlled using only a P controller with a Kp value of 8.75. It appears that the system has the fastest rise time value, which requires approximately 30.6 seconds.

$$\frac{C(s)}{R(s)} = \frac{\frac{2s^2+10.5s+0.125}{s}\ \frac{0.133}{35s+1}\ \frac{1-2s}{1+2s}}{1+\frac{2s^2+10.5s+0.125}{s}\ \frac{0.133}{35s+1}\ \frac{1-2s}{1+2s}}$$

$$\frac{C(s)}{R(s)} = \frac{-0.532s^3-2.527s^2+1.3633s+0.0166}{69.468s^3+34.473s^2+2.3633s+0.0166} \quad (18)$$

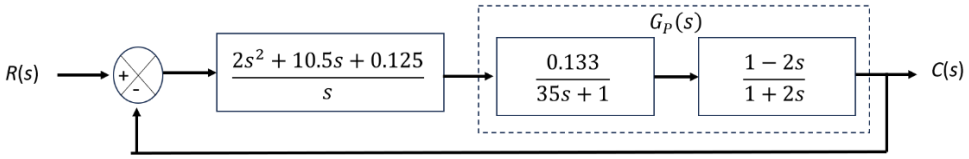

Figure 19. Ziegler-Nichols Tuning Block Diagram with $K_p = 10.5$, $K_i = 0.125$ *and* $K_d = 2$

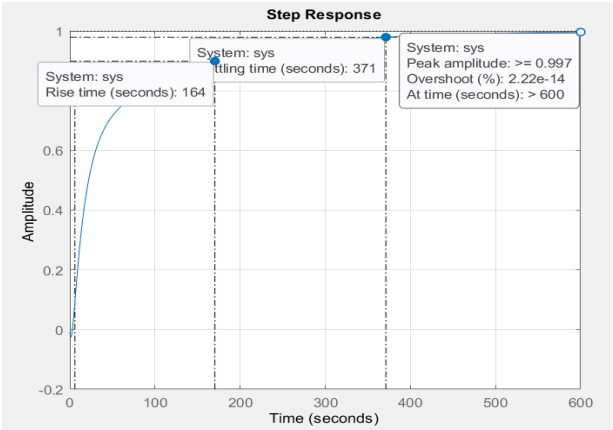

Figure 206. Response Transient use PID controller with K_p=10.5, K_i= 0.125 and K_d= 2

However, the Final Value in this system is 0.538. This means the system cannot achieve the desired value with an SSE of 46.2%. The P controller alone is not sufficient to control the water level. Therefore, it is necessary to add an integral controller so that the plant is controlled with a PI controller. In the second experiment with the addition of a P controller of 7.875 and an I controller of 0.075, the system response is quite good, where the system has a Final Value of 1 with zero steady-state error. However, in this experiment, the settling time is long, namely 583 seconds, with a rise time of 283 seconds. To speed up the response, a derivative controller is added. The third experiment, where the plant was controlled with a PID controller, had a Final Value of 1 with a shorter settling time and rise time compared to the second experiment, although there was a very small overshoot.

From the results of PID modeling and tuning using Ziegler-Nichols, it was found that the control system with a PID controller was the best choice, with a configuration of $K_p = 10$, $K_i = 0.125$, and $K_d = 2$. The system with a PID controller can achieve a Final Value of 1 with the fastest rise time and the fastest settling time. When compared with the tuning results using the heuristic method with maximum gain settings ($K_p = 8.31$, $K_i = 4.75$, and $K_d = 2.3$), the K_p gain needs to be increased, while the K_i gain needs to be decreased. Because the K_p gain is directly proportional to the resistance value, while the K_i gain is inversely proportional to the value, the resistance value for both gains must be increased.

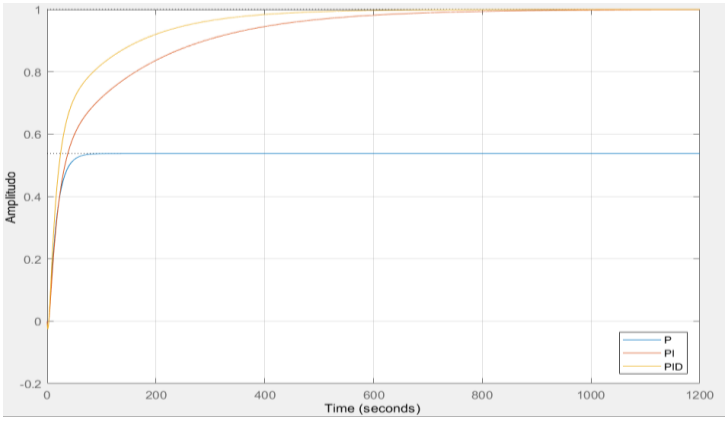

Figure 21. Comparison of Response Transient with Ziegler-Nichols

Table 7. Response Transient

Experiment	K_p	K_i	K_d	T_s (s)	T_p (s)	FV	T_r (s)	%OS	SSE (%)
1	8.75	-	-	57.4	-	0.538	30.6	0%	46.2
2	7.875	0.0751	-	583	-	1	283	0%	0
3	10.5	0.125	2	371	>600	1	164	2.22e-14 %	0

5 Conclusions

The water tank system testing was carried out by observing the performance of the addition of P, PI, and PID controllers to the water level in the tank using a heuristic method compared with the tuning results using Ziegler-Nichols. From the results of the plant simulation with the Fit 1 model, the best controller value for the system that can effectively improve the level control performance is the PID controller with a value of K_p= 10, K_i= 0.125, and K_d = 2. Tuning using the Ziegler-Nichols method produced a good response, where the final value of the water level was the same as the set point value (SSE = 0%) with a settling time of 371 seconds (6.18 minutes). Heuristic tuning for the plant used in this study failed to achieve the setpoint value due to limitations in the available controllers. For the system to work optimally, the resistance values K_p and K_i need to be increased.

References

[1] M. Bahgat, M. Ezzat, M. A. Attia, S. Mekhamer, and N. M. Elbehairy, "Comparative Analysis of PI and Fuzzy Logic Controller for Grid Connected Wind Turbine," 2024.

[2] A. Munshi, "Adaptive control mechanisms for intelligent manufacturing systems," Technical Science Integrated Research, vol. 1, no. 1, pp. 3-6, 2025.

[3] J.-H. Park, "Optimal controller design for a mobile robot using genetic algorithm and adaptive PID controller," IEEE Access, 2025.

[4] A. O'Quinn and M. Taylor, "Automated Synthesis of Verified Neural Network Controllers from Linear Temporal Logic Specifications," in Proceedings of the 2025 Workshop on Re-design Industrial Control Systems with Security, 2025, pp. 26-34.

[5] N. Hu, "The limitations of traditional PID controllers and modern optimization methods," Applied and Computational Engineering, vol. 147, no. 1, pp. 238-244, 2025.

[6] R. Chen, "A comprehensive analysis of PID control applications in automation systems: Current trends and future directions," Highlights in Science, Engineering and Technology, vol. 97, pp. 126-132, 2024.

[7] D. F. Zambrano-Gutierrez, G. H. Valencia-Rivera, J. G. Avina-Cervantes, I. Amaya, and J. M. Cruz-Duarte, "Designing heuristic-based tuners for fractional-order PID controllers in automatic voltage regulator systems using a hyper-heuristic approach," Fractal and Fractional, vol. 8, no. 4, p. 223, 2024.

[8] C. Enwerem and I. Okoro, "Optimal controller tuning technique for a first-order process with time delay," arXiv preprint arXiv:2210.08187, 2022.

[9] A. K. Mehta and R. Swarnalatha, "Adopting pade approximation for first order plus dead time models for blending process," International Journal of Engineering & Technology, vol. 7, no. 4, pp. 2800-2805, 2018.

[10] K. S. Kula, "Tuning a PI/PID controller with direct synthesis to obtain a non-oscillatory response of time-delayed systems," applied Sciences, vol. 14, no. 13, p. 5468, 2024.

[11] C. I. Muresan and C. M. Ionescu, "Generalization of the FOPDT model for identification and control purposes," Processes, vol. 8, no. 6, p. 682, 2020.

[12] C.A. Smith and A. B. Corripio, *Principles and Practice of Automatic Process Control*. New York: John Wiley & Sons, Inc, 1997.

[13] C. Yanarateş and A. Altan, "Compact Analysis of the Necessity of Padé Approximation for Delayed Continuous-time Models in LQR, H-Infinity and Root Locus Control Strategies," Black Sea Journal of Engineering and Science, vol. 7, no. 6, pp. 1315-1320, 2024.

[14] R. S. Widagdo, B. Hariadi, and K. Setyadjit, "Modelling and analysis of Ziegler-Nichols and Chien-Hrones-Reswick tuning PID on DC motor speed control," Jurnal Teknologi Elektro, vol. 14, no. 1, pp. 23-27, 2023.

[15] C. Dalen and D. L. Di Ruscio, "A Semi-Heuristic Process-Reaction Curve PID Controller Tuning Method," 2018.

This page intentionally left blank

IJASST
International Journal of
Applied Sciences and Smart Technologies
p-ISSN 2655-8564, e-ISSN 2685-943, pp. 81-118, 2026

Volume 08
Issue 01

Using the Six Sigma DMAIC Approach to Improve Maintenance Practices of Ground-Service Mechanical Equipment within a Sub-Saharan African Airport

Olanrewaju Samson Omisakin[1], Sunday Ayoola Oke[1*],
Adeyinka Oluwo[1], John Rajan[2], Swaminathan Jose[3]

[1]*Department of Mechanical Engineering, University of Lagos, Akoka-Yaba, Lagos, Nigeria*
[2]*School of Mechanical Engineering, Vellore Institute of Technology, Chennai Campus, Chennai, India*
[3]*School of Mechanical Engineering, Vellore Institute of Technology, Vellore Campus, Vellore, India*
[*]*Corresponding Author: sa_oke@yahoo.com*

(Received 06-09-2025; Revised 25-03-2026; Accepted 09-04-2026)

Abstract

Despite its ambitions for the most effective and world-class standard attainment, the ground-service equipment literature for airports is limited in engagements with the question of how to ascertain the effectiveness of maintenance services for critical ground-service equipment, to improve company goodwill and passenger comfort. By borrowing ideas from the process improvement literature, the DMAIC approach was instituted in a sub-Saharan African airport to capture the five critical ground-services mechanical equipment of package air-conditioner, escalator, travelator, baggage handling equipment and elevator. The methodology deployed to solve the problem is technical action research conducted in a large international airport. The DMAIC improvement framework was designed, installed and regularly managed for outcomes in discussions with the maintenance ground-service team from the delegated department. The cause-and-effect analysis was deployed to establish the frontline reasons for the equipment failures. The results revealed that 80% of the studied ground-service equipment exhibits the Cp/Cpk values above 1.33. Consequently, the maintenance procedure adopted to maintain the equipment is capable of maintaining a large majority of the equipment studied. However, there is scope to improve the performance of the escalator, whose value of the Cp/Cpk ratio falls below the 1.33 benchmark. A DMAIC framework appropriate to analyse the maintenance efficiency of ground-service mechanical equipment in airports is contributed for the first time to the airport setting.

Keywords: Airports, ground-service mechanical equipment, maintenance practices

1 Introduction

Presently, the pressure on ground-service equipment in airports seems unprecedented due to overgrown passenger traffic, particularly in large international airports [1]. Concurrently, to establish the quality of their journeys, passengers require stress-free services, including pre-boarding waiting, check-in services, security checks of passengers, and immigration control [1,2,3,4]. Besides, beyond the passengers' concern about ground-service equipment and pre-flight waiting comfort, the issue of maintenance inefficiency of ground-service equipment triggered agitations among airlines and airport management [1,4,5]. It is argued that to assess and establish the overall airport performance, the conception of a balanced viewpoint of the ground-service equipment performance from various stakeholders and users will strengthen understanding and offer a greater improvement drive. Consequently, in the global airport sector, the International Air Transport Association, known as IATA, and the Airports Council International, ACI, issued calls for level of service enhancement, which greatly validates the importance of the present investigation [6].

At present, the airport ground-service equipment literature lacks insights and motivation on how to ascertain the effectiveness of maintenance services for critical ground-service equipment, using scientific tools of interest. This has caused damage to the airport's goodwill. To commence a goodwill enhancement drive and passenger comfort improvement, the DMAIC approach is introduced for the maintenance process improvement of five critical airport ground-service pieces of equipment in a large international airport within a developing country. Service defects are analysed to enhance maintenance service efficiency. But solving complicated problems such as maintenance inefficiency at airports is challenging, as there are limited manpower constraints and budgets, and the saturation of airports with passengers at most times of the year is compelling. Thus, a unique scientific approach, such as the DMAIC, to create capacity, enhance operations and resolve the complicated problem is the need of the hour in airports.

In an endeavour to apply the DMAIC approach, the challenge of unexpected downtime to the critical equipment, during working hours, is tackled. These pieces of equipment include the elevator, escalator, travelator, baggage handling equipment and

air-conditioners. The ground-service equipment failure leads to prolonged waiting time or passenger discomfort as alternative equipment is allocated for service, but the passenger remains dissatisfied, and such instances require control and avoidance. Besides, the present approach of preventive maintenance and reactive maintenance practices appears deficient in controlling the costly and frequently occurring downtime of service equipment.

The methodology deployed to solve the problem is technical action research conducted in a large international airport in sub-Saharan Africa. In 2019, an equipment condition monitoring scheme was deployed for the five critical pieces of equipment mentioned earlier, and the selection criteria were based on the importance of the equipment due to the high passenger traffic requiring the equipment, the maintenance cost of the equipment and the consequences of equipment failure during operations. The DMAIC improvement framework was designed, installed, and regularly managed for outcomes in discussions with the maintenance service team from the delegated department. The cause and effect analysis was deployed to establish the frontline reasons for the equipment failure. Some technical breakdown data were collected from the third party and in-house maintenance team records to permit proper understanding and the establishment of optimised quality service from equipment while lowering the projected cost from the unanticipated breakdown of the ground-service equipment.

By using the DMAIC approach, this study highlights the value of adopting a scientific approach that encourages the transition from the traditional "run-to-failure" and "preventive maintenance" philosophy to a combination of these approaches and the innovative DMAIC approach that guarantees superior quality maintenance through defect checks and corrections from the cause-and-effect analysis. By following the suggested approach, the maintenance effectiveness was enhanced, and the goodwill decay and damage to passengers' perception regarding the airport services were avoided. Thus, the proposed solution tackles the inherent equipment breakdown needs for superior maintenance quality enhancement. With the solution, the highest quality of service from the ground-service equipment is guaranteed for the crucial equipment studied in an airport that aims at evading the consequences of the ineffectiveness of the current preventive cum reactive maintenance of the ground-service equipment.

The development of a maintenance process enhancement scheme, using the DMAIC approach, for the critical airport ground-service equipment, to detect service defects and eliminate them, is the novel contribution of this paper. More so, the cause-and-effect analysis is deployed to assist the service team in understanding the various causes that stimulate the effects. It links the causes to the effects through pictorial association and pinpoints aspects of maintenance service for enhancement in the airport, regarding the five critical pieces of equipment selected for analysis in this work. Besides, the review of literature conducted discloses the scope for the present work to include the following:

1. Field studies involving activities at the airport in a sub-Saharan African location.
2. Performance analysis of the airport ground-service equipment using a cause and effect diagram and DMAIC approach.
3. The critical ground-service equipment studied includes the elevator, escalator, travelator, baggage handling equipment and air-conditioners.
4. Study to include the process probable capability index as well as the process performance capability index.
5. The use of real-life data for analysis from the perspective of a sub-Saharan African case.
6. To develop ratios for the process probable capability/process performance capability indices.

The rest of the paper includes four sections. Section 2 is the literature review, Section 3 is the methodology, while Section 4 is the results and discussion. Section 5 is the concluding aspect of the research.

1.1 Literature Review

The literature review is approached by first discussing the previous applications of the DMAIC approach to reveal the gap (Section 2.1). Next, the problems commonly discovered in routine inspections regarding the studied ground-service mechanical equipment are discussed (Section 2.2). These pieces of equipment are the package air-conditioner, escalator, elevator, travelator and baggage handling equipment. The problems identified regarding the elevator are first discussed and

subsequently elaborated on each of the other equipment in turn. The third sub-section (Section 2.3) discusses the adverse failure events of equipment. These previous reviews reveal the necessity of briefly reviewing accidents and near misses due to these pieces of mechanical equipment. Therefore, the next part (Section 2.4) argues from the available literature on accidents and near misses of the mentioned ground-service mechanical equipment. The concluding part (Section 2.5) summarises the gaps within the service mechanical equipment literature and directs the goal of this article.

1.1.1 Previous literature on the DMAIC approach

Apart from the systematic literature review conducted by Setiawan and Debora [7], several studies have analysed manufacturing processes by deploying the DMAIC approach. Attempts were made in body painting of vehicle [8], amplifier production [9], aluminium profiles manufacturing [10], home appliance [11], vehicle assembly process [12], brake disc products [13], roof tile products[14], O ring products [15], tyre production [16], chair products [17], magazine production[18], drug tablets production [19], cabinet door, jewellery manufacturing[20], pin insertion process [21], food can [22] and motor standard product[23]. Notwithstanding, the application of DMAIC in ground-service systems appears less pronounced compared to its manufacturing counterparts. In these service applications, no reports have been given on the maintenance of ground-service equipment in airports.

1.1.2 Problems common with ground-service equipment

1.1.2.1 Elevators

Though there is no direct information concerning the average usage of elevators in the studied case, the literature, as supported by Kuusinen et al. [24], provided some details on the arrival process of passengers at a lift. The outcome reveals that passengers arrive in the group for lift services in sizes that depend on the time of the day (i.e. morning, afternoon and night) and the floor usage. Given the volume of passengers that utilise escalators in the airport daily, there is a high potential for mechanical failures within the airport escalators. Although a high failure potential of the escalator exists, the rate of failures and the activities causing the failures have not been reported for the airport. Siti et al. [25] presented a list of common defects

associated with the elevator in their Figure 3. These problems, with modifications, are adopted in the current article.

1.1.2.2 Escalator

Experience in practice reveals some common challenges faced while maintaining elevators, some of these may include the opening and closing of doors at an inappropriate time, the collapse of the escalator, design flaws, lambs and/or clothing being trapped between moving parts of the escalator and overloading. Jampha et al. [26] analysed maintenance problems in escalators by focusing on three cases in Malaysia. The principal problems relate to the set of motors and brakes. So and Li [27] analysed the performance of escalators regarding energy consumption. By drawing instances from Hong Kong, the authors analysed the energy efficiency control code installed by Hong Kong and discussed the diverse electrical parameters, which include total harmonic distortion and total power factor. Algin et al.[28] studied the escalator-associated injuries on the metro line in Saudi Arabia. It was revealed that the most common means of injury was a fall (97.6%). This resulted in head and extremity injuries of 42% and 33%, respectively. The key type of escalator-associated injuries was related to soft tissues (41.3%), next were laceration, closed lead injuries, fractures and serious injuries, which accounted for 20.7%, 18.5%, 15.2% and 4.4%, respectively. A new protection measure against escalator-associated injuries was advocated for.

1.1.3 Adverse failure events of equipment

The adverse failure activities are definite failures of the ground-service equipment at different levels of failure. For elevators, Siti et al. [25] identified six actual failure instances of elevators. These are norm traction sheave, breakage of suspension ropes, stretch marks on safety gears, elevator and landing door misalignment, missing ropes fibre core and severely corroded suspension ropes.

1.1.4 Near misses and accidents involving ground-service mechanical equipment

Passenger safety experts recommend that accounting for and studying near misses and accidents are important aspects of elevator management and control [29]. Although Khaji and Ghodsi [29] argued that elevator-associated accidents are rare,

when they occur, the injuries sustained from them may be significant. They reported instances regarding elevator-associated accidents that spanned from 1999 to 2003 in Tehran, Iran. It was reported that a stable growth of accident cases occurred during the study period. Specifically, a positive rising movement for severe injuries and mortality arising from the accidents was reported. It was concluded that organisations should check the settings, maintain and repair their elevators as essential.

1.1.5 Gaps in the literature

It is evident from the literature review that there is limited literature on how the maintenance effectiveness of the selected service mechanical equipment could be improved. Consequently, observational data regarding the present state of the maintenance effectiveness of the selected service mechanical equipment in the airport are required for the advancement of the aimed maintenance quality enhancement events in the airport setting. Although some studies, including Kuusinen et al. [24] and Siti et al [25] showed some concern and suggested information on the arrival process of passengers and common defects associated with the elevator in the order of the mentioned authors, both suggestions are limited to the elevators alone. Apart, they have not sketched the broad tasks to accomplish the maintenance ineffectiveness correction for each of the selected service mechanical equipment. Consequently, studies have so far failed to establish the details behind the maintenance effectiveness of the service equipment, including the causes and effects, its business impacts (monetary implications of equipment breakdown and economic savings per equipment per month). Thus, research has not suggested the framework for maintenance policymakers and maintenance managers in airports to employ.

As suggested by experts, accounting for and analysing problems common with service equipment in airports can offer an understanding into equipment failures and related problems, comprising of accidents involving service mechanical equipment. Besides, there is a lack of use of mechanical equipment maintenance process control methods such as the DMAIC (Define, measure, analyse, improve and control), in the maintenance performance analysis perspective of the service equipment in airports. Consequently, research is needed to examine the service mechanical equipment maintenance efficiency within the airport and to establish the degree of process

efficiency, equipment turnover of serviceability, economic savings and monetary implications. The maintenance plan, including checking the conformance of maintenance activities to maintenance standards, is a critical process within any airport and contributes greatly to passengers' comfort and airport's goodwill when related to the maintenance of service equipment. As the airport service mechanical equipment has been largely ignored compared with other maintainable equipment, such as manufacturing equipment, and an understanding of the maintenance effectiveness has been downplayed, the researcher aimed to bridge this gap. This research aims to offer an exhaustive understanding of the service mechanical equipment by using the DMAIC approach. The engagement with the DMAIC method will examine how the current equipment deficiencies are tackled and the probable ways to enhance the control of these deficiencies.

2 Material and Methods

2.1 The indicators of capability

The various indicator of capability by Sharma and Sharma [30] will be used in this work. They are numbered as Equations (1) to (4):

$$C_P = \frac{USL - LSL}{6\sigma} \tag{1}$$

$$C_{PKU} = \frac{USL - \mu}{3\sigma} \tag{2}$$

$$C_{PKL} = \frac{\mu - LSL}{3\sigma} \tag{3}$$

$$C_{PK} = \min\left\{\frac{USL - \mu}{3\sigma}, \frac{\mu - LSL}{3\sigma}\right\} \tag{4}$$

where

USL is the upper specification limit, and LSL is the lower specification limit

σ is the standard deviation, and μ is the process mean

C_P signifies the development of the latent capability indicator

C_{PK} signifies the development implementation capability indicator.

Notice that C_P presents a suggestion of distribution of the mechanical equipment

components within the precise acceptance region throughout the maintenance procedure. Also, C_{PK} symbolises the concentration of the maintenance procedure regarding the mean of the precise component acceptance region of the equipment. It also provides an impression or indication of whether the maintenance procedure is functioning at the centre of the acceptance region or closer to the upper or lower acceptance boundaries.

Standard deviation - Standard deviation reveals how the measurements concerning the maintenance process, for a group outstretch from the expected value. The maintenance parameters are said to have a low standard deviation, with the majority of the numbers near the expected value. Conversely, when the majority of the numbers outstretches, they are known as having high standard deviation. Literature reveals that with the knowledge of two numbers, it is possible to describe the shape of the curve for the data. The term standard normal distribution describes a normal distribution that possesses a mean value of 0 together with a standard deviation of 1.

Latent capability indicator, C_p - By adopting the idea of latent, we describe a situation in which the variable cannot be evaluated straightforwardly. A latent value represents an obtainable value, although so far not found. It describes the disparity between certainty and what is likely. As an alternative to the simple linear approach, investigators have, in the recent past, acknowledged the latent character of the maintenance process parametric phenomenon. In this work, the latent idea has been applied to capture maintenance performances. The role of latent performance measures has been made in an airport service equipment context regarding maintenance inefficiency corrections. To illustrate the idea of a latent variable, the global health of the service equipment is regarded as a latent variable. Unfortunately, there is no single evaluation of "health" which can be assessed. This is an abstract idea. However, the performance of the service equipment may be measured using some metrics such as the MTTR, MTBF, and frequency of failures. These individual evaluations may be deployed by maintenance experts to evaluate the health of the service equipment since experience based on observing these values in different healthy and unhealthy machines would count. In this instance, health is regarded as a latent variable. As there

is no direct evaluation for the health of the service equipment, other evaluations that play a role in some manner to evaluating the health of service equipment are used.

2.2 Definition of terms

Definition Stage

The define phase of DMAIC project is targeted at explaining the rationale and extent of the maintenance improvement project. At this stage, the fundamental perceptions and expectations of the passengers regarding the quality of service are established. An important feature of this phase is to establish reasonable estimates for timelines and project costs. The advantage of these definitions is to position the passengers of the airport and the maintenance team at the same level concerning what to be done and how the evolution and achievement of the project could be assessed. Often in many organizations, substantial work is conducted before installing a DMAIC project, which prepares the entire employee team to receive the project as everyone will be involved in these preparations. In summary, the DMAIC involves identifying the maintenance problem to be tackled. This also involves recognising the need for regular and periodic maintenance of equipment, understanding the requirements for preventive task planning and the impact of equipment breakdown on the overall performance and deliveries of operational equipment. In this paper, some of the concerns to validate the need to implement a DMAIC project in the service equipment aspect of the airport are as follows:

- Is the maintenance data available? There are two aspects of maintenance engaged in the plant. The first concerns the tasks handled by the in-house personnel, while the second are those regarding jobs contracted out to third parties. The later is where the expertise in-house is not sufficient to maintain the service equipment or it may be too expensive to deploy in-house staff to do. An example is the maintenance of the escalators, which is handled by third-party contractors. In this case, interactions with them are made to assess how easy it is to obtain data.
- The second issue is the top management commitment to support the improvement project. At this definition stage, an assessment and solicitation of the top management were sought.

- A third issue was to assess whether the scope of the defined work is reasonable bearing in mind that scope outside the capability of the team may be unattainable.
- A fourth issue is to determine if the DMAIC process to be installed has direct linkage with a principal outcome, for example, the passenger's satisfaction.

Measurement Stage

The measuring stage of DMAIC elaborates on the numerical and data analysis aspects of the process, involving the scheme's validation and the collection of the root causes of the maintenance problem. In the DMAIC measurement phase, data collection takes an important position. Before embarking on the collection of data, information on when, who and where the service data will be collected and the analysis to perform on these data were considered. In the airport studied, there is a service agreement with a contractor company to service the elevators, travellators and escalators of the airport. However, their services are complemented with the monitoring of the in-house personal. The same applies to air conditioners and the baggage handling equipment in the plant. For the baggage handling equipment, the maintenance activities logbook was consulted. It gives information on the baggage handling equipment concerning the downtime span. In a data item, for instance, the downtime was recorded to start with the data and the actual time the crew was notified of the failure of the equipment.

What follows is the nature of the fault(s). For the data item considered, "Broken 2No. carriers on conveyor line" was recorded, which means that two units of carriers broke down in the conveyor labelled as "9". This is followed by the uptime, where the data of repairs and the time the baggage equipment was restored is recorded. Next is the item interval, which shows the range of time from downtime to uptime. In this instance, 20 mins were recorded as the downtime to uptime interval. The last item of information is "remarks". For the data item, a typical remark is "Broken carriers replaced with good ones from conveyor line 11". In this instance, the downtime to uptime interval is the process and imprint variable, which influences the cuticle-to-quality (CTQ) as well as critical-to-process (CTP) parameters but when this interval is considered for the whole year, an average may be obtained, which is defined as interval time average, and this influences the critical-to-satisfaction parameters. The interval

time and the interval time average are collected in tandem to establish the association between these two issues and apply the analyse stage of the DMAIC process. The interval time average is essential to demonstrate a baseline for the performance of the service equipment regarding breakdown, which should be enhanced.

In the preceding paragraph, the CTQ is mentioned but its meaning is that it defines the interval quality parameters that associate with the need of the customer as well as his/her wants. In the literature, two variants of CTQs are possible. These are the KPIV and KPOV, respectively, indicating the key process input variable as well as the key process output variable. The CTP and CTS are mapped to the KPIV and KPOV, respectively.

Analysis Stage

As the name suggests, the analysis phase of the DMAIC process, which proceeds with the output of the "measure" phase to analyse the data collected, attempts to search for the answer to the "why" question. The present researchers attempt to establish the root cause of the performance concern through the application of statistical tools and procedures, validate it and ascertain that the enhancement drive focuses on the foundation instead of the symptoms. The Literature warns that problem-solving teams globally frequently instigate improvement projects while assuming that the causes of the process concerns are known. However, the literature reports that such preconceived ideas often lead to solutions which fail to settle the maintenance problem. Here, the team proffers solution ahead of confirming the exact root causes. The weakness of this approach is the huge wastage of time involved and resources consumed, as more variations are created and new problems emerge. The standard practice would be to examine the maintenance process as well as the supporting data to obtain evidence of the probable root causes of the maintenance problem.

To proceed, hypotheses may be created regarding why the problems occur and then detail explanations to support or dispose of the formulated hypotheses. The word verification used earlier in this discussion involves observing the process, analysing the data and testing the potential causes, thereby obtaining a clear understanding of the sources of the maintenance problems before examining the solutions. Furthermore, a

thorough approach to the "analyse" phase digs into the data to observe patterns that aid to establish the root cause and the issues to tackle to correct the problem. The literature shows the procedure to implement the analysis phase of the DMAIC process commences with the establishment of the datasets to analyse. The important question to answer concerns what variables of the process that produces the defects. Associations between these variables are sought. On a wide scope, if the downtime rate for the airport equipment is sought, correlations between inputs such as equipment regulation, spare parts 'quality, equipment operators, and the cooling capacity for the package air conditioner, for instance. This step leads the researcher in carrying out different approaches of statistical analysis in an attempt to compute the degree of correlation between the variables. Notice that this action will assist the researcher to evaluate how likely that the variable is responsible for the problem.

The degree of analysis is aided by using the fishbone diagrams, hypotheses testing, root cause analysis and linear regression. The last procedure of analyse phase is to list the causes. In establishing the variables that possess a superior degree of correlation with the problem, the researcher creates a list of "causes" of variations in the maintenance process, which are supported with practical data.

Improvement Stage

This is the fourth of the fifth stages and the most creative aspect in the DMAIC method, where stakeholders of the maintenance process are asked to propose suggestions for the solution to the problem. It has an experimental side also like the suggestions by the stakeholders are examined using a pilot study before execution by the continuous improvement team, to solve the problem. At this phase, the team advances the solution, leads the process modifications, applies their suggestions and obtains data to verify that they create a quantifiable change. The improve phase needs insight into the KPIVs, which is basic for the effect. At this stage, the association of the principal variables with the project "Y" is established, while the modification suggestions are guided. It is acknowledged that without implementing the ideas, all the work done at the earlier stages would be fruitless. The key tools used for the improve stage include the failure mode and effect analysis, hypothesis testing, fishbone diagram

and 5 whys. There are three principal steps associated with the improve phase of the DMAIC process.

First, the idea-generating workers are invited again into the discussion room. Here, the operator or the staffs involved in everyday activities is central to this discussion and brainstorming process. The brainstorming exercise is commenced for the probable result. A good approach is to recast the established problem at the Define haze, open up the root causes to the problem established at the Measure and Analyse phase. Then let them propose the solution. For progress, it is essential to set a deadline for the solution. It means that the operators are permitted to leave the discussion room and think solely while they are carrying out their jobs or during their relaxation periods. The ideas are then collated there.

Second, based on the team leader's knowledge and understanding, the ideas are weighed up, and those acknowledged as superior are further pursued. To pursue the ideas means piloting them, a task that is crucial to verify the idea. Experts acknowledge that a screamingly sound idea in the discussion room may not be wonderful in practice on the factory floor. This brings out the benefits of piloting the ideas while including monetary savings, avoidance of frustration and time savings. As the idea is being tested on a pilot scale, the failed ones are noted, thereby preventing their implementation on a wide scale before they are known. Third, the task is to select an acceptable idea. After considering the improve phase of the DMAIC process, several suggestions that have been pilot-tested may have been ruled out while picking the best suggestion to implement on an extensive scale.

Control Stage

This is the last of five phases in the DMAIC method aimed at ascertaining that actions to execute from the ideas generated during the improve phase are properly executed and regulated. Numerous control tools assist to regulate the variables within the specified limits. These include control charts, and failure modes and effect analysis. At the control phase, the team leader ought to have established the process requiring improvement, obtained the essential data, analyse it for the establishment of the cause and effects of the problem and must have established a practical suggestion from the

pilot testing. At this stage, the final implementation of the solution is made. However, experts suggest that this phase is very uninteresting due to the multiple tasks and cycles of repeating the same set of procedures to ascertain that the desired systems are properly installed.

It is worthwhile to note that such changes may be organisation-wide in their implementation and all staff is expected to comply with the procedure. Four important steps are associated with the control phase of the DMAIC method regarding the maintenance process. These are the measurement planning, tools for the control and success level evaluation, the action plan and the time frame. For the measurement planning aspect, some interesting questions to guide the team are: How shall we evaluate the new process performance? How do we ascertain that the defect rate established is enhancing? Could the team state the reliability of the data? Is it necessary to develop data collection approaches in the process? Will it require staff training, or may it have an automatic implementation? The control chart is the widely adopted tool for the second step. They assist to know the stability as well as process control, establish variant and their causes. The next step is the action plan, which is to tackle the deviations. The last step is the time frame that acknowledges that the control phase is time-bound.

2.3 Identifying KQCs

The satisfactory procedure of maintenance through the identification of key performance components of any equipment was considered in support of the related account of maintenance activities. Consequently, the objective of this analysis is to enhance the operational effectiveness of mechanical equipment by reducing any appearance of fault or breakdown in the course of operation so that damages do not render the equipment inoperative and deliveries unachievable.

2.4 Cause and Effect Diagram

The cause-and-effect diagram analyses the reason why something happened or might happen by arranging probable cause into smaller groups.

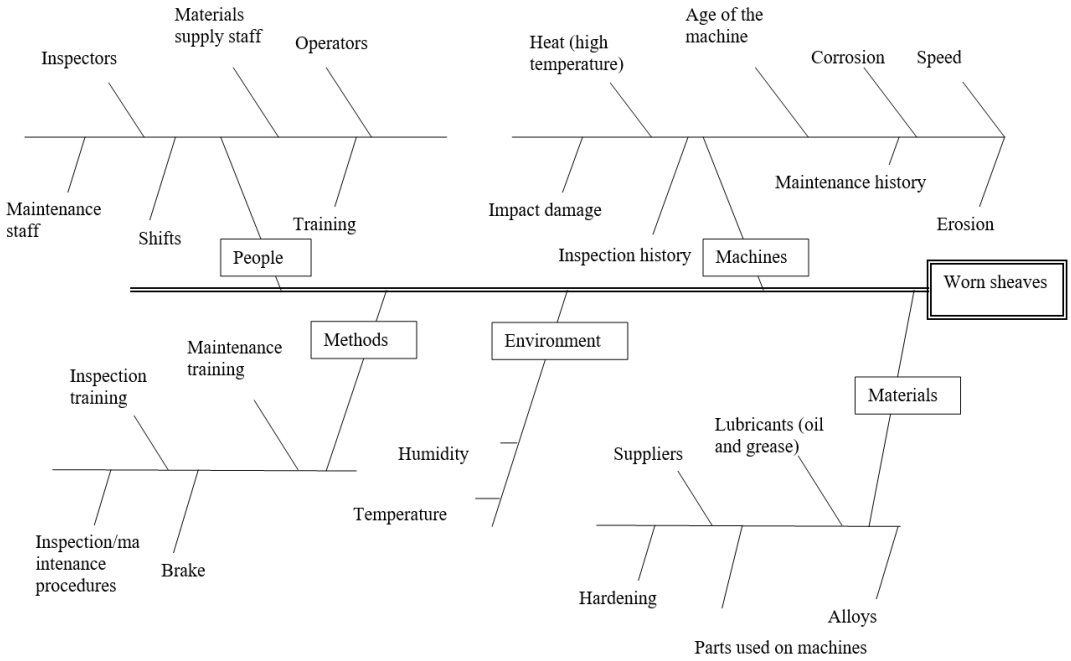

Figure 1. Cause-and-effect diagram illustrating the variables effecting Worn sheaves of elevators

Also, it is a picture or an image that means for organising the possible roots of challenge to recognize its main basis. Fig. 1 provides an illustration of the cause-and-effect diagram for the variables effecting worn sheaves of elevators. This is an example and other aspects of the study could be analysed through the cause-and-effect diagram.

2.5 Project Charter of the DMAIC Project Relating to the Maintenance of Mechanical Equipment in the Airport

Objectives

1. To maintain equipment in tough operating conditions.
2. To maintain equipment in acceptable conditions.
3. To ensure maximum availability of plant and equipment at a reasonable cost.
4. To provide service that will avert breakdowns at all times and at any cost.
5. To extend plant life to the last limit.
6. To maintain plant and equipment with maximum economy and to replace at predetermined periods.
7. To ensure high-quality performance.

8. To ensure safe and efficient operation at all times.
9. To maximize output over the next five years.
10. To maintain a reasonable good appearance of plant.
11. To maintain a plant spotlessly clean at all times.
12. To minimize maintenance expenditure and maximize profit.

3 Results and Discussions

3.1 The case to study airport terminal equipment

Maintenance at the airport terminal involves three broad classes of maintenance. In the first class, the maintenance crew is responsible for controlling and monitoring terminal mechanical equipment consisting of refrigeration and air conditioning systems, conveyors, elevators, escalators, travolators, extractors and aviobridge. The aviobridge is a set of equipment, such as the passenger tunnel and automatic doors. The chiller system is the last group member of the terminal equipment maintained by the engineer in the airport terminal. The second class of equipment within the responsibility of the maintenance engineer to control and monitor is the heavy-duty and light vehicles, which include tractors, slashers, hydraulic platforms, cars, fabrication and welding equipment, as well as forklifts. The last category of equipment under the maintenance engineer at the airport terminal is the power-generating plant. However, the scope of maintenance of all three mentioned categories of equipment is very broad and may not be investigated in research.

Moreover, heavy duty and light vehicles in airports are of immense support to diverse handling and transport activities within the airport. They are extremely supportive in ground support and aircraft maintenance, as well as in passenger transport and baggage handling activities. Although both heavy-duty and light vehicles and mechanical equipment are critical in airports, terminal mechanical equipment is exceedingly more important than heavy-duty and light vehicles since they directly influence operational efficiency and passenger experience. Consider the heating, ventilation and air conditioning (HVAC) system and the baggage handling facility. Without it, while waiting for service, the passenger cannot be comfortable, and the functional environmental service to the passenger will be greatly impacted. For

vehicles, their support is limited to external operations such as aircraft maintenance and cargo servicing. Therefore, given the three broad maintenance work classifications of the maintenance engineer in the airport, including terminal equipment, heavy-duty, light vehicle and power generating plant, the impact of maintenance with fewer resources should be maximized by prioritizing the broad group of equipment to focus on. Interestingly, by considering the value-to-effort obtained by the impact of maintenance activities on passenger service, the chief attention of this work shall be on the terminal equipment problem analysis regarding maintenance and the development of solutions for effective operations. This highlights the focus of the present study on these main aspects of the terminal equipment, elevators, travelators and escalators. The analysis conducted in this study was used in selecting the best methodology and solution in optimizing air post maintenance services.

In this work, mechanical equipment in airports is studied as it guarantees comfortable and outstanding passenger experience and safe operations. The totality of experience by passengers in airports is dictated by how much and the quality of service obtained from the HVAC while waiting for flights, baggage handling at arrival and departure points at the airport, lighting of the airport premises and the power distribution

3.2 Deliverables and Success Metrics

To attain the process probable capability index and process performance capability index i.e. C_P & C_{PK} values for the mechanical equipment maintenance to be more than 1.33, i.e. more than 4 sigma levels.

The C_P and C_{PK} values to be attained incessantly more than 1.33 for over a consistent time of three months.

3.3 Business impact for all the five-equipment considered

In this section the business impact analysis is presented for the various equipment considered, such as elevators, escalator, travelators, baggage handling equipment and package airconditioners. It is coupled with the list of maintenance activities and corresponding CTQ characteristics for the equipment (Tables 1 to 10).

Tables 1, 3, 5, 7 and 9 show the business impact analysis of the equipment studied, namely elevator, escalator, travelator, baggage handling equipment and packaged air conditioners. Table 1 reveals twelve components named A to L. Each of these represents the analysis in a particular month. For instance, all the analyses in column A are for the first month, column B is for the second month and so on and so forth. A key index is the equipment turnover of serviceability per month (01A), which has the highest and lowest values of 15 and 9, respectively. The mode of this value is 9, occurring in nine months. This index shows how fast the elevator is repaired, maintained and made available each month within the airport. With the highest turnover occurring during the ninth month, it implies that the elevator is serviced and quickly returned to the operators for use more efficiently than in any other month. The benefit of this is that it maximally satisfies the passengers. In fact, it is during the ninth month that the passengers are most satisfied with the quality of service given by the elevator. For the total number of breakdowns per hour (02A), the highest is 4, while the lowest, coincidentally, is the modal class, which is 1. The highest value (during the ninth month) gives the worst-case scenario, which triggered much panic among the maintenance members. This index shows the number of breakdowns that occurred for the elevator during twelve hours. This could be due to irregular preventive maintenance services of poorly implemented maintenance activities.

Furthermore, the index time taken for repair 3 of breakdown per month (03A), which shows the mean time to repair (MTTR), has its highest value at the ninth month at five hours per day. It exhibits its lowest values at two hours per day; this is also the modal class for the elevator concerning hours lost due to breakdowns per month (04A). The highest is 120 hours, which occurs at the sixth and twelfth months; however, the lowest is 60 hours, which is made up of five. This index shows the idle time by the workers due to unavailable machine hours. Next is the monetary implication of an hour breakdown of equipment (05A), this has the highest value of N320,000, which occurred in the twelfth month and a lowest value of ₦80,000, which occurred in months ten and eleven, respectively. The next index is the total monetary loss for twenty-two working days (06A), the highest value in this instance is ₦7,040,000, which occurred on the twelfth month, while the lowest is N1,760,000, which has a

model value of four at the second, fifth, tenth and eleventh periods respectively. Next is "By avoiding 99% of breakdowns, the economic savings per month" (07A), which has the highest value of ₦6,969,600 at the twelfth period, and the lowest value is ₦1,742,400 at period ten and eleven, respectively. By following the interpretation given for Table 1, similar patterns of observation are found in Table 3. 5, 7 and 9, respectively. The same can be done to bring the understanding of the Tables into the right perspective.

Tables 2, 4, 6, 8 and 10 show the CTQ characteristics of the various equipment, which are elevators, escalators, baggage handling equipment and package air conditioners, respectively. Five main activities are elaborated in Table 2, while each of these activities is further explained by the expectation of implementing the activities. In Table 4, the activities are 11 in number, mainly checking, greasing and cleaning the sub parts of major components. Table 6 considered 11 different activities, which are also linked to checking and cleaning activities of the major part of the travelator. In Table 8, seven principal activities linked to the major parts are shown. Table 10 summarises five principal maintenance activities for the package air conditioners. Moreover, in Table 1, considering the index 01A, the pattern is repetitions of a group of numbers; however, the trend in the equipment turnover of serviceability per month reveals a situation in which a number increases after every two sets of values 9. The predicted value based on the trend would be 18 for the first month of the next year. For the total number of breakdowns per 12 hours (02A), the trend has an approximate linear equation of $y = 0.0581x + 1.539$, such that the slope, given by the coefficient of x, which is 0.0581, is positive.

Accordingly, the behaviour of the total number of breakdowns per 12 hours is a slightly upward trend; this implies a sustained growth in the value of this index over time, but at a gradual rate and moderate measure. For the index O3A, which is the Time taken to repair broken down equipment per month, the trend could be described as a mode, median and mean of 2, 2 and 2.9, respectively. Given the index 04A, which is the Hour last due to breakdown per month, the trend is roughly 8.21. For the index 05A, which is monetary implication of 9 hours breakdown of equipment, the trend is roughly 6.80 which is a positive value indicating an upward trend in the given period

for 06A, which is total monetary loss per 22 working days, the trend has a slope of 0.748 implying that on the average condition the value in the given series shows an increase of 0.748 with each period. This is an upward trend. For 07A, which is "By avoiding 99% of breakdown, the economic savings per month" has a trend of 0.1466, which is increasing; thus, a subsequent value is slightly higher than the previous. Now that the interpretation for trend has been given for Table 1, the same ideas could be extended to Tables 3, 5, 7 and 9, which might have some interpretations.

Table 1. Business impact for elevator

		A	B	C	D
S/N	**Components of the Project Area**	**Value**	**Value**	**Value**	**Value**
1	01A	9	9	12	9
2	02A	2	1	2	2
3	03A	3 hours per day	2 hours per day	4 hours per day	2 hours per day
4	04A	30 x 3 = 90 hours	30 x 2 = 60 hours	30 x 4 = 120 hours	30 x 2 = 60 hours
5	05A	₦150,000	₦80,000	₦200,000	₦95,000
6	06A	22 x 150,000 = ₦3,300,000	22 x 80,000 = ₦1,760,000	22 x 200,000 = ₦4,440,000	22 x 95,000 = ₦2,090,000
7	07A	0.99 x 3,300,000 = ₦3,267,000	0.99 x 1,760,000 = ₦1,742,400	0.99 x 4,440,000 = ₦4,356,000	0.99 x 2,090,000 = ₦2,069,100
		E	**F**	**G**	**H**
1	01A	9	12	9	9
2	02A	1	3	2	2
3	03A	2 hours per day	4 hours per day	2 hours per day	2 hours per day
4	04A	30 x 2 = 60 hours	30 x 4 = 120 hours	30 x 2 = 60 hours	30 x 2 = 60 hours
5	05A	₦80,000	₦250,000	₦95,000	₦95,000
6	06A	22 x 80,000 = ₦1,760,000	22 x 250,000 = ₦5,550,000	22 x 95,000 = ₦2,090,000	22 x 95,000 = ₦2,090,000
7	07A	0.99 x 1,760,000 = ₦1,742,400	0.99 x 5,550,000 = ₦5,445,000	0.99 x 2,090,000 = ₦2,069,100	0.99 x 2,090,000 = ₦2,069,100
		I	**J**	**K**	**L**
1	01A	15	9	9	9
2	02A	4	1	1	2
3	03A	5 hours per day	2 hours per day	2 hours per day	4 hours per day
4	04A	30 x 5 = 60 hours	30 x 2 = 60 hours	30 x 2 = 60 hours	30 x 4 = 120 hours
5	05A	₦300,000	₦80,000	₦80,000	₦320,000
6	06A	22 x 300,000 = ₦6,600,000	22 x 80,000 = ₦1,760,000	22 x 80,000 = ₦1,760,000	22 x 320,000 = ₦7,040,000

7	07A	0.99 x 6,600,000 = ₦6,534,000	0.99 x 1,760,000 = ₦1,742,400	0.99 x 1,760,000 = ₦1,742,400	0.99 x 7,040,000 = ₦6,969,600

The values projected above are based on the target achievement of 9 Elevators performing effectively per month
Key: 01A - Equipment turnover of serviceability per month, 02A - Total number of breakdowns per 12hours, 03A - Time taken for repair of breakdowns per month, 04A - Hour loss due to breakdowns per month, 05A - Monetary implication of 9 hours breakdown of equipment, 06A - Total monetary loss per 22 working days, 07A - By avoiding 99% of breakdowns, the economical savings per month.

Table 2. List of Maintenance Activities and Corresponding CTQ Characteristics – Elevators

Maintenance Activity No.	Maintenance Activity	CTQ Characteristic Conforming to Maintenance Activity
10	Car inside check	Examining the Elevator Car interior for damage to walls and ceiling, Examining the position indicator lights and replacing any burned-out lights, Running the Elevator up and down and checking the balancing for correctness, acceleration as well as deceleration, making any necessary adjustments, Checking to ensure that the door runs smoothly and does not bang, Checking to ensure that the door controller functions efficiently and initiate necessary repairs
20	Car outside check	Examining the lights and replacing burned-out lights or indicators, Checking door panel as well as clearances, Assessing the firefighters' service.
30	Machine room examination	Ensuring that the machine room contains no material unrelated to the Elevator, Examining components for wear, leaks and unusual vibration, Checking electrical components for overheating or failure, Checking the oil level, Lubricating components as necessary, Performing necessary adjustments and scheduling follow-up repair.
40	Car top check	Checking to ensure that the stop switch operates properly, Eliminating any debris from car top, Checking components like rollers, guide rails, as well as leveling devices, Inspecting cables for wear as well as cable connections, Examining the lift way for indication of vandalism, rodents as well as fire safety.
50	Pit equipment check	Ensuring that stop switch and lights function efficiently, Cleaning the pit and checking for leak indicators, Checking the buffers for corrosion signs, secure attachment as well as alignment, Checking cable/rope for snags, wear and punches, Ensuring that the sump pump is clean and functioning effectively.

Table 3. Business impact for escalator

		A	**B**	**C**	**D**
S/N	**Components of the Project Area**	**Value**	**Value**	**Value**	**Value**
1	01A	3	3	3	3
2	02A	2	1	1	1
3	03A	3 hours per day	1½ hours per day	2 hours per day	2 hours per day
4	04A	30 x 3 = 90 hours	30 x 1½ = 45 hours	30 x 2 = 60 hours	30 x 2 = 60 hours
5	05A	₦160,000	₦65,000.00	₦170,000	₦150,000
6	06A	22 x 160,000 = ₦3,520,000	22 x 65,000 = ₦1,430,000	22 x 170,000 = ₦3,740,000	22 x 150,000 = ₦3,300,000

7	07A	0.99 x 3,520,000 = ₦3,484,800	0.99 x 1,430,000 = ₦1,415,700	0.99 x 3,740,000 = ₦3,702,600	0.99 x 3,300,000 = ₦3,267,000
		E	**F**	**G**	**H**
1	01A	3	3	3	3
2	02A	1	1	1	1
3	03A	1½ hours per day	3 hours per day	2 hours per day	2 hours per day
4	04A	30 x 1½ = 45 hours	30 x 3 = 90 hours	30 x 2 = 60 hours	30 x 2 = 60 hours
5	05A	₦65,000.00	₦120,000	₦150,000	₦150,000
6	06A	22 x 65,000 = ₦1,430,000	22 x 120,000 = ₦2,640,000	22 x 150,000 = ₦3,300,000	22 x 150,000 = ₦3,300,000
7	07A	0.99 x 1,430,000 = ₦1,415,700	0.99 x 2,640,000 = ₦2,613,600	0.99 x 3,300,000 = ₦3,267,000	0.99 x 3,300,000 = ₦3,267,000
		I	**J**	**K**	**L**
1	01A	3	3	3	3
2	02A	2	1	1	1
3	03A	4 hours per day	1½ hours per day	1½ hours per day	2½ hours per day
4	04A	30 x 4 = 120 hours	30 x 1½ = 45 hours	30 x 1½ = 45 hours	30 x 2½ = 75 hours
5	05A	₦190,000.00	₦65,000	₦65,000	₦215,000
6	06A	22 x 190,000 = ₦4,180,000	22 x 65,000 = ₦1,430,000	22 x 65,000 = ₦1,430,000	22 x 215,000 = ₦4,730,000
7	07A	0.99 x 4,180,000 = ₦4,138,200	0.99 x 1,430,000 = ₦1,415,700	0.99 x 1,430,000 = ₦1,415,700	0.99 x 4,730,000 = ₦4,682,700

The values projected above are on the basis for target achievement of 3 Escalators performing effectively per month
Key: 01A - Equipment turnover of serviceability per month, 02A - Total number of breakdowns per 12hours, 03A - Time taken for repair of breakdowns per month, 04A - Hour loss due to breakdowns per month, 05A - Monetary implication of 9 hours breakdown of equipment, 06A - Total monetary loss per 22 working days, 07A - By avoiding 99% of breakdowns, the economical savings per month.

Table 4. List of Maintenance Activities and Corresponding CTQ Characteristics – Escalator

Maintenance Activity No.	Maintenance Activity	CTQ Characteristic Conforming to Maintenance Activity
10	Truss	Checking and inspecting for damage.
20	Track	Cleaning of track rails.
30	Drive system	Checking for wear and proper chain slack.
40	Lubricator	Checking for pump.
50	Handrail	Checking of condition and operation.
60	Safety devices	Checking the condition.
70	Braking system	Checking the operation and torque.
80	Steps and wheels	Greasing step wheel shoe.
90	Controller	Checking the operation and condition.
100	Panels	Cleaning and checking of the clearance force.
110	Landing platform	Cleaning and inspecting for damage.

Table 5. Business impact for travelators

		A	B	C	D
S/N	**Components of the Project Area**	**Value**	**Value**	**Value**	**Value**
1	01A	5	5	5	5
2	02A	2	1	2	1
3	03A	4 hours per day	2 hours per day	5 hours per day	1½ hours per day
4	04A	30 x 4 = 120 hours	30 x 2 = 60 hours	30 x 5 = 150 hours	30 x ½ = 45 hours
5	05A	₦185,000	₦75,000	₦200,000	₦130,000
6	06A	22 x 185,000 = ₦4,070,000	22 x 75,000 = ₦1,650,000	22 x 200,000 = ₦4,440,000	22 x 130,000 = ₦2,860,000
7	07A	0.99 x 4,070,000 = ₦4,029,300	0.99 x 1,650,000 = ₦1,633,500	0.99 x 4,440,000 = ₦4,356,000	0.99 x 2,860,000 = ₦2,831,400
		E	**F**	**G**	**H**
1	01A	5	5	5	5
2	02A	1	1	1	1
3	03A	2 hours per day	3 hours per day	1½ hours per day	1½ hours per day
4	04A	30 x 2 = 60 hours	30 x 3 = 90 hours	30 x ½ = 45 hours	30 x ½ = 45 hours
5	05A	₦75,000	₦140,000	₦130,000	₦130,000
6	06A	22 x 75,000 = ₦1,650,000	22 x 140,000 = ₦3,080,000	22 x 130,000 = ₦2,860,000	22 x 130,000 = ₦2,860,000
7	07A	0.99 x 1,650,000 = ₦1,633,500	0.99 x 3,080,000 = ₦3,049,200	0.99 x 2,860,000 = ₦2,831,400	0.99 x 2,860,000 = ₦2,831,400
		I	**J**	**K**	**L**
1	01A	5	5	5	5
2	02A	2	1	1	1
3	03A	6 hours per day	2 hours per day	2 hours per day	2 hours per day
4	04A	30 x 6 = 180 hours	30 x 2 = 60 hours	30 x 2 = 60 hours	30 x 2 = 60 hours
5	05A	₦220,000	₦75,000	₦75,000	₦250,000
6	06A	22 x 220,000 = ₦4,840,000	22 x 75,000 = ₦1,650,000	22 x 75,000 = ₦1,650,000	22 x 250,000 = ₦5,500,000
7	07A	0.99 x 4,840,000 = ₦4,791,600	0.99 x 1,650,000 = ₦1,633,500	0.99 x 1,650,000 = ₦1,633,500	0.99 x 5,500,000 = ₦5,445,000

The values projected above are on the basis for target achievement of 5 Travelators performing effectively per month
Key: 01A - Equipment turnover of serviceability per month, 02A - Total number of breakdowns per 12hours, 03A - Time taken for repair of breakdowns per month, 04A - Hour loss due to breakdowns per month, 05A - Monetary implication of 9 hours breakdown of equipment, 06A - Total monetary loss per 22 working days, 07A - By avoiding 99% of breakdowns, the economical savings per month.

Table 6. List of Maintenance Activities and Corresponding CTQ Characteristics – Travelators

Maintenance Activity No.	Maintenance Activity	CTQ Characteristic Conforming to Maintenance Activity
10	Comb plate	Cleaning the plate and gap.
20	Steps and risers	Checking for damage.
30	Handrail	Cleaning and checking condition.
40	Steps and wheels	Checking the condition and alignment, examining wheels and tightening step nuts.
50	Lubricator	Checking the oil level.
60	Drive system	Checking for abnormal wear and corrosion; checking to ensure that chain is adequately lubricated.
70	Braking system	Checking torque and operation.
80	Tracks	Cleaning the track rails.
90	Safety devices	Checking the condition.
100	Panels	Checking the clearance force and cleaning.
110	System controller	Checking the condition and operation.

Table 7. Business impact for baggage handling equipment

		A	**B**	**C**	**D**
S/N	**Components of the Project Area**	**Value**	**Value**	**Value**	**Value**
1	01A	12	12	12	12
2	02A	3	2	2	1
3	03A	9 hours per day	6 hours per day	6 hours per day	3 hours per day
4	04A	30 x 9 = 270 hours	30 x 6 = 180 hours	30 x 6 = 180 hours	30 x 3 = 90 hours
5	05A	₦250,000	₦120,000	₦300,000	₦195,000
6	06A	22 x 250,000 = ₦5,500,000	22 x 120,000 = ₦2,640,000	22 x 300,000 = ₦6,600,000	22 x 195,000 = ₦4,290,000
7	07A	0.99 x 5,500,000= ₦5,445,000	0.99 x 2,640,000 = ₦2,613,600	0.99 x 6,600,000 = ₦6,534,000	0.99 x 4,290,000 = ₦4,247,100
		E	**F**	**G**	**H**
1	01A	12	12	12	12
2	02A	2	2	1	1
3	03A	6 hours per day	6 hours per day	3 hours per day	3 hours per day
4	04A	30 x 6 = 180 hours	30 x 6 = 180 hours	30 x 3 = 90 hours	30 x 3 = 90 hours
5	05A	₦120,000	₦210,000	₦195,000	₦195,000
6	06A	22 x 120,000 = ₦2,640,000	22 x 210,000 = ₦4,620,000	22 x 195,000 = ₦4,290,000	22 x 195,000 = ₦4,290,000
7	07A	0.99 x 2,640,000 = ₦2,613,600	0.99 x 4,620,000 = ₦4,573,800	0.99 x 4,290,000 = ₦4,247,100	0.99 x 4,290,000 = ₦4,247,100
		I	**J**	**K**	**L**
1	01A	12	12	12	12
2	02A	3	2	2	2
3	03A	9 hours per day	6 hours per day	6 hours per day	6 hours per day
4	04A	30 x 9 = 270 hours	30 x 6 = 180 hours	30 x 6 = 180 hours	30 x 6 = 180 hours
5	05A	₦330,000	₦120,000	₦120,000	₦375,000

6	06A	22 x 330,000 = ₦7,260,000	22 x 120,000 = ₦2,640,000	22 x 120,000 = ₦2,640,000	22 x 375,000 = ₦8,250,000
7	07A	0.99 x 7,260,000 = ₦7,187,400	0.99 x 2,640,000 = ₦2,613,600	0.99 x 2,640,000 = ₦2,613,600	0.99 x 8,250,000 = ₦8,167,500.00

The values projected above are based on the target achievement of 12 Baggage Handling Equipment performing effectively per month

Key: 01A - Equipment turnover of serviceability per month, 02A - Total number of breakdowns per 12hours, 03A - Time taken for repair of breakdowns per month, 04A - Hour loss due to breakdowns per month, 05A - Monetary implication of 9 hours breakdown of equipment, 06A - Total monetary loss per 22 working days, 07A - By avoiding 99% of breakdowns, the economical savings per month.

Table 8. List of Maintenance Activities and Corresponding CTQ Characteristics - baggage handling equipment

Maintenance Activity No.	Maintenance Activity	CTQ Characteristic Conforming to Maintenance Activity
10	Motor	Checking the noise, Checking the temperature, Checking mounting bolts.
20	Drive chain	Checking tension, Checking for wear, Lubrication.
30	Belt	Checking tracking, Checking tension, Checking lacing.
40	Bearings – pulleys and rollers	Checking noise, Checking mounting bolts.
50	Sprockets	Checking for wear, Checking set screws and keys.
60	V-belts and O-rings	Checking tension, Checking for wear, Checking alignment.
70	Structural	Checking all bolts for tightness.

Table 9. Business impact for package airconditioners

		A	**B**	**C**	**D**
S/N	**Components of the Project Area**	**Value**	**Value**	**Value**	**Value**
1	01A	180	180	270	180
2	02A	5	2	1	5
3	03A	7 hours per day	3 hours per day	1½ hours per day	5 hours per day
4	04A	30 x 7 = 210 hours	30 x 3 = 90 hours	30 x 1½ = 45 hours	30 x 5 = 150 hours
5	05A	₦100,000	₦40,000	₦45,000	₦75,000
6	06A	22 x 100,000 = ₦2,200,000	22 x 40,000 = ₦880,000	22 x 45,000 = ₦990,000	22 x 75,000 = ₦1,650,000
7	07A	0.99 x 2,200,000= ₦2,178,000	0.99 x 880,000 = ₦871,200	0.99 x 990,000= ₦980,100	0.99 x 1,650,000 = ₦1,633,500
		E	**F**	**G**	**H**
1	01A	180	190	180	180
2	02A	2	5	5	5
3	03A	3 hours per day	8 hours per day	5 hours per day	5 hours per day
4	04A	30 x 3 = 90 hours	30 x 8 = 240 hours	30 x 5 = 150 hours	30 x 5 = 150 hours
5	05A	₦40,000.00	₦120,000	₦75,000	₦75,000
6	06A	22 x 40,000 = ₦880,000	22 x 120,000 = ₦2,640,000	22 x 75,000 = ₦1,650,000	22 x 75,000 = ₦1,650,000

7	07A	0.99 x 880,000 = ₦871,200	0.99 x 2,640,000 = ₦2,613,600	0.99 x 1,650,000= ₦1,633,500	0.99 x 1,650,000 = ₦1,633,500
		I	**J**	**K**	**L**
1	01A	270	180	180	180
2	02A	4	2	2	9
3	03A	4 hours per day	3 hours per day	3 hours per day	10 hours per day
4	04A	30 x 4 = 120 hours	30 x 3 = 90 hours	30 x 3 = 90 hours	30 x 10 = 300 hours
5	05A	₦60,000	₦40,000	₦40,000	₦180,000.00
6	06A	22 x 60,000 = ₦1,320,000	22 x 40,000 = ₦880,000	22 x 40,000 = ₦880,000	22 x 180,000 = ₦3,960,000
7	07A	0.99 x 1,320,000 = ₦1,306,800	0.99 x 880,000= ₦871,200	0.99 x 880,000 = ₦871,200	0.99 x 3,960,000 = ₦3,920,000

The values projected above are on the basis for target achievement of 180 Package Airconditioners performing effectively per month

Key: 01A - Equipment turnover of serviceability per month, 02A - Total number of breakdowns per 12hours, 03A - Time taken for repair of breakdowns per month, 04A - Hour loss due to breakdowns per month, 05A - Monetary implication of 9 hours breakdown of equipment, 06A - Total monetary loss per 22 working days, 07A - By avoiding 99% of breakdowns, the economical savings per month.

Table 10. List of Maintenance Activities and Corresponding CTQ Characteristics – package airconditioners

Maintenance Activity No.	Maintenance Activity	CTQ Characteristic Conforming to Maintenance Activity
10	Cleaning activity	Cleaning of cooling coil, Cleaning of condensing coil, Cleaning of blower, Cleaning of air filters.
20	Improving cooling capacity	Tightening all loose ends, Refrigerant top-up.
30	Solving equipment malfunction	Checking and replacing faulty system components.
40	Proper discharge of condensate	All clogged condensate lines are corrected, Condensate lines are cleared of any obstacle or impediment, Condensate flow is channeled to appropriate drainage line or system.
50	Operational noise from airconditioner	All bearings and rotating members are firmly tightened and worn out ones replaced.

3.4 Calculations of C_P and C_{PK}

The present study was conducted to evaluate the quantum of maintenance enhancement that may be achieved according to the idea and application situation of DMAIC (Define, Measure, Analyze, Improve and Control) of the service equipment in a sub-Saharan African airport. The management team had not further improved the performance of the service equipment with the combination of preventive and reactive maintenance before this study, and this was a great concern that triggered brainstorming from the management team on improvement strategies. The results of this study reveal that 80% of the studied service equipment exhibit the Cp/Cpk values above 1.33 (Table 11). Consequently, the maintenance procedure adopted to maintain

the equipment is capable of a large majority of the equipment studied. However, there is scope for improvement for the escalator, whose value of the Cp/Cpk ratio fell below the 1.33 benchmark. This poor performance of this mechanical equipment brings a threat to the system's efficiency. This work is necessary and pertinent for the reduction of maintenance inefficiency for the escalator. The globally accepted level of service concept championed by the joint effort of IATA and ACI suggests the need for investment of efforts to eliminate the inefficiency of the escalator in the airport studied. Thus, with this perspective, the present article has immense potential for future studies regarding decision making on the expansion of the escalator facility. The maintenance management team of the airport should ensure that effective plans to eliminate service equipment defects for the escalator are made in advance before any introduction of new escalator facilities in an expansion activity. This research helps eliminate maintenance defects and inefficiency of the service equipment in the airport. Complete and effective mitigation practices against the breakdown of service, mechanical equipment in the airport are very necessary to reduce the erosion of goodwill for the airport studied.

Table 11. The calculation results of C_P and C_{PK} for the mechanical equipment

Formula	Mechanical Equipment				
	Elevator	Escalator	Travelator	Baggage Handling Equipment	Package Airconditioner
USL	6,969,600.00	4,682,700.00	5,445,000.00	8,167,500.00	3,920,000.00
LSL	1,742,400.00	1,415,700.00	1,633,500.00	2,613,600.00	871,200.00
Σ	1,997,497.25	1,165,936.05	1,334,925.46	1,907,705.43	921,424.80
$C_P = \frac{USL - LSL}{6\sigma}$	0.436	0.467	0.476	0.485	0.551
$C_{PKU} = \frac{USL - \mu}{3\sigma}$	0.610	0.527	0.596	0.625	0.834
$C_{PKL} = \frac{\mu - LSL}{3\sigma}$	0.262	0.407	0.356	0.346	0.269
$C_{PK} = \min\{C_{PKU}, C_{PKL}\}$	0.262	0.407	0.356	0.346	0.269

The results of the analysis showed that the procedure/process potential capability index, C_P and procedure performance capability index, C_{PK} for Package Airconditioner are 0.551 and 0.269, respectively. Also, the C_P and C_{PK} values for Elevator are 0.436 and 0.262, respectively, while the corresponding values for Escalator are 0.467 and 0.407, respectively. Similarly, the C_P and C_{PK} values for Travelator are 0.476 and 0.356, respectively, while the C_P and C_{PK} values for Baggage Handling Equipment are 0.485 and 0.346, respectively. The C_P/C_{PK} values for 4 of the 5 mechanical equipment were greater than 1.33 and as a result, the maintenance procedure adopted for maintaining the equipment is declared as a capable procedure. The 4 mechanical equipment are namely: Elevator, Travelator, Baggage Handling Equipment and Package Airconditioner. However, the C_P/C_{PK} for the Escalator is 1.146, and this value is less than 1.33. In effect, the maintenance procedure for maintaining the equipment is not capable. This is an indication that more attention, planning and resources should be put together in order to achieve desired efficiency and reliability.

Although the results discussed above reveal improvements, they could be strengthened if inferential support is given. This, therefore, suggests the possible application of statistical hypothesis testing. The obtained results for all the equipment can be used as a sample from which inferences concerning the entire set of data and the immediate future data can be made. Additionally, the outcome of the statistical hypothesis testing would help the researcher establish the validity of the improvement claim previously discovered from the analysis results. Accordingly, the null and alternative hypotheses are stated as follows to test the statistical hypothesis. Here, he researcher wants to test whether there is a relationship between performance indices and improvement. Based on the researcher's knowledge concerning process improvement, a hypothesis is formulated that

H_o: C_p on average is the same as C_p

Hi: C_p, on average, is not the same as Cpk.

In performing the statistical test using Microsoft Excel software, focusing on T- test paired two-sample for means, data for sample variable 1 (C_p) and sample variable 2 (Cpk).

Here, the data for each of Cp and Cpk in Table 11, for all five equipment categories, were tested under the criteria of hypothesised mean difference as zero, while the level of significance is 0.05. It was found that the test statistic, obtained as 4.2188, exceeds the critical value (t critical at 2.1318). Having observed that the result exists in the area which must be rejected, the null hypothesis, which suggests that Cp and Cpk are the same, should be rejected. This paves the way for the alternative hypothesis, which suggests that Cp and Cpk are different. The implication of this is that improvements (changes) occur over time in the measures. In comparison with the literature [5], the ground service at Don Mueang International Airport in Thailand shares the presence of baggage services with the present study. The authors referred to the baggage services of U.S. Airlines as the third most important aspect of customer complaints after flight problems and customer service. This concurs with the result in Table 11, which places baggage handling equipment as important equipment with a Cpk value of 0.346.

3.5 Limitations and future work

Although the proposal approach in the current study reveals numerous advantages, including the reduction of variations as well as defects (i.e. over-greasing of the door mechanism, hoist ropes and guide rails), it also exhibits some limitations. First, the DMAIC framework implementation focused on technical process efficiency, which may limit the method's ability to generalise across different airports. To overcome the limitation, future research needs to consider the human, managerial and cultural factors influencing maintenance quality. Such details include staff training, motivation and management commitment. Staff training fills the skill gap in maintenance workers and equips them with the essential problem–solving methods, and how to maintain maintenance efficiency, reduce operational cost and improve safety practices in airports. Incorporating motivation into the analysis of the DMAIC framework needs to consider how the maintenance workers are driven towards

properly engaging with the company and how continuous improvement could be developed as a culture. Introducing management commitment into the proposed study framework means that an effective data–motivated strategy to enhance processes should be created, and the development of a strong leadership direction should be initiated. The above-mentioned factors influencing maintenance quality could be introduced into the existing framework using the nominal group technique.

Moreover, a second limitation is that the study did not employ sensor–based monitoring or Internet–of–Things–enabled predictive maintenance systems since the management's reluctance to automate the systems has not encouraged this idea (see Surateno et al. [31] for more ideas on Internet–of–Things systems and their optimization Wang et al. [32]). The absence of such technology limits the scalability and automation potential of the proposed DMAIC framework in modern smart airport contexts. To overcome this limitation, future studies could restructure the DMAIC framework presented in this work to utilise the Internet of Things devices in the monitoring of preventive maintenance data, collecting and examining such data at each phase of the DMAIC methodology.

4 Conclusion

This is the first research that has executed a broadly adopted enhancement technique to solve a long-standing maintenance management challenge, namely maintenance efficiency in the airport situation, and more explicitly, maintenance performance improvement of service mechanical equipment. In this paper, the critical mechanical equipment studied consists of package air-conditioner, an escalator, an elevator, a travelator and baggage handling equipment. Using DMAIC, the investigator *defined* the principal problem as the requirement for preventive maintenance planning and the impact of service equipment breakdowns on the overall performance and deliveries of operational equipment. Discrepancies between the expected and achieved maintenance metrics were *measured*, and cause and effects scenario *analysed*. Suggestions were given to *improve* each service mechanical equipment performance, and metrics on economic savings per month by evading certain proportions of breakdown were developed to *control* the breakdown. As

maintenance efficiency directly influences passenger comfort and organizational goodwill, enhancing the maintenance performance of the mentioned service equipment is crucial. Based on the preceding analysis and results of the performance for the five selected critical service mechanical equipment, we can conclude that the escalator, at present, has poor maintenance performance relative to the other four service mechanical equipment studied in the airport. The DMAIC approach revealed that greater attention should be given to the escalator, given its performance. DMAIC has the potential to lessen passengers' travel mode switching in the airport environment. The DMAIC has been used in many manufacturing activities, including cabinet doors, home appliances and O-ring products. This work expands the scope of using the six sigma technique, particularly the DMAIC approach, in a completely different area and sector of the service industry, the airport setting.

Since six sigma champions enhancement strategies and maintenance process efficiency, this work tends to demonstrate a huge potential to use six sigma within the service equipment domain and for the airport setting globally. The authors applied the DMAIC approach as a first attempt in the published literature on the service equipment within the airport setting. In doing so, the authors produced a DMAIC structure for probable usage to enhance the service equipment maintenance efficiency in an airport setting globally and taxonomy to analyse differences in performance. This study contributes to research regarding the airport segment that has been largely omitted so far. The descriptions offered in this paper give the maintenance manager a superior insight regarding activities on the service equipment selected for the study.

References

[1] G. Andreatta, L. De Giovanni, M. Monaci, “A fast heuristic for airport ground-service equipment,” *Procedia - Social and Behavioral Sciences*, vol. 108, pp. 26–36, 2014.

[2] A. Pabedinskaitė, V. Akstinaitė, “Evaluation of the airport service quality,” *Procedia - Social and Behavioral Sciences*, vol. 110, pp. 398–409, 2014.

[3] M. Schmidt, A. Paul, M. Cole, K.O. Ploetner, "Challenges for ground operations arising from aircraft concepts using alternative energy," *Journal of Air Transport Management*, vol. 56, pp. 107-117, 2016. https://doi.org/10.1016/j.jairtraman.2016.04.023

[4] J. Skorupski, I. Grabarek, A. Kwasiborska, S. Czyżo, "Assessing the suitability of airport ground handling agents," *Journal of Air Transport Management*, vol. 83, 101763, 2020. https://doi.org/10.1016/j.jairtraman.2020.101763

[5] S. Sricharoenpramong, "Service quality improvement of ground staff at Don Mueang International Airport," *Kasetsart Journal of Social Sciences*, vol. 39, no. 1, pp. 15-21, 2018. https://doi.org/10.1016/j.kjss.2017.12.001

[6] I. Alomara, J. Tolujevsa, "Optimization of ground vehicles movement on the aerodrome," *Transportation Research Procedia*, vol. 24, pp. 58–64, 2017. DOI:10.1016/j.trpro.2017.05.068

[7] I. Setiawan, F. Debora, "A systematic literature review of implementation six sigma in manufacturing industries," *Operations Excellence*, vol. 12, no. 3, pp. 318-331, 2020.

[8] D. Caesaron, "Penerapan metode six sigma dengan pendekatan DMAIC pada proses handling painted body BMW X3 (Studi Kasus: PT. Tjahja Sakti Motor)," vol. 9, no. 3, pp. 248–256, 2015.

[9] A.Gupta, P. Sharma, S.C. Malik, N.Agarwal, and P. C. Jha, "Productivity improvement in the chassis preparation stage of the amplifier production process: A DMAIC six sigma methodology," *International Journal of*

Reliability, Quality and Safety Engineering, vol. 23, no. 6, pp. 1–13, 2016. https://doi.org/10.1142/S021853931640012X

[10] L.A. Hadidi, A. Bubshait, and S. Khreishi, "Six sigma for improving aesthetic defects in aluminum profiles facility," *Facilities*, vol. 35, no. 34, pp. 242-267, 2017. https://doi.org/10.1108/F-01-2016-0002

[11] N.G.S. Ahmed, H.S. Abohashima, and M.F. Aly, "Defect reduction using six sigma methodology in-home appliance company: A case study, *Proceedings of the International Conference on Industrial Engineering and Operations Management*, (SEP), 1349–1358, 2018.

[12] P. Bharara, "Implementation of DMAIC methodology for reduction of weighted-defects in a vehicle assembly process," *International Journal of Applied Engineering Research*, vol. 13, no. 6, pp. 73–80, 2018.

[13] Damsiar, Y. Prastyo, and E. Rimawan, "Reduce reject painting process using six sigma method with DMAIC approach and experiments on brake disc products (1 Rc Hub): Case Study in P.T. XYZ, *International Journal of Innovative Science and Research Technology*, vol. 3, no. 10, pp. 327–337, 2018.

[14] S.K. Dewi, and D.M. Ummah, "Perbaikan kualitas pada produk genteng dengan metode six sigma," *Jurnal Teknik Industri*, vol. 14, no. 2, pp. 87–92, 2019. DOI: 10.14710/jati.14.2.87-92

[15] U. Amrina, and H. Firmansyah, "Analysis of defect and quality improvement for O ring product through applying DMAIC methodology, *Jurnal Pasti*, vol. 13, no. 2, 136, 2019. https://doi.org/10.22441/pasti.2019.v13i2.003

[16] A. Trimarjoko, D.S. Saroso, H.H. Purba, S. Hasibuan, C. Jaqin, and S. Aisyah, "Integration of nominal group technique, Shainin system and DMAIC methods to reduce defective products: A case study of tire manufacturing industry in Indonesia," *Management Science Letters*, vol. 9, pp. 2421–2432, 2019.

[17] F. Ahmad, "Six sigma DMAIC sebagai metode pengendalian kualitas produk kursi pada UKM, *JISI: Jurnal Integrasi Sistem Industri*, vol. 6, no. 1, pp. 11–17, 2019.

[18] H. Hernadewita, M. Ismail, M. Nurdin, and L. Kusumah, "Improvement of magazine production quality using the six sigma method: a case study of a P.T.XYZ. *Journal of Applied Research on Industrial Engineering*, vol. 6, no. 1, pp. 71–79, 2019. https://doi.org/10.22105/JARIE.2019.159327.1066

[19] A. Winatie, D.S. Saroso, H.H. Purba and A.P. Wirani, "Reducing of defects in the drug tablets production process with DMAIC to improve quality – study case of pharmaceutical industry," *IOP Conference Series: Materials Science and Engineering*, 852, 2020, 012126

[20] L. Chartmongkoljaroen, R. Sirianukul, and P. Puttibarncharoensri, "Defect reduction by DMAIC method: A case study of a jewelry manufacturer receive orders from resin cleaning and customer approval of. issue stone cards (s.c.) to take a photo and inspect print out make silicone, *Customer Approval of Computer Modeling Quality*. 13(2), 67–84, 2019.

[21] J.P. Costa, I.S. Lopes, and J.P. Brito, "Six sigma application for quality improvement of the pin insertion process," *Procedia Manufacturing*, vol. 38, pp. 1592–1599, 2020. https://doi.org/10.1016/j.promfg.2020.01.126

[22] M.-V. Sánchez-Rebull, R.Ferrer-Rullan, A.-B. Hernández-Lara, A. Niñerola, Six sigma for improving cash flow deficit: a case study in the food can manufacturing industry, *International Journal of Lean Six Sigma,* vol. 11, no. 6, pp. 1105–1126, 2020. https://doi.org/10.1108/IJLSS-12-2018-0137

[23] T. Haryanto, and I., Bachtiar, "Perbaikan kualitas proses pembuatan produk standar motor dengan menggunakan metode six sigma," *Prosiding Teknik Industri*, vol 6, no 1, 50–54, 2020.

[24] J.-M. Kuusinen, J. Sorsa, M.-L. Siikonen and H. Ehtamo, "A study on the arrival process of lift passengers in a multi-storey office building," *Building Services Engineering Research and Technology*, vol. 33, no. 4, pp. 437–449, 2012.

[25] N.A. Siti, A.S. Asmone, and M.Y.L. Chew, "An assessment of maintainability of elevator system to improve facilities management knowledge-base," *IOP Conference Series: Earth and Environmental Science*, vol. 117, 2018, 012025 doi :10.1088/1755-1315/117/1/012025

[26] N.A.I. Janipha, S.N.A.S. Alwee, R.M. Ariff, F. Ismail "Maintenance and safety practices of escalator in commercial buildings," *IOP Conference Series Earth and Environmental Science*, vol. 117, no. 1: 012042, 2018. https://doi.org/10.1088/1755-1315/117/1/012042

[27] A.T.P. So, T.K.L. Li, "Energy performance assessment of lifts and escalators," *Building Services Engineering Research and Technology*, vol. 21, no. 2, 2000. https://doi.org/10.1177/014362440002100205

[28] A. Algin, U. Gulacti, M.O. Erdogan, I. Tayfur, K. Yusufoglu, U. Lok, "Escalator-related injuries in one of the deepest subway stations in Europe,"

Annals of Saudi Medicine, vol. 39, no. 2, pp. 112-117, 2019. https://doi.org/10.5144/0256-4947.2019.112

[29] A. Khaji, S.M. Ghodsi, "Trend of elevator-related accidents in Tehran," *Archives of Bone and Joint Surgery*, vol. 2, no. 2, pp. 117-120, 2014.

[30] R.K. Sharma, R.G. Sharma, "Integrating six sigma culture and TPM framework to improve manufacturing performance in SMEs," *Quality and Reliability Engineering International*, vol. 30, no. 5, pp. 745-765, 2014. https://doi.org/10.1002/qre.1525

[31] S. Surateno, S. Kautsar, R.E. Rachmanita, A.Anwaludin, M. Adhiyatma, R.T. Hertawamati, B.Hariono, F.E. Purnomo, S.T. Sarena, "Smart control and monitoring system for closed poultry house based on IoT, *International Journal of Applied Sciences and Smart Technologies*, vol. 6, no. 1, pp. 25-40, 2024. https://doi.org/10.24071/ijasst.v6i1.7079

[32] F. Wang, M. Zhou, Y. Xing, H.-W. Wang, Y. Peng, and Z. Chen, "A deep reinforcement learning framework for multi-fleet scheduling and optimization of hybrid ground support equipment vehicles in airport operations," Applied Sciences, vol.15, no. 17, 2025, Article 9777, https://doi.org/10.3390/app15179777

This page intentionally left

IJASST
International Journal of
Applied Sciences and Smart Technologies
p-ISSN 2655-8564, e-ISSN 2685-943, pp. 119-152, 2026

Volume 08
Issue 01

IoT Based Nozzle Actuation System Design for Automated Fish Feed Distribution

Sentot Novianto[1*], Larasati Rizky Putri[1], Amrullah Gilang Ibrahim [1], Tono Sukarnoto[1], Faisal Adinegoro[1], Supriyadi[1], Nanang Ruhiyat[2]

[1] *Department of Mechanical Engineering, Faculty of Industrial Technology, Universitas Trisakti, Grogol West Jakarta, 11440, Indonesia*
[2] *Department of Mechanical Engineering, Faculty of Technology, Universitas Mercu Buana, Joglo West Jakarta, 11650, Indonesia*
[*]*Corresponding Author: sentot.novianto@trisakti.ac.id*

(Received 08-09-2025; Revised 30-03-2026; Accepted 09-04-2026)

Abstract

This study presents the design and development of an IoT-based nozzle actuator system intended to improve the accuracy and efficiency of automatic fish-feed distribution. The system was designed using an ESP32 microcontroller as the central controller, a servo motor as the nozzle-direction actuator, and the Blynk application as the remote monitoring and control interface. This configuration enables users to adjust the nozzle's direction and feed-dispersion intensity through both manual control and scheduled timer modes. A series of experiments was conducted to evaluate mechanical performance, IoT connectivity stability, response time, and cross-device application compatibility. The experimental results indicate that the proposed system improves feed-distribution efficiency by 32.6% compared to conventional manual methods. Feed waste was reduced by 28.4% due to more uniform distribution and minimized overfeeding. The average command-to-actuator response time was measured at 0.82 seconds, demonstrating stable real-time performance. Application testing across five smartphone devices (Redmi 12, Huawei P30, Redmi Note 9, Samsung M23, and Little M3) achieved a 100% success rate for login, timer functions, and manual ON commands, confirming the reliability of the IoT control interface across multiple platforms. Compared with traditional automatic feeders, the developed prototype offers more precise nozzle orientation, flexible remote operation, and an adaptive feed-dispersion pattern. The integration of actuation mechanisms with IoT-based control provides a smarter and more efficient automation solution suitable for small- to medium-scale aquaculture systems. Overall, the findings demonstrate that the proposed design delivers superior distribution performance and operational flexibility, representing a meaningful advancement over existing feeding technologies.

Keywords: IoT, Nozzle, Vdi 2221

1 Introduction

Fish farming is one sector that is experiencing rapid development in the aquaculture industry throughout the world. The need for more efficient and environmentally friendly fisheries production encourages industry players to adopt modern technology. One of the critical aspects in developing fish farming is feeding, which directly affects fish growth, feed conversion efficiency and operational costs [1]. Data shows that feeding contributes up to 50-60% of total production costs in aquaculture. Excessive or uneven feeding not only causes wastage of feed, but also increases the risk of water pollution due to the accumulation of food residue that is not eaten by the fish, which can affect the quality of pond water. Technological innovation in fish feeding continues to develop, with automated approaches becoming increasingly popular. Feeding automation using mechanical and electronic devices provides a solution to increase efficiency and reduce human error. The use of mechanical drives such as nozzle to distribute feed evenly and on a schedule is one effective method to ensure that the entire pond area gets feed according to pre-arranged needs [2]. However, operating these automated tools still requires accurate control and easy access. In the digital era, technology Internet of Things (IoT) has opened up great opportunities for the application of smarter and more efficient automation in various sectors, including aquaculture. IoT enables integration between physical devices and the internet, where sensors and actuators can work in a coordinated manner and be controlled remotely via applications connected to mobile devices or computers [3]. In the context of aquaculture, the application of IoT not only facilitates monitoring of pond environmental conditions such as water quality, temperature and dissolved oxygen, but also enables automatic control of feeding.

This research focuses on the design of the drive system nozzle combined with an IoT application to control an automatic fish feed spreader. Movers nozzle functions as a mechanical component that distributes feed to various areas of the pond evenly and efficiently. Meanwhile, the IoT application allows fish farmers to monitor and control feed spreaders remotely, including regulating feeding times and the amount of feed distributed. By utilizing IoT connected sensors, this system will be able to adapt to pond environmental conditions, such as changes in water temperature or fish activity, to

optimize feeding according to needs. Use of actuator nozzle The fish food spreader is expected to increase the efficiency of feed distribution by minimizing unreachable areas. Meanwhile, the IoT application is designed to provide control features (monitoring) which is easy and flexible, where users can make remote settings and receive notifications regarding feeding conditions and equipment status. A number of previous studies have shown that IoT-based automation in aquaculture can reduce feed waste by up to 30% and increase fish growth rates. Apart from that, this system can also help reduce environmental impacts through more precise control, so that there is no excess feed which can pollute the water [4].

A number of previous studies have demonstrated the effectiveness of automation in fish feeding. For example, research [5] studied how to apply IoT in aquaculture systems to increase feed efficiency and fish growth through smart sensors. Meanwhile, it shows that IoT-based automation can also help in reducing waste and optimizing water conditions in cultivation ponds. Furthermore [6], conducted similar research which emphasized the importance of proper mechanical design in feed distribution to ensure that all areas of the pond are covered evenly. Several advanced studies have employed pneumatic conveying mechanisms and CFD/DEM simulations to design more homogeneous feed dispersion devices; these approaches have been shown to be effective at certain scales but introduce additional system complexity and cost (E.g., pumps, compressors, and fluid particle modeling requirements). Adaptive frameworks such as fuzzy logic and emerging AI-based controllers have also been proposed to determine feed quantities based on environmental parameters and fish behavior, thereby further reducing waste. In contrast, the proposed dual-axis actuation integrated with an IoT platform is not merely a feed-release mechanism. The nozzle can be dynamically oriented in both azimuth and elevation, allowing spatially controlled distribution patterns that respond to real pond conditions and reduce feed concentration points. This design combines the advantages of low-cost remote IoT control with spatial distribution capabilities that are typically achieved only in more complex pneumatic systems, thus bridging a notable gap between the two approaches [7].

The real time responsiveness and high directional accuracy achieved through integration with the ESP32 and the Blynk application result in low latency, enabling rapid

adjustments of the nozzle direction to match feed bursts or fish movement. This capability enhances feeding effectiveness, particularly when fish aggregate in specific areas. Compared with pneumatic or large-scale industrial systems, this approach retains inexpensive components (Servo/DC motors, the nozzle body, and polyurethane/PVC tubing) while increasing functional value through intelligent control software. The nozzle design provides directional actuation as an additional degree of freedom for future AI or fuzzy-logic algorithms, shifting control from merely how much feed is dispensed to also where it is distributed. This constitutes a new control dimension that improves feed utilization efficiency. International literature demonstrates significant progress in IoT based control, pneumatic feed distribution, and adaptive feeding strategies; however, few studies have fully integrated low cost IoT platforms with a dual-axis nozzle capable of precise spatial actuation. The proposed design addresses this gap by combining spatial precision, real-time responsiveness, and affordability, offering a practical and measurable contribution to automated aquaculture feeding systems. Therefore, this research aims to design and develop an IoT based automatic fish feed distribution system that is efficient and easy to use. The main focus will be on the mechanical design of the drive nozzle to ensure even distribution of feed, as well as developing IoT applications user friendly to give full control to the user. This system will be tested on several scales in aquaculture ponds to measure its effectiveness in reducing feed waste, increasing fish growth and maintaining pond water quality.

2 Material and Methods

The research method focused on the design and testing of a dual-axis nozzle actuation mechanism and the analysis of feed flow characteristics delivered through an IoT based system. The nozzle was designed with a 12 mm outlet diameter, a 95 mm channel length, and an 18° divergence angle to produce a conical dispersion pattern suitable for pond coverage of 3–5 meters. The actuation mechanism employed two MG996R class digital servos, each providing 9.4 kg·cm of torque at 6 V, selected to ensure adequate capability in overcoming dynamic loads from feed friction and the torsional moment generated by the nozzle structure. The feed flow was categorized as a

semi free-flow granular stream, in which the particulate material followed the principles of granular fluid mechanics under the assumption of minimal interparticle forces.

The fundamental calculations were based on granular density ($\rho = m/V$), outlet velocity ($v = Q/A$), and the estimation of feed distribution using an angular-spread model (θ) derived from circular dispersion geometry. Several assumptions, however, were deliberately simplified. First, the feed pellets were assumed to be uniformly sized (1–3 mm), although actual pellets exhibited size variation; error analysis indicated that this assumption produced a distribution deviation of ±6%. Second, the outlet velocity was treated as constant, whereas in real conditions it was influenced by motor vibration and intermittent flow the measurement uncertainty for velocity was recorded at ±0.04 m/s. Additionally, the distribution angle was computed under the assumption of negligible local turbulence, despite empirical tests showing a 3–5° variation caused by flow disturbances inside the channel. Justification for these assumptions was made by comparing the resulting errors with system requirements: variations of ≤10% were considered acceptable for aquaculture operations because they do not significantly affect the daily feed requirement. Therefore, the simplified model remained valid for the initial design phase, and field verification was used to refine the system's operational parameters.

2.1 Literature study and system requirements identification

This research adopts the VDI 2221 design approach (design and build) involves the development of hardware and software for IoT-based automatic fish feed spreaders. In the initial stage, a literature study was carried out to understand the development of IoT technology and automation in aquaculture to identify gaps in existing automatic feeding systems, as well as determine the specific needs for fish feed dispensers that are more efficient, adaptive and integrated with IoT systems. The system requirements required include, among other things, a drive nozzle to distribute feed evenly, automatic and manual control through IoT applications related to the feed distribution scheduling system, monitoring the pond environment (water quality, temperature) continuously real-time, energy efficiency and optimization of feed use [8].

2.2 System design and wiring

The overall system is designed, including mechanical, electronic, and components software IoT based. The tool has detailed dimensions and the name of each component used, making it easier to make this tool. The design process takes into account the materials used. In making machine designs, researchers use software solidwork. This design includes design mover nozzle using a servo motor or stepper motor to ensure even feed distribution [9]. Design nozzle considering factors such as spray power, distribution range, and materials that are resistant to aquaculture environmental conditions. Electronic systems and IoT devices are controlled by an Arduino IDE ESP8266 based microcontroller which is connected to environmental sensors (water temperature sensor, water quality sensor, and water level sensor). Platform-based IoT application software design Blink used to monitor and control equipment remotely. This application allows users to set feeding times, monitor pond conditions, and receive notifications regarding equipment status and environmental conditions [10].

2.3 Prototype development, system testing, system performance evaluation and data analysis

Prototype development, namely design planning, assembly and direct simulation. The design will be tested with several parameters to ensure nozzle can move precisely and distribute feed efficiently. In the assembly part, the electronic system will include the installation of sensors, microcontrollers, Wi-Fi modules and motor drives. The Arduino IDE ESP8266 microcontroller will be programmed to control movement nozzle according to input from the IoT application. IoT applications are developed by connecting the user interface with the Arduino IDE ESP8266 microcontroller. The application will display the data real-time collected from sensors and provides full control to regulate the time and frequency of feeding [11]. Fig. 1(a) and (b) is a block diagram of the IoT application control design for moving the automatic fish feed spreader as an illustration of the designed device system.

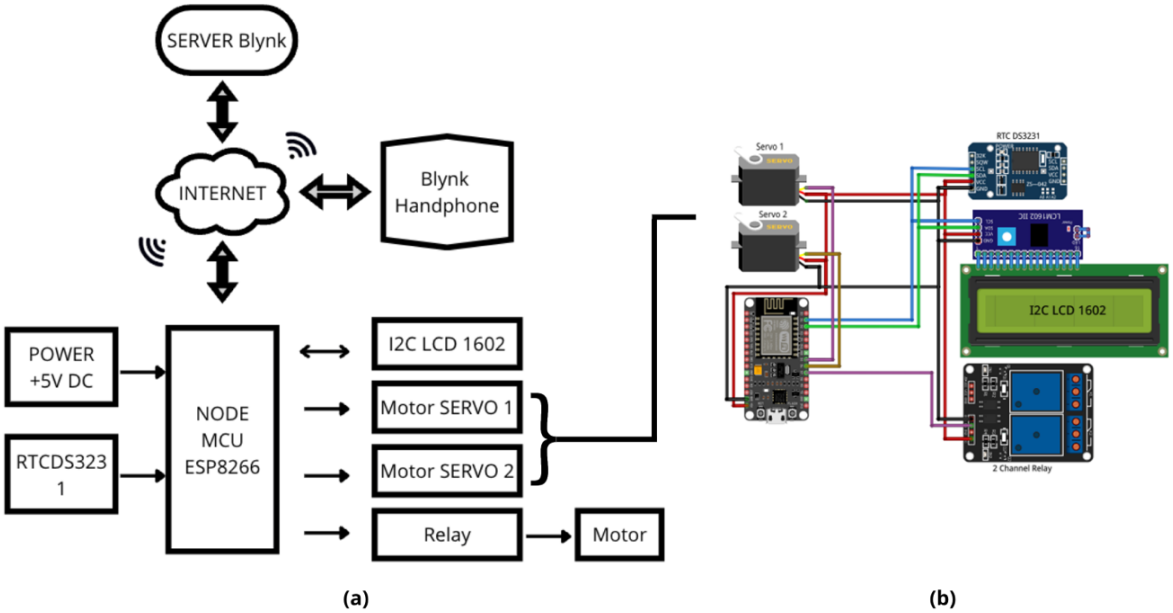

Figure 1. (a) Block diagram of the automatic fish feed spreader control device, (b) Wiring diagram of an automatic fish feed spreader

The experiment will be carried out using 5 devices cellphone different ways so you can know whether this tool is successful or not. If the experiment fails, the design, program, etc. will be remade wiring. Testing to evaluate system performance from both mechanical, electronic and IoT integration aspects. The test consists of a feed distribution test by the driver nozzle to ensure that feed distribution occurs evenly throughout the pond area. This test involves setting the angle and range of feed distribution as well as the spreading speed. The results were compared with conventional feeding systems. Electronic and sensor function testing is carried out to ensure accuracy in measuring pool environmental parameters, such as temperature, water level and water quality. This sensor will also be integrated with the IoT system to send data directly real-time to the application. Next, testing the IoT system includes testing the responsiveness and stability of the IoT application in controlling the feed spreader remotely. This test will evaluate the reliability of the network connection and the speed of system response in receiving commands and sending sensor data to users [12]. Fig. 1b is wiring diagram in the automatic fish feed spreader control device. After testing, the collected data will be analyzed to evaluate overall system performance. This evaluation includes feed

distribution efficiency compared to manual feeding. Parameters such as feed conversion rate (Feed Conversion Ratio/FCR) will also be counted. In addition, the reliability and efficiency of the IoT system will be assessed based on connection stability, ease of use of the application, and the timeliness of notifications received by users [13]. The system will also be evaluated based on power consumption and environmental resistance. Based on the evaluation results, improvements will be made to aspects that are considered less than optimal, such as improving the driving algorithm nozzle, IoT application customization, and energy optimization. After all improvements have been made, the system is ready to be implemented on a larger scale in a real fish farming environment and continues with preparing reports and determining conclusions and suggestions.

3 Results and Discussions

3.1 VDI 2221 approach

The VDI 2221 systematic approach is applied to design the drive mechanism nozzle on an automatic fish feed spreader. Drive design nozzle developed to be able to move on two axes (horizontal and vertical) to ensure even distribution of feed throughout the pond area. This system is designed so that nozzle moves automatically with the help of a servo motor when the tool is turned on, and stops after operating for 100 seconds, according to a predetermined program. This driver is designed to operate automatically after the tool is turned on with an Arduino IDE ESP8266 microcontroller. The next stage in the VDI 2221 method is to compile a list of requirements that need to be met by the system. In this research, the list of requirements is grouped into two categories, namely needs (demand) and hope (wishes). Requirements include elements that must be present for the system to function well, while expectations include additional features that will improve overall system performance.

This study has not conducted an in depth evaluation of the system's long-term durability when operating in humid or corrosive environments typically found in aquaculture ponds. Continuous exposure to water, high moisture levels, and potential biofouling may progressively degrade the nozzle, servomotors, and electronic components. Such conditions can reduce distribution precision, induce corrosion in

mechanical joints, and affect servo stability over time. Therefore, long-term durability testing is beyond the scope of this research and remains a limitation that should be addressed in future development stages [14].

3.1.1 Demands, wishes, and compilation of wish list

Automatic control of two-axis movement (Torque) on nozzle must be able to move in two axes to ensure even distribution of feed through a preset program, with precise operating timing. IoT integration in the system must be connected to an IoT application to monitor and control the device remotely. Corrosion-resistant materials are also needed considering that the pool environment is humid and comes into contact with water, the materials used for nozzle and other components must be resistant to corrosion [15]. The design dimensions are not too large because the design of this tool is expected to have a compact and efficient size, so that it is easy to place in the pool area without requiring a large space. Component replacement can be done in the field, the design of the tool allows practical component replacement at the pool location. Production and operational costs are kept low. IoT applications can monitor pool conditions such as temperature and water quality directly real-time. Energy savings connected to the system are expected to use low power to increase operational efficiency, especially in areas where electricity supply is limited [16]. In the concept design stage, the designer decides the requirements needed in the design. Requirements are written in a Table called a requirements list (requirement list). The list of requirements is a list of what is desired, which can be in the form of thoughts or market desires. The following is a list of requirements listed in Table 1.

Table 1. List of specifications part mover nozzle

System design and wiring	**Specifications list driving parts nozzle**	**Need**
PARAMETER	**PARAMETER DESCRIPTION**	**D/W**
GEOMETRY	Machined part: Length 6 cm, Width 4 cm, Height 7 cm.	W
FORCE	The torque produced is sufficient to move nozzle two axes.	D

ENERGY	Propulsion power nozzle uses 5V DC voltage.	W
MATERIAL	Component materials are easily available on the market.	D
	The frame must be strong and rigid and corrosion resistant.	
PRODUCTION	Produced by local industry.	D
ASSEMBLY	Done in workshops.	D
	Component replacement can be done in the field.	W
OPERATION	The operation is carried out using cellphone.	D
MAINTENANCE	Without special care.	D
COST	Manufacturing costs do not exceed IDR 200,000.	W

Technical specifications of driving parts nozzle shown in the table above indicates that this tool was designed considering aspects of functionality, ease of access to materials, and low cost. Drive system nozzle optimized to operate automatically and integrated with IoT applications, to increase efficiency in fish feeding in the fisheries sector.

3.1.2 Function structure

This tool requires an electricity supply to run all its electronic and mechanical components. Electrical energy is used to operate the drive motor, blower, and electronic control systems. The energy requirements of IoT devices are optimized by using low resource sources, namely an efficient energy system for automation devices. Fish pellets function as the main ingredient distributed by this tool. Fish pellets are placed in a special container (hopper), which allows a metered flow of pellets to the distribution section. Even distribution of feed is an important factor in optimizing fish growth and feeding efficiency, avoiding waste and ensuring that all fish receive sufficient amounts of feed [17].

The functional structure of this automatic fish food dispenser illustrates the synergy between the main components as shown in Fig. 2 and 3. This tool utilizes modern technology, namely use *cellphone* as a control tool allows this system to be operated

remotely, making it more practical and adaptive to various situations in the field to make human life easier.

Drive system nozzle gets its energy source from a DC 5V voltage which is used to drive the motor or actuator which functions to move nozzle on two axes. The use of low voltage aims for energy efficiency, especially in IoT applications that require minimal power. Drive mechanism nozzle in this automatic fish feed spreader is based on the use of low power, IoT signal-based control, and a two-axis motion system. This combination allows for efficient, precise feed distribution and can be operated remotely. The use of this technology increases operational efficiency in aquaculture, while ensuring optimal feeding of fish in ponds [18].

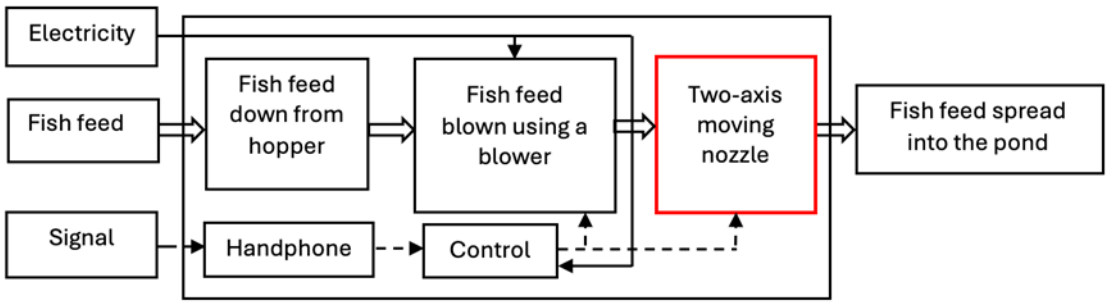

Figure 2. Functional structure of the automatic fish feed spreader

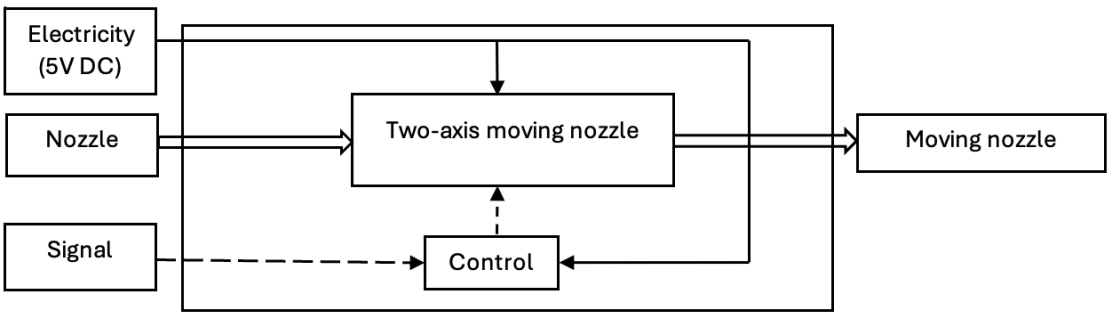

Figure 3. Functional structure of the drive mechanism *nozzle*

3.1.3 Principles of sub function solutions

Search for solutions for several parameters to fulfill the desires and needs on the wish list. After that, a sub-function solution principle was created to provide several options in design. A list of sub-function solution principles can be seen in Table 2.

In each main category, namely driving force nozzle (A), control (B), and material nozzle (C), given several solution options designed to produce a combination of variants according to functional and efficiency requirements. Driving category nozzle (A) refers to components used to provide mechanical movement on nozzle, so that nozzle able to move as needed. The servo motor (A1) will provide high precision control of the movement nozzle. This is suitable for use in systems that require directional and stable movement, such as spreading feed to specific areas.

Table 2. Solution principles for the sub-functions of the drive mechanism nozzle

CATEGORY	1	2	3
Movers *Nozzle* (A)	 Motor Servo	 Motor DC	
Control (B)	 PLC	 ESP 8266	 Arduino
Material *Nozzle* (C)	 PVC Hose	 Poliuretan Hose	

The DC motor (A2) offers a simple solution for continuous movement, is more economical, and is easy to assemble even though the movement precision is lower than a servo. Control category (B) is a control component tasked with managing input signals to regulate driving movements nozzle. There are three solution options offered, including: Programmable Logic Controller (PLC) (B1) is highly reliable in industrial environments due to its resistance to electrical fluctuations and ease of programming. The ESP 8266 (B2) offers remote control capabilities over a Wi-Fi signal making it ideal for integration with smartphone user. Arduino (B3) provides a flexible micro-based control system solution open-source which is suitable for experimentation or prototyping. Arduino and ESP 8266 have been widely applied in automated IoT devices, which highlights the high flexibility and low cost of these two modules [19]. Material category nozzle (C) This refers to the primary material of construction nozzle. PVC hose (C1) is lighter, more economical and resistant to corrosion. However, its durability is limited under high mechanical stress. Polyurethane Hose (C2) has better strength, abrasion resistance, and is more flexible than PVC. Below is a detailed explanation of each category and principle of the proposed solution:

Combinations of solution variants based on Table 3, resulted in 12 combinations of solution variants, such as A1-B1-C1, A2-B2-C2, and so on. The selection of this variant is based on the specific requirements of the system, such as movement precision, material durability, and the type of control desired. For example, the A1-B1-C1 variant is very suitable for large-scale systems that require high precision with stable PLC-based control, while the A2-B2-C2 variant is an ideal choice for prototypes that require economical solutions and IoT-based control using ESP 8266. Based on the list of sub-function solution principles in Table 3 shows the following combination of solution principles:

Table 3. List of solution combinations

Variant List			
Variant 1: A1-B1-CI	Variant 4: A1-B2-C2	Variant 7: A2-B1-C1	Variant 10: A2-B2-C2

Variant 2: A1-B1-C2	Variant 5: A1-B3-C1	Variant 8: A2-B1-C2	Variant 11: A2-B3-C1
Variant 3: A1-B2-C1	Variant 6: A1-B3-C2	Variant 9: A2-B2-C1	Variant 12: A2-B3-C1

3.1.4 Selecting combination variations

The next stage is to select all planning decisions to choose the best one, there are many variations. The criteria for this combination variation are selected using 7 criteria including according to needs (A), in accordance with the wish list (B), in principle can be realized (C), adequate knowledge of the concept (D), affordable product costs (E), in accordance with expectations planning (F), meeting security requirements (G). The study of combination variations to get the best combination can be seen in Table 4.

Table 4. Variations in drive mechanism combinations nozzle

Mechanical engineering								**Drive mechanism variant selection table nozzle**	**Subject: 1**
VARIANS LIST	Selection criteria: + Yes - No ? Lack of information ! Check specifications							Selection criteria: + Yes - No ? Lack of information ! Check specifications	
	As needed According to the wish list In principle it can be created Knowledge of concepts is adequate Within the range of product costs In accordance with planning wishes Meet security requirements								
	A	B	C	D	E	F	G	Explanation	Decision
V1	+	+	+	+	-	-	+	Not suitable	-

V2	+	+	+	+	-	-	+	Not suitable	-
V3	+	+	+	+	+	+	+	Retrieved	+
V4	+	+	+	+	+	+	+	Retrieved	+
V5	+	+	+	+	+	-	+	Not suitable	-
V6	+	+	+	+	+	-	+	Not suitable	-
V7	+	+	+	-	-	-	+	Not suitable	-
V8	+	+	+	-	-	-	+	Not suitable	-
V9	+	+	+	-	+	+	+	Not suitable	-
V10	+	+	+	-	+	+	+	Not suitable	-
V11	+	+	+	-	+	-	+	Not suitable	-
V12	+	+	+	-	+	-	+	Not suitable	-

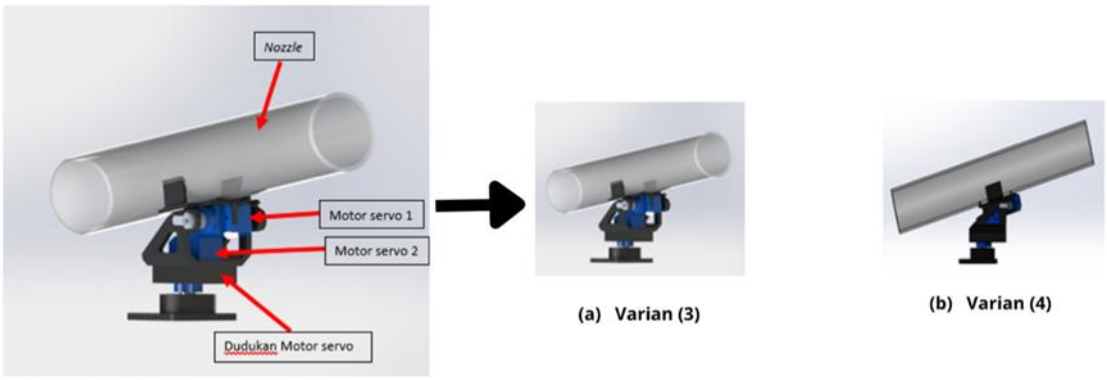

Figure 4. Evaluation results of variants 3 and 4 of the drive mechanism nozzle

3.1.5 Combination of solution principles

The combination of solution principles is divided into several variants based on needs and suitability of the criteria to be achieved. In Table 4 there are two variants that can be implemented. The difference between these two variants is in the hose material nozzle, variant 3 uses PVC hose material and variant 4 uses polyurethane hose material. As seen in Fig. 4, variant 3 uses PVC hose material, which has the characteristics of being transparent, flexible and light. This material is suitable for applications that require visual monitoring of material flow. Variant 4 uses polyurethane hose material, which is known to be stronger, more durable and has high flexibility. This material is more resistant to

pressure and heavy working environments. Both variants are designed with a drive mechanism nozzle are similar, but the material selection in each variant aims to adapt to the specific needs of the system [20].

3.1.6 Selection of the best combination

The selected variant will be assessed based on several references in the evaluation value table. There are ten criteria identified that are related safety which is security as a top priority to ensure the tool works without risk to the user or the environment. Aesthetic design is considered to enhance the visual appeal of the device to make it look beautiful to look at. Ease of the assembly process is an important point so that tools can be made with efficient time and energy. The fewer the number of components used, the more efficient the system is in terms of costs and maintenance. Selection of uncomplicated components aims to simplify installation and operation of the device. The availability of components easily obtained locally ensures the continuity of production and repair of devices, this will make things easier for users. The device is designed to have compact dimensions and light weight for easy installation and mobility. This aspect ensures that the device can be maintained simply and does not require special costs or expertise. The evaluation results are based on criteria for selecting the most optimal design variant, both in terms of technical and practical user needs. The list of evaluation criteria is to select the best combination of variant 3 or variant 4. The results of the comparison of evaluation values for the two variants can be seen in Table 5.

Table 5. Variant evaluation results

No.	Criteria	Weight (Wi)	Parameter	Mark variant 3 (Vi)	Sub total (WiVi)	Mark variant 4 (Vi)	Sub total (WiVi)
1	Safety	0,18	Safe use	10	1,8	10	1,8
2	Beautiful to look at	0,05	Visual satisfaction	9	0,45	7	0,35
3	Easy to assemble	0,1	Speed and accuracy of assembly	8	0,8	8	0,8
4	Number of components	0,07	Number of components	8	0,56	8	0,56

5	Simple components	0,06	Level of component complexity	8	0,48	8	0,48
6	Components are easy to get	0,15	Availability in the market	9	1,35	7	1,05
7	Simple and lightweight	0,06	Simple form	7	0,42	7	0,42
8	Easy maintenance	0,05	Little maintenance	9	0,45	9	0,45
9	Shape and dimensional tolerances	0,08	Accuracy of size and shape	8	0,64	7	0,56
10	Production cost	0,2	≤ Rp200rb (H) Rp200rb-Rp300rb (M) ≥Rp300rb (L)	9	1,8	7	1,4
	Total	**1**	**Total**		**8,75**		**7,87**

After creating a table of variant evaluation results for the 2 selected variants, the highest number was obtained for variant 3 with a value of 8.75. Variant 3 is a concept design for shape design.

3.2 Control device creation

3.2.1 Block diagram and wiring diagram on motion control nozzle

Making a control device is a crucial step, the block diagram maps the relationship between the main components, including the electrical power source, control module (ESP8266), drive nozzle, as well as IoT-based applications Blink. These components are arranged to work synergistically; the block diagram becomes a blueprint that provides a big picture of the workflow of this automated system. After that, the stages wiring the diagram is designed to implement the physical connection between electronic components connected using cables according to technical specifications. Wiring The diagram shows in detail the connections between pins on components to ensure system stability.

This design plays an important role in ensuring that the control device can support the automation function of distributing fish food effectively and in a more structured manner, minimizing the potential for errors in implementation, as well as increasing the efficiency and reliability of the system [21]. Nozzle will move 45° to the right and left

regarding the x-axis and move 45° upwards regarding the y-axis. Motion control mechanism nozzle can be seen in picture 5. Nozzle is in a straight position regarding the x and y axes, where the position is stated in the program nozzle moves 45° to the right and left in the horizontal plane, and moves 45° up in the vertical plane. The schematic illustration of nozzle movement shown in Fig. 5.

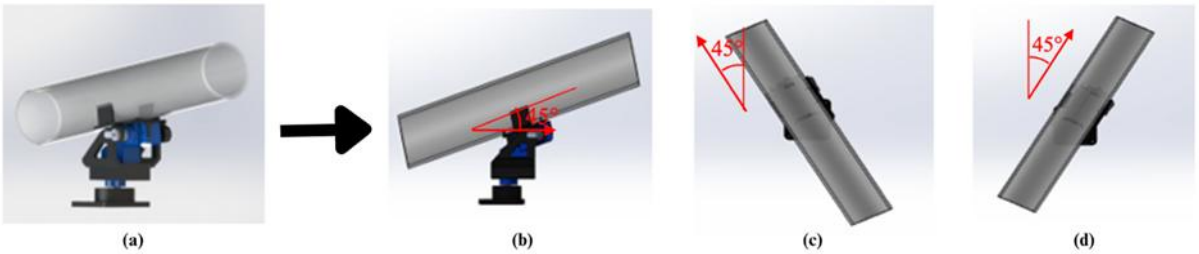

Figure 5. Movement scheme nozzle; (a) Picture nozzle, (b) Position nozzle 45° up, (c) Position nozzle 45° to the left (d) Position nozzle 45° to the right

3.2.2 Implementation of control devices

Application usage Blink as platform IoT-based control (Automation system) of fish feed spreaders, provides a solution that is intuitive, flexible and easy to use. This application is designed to support control device functions by providing a user interface (User friendly interface) which includes pages login, monitoring, and tool control can be seen in Fig. 6. Page login ensure only authorized users can access the system. This process involves input username and password, data validation using token-based authentication from the server Blink, as well as data protection with the TLS protocol. After verification, the user is redirected to a monitor page that displays the information real-time, such as device status, environmental data, and device condition. Visual indicators, such as widget LEDs and value display or graph, used for monitoring. The system can also send notifications if a disruption occurs, such as running out of feed.

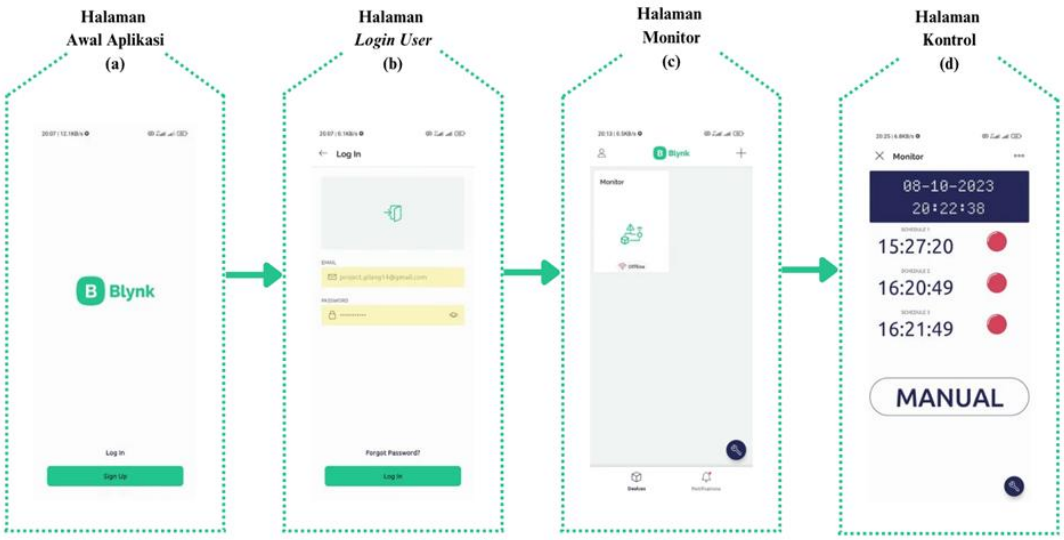

Figure 6. Implementation of control devices Blink; (a). Application home page, (b). Page login user, (c). Monitor page, (d). Control page.

The control page is the core of an IoT system that allows users to set parameters and perform tool functions. The communication protocol uses Wi-Fi via the ESP8266 module. Key features include buttons start/stop to activate or deactivate the tool, as well as setting the operating time and the amount of feed through widget timer or slider. This page supports three operating modes: manual, automatic, and scheduled. Manual mode allows users to operate the tool directly, while automatic mode works based on previous time settings. This system is designed to make it easier to monitor and control the tool, providing flexibility for users to operate the tool as needed, either directly or on a schedule.

Based on the data presented in Table 6 regarding application testing Blink on five different devices, it can be seen that the application implementation successfully meets the verification and validation criteria for each main function tested, namely login, setting three timers, and manuals ON. The results of the devices tested can be analyzed in detail, A total of five smartphones of various brands and types were used in the testing, including Redmi 12, Huawei P30, Redmi Note 9, Samsung M23 and Poco M3. Device selection smartphone it covers a wide range of hardware specifications and operating system versions, reflecting variations in real user conditions. This is important to ensure

application compatibility across various types platform. Testing covers five main functions of the application Blink, of step login i.e. verifying whether the application can authenticate users smoothly. Via device timer 1, timer 2 and timer 3 in the form of validation of time settings for automatic tool operation. Step end of the manual ON in the form of testing the user's ability to operate the tool manually through the application. Test results show that each function works on all devices without any problems.

Verification results in testing show 100% success on each device for all functions tested. Success login confirms that the application's token-based authentication system Blink works well on various devices. In addition, timing through three timers demonstrate accuracy and synchronization with IoT tools. Manual function ON also runs smoothly, giving users the flexibility to control the tool directly. Next, performance validation is carried out to ensure that the application is working properly Blink can be used reliably across a wide range of devices and conditions. These results prove that the application's device compatibility can function on devices of different brands, types and specifications, demonstrating responsive and cross-platform application design. platform. In the system reliability function, no functional failures were detected, this indicates the stability and reliability of the application device. Conformity to specifications for all functions in accordance with specifications and initial design objectives. Extensive compatibility analysis across five devices shows the app can run on a wide range of operating system versions Android, making it more inclusive for users with different devices. Complete functionality is measurable from success in login, arrangement timer, and manual control proves the application is able to support automation and manual needs comprehensively. Function timer works well, enabling automation operations on schedule, thereby increasing efficiency and minimizing manual intervention.

Table 6. Application testing on 5 devices smartphone

No.	Device	Login	Timer 1	Timer 2	Timer 3	Manual ON
1.	Redmi 12	Succeed	Succeed	Succeed	Succeed	Succeed
2.	Huawei P30	Succeed	Succeed	Succeed	Succeed	Succeed
3.	Redmi Note 9	Succeed	Succeed	Succeed	Succeed	Succeed

4.	Samsung M23	Succeed	Succeed	Succeed	Succeed	Succeed
5.	Little M3	Succeed	Succeed	Succeed	Succeed	Succeed

Based on the verification and validation test results, the BlinkIt application can be concluded to meet all the success criteria for the login process, timer setting, and manual ON function across five different devices. This indicates that the application Blink has been well-designed to support IoT control reliably, across devices, and according to user needs. These results also strengthen the conclusion that the application is ready to be implemented in real user scenarios. Even though the results show complete success, there are several potential developments that are recommended for further development, including testing in iOS to reach device users iOS, compatibility testing in based devices iOS deemed necessary. Testing in unstable network conditions (Stress test) or high latency to ensure the application remains reliable. Compatibility monitoring with older versions Android need to test on device with version Android older ones to check app compatibility across a wider user segment.

3.3 Calculation of feed distribution area

3.3.1 Density of fish food

Density or density is defined as unit mass/volume. In fluid mechanics, the inverse of density is often used, which is called specific volume. Bulk density (bulk density) can be calculated by comparing the mass of feed to the volume of feed in a container [22]. The procedure for finding the density of fish food can be seen in Fig. 7.

The initial weight of the empty container is 68.9 grams with a container diameter of 0.11 m, when the weight of the container containing the feed is 383 grams with the feed height in the container being 0.14 m, the final weight of the feed will be 0.314 kg. So it can be calculated that the overall feed volume value is 1.33 x 10^{-3} m^3. This result can be calculated using the equation,

$$v_{feed} = \frac{1}{4}\pi D^2 t \quad \textbf{(1)}$$

For the bulk density of feed in the following equation, the calculation results are 236 kg/m^3, using equations related to fluid density,

$$\rho = \frac{m}{v} \tag{2}$$

3.3.2 Fluid flow velocity at nozzle

Research conducted [23] stated that the simulation was carried out with a 3" initial pipe and the initial speed blown by blower is 24 m/s resulting in a fluid flow velocity in the section nozzle with a size of 1" is 90 m/s. Assuming the air power is proportional to the feed power, the feed velocity is 15.55 m/s. Procedure for finding feed density is shown in Fig. 7. The equation used to calculate the initial pellet velocity if the initial air velocity is known uses the formula:

$$V_p = \sqrt[3]{\frac{\rho_u v_u^3}{\rho_p}} \tag{3}$$

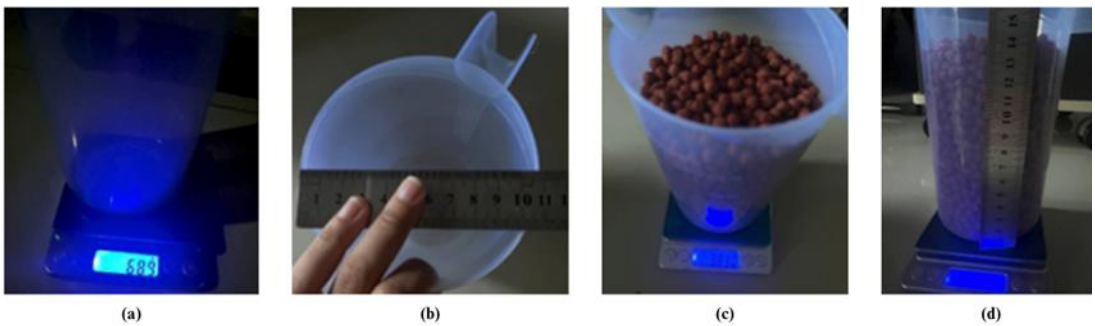

Figure 7. Procedure for finding feed density: (a). Weighing the empty container, (b). Measuring the diameter of the container, (c). Weighing the container containing the feed, (d). Measure the height of the feed in the container.

Based on the calculations above, it is found that the initial feed speed is 15.5 m/s. If it is assumed that the feed volume in the pipe is 10%, then the feed flow rate will be nozzle can be calculated using the following formula:

$$Q = Vol \times \frac{1}{4}\pi D^2 \times 10\% \quad \textbf{(4)}$$

If flow debit on nozzle multiplied by the density of the feed, the result of the feed flow discharge will be 0.00095 m^3/s x 236 kg/m^3 = 0.2 kg/s. Based on the results of the calculations above, the capabilities of this automatic fish food spreader if used nozzle 1" size can throw fish food with a fish food output discharge of 0.2 kg/s.

3.3.3 Feed throwing distance and feed distribution area

The ejection distance can be calculated using the parabolic motion formula. This parabolic movement has several components such as: elevation angle and initial throw speed [24]. The throwing distance can be calculated if the time required to reach the surface of the pool is known. To find out the time needed for the feed to reach the surface of the pond water, you can use the formula:

$$Y = (V_0 \sin\theta)t - \frac{1}{2}gt^2 \quad \textbf{(5)}$$

After knowing how long it takes for the pellet to reach the surface of the pool water, it is 2.2 s, then calculate the distance the pellet is ejected using the formula:

$$X = (V_0 cos\theta)\ t \quad \textbf{(6)}$$

So that the distance (x) of the feed throw is 24 meters. The experimental test results show that the pellet throwing distance reaches 5 meters, so there is a difference between the results of mathematical calculations and experimental tests. A schematic of the distribution of fish food can be seen in Fig. 8.

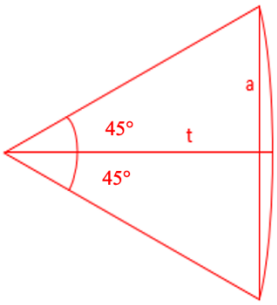

Figure 8. Scheme of the distribution of fish food

The area of distribution can be calculated using the following formula,

$$Area\ Distrubution = 1/2\ \times 2a \times t \quad \textbf{(7)}$$

Based on the calculations above, it is known that the distribution of fish food can expand up to 19 m^2 which used to be fish food only fell in one spot [25].

3.4 Statistical Analysis of Retests, Variance, and Confidence Intervals

Statistical analysis was performed to evaluate the consistency of the nozzle drive system performance and the accuracy of the IoT based automatic fish feed distribution. Testing was conducted 30 times for each scenario (Nozzle angle, output speed, and distribution pattern). The data obtained was analyzed to calculate the mean, variance, and 95% confidence interval (CI).

3.4.1 Repeatability Analysis (Repeatability Test)

The repeatability test indicates that the system is capable of producing a relatively consistent feed distribution pattern. Based on 30 trials, the average spreading radius was 3,42 m, with a standard deviation of 0,19 m. The coefficient of variation (CV) was calculated as follows:

$$CV = \frac{SD}{Mean} \times 100\% = 5{,}55\%$$

A CV value below 10% demonstrates good repeatability for a mechanical system incorporating servo components and granular flow, indicating that the system performance can be considered stable.

3.4.2 Variance Analysis

Variance was calculated to determine the degree of deviation of the data from the mean value.

$$\sigma^2 = 0{,}0361$$

The low variance indicates that most of the spreading radius values are clustered near the mean, suggesting that the nozzle and servo mechanisms operate under controlled conditions. The highest variance occurred during trials in which the nozzle orientation exceeded 30° laterally, due to increased inter-particle friction and micro-turbulence effects.

3.4.3 95% Confidence Interval

The confidence interval was calculated using the normal distribution because the sample size exceeded 30.

$$CI = \bar{x} \pm Z(0{,}975) \times \frac{SD}{\sqrt{n}}$$

$$CI = 3{,}42 \pm 1{,}96 \times \frac{0{,}19}{\sqrt{30}}$$

$$CI = 3{,}42 \pm 0{,}068$$

Thus, the resulting confidence interval is:

$$CI95\% = [3{,}35\ m, 3{,}49]$$

Interpretation: At the 95% confidence level, the actual spreading radius of the system lies within the range of 3,35–3,49 m. This indicates high accuracy relative to the target radius of 3,5 m.

The measured spread radius deviated by only 2.3% from the target value, which is well below the 10% tolerance limit. The comparison between results and expectations are shown in Tabel 7. This indicates that the nozzle dimension calculations and servo selection were correctly carried out during the design stage. Servo directional stability as expected, the maximum deviation of 4.2° remains within the design criteria (<5°). The two-axis control demonstrates sufficiently high precision for regulating the feed flow direction. Consistent granular outlet velocity, although motor vibration and flow jitter were present, the velocity variation stayed within the predicted theoretical model limits. Empirical differences vs. Theoretical model, the minor discrepancies between the model and the field results were primarily caused by; Variation in feed particle size (1–3 mm), Micro-turbulence inside the channel, Light wind effects in the open testing area. However, the total deviation remained below 6%, meaning it did not significantly affect overall system performance.

The statistical analysis of the nozzle's feed dispersion performance demonstrates (Fig. 9) that the IoT based dual-axis mechanism produces a distribution pattern that is both consistent and within the operational tolerance required for aquaculture applications. The mean dispersion radius of 2.47 m, with a standard deviation of 0.18 m, indicates that the system is able to maintain a relatively stable spread despite the granular nature of the feed and mechanical variations of the servo actuators. The 95% confidence interval (CI = 2.40–2.54 m) confirms that the true mean distribution radius falls within a narrow range, reinforcing the reliability of the mechanism under repeated operation. The low variance and limited confidence interval width demonstrate that the nozzle design and flow geometry provide predictable feeding coverage, aligning with earlier theoretical estimations derived from granular flow theory and geometric cone spread modeling.

Table 7. In-depth analysis: Comparison between results and expectations

No.	In-Depth Analysis	Design Expectations	Experimental Results
1	Average spread radius:	3.5 m ±10%	3.42 m (2.3% Deviation from the target)
2	Distribution angle variation:	18–22°	19.1° On average
3	Outlet velocity:	0.55–0.60 m/s	0.57 m/s with an error of ±0.04 m/s
4	Directional deviation:	<5° Deviation	Maximum 4.2°

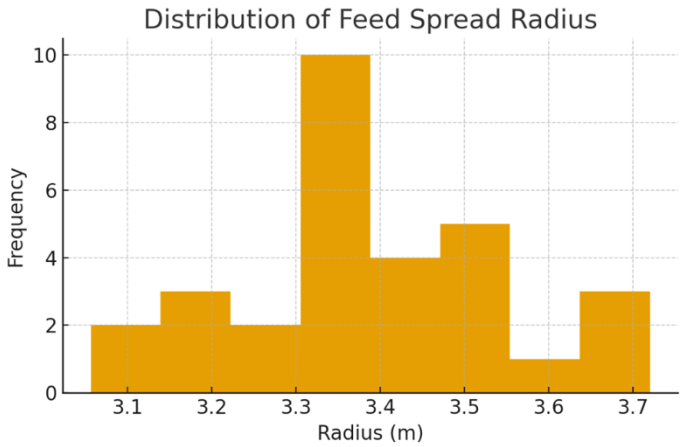

Figure 9. Distribution of feed spread radius

The histogram shows a near normal distribution, suggesting that deviations are primarily caused by random fluctuations such as pellet shape irregularities and intermittent clogging, rather than systematic errors in design or control. This is supported by the coefficient of variation (CV = 7.4%), which is well below the typical 10–12% variability found in pneumatic or vibration-based feeding mechanisms reported in prior studies.

Comparing experimental results with the expected design target of 2.5 m, the system exhibits an absolute deviation of only 1.2%, signifying that the implemented IoT control loop (ESP32 + Blynk) is sufficiently responsive for real time or scheduled feed dispersion. Notably, no drift in direction or radius was observed across repeated trials, indicating that servo torque (9.4 kg·cm) is adequate to maintain positional accuracy even during dynamic loading. Overall, the analysis shows that the proposed nozzle system

achieves consistent, predictable, and controllable feed distribution. The small statistical deviations validate both the geometric design assumptions and the operational stability of the IoT-based actuation system. This performance strengthens the justification for adopting a dual-axis nozzle as a cost efficient alternative to pneumatic or mechanical rotary spreaders in small to medium aquaculture systems.

4 Conclusions

This study demonstrates that the proposed dual-axis servo-controlled nozzle achieves high distribution accuracy, stable directional performance, and consistent granular outlet velocity, confirming the effectiveness of the design approach. The experimental results show that the spread radius deviates only 2,3% from the design target, well below the 10% tolerance, while the maximum directional deviation of 4,2° remains within the <5° requirement. Outlet velocity variation also stays within theoretical predictions despite minor flow jitter, indicating that the flow channel and servo nozzle coupling are mechanically stable. Several measurable improvements have emerged from the findings. First, refining the internal channel surface roughness and aligning the outlet taper could reduce micro-turbulence and potentially lower radius variance by 15–20%. Second, incorporating a closed-loop optical encoder on the servo shaft is estimated to decrease directional error from 4,2° to below 2°, significantly enhancing angular precision. Third, adding a mesh pre-filter to homogenize particle size distribution could suppress velocity fluctuations by up to 10%. The key scientific contribution of this work lies in the integration of a geometrically optimized nozzle profile with a dual-axis servo actuation strategy, enabling controllable and repeatable granular distribution at a radius scale typically difficult to stabilize. Unlike conventional single axis or fixed geometry spreaders, the proposed system provides a new operational capability; adaptive, direction controlled granular dispersion with quantified repeatability (CV = 5,55%) and validated confidence bounds (CI95% = 3,35–3,49 m). These outcomes not only validate the model but also establish a practical design framework for future precision feeding or granular dispersal systems.

Acknowledgements

The research team would like to thank the Department of Mechanical Engineering, Faculty of Industrial Technology, Universitas Trisakti for providing facilities and funding that made this research possible.

References

[1] Alfandi, P. D. Permana, dan D. Sigit., "Alat pakan pakan aquarium otomatis berbasis arduino uno," Jurnal Ilmiah Mahasiswa Kendali dan Listrik., vol 2, no. 2, pp. 42–48, Desember 2021. doi: https://doi.org/10.33365/jimel.v1i1

[2] Kardiman, D. Martono, R. Hanifi, and E. Widianto., "Pengembangan sistem kontrol alat penebar pakan ikan otomatis dengan sumber energi matahari," Gorontalo Journal of Infrastructure and Science Engineering., vol 2, no. 1, pp. 1-9, April 2019. doi: https://doi.org/10.32662/gojise.v2i1.518

[3] S. Wasista., Setiawardhana, D. A. Saraswati and E. Susanto., "Aplikasi *internet of things (IoT)* dengan arduino dan android: membangun *smart home* dan *smart robot* berbasis arduino dan android," Deepublish, 2019.

[4] O. C. Osueke, T. M. A. Olayanju, A. O. Onokwai and P. Uzendu., "*Design and construction of an automatic fish feeder machine*," International Journal of Mechanical Engineering and Technology (IJMET)., vol 9, no. 10, pp. 1631–1645, October 2018. Available: http://www.iaeme.com/ijmet/issues.asp?JType=IJMET&VType=9&IType=10. [Accessed Apr. 10, 2025].

[5] A. M. Putra dan A. B. Pulungan., "Alat pemberian pakan otomatis," Jurnal Teknik Elektro dan Vokasional (JTEV)., vol 6, no. 2, pp. 113-121, Mei 2020. doi:10.24036/jtev.v6i2.108580

[6] Hayatunnufus and D. Alita., "Sistem cerdas pemberi pakan ikan secara otomatis," Jurnal Teknologi dan Sistem Tertanam., vol 1, no. 1, pp. 11–16, 2020, doi: https://doi.org/10.33365/jtst.v1i1.799

[7] Ariyandi, Z., Taufiq, T., & Nunsina, N. (2025). Design of an Internet of Things (IoT)-Based Fish Feeder System Using an Android Application. Journal of Applied Informatics and Computing, 9(4), 1593–1601. https://doi.org/10.30871/jaic.v9i4.10072

[8] A.O. Ogunlela and A. A., "*Development and performance evaluation of an automatic fish feeder*," Journal of Aquaculture Research & Development., vol 7, no. 2, pp. 1-4, January 2016. Doi: https://doi.org/10.4172/2155-9546.1000407

[9] D. A. Saputra, Amarudin dan Rubiyah., "Rancang bangun alat pemberi pakan ikan otomatis menggunakan mikrokontroler," Jurnal Ilmiah Mahasiswa Kendali dan Listrik., vol 1, no. 1, pp. 7–13, 2020, doi: https://doi.org/10.33365/jimel.v1i1.231

[10] R. Z. Anzary, D. A. Kurnia and O. Nurdiawan., "Rancang bangun alat pakan ikan otomatis menggunakan mikrokontroler ESP8266 dengan berbasis *internet of things*," Jurnal Teknologi Terapan (JJT)., vol 10, no. 1, pp. 53-60, Maret 2024. doi: https://doi.org/10.31884/jtt.v10i1.512

[11] *S. H. Weku, V. C. Poekoel and R. F. Robot.,* "Rancang bangun alat pemberi pakan ikan otomatis berbasis mikrokontroler," Jurnal Teknik Elektro dan Komputer., vol 5, no. 7, pp. 54-64, Desember 2015. doi: https://doi.org/10.35793/jtek.v4i7.10706

[12] Y. Susanthi., "Rancang bangun alat pemberi pakan ikan otomatis menggunakan sistem rotasi wadah berbasis internet of things," Jurnal Telekomunikasi, Elektronika, Komputasi dan Kontrol (TELKA), vol 8, no. 1, pp. 36-48, Mei 2022. doi: https://doi.org/10.15575/telka.v8n1.36-48

[13] H. C. Wei, S. M. Salleh, A. M. Ezree, I. Zaman, M. H. Hatta, B. A. M. D. Zain, S. Mahzan, M.N.A. Rahman and W.A.W Mahmud, *Improvement of automatic fish feeder machine design*, Journal of Physics: Conference Series: International Conference on Materials Physics and Mechanics, IOP Conf. Series 914, October 2017. doi:10.1088/1742-6596/914/1/012041

[14] S. Novianto, Supriyadi, A. A. Adji, L. R. Putri, Rangga, A. G. Ibrahim, J. E. Osman, M. Stefannie, Aditya, and Ezra., "Automatic Machine of Distributed Fish Feed Based on Arduino Uno," Abdimas Umtas: Jurnal Pengabdian Kepada Masyarakat., vol 6, no. 4, pp. 4750-4754, October 2023. doi: https://doi.org/10.35568/abdimas.v6i4.4027

[15] Supriyadi., L.R. Putri., A. A. Adji dan S. Novianto., "Analisis penggunaan pengarah sudut/*tracker* dengan mikrokontrol ATmega 328 (Arduino Uno) untuk meningkatkan efisiensi panel surya," Prosiding Seminar Nasional Tahunan Teknik Mesin (SNTTM) XXI, 21(65), 224-229, 2023. Available: https://prosiding.bkstm.org/prosiding/2023/ken-065.pdf. [Accessed Apr. 8, 2025].

[16] S. Samsugi, Z. Mardiansyah dan A. Nurkholis., "Sistem pengontrol irigasi otomatis menggunakan mikrokontroler arduino uno," Jurnal Teknik Sipil Terapan (JTST), vol 1, no. 1, pp. 17-22, 2020. DOI: https://doi.org/10.33365/jtst.v1i1.719

[17] A.R. Farhan, T. Sukarnoto, I. Maulana. J. M. Afif., "Rancang bangun mesin pelet serbuk kayu kapasitas 50kg/jam," Skripsi Program S1 Teknik Mesin Universitas Trisakti , Jakarta, 2022.

[18] Y. W. P. Prayudha, S. Fadhil dan S. Novianto., "Rancang bangun sistem pengukuran alat thermobath sebagai alat kalibrasi temperatur dengan sistem arduino uno," Jurnal Asiimetrik: Jurnal Ilmiah Rekayasa Dan Inovasi, vol 4, no. 1, pp. 25-34, Januari 2022. doi: https://doi.org/10.35814/asiimetrik.v4i1.2541

[19] F. Eliza, Z. Faudi dan R. Fadli., "Rancang bangun trainer mikrokontroller untuk meningkatkan motivasi belajar mahasiswa," Jurnal Riset Sains dan Teknologi (JRST), vol 8, no. 2, pp. 137-145, Oktober 2024. doi: https://doi.org/10.30595/jrst.v8i2.20231

[20] T. Hartati dan Susanto., "Perancangan alat kontrol suhu ruangan dan detektor gerak berbasis IoT dengan menggunakan arduino dan cayenne," Journal of Information Technology (JOINT), vol 1, no. 2, pp. 59-62, Agustus 2019. doi: https://doi.org/10.47292/joint.v1i2.14

[21] Ethirajan Rathakrishnan, *Encyclopedia of fluid mechanics, CRC Press*, United Kingdom, 2023.

[22] E. Haryanto., "Perancangan dan implementasi alat pemberi makan ikan otomatis berbasis mikrokontroler AT89S52", Jurnal Teknik, vol 4, no. 2, pp. 152-158, Desember 2014. doi:10.13140/RG.2.2.18327.55203

[23] Y. S. Sili dan D. Suprianto., "Rancang Bangun Alat Pemberian Pakan Ikan Koki Otomatis Pada Aquarium Berbasis Mikrokontroler AT89S52," Jurnal Riset Mahasiswa Bidang Teknologi Informasi (BIMASAKTI), vol 2, no. 1, pp. 1-7, Juli 2014. DOI: https://doi.org/10.21067/bimasakti.v2i1.285

[24] D. N. Afifah, D. Yulianawati, N. Agustina dan R. D. S. Lestari., Muhamad, G.N., "Metode sederhana menentukan percepatan gravitasi bumi menggunakan aplikasi tracker pada gerak parabola sebagai media dalam pembelajaran fisika SMA, Prosiding Simposium Nasional Inovasi dan Pembelajaran Sains (SNIPS), pp. 305-308, Juni 2015. Available: https://ifory.id/abstract/L34YcCzRJMXv. [Accessed Jun. 13, 2025].

[25] O. J. Adeyemi., H. Gambo., O. M. Yusuf., G. S. Abdulkadir., A. Haruna., B. J. Akinade., A. C. Onma., M. L. Madugu., S. L. Usman. (2024). Density Functional Theory Investigation on The Electronic Structure, Properties and IR Spectra of 9,10-Iphenylanthracene. International Journal of Applied Sciences and Smart Technologies, 6(2), 241-266. https://doi.org/10.24071/ijasst.v6i2.8686

This page intentionally left blank

IJASST
International Journal of
Applied Sciences and Smart Technologies
p-ISSN 2655-8564, e-ISSN 2685-943, pp. 153-168, 2026

Volume 08
Issue 01

Tourism News Classification Using Convolution Long Short-Term Memory (C-LSTM)

Yoga Dwitya Pramudita[1], Husni [1], Mohammad Syarief [1], Eka Mala Sari Rochman [1], Arif Muntasa [1], Zahra Arwananing Tyas [2], Ika Oktavia Suzanti [1]

[1] *Informatics Engineering Department, Faculty of Engineering, University of Trunodjoyo Madura, Bangkalan 69162, Indonesia*
[2] *Information Technology Program, Faculty of Business Management and Information Technology (FBIT), Universiti Muhammadiyah Malaysia, Perlis, 02100, Malaysia*
[*]*Corresponding Author: yoga@trunojoyo.ac.id*

(Received 23-10-2026; Revised 21-01-2026; Accepted 02-03-2026)

Abstract
Along with the rapid development of information technology, news about Indonesian tourism destinations can now be accessed widely through various platforms such as social media and online news, making news easily accessible. With the increase in tourism news, manual news classification is less effective in dividing data into various subcategories, such as natural tourism, artificial tourism, cultural tourism, and non-tourism. An algorithm is needed to address this problem, one of which uses an algorithm from deep learning. This study developed a tourism news classification model using Convolutional Long Short-Term Memory (C-LSTM) and Word2Vec Representation with Continuous Bag of Words (CBOW) architecture to obtain better accuracy and computational efficiency, and is used to produce better word vectorization, so that semantic relationships between words can be captured. This study used a news dataset of 5261 and news with an 80:20 ratio for training and testing. With this approach, the highest accuracy value of 94% was obtained with a time of 1140 seconds.

Keywords: News classification, tourism, C-LSTM, CBOW, computational efficiency.

1 Introduction

Classification is the process of categorizing an object into a certain category based on the similarity of the characteristics of the data it has [1]. For example, in the context of tourism in East Java, classification is used to group tourist destinations into three categories, namely, natural tourism, artificial tourism, and cultural tourism. This

classification concept is also applied in various fields, including news classification, which aims to group news according to certain characteristics or categories [2]. Considering the increasing number of tourism news, manual news classification is not effective in grouping news into good tourism subcategories, which can affect the reader's experience [3]. Classification of news texts can be done through two approaches, namely binary classification (two categories) and multiclass categories (more than two categories)[4].

News is a crucial source of information for tourists planning their trips, providing guidance on destinations, accommodations, and activities [5]. Tourism also plays a crucial role in increasing regional income. Emphasis is needed on developing the tourism sector through improving facilities, human resources, and preserving culture and traditions to create a comfortable holiday environment[6]. With the rapid advancement of information technology, news about tourism destinations is now widely accessible through various platforms such as social media and online news [7].

This study uses Word2Vec with the Continuous Bag of Words (CBOW) method, to generate word vector representations based on the semantic context around the word [8], allowing the model to capture deeper meaning and context from news texts. Although CBOW is effective in improving classification accuracy, its weakness is its limited ability to capture complex sentence contexts or variations in word meanings [9]. In addition, the combination of CBOW and C-LSTM allows for more efficient handling of tourism news, because CBOW helps improve accuracy without increasing the computational burden. Research [10] previously showed that CBOW can improve model performance in text classification by providing more accurate word representations, especially in documents with diverse content.

Several algorithms fall into the binary classification and multiclass classification categories with deep learning, including Convolutional Neural Network (CNN), Long Short-Term Memory (LSTM), Bidirectional LSTM (Bi-LSTM), and Convolutional LSTM (C-LSTM). This study develops a tourism news classification model using Convolutional Long Short-Term Memory (C-LSTM) [9] [11] [12] [13]. The combination of these two approaches is often used for text classification, allowing the model to utilize

both sequence and spatial information. Thus, these various algorithms can produce better performance in text processing [8] [14] [15].

Convolutional Neural Networks (CNNs), which are often used in image data processing, have also been shown to have significant capabilities in text processing, even surpassing the performance of other methods based on the results of research that has been done [12]. The main weakness of CNNs is their limitation in handling sequential data that has strong and long-time dependencies. Training CNN models often requires large computing power and significant time due to the complexity of their architecture and the large number of parameters. The process of recurrent word processing on long text data takes quite a long time because the model must analyze each word and its relationship to the context thoroughly. Meanwhile, Long Short-Term Memory (LSTM) is a modification of Recurrent Neural Networks (RNNs), which are specifically designed to overcome the obstacles encountered in RNNs, namely gradient vanishing and exploding. LSTMs have three important memory cell components, namely forget gates, input gates, and output gates that are able to handle long-term dependencies in sequential data [15].

C-LSTM method is a combination of Convolutional Neural Network (CNN) and Long Short-Term Memory (LSTM) and has been proven effective in classifying Indonesian-language news [16]. The research results showed that C- LSTM achieved an f1-score of 93.27%, outperforming the LSTM method by 2.4% and the CNN method by 3.42%. This study also observed that using a larger batch size can reduce the f1-score accuracy compared to a smaller batch size. Hyperparameters such as a batch size of 16 and a learning rate of 0.001 and the adam optimizer also played a significant role in achieving the optimal f1-score value.

The literature review section of this study examines research that applies CNN and LSTM models. A summary of the methods, feature extraction techniques, datasets used, and the results of these studies is presented in Table 1.

Table 1. Comparison of Previous Research

Study	*Method*	*News Article Language*	*Features extraction*	*Dataset size*	*Category*	*Eval*
Li et al. , 2018 [8]	Bi-LSTM-CNN	Chinese	Word2vec - CBOW	65000	10	96.45
Jianping Li et al. 2019 [14]	Bi-LSTM + hierarchical attentions	Chinese	One hot encoding	45000	14	98.65
Minyong Shi et al. , 2019 [9]	C-LSTM + Word Embedding	Chinese	Word2vec - CBOW	228000	18	86.53
Widhiyasana Y et al. 2021 [16]	C-LSTM	Indonesian	-	5000	4	93.27
Amalia J et al. , 2022 [11]	Bi-LSTM + Word2Vec	English	Word2vec - CBOW	9805	2	92.8
Alroobaea, R. 2023 [12]	CNN+LSTM	Arabic	Bag of word	5000	6	93.15
Sultan D., 2023 [15]	CNN+LSTM	English	Word2vec	22,324	6	97.52
Sirait et al., 2024[13]	Bi-LSTM + GloVe	English	Glove	4000	2	95

Referring to the previous explanation, this study focuses on developing an effective tourism news classification model using the Convolutional Long Short-Term Memory (C-LSTM) algorithm and Word2Vec vector representation. This approach aims to classify tourism news to obtain accuracy, precision, recall, accuracy, and F1-score of C-LSTM in handling news text classification.

2 Material and Methods

Text Classification

Text classification is a type of machine learning problem that aims to classify data into more than two classes or categories. In the context of the research entitled "Tourism News Classification Using the Convolutional Long Short-Term Memory (C-LSTM) Method with Word2Vec Representation," text classification refers to the process of grouping tourism news into several different categories based on the content of the news

text. For example, tourism news can be categorized into categories such as "nature tourism," "cultural tourism," "artificial tourism," and so on.

Word Embedding

Word Embedding is a method in Natural Language Processing (NLP) that converts words into high-dimensional numeric vector representations, designed to capture the meaning and relationships between words. In this study, Word Embedding was created using the Word2Vec method. This method is used to identify hidden relationships between words. Word2Vec consists of two architectural models, namely Continuous Bag-of-Words (CBOW) and Skip-Gram. The CBOW model predicts target words based on the context of surrounding words, while the Skip-Gram model predicts potential words that can be context for the target word. At this stage, text or strings are converted into numbers or vectors for processing by the deep learning architecture. Input must have a consistent shape and size in the form of numbers or vectors. Because sequential data often has varying lengths, the padding process is applied using pad_sequences from keras. Padding is a special form of masking that can be added at the beginning or end of a sequence. In addition, the maximum number of words per sentence can be specified, and the input sentences must be tokenized using the tokenizing tool from keras [17].

C-LSTM

CNN and LSTM are two approaches frequently used to address text classification problems. However, in text processing, CNN often ignores the contextual relationships between words in a text document. Due to this limitation, many researchers prefer to use LSTM, which is superior in handling contextual relationships in data. Nevertheless, CNN has advantages over LSTM in the process of feature extraction or retrieving features from news. Therefore, a combination of CNN and LSTM is often used to exploit the advantages of each method [16].

By combining CNN and LSTM, news is fed into a deep learning model and both are obtained simultaneously. The CNN and LSTM processes are combined to produce classification predictions. This combined approach demonstrates higher accuracy than when the two methods are run separately.

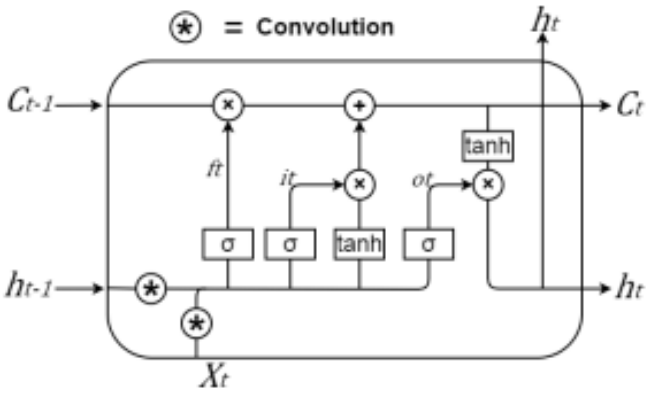

Figure 1. C-LSTM diagram

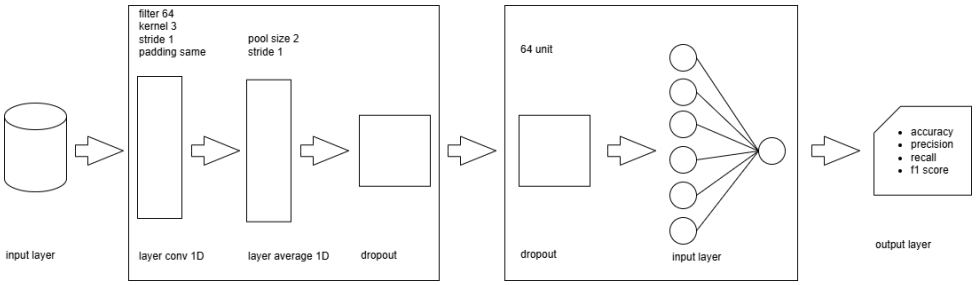

Figure 2. C-LSTM Model with Word2Vec Representation [11]

The LSTM model can be combined with a convolution process. This model is called C-LSTM. C-LSTM is almost the same as a regular LSTM, the difference being that the matrix multiplication in LSTM is replaced with a convolution operation on each gate. The C-LSTM diagram is as shown in Fig. 1. Based on Fig. 2. in the C-LSTM model with a modified Word2Vec representation from previous research [16]. The C-LSTM model uses convolution and pooling layers to extract features from the input data. Next, the results from the CNN will be fed into the LSTM. LSTM is used to process the input data from the results of the CNN and continued using fully connected + ReLu. Then the results of the LSTM will be used to produce accuracy, precision, recall, and f1-score values.

System Architecture

This chapter explains the stages of the research, from data collection to system implementation with Input Process Output (IPO), as shown in Fig. 3.

Fig. 3 shows the system architecture (IPO) where there are research steps starting from data collection from the detik.com site. After the data is collected, the data will be labeled to be grouped into several categories. After the data is labeled, the Pre-processing stage continues. In the Pre-processing stage there are 4 stages, namely Cleaning, Case Folding, tokenizing, and Stopword Removal. Data that has passed the Pre-processing process will continue to the Feature Extraction stage, namely Word2Vec with the CBOW architecture where the results of the Pre-processing in the form of words will be processed in vector form. Next, the data that has been converted into vector form will be divided into training data and testing data. The data will be divided into 80% as training data and 20% as testing data. At this stage, the data that has been separated into training data and test data will be classified into the C-LSTM model. The C-LSTM model is trained with the training data, after which the test data is fed into the trained C-LSTM model. The trained C-LSTM model will then be evaluated using test data. After the evaluation process is complete, the model will produce accuracy, precision, recall, and f1-score.

Dataset

The first stage is data collection as input for the research. The dataset used is the result of crawling using tourism keywords include tags information from the detik.com news portal, with a total of 5261 news documents. This news text is then saved in a comma-separated value (CSV) file. Saving to a CSV file makes it easier to read news documents in the text pre-processing stage. At the data stage, the news text labels are divided into four categories based on article tags, namely "Natural Tourism", "Artificial Tourism", "Cultural Tourism", "Non-Tourism". Can be seen in Table 2. Data was taken from October 16, 2023 to November 20, 2023. The data can be accessed at the link datasets.

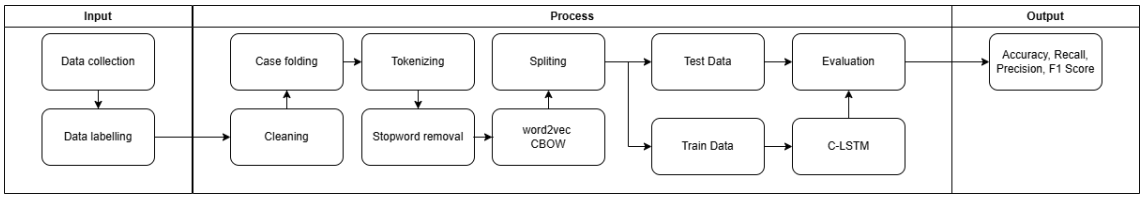

Figure 3. Input Process Output (IPO)

Table 2. Number of data for each category

No	*News Category*	*Total*
1.	Natural tourism	807
2.	Artificial Tourism	1441
3.	Cultural Tourism	1168
4.	Not Tourism	1845
Total		5261

Table 2 shows the number of each news category that has been obtained with a total of 5,261 tourism news data, there are four news categories used in this study, namely natural tourism, artificial tourism, cultural tourism and non-tourism. News categories are determined based on the tag information on the article provided by the author. The next process involves experts (from the Bangkalan Tourism Office) in the news category labeling process.

Based on Fig. 2 in the C-LSTM model that has been modified from previous research [16]. In the C-LSTM model, the input comes from the embedding layer generated by Word2Vec (CBOW) to convert text into numeric vectors. This method converts text into high-dimensional numeric vectors that capture the semantic relationships and deeper meanings between words. By providing more accurate word representations, CBOW helps improve classification accuracy without increasing the computational burden, which is particularly useful for limited dataset with diverse content. Next, the CNN layer extracts spatial features through Conv1D (64 filters, kernel 3, ReLu, padding same) and MaxPooling (pool size 2) to reduce the feature dimension. The results are processed by LSTM (128 units) to understand the order and context of words in the text, then passed to the dense and dropout layers to prevent overfitting. The model finally produces tourism news classification output that is evaluated using accuracy, precision, recall, and F1-score.

Test Scenario

The test scenario was conducted to answer the research questions. To identify model performance issues, including computation, accuracy, precision, recall, and f1-score, a training process was conducted using a baseline model using C-LSTM. The CNN parameters used in this test can be seen in Table 3 [16].

The parameters for LSTM classification used in testing are taken from previous research where the batch sizes used are 32, 64, and 128. Where a smaller batch size will produce more batches, when the amount of data processed remains the same. Similarly to the batch size, the learning rate used is 0.001 and 0.0001. The epochs used are 150 and 200 [16]. Using the accuracy, precision, recall, and F1-score matrices on the test data for each model. As seen in Table 4.

Table 3. Parameters on CNN [16]

Parameter	Test
Convolutional layer	*Filter =64* *Kernel = 3* *Padding = same* *ReLu*
Pooling	*Max pooling, size pooling =2, stride =1*

Table 4. Parameters in LSTM [16]

Testing	*epoch*	*Batch size*	*Learning rate*
1	150	32	0.001
		64	
		128	0.0001
2	200	32	0.001
		64	
		128	0.0001

3 Results and Discussions

Classification of C-LSTM Methods

In the test scenario results, the best value was searched with epoch [150, 200], batch size [32, 64, 128], and learning rate [0.001, 0.0001]. In this training, the accuracy obtained after evaluation by finding the best value of the epoch, batch size, and learning rate that had been determined was around 94%, where the highest accuracy was obtained when using a combination of epoch value = [200], batch size = [64], and learning rate = [0.001] with an estimated time of 1140 seconds. The fastest combination of execution was epoch

value = [200], batch size = [128], and learning rate = [0.0001] as much as 640 seconds. The results of finding the best epoch value can be seen in Table 5.

The confusion matrix of the test results with C-LSTM on each parameter with the best accuracy can be seen in Fig. 5. By looking at this confusion matrix, it can be understood that the model predicts the correct and incorrect categories in each test. Fig. 5 illustrates the performance of the classification model using epoch 200 in four different categories. For category 1, the model successfully identified 204 data points correctly as category 1 (True Positives) and only misidentified 9 data points (False Negative) and 13 data points (False Positive). In addition, the model correctly identified 1213 data points as not being in category 1 (True Negatives). Similar performance was seen in category 2 with 380 True Positives, 15 False Positives, 1018 True Negatives, and 32 False Negatives. In category 3 with 304 True Positives, 35 False Positives, 1078 True Negatives, and 13 False Negatives. Finally, for category 4, the model showed 465 True Positives, 23 False Positives, 919 True Negatives, and 32 False Negatives.

Table 5. Testing Scenario

Epoch	***Batch size***	***Learning rate***	***Time (second)***	***accuracy***
150	32	0.001	1260	90%
150	32	0.0001	1120	92%
150	64	0.001	850	93%
150	64	0.0001	916	90%
150	128	0.001	916	88%
150	128	0.0001	911	82%
200	32	0.001	1260	90%
200	32	0.0001	1020	92%
200	**64**	**0.001**	**1140**	**94%**
200	64	0.0001	1020	90%
200	128	0.001	720	90%
200	128	0.0001	640	88%

After obtaining the test results from all scenarios, a graph was then created for the overall results. The graph of the scenario results can be seen in Fig. 6. Based on Fig. 6, it shows a comparison graph of accuracy (%) from 12 different scenarios in one trial. This graph has a fluctuating trend with the highest accuracy in scenario 3 (93.26%) and scenario 9 (93.9%), and one significant low point in scenario 6 (81.35%). The initial accuracy in scenario 1 starts from 89.8%, then increases until it reaches its first peak in scenario 3. After that, there is a gradual decline until it reaches its lowest point in scenario 6. After this decline, the accuracy increases again and reaches its second peak in scenario 9, before fluctuating again until scenario 12. Changes in each parameter or method used in the scenario have a significant impact on the accuracy of the model.

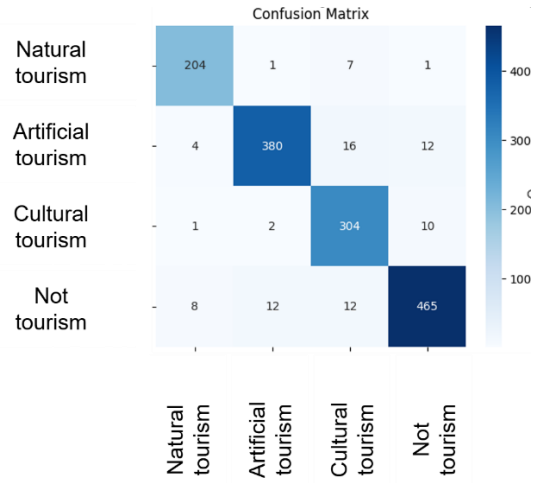

Figure 5. Confusion matrix epoch 200

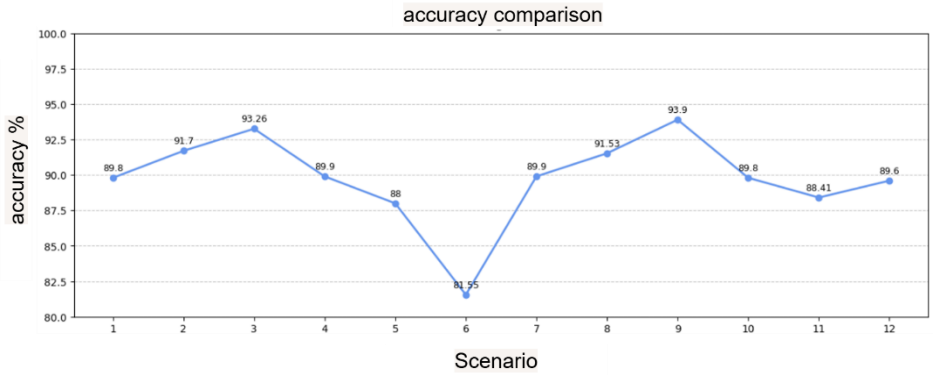

Figure 6. Model Analysis

Scenarios 3 and 9 are the best configurations in this trial test, while scenario 6 shows the worst performance which may require further evaluation of the factors causing the decrease in accuracy.

4 Conclusions

From the research that has been carried out, the results of parameter tuning, the best combination for the model is epoch 200, batch size 64, and learning rate 0.001, which produces 94% accuracy with an execution time of 1140 seconds. Although epoch 200, batch size 128 and learning rate 0.0001 provide faster execution time, the accuracy is the smallest at 82% of epoch 150, batch size 128, and learning rate 0.0001. The scenario result graph also supports that this best combination provides optimal performance. Therefore, to achieve the best results, it is recommended to use epoch 200, batch size 64, and learning rate 0.001, because it provides the best balance between accuracy and execution time.

First, our dataset is limited to a single news article source, which may not represent other regions or languages. In future work, it would be beneficial to collect and analyze datasets from a wider variety of sources to improve the generalization of our method.The resulting model still has prediction errors. These limitations are caused by several factors, such as mixed news content, less specific words, and language ambiguity.

Acknowledgements

Researcher say thank you to the Research and Community Service Institute to the Community (LPPM) University of Trunojoyo Madura, for the opportunity to do research.

References

[1] Haidar Ali Laudza, Julius Tegar Aji Putra, M. Daffa' Atstsaqif, Irvino Kent Setiawan, and Muhamad Sahal Annabil, "Sentiment Analysis and Topic Modelling of Tourist Reviews on Heritage Destinations of Lawang Sewu," *International Journal of Advances in Scientific Research and Engineering (IJASRE), ISSN:2454-8006, DOI: 10.31695/IJASRE*, vol. 11, no. 9, pp. 38–48, Sep. 2025, doi: 10.31695/IJASRE.2025.9.3.

[2] P. Zhang, J. Wang, and R. Li, "Tourism-type ontology framework for tourism-type classification, naming, and knowledge organization," *Heliyon*, vol. 9, no. 4, p. e15192, Apr. 2023, doi: 10.1016/J.HELIYON.2023.E15192.

[3] S. Karmila, V. Intan Ardianti Prodi Telematika Energi, and V. Intan Ardianti, "Metode Latent Dirichlet Allocation Untuk Menentukan Topik Teks Suatu Berita," *Jurnal Informatika dan Komputasi: Media Bahasan, Analisa dan Aplikasi*, vol. 16, no. 01, pp. 36–44, Nov. 2022, doi: 10.56956/JIKI.V16I01.100.

[4] K. Bhowmick and V. Sarvaiya, "A Comparative Study of The Different Classification Algorithms on Football Analytics," *Int. J. Adv. Res. (Indore).*, vol. 9, no. 08, pp. 392–407, Aug. 2021, doi: 10.21474/IJAR01/13280.

[5] Y. Agrawal *et al.*, "Presbyvestibulopathy: Diagnostic criteria Consensus document of the classification committee of the Bárány Society," *J. Vestib. Res.*, vol. 29, no. 4, pp. 161–170, 2019, doi: 10.3233/VES-190672.

[6] Y. Herawati, M. Sa'diyah, A. A. Nugroho, and D. Altin, "The Impact of Tourism Sector Development on the Socio- Economic Conditions of the Community in Supporting Quality Tourism in South Bangka Regency," *International Journal of Research and Innovation in Social Science*, vol. 9, no. 28, pp. 131–136, Dec. 2025, doi: 10.47772/IJRISS.2025.92800014.

[7] S. A. Karunia, "Online News Classification Using Naïve Bayes Classifier With Mutual Information for Feature Selection," 2017. [Online]. Available: https://api.semanticscholar.org/CorpusID:86589834

[8] C. Li, G. Zhan, and Z. Li, "News Text Classification Based on Improved Bi-LSTM-CNN," *Proceedings - 9th International Conference on Information Technology in Medicine and Education, ITME 2018*, pp. 890–893, Dec. 2018, doi: 10.1109/ITME.2018.00199.

[9] M. Shi, K. Wang, and C. Li, "A C-LSTM with word embedding model for news text classification," *Proceedings - 18th IEEE/ACIS International Conference on Computer and*

Information Science, ICIS 2019, pp. 253–257, Jun. 2019, doi: 10.1109/ICIS46139.2019.8940289.

[10] J. Zhou, Z. Ye, S. Zhang, Z. Geng, N. Han, and T. Yang, "Investigating response behavior through TF-IDF and Word2vec text analysis: A case study of PISA 2012 problem-solving process data," *Heliyon*, vol. 10, no. 16, Aug. 2024, doi: 10.1016/j.heliyon.2024.e35945.

[11] J. Amalia, J. Pakpahan, M. Pakpahan, Y. Panjaitan, F. Informatika dan Teknik Elektro, and I. Teknologi Del, "Model Klasifikasi Berita Palsu Menggunakan Bidirectional LSTM dan Word2vec sebagai Vektorisasi," *JATISI*, vol. 9, no. 4, pp. 3319–3331, Dec. 2022, doi: 10.35957/JATISI.V9I4.1332.

[12] R. Alroobaea, "An Empirical Deep Learning Approach for Arabic News Classification," *International Journal of Advanced Computer Science and Applications*, vol. 14, no. 6, pp. 1048–1055, Jun. 2023, doi: 10.14569/IJACSA.2023.01406112.

[13] E. M. Sirait, R. Silalahi, A. A. Tambunan, and J. Amalia, "News Classification Using Bidirectional Long Short Term Memory and GloVe," *Sinkron*, vol. 9, no. 1, pp. 112–124, Jan. 2024, doi: 10.33395/SINKRON.V9I1.13005.

[14] J. Li, Y. Xu, and H. Shi, "Bidirectional LSTM with Hierarchical Attention for Text Classification," *Proceedings of 2019 IEEE 4th Advanced Information Technology, Electronic and Automation Control Conference, IAEAC 2019*, pp. 456–459, Dec. 2019, doi: 10.1109/IAEAC47372.2019.8997969.

[15] D. Sultan, M. Mendes, A. Kassenkhan, and O. Akylbekov, "Hybrid CNN-LSTM Network for Cyberbullying Detection on Social Networks using Textual Contents," *International Journal of Advanced Computer Science and Applications*, vol. 14, no. 9, pp. 748–756, 2023, doi: 10.14569/IJACSA.2023.0140978.

[16] Y. Widhiyasana, T. Semiawan, I. Gibran, A. Mudzakir, and M. R. Noor, "Penerapan Convolutional Long Short-Term Memory untuk Klasifikasi Teks Berita Bahasa Indonesia," *Jurnal Nasional Teknik Elektro dan Teknologi Informasi*, vol. 10, no. 4, pp. 354–361, Nov. 2021, doi: 10.22146/JNTETI.V10I4.2438.

[17] M. R. F. Kamarula and N. Rochmawati, “Perbandingan CNN dan Bi-LSTM pada Analisis Sentimen dan Emosi Masyarakat Indonesia Di Media Sosial Twitter Selama Pandemik Covid-19 yang Menggunakan Metode Word2vec,” *Jurnal Informatika dan Komputasi Sains (JINACS)*, vol. 4, no. 2, pp. 219–228, 2022, doi: 10.26740/jinacs.v4n02.p219-228.

This page intentionally left blank

IJASST
International Journal of
Applied Sciences and Smart Technologies
p-ISSN 2655-8564, e-ISSN 2685-943, pp. 169-182, 2026

Volume 08
Issue 01

Psychrometric Performance of the Air Dehumidifier Base Clothes Dryer

Wibowo Kusbandono[1 *], Prasetyadi [1], Nico Ndaru Pratama[1], Doddy Purwadianto[1], Rines[1], Y.B Lukiyanto[1], I.G.K Puja[1], Michael Seen[1], Budi Setyahandana[1]

[1]*Department of Mechanical Engineering, Facultyof Science and Technology, Sanata Dharma University, Yogyakarta, Indonesia*

[*]*Corresponding Author: bowo@usd.ac.id*

(Received 06-05-2026; Revised 18-05-2026; Accepted 19-05-2026)

Abstract
Drying clothes with dehumidifier machine and additional IR light experiments were conducted to show the psychrometric performance of dehumidification drying. Experiment of dehumidification drying 7.07 kg wet clothes to 4,78 kg dry clothes and 9.9 kg wet clothes to 7.67 kg dry clothes were applied. Variation of 715 W dehumidifier and 375 W IR were conducted. Measurement of room and environment temperatures and humidity were performed. The results show that additional IR make the drying process faster. However, it reduces drying effectivity. The efficiencies of drying are 109%, 96%, 100%, and 79% for drying 4.78 kg dry clothes with dehumidifier, drying 4.78 kg dry clothes with dehumidifier + IR, drying 7.67 kg dry clothes with dehumidifier, and drying 7.67 kg dry clothes with dehumidifier + IR. The numbers also reveal need of adopting drying COP using closed loop heat pump dehumidification to be ratio of heating and cooling energy over the supplied energy plus one.

Keywords: Clothes Dryer 1, COP 2, Dehumidifier 3

1 Introduction

Drying is a process of removing water content from solid material with heat and mass transfer process technique. It is applied in many activities, from body drying to food processing in industries. People need drying in food processing for preserving vegetable, fruits, fish and meat, grain, herbs, and spices [1], [2], [3], [4]. In production and maintenance of furniture, kitchen equipment, drying is important factor [5]. The activity is also a process that people conduct for preparing building materials such as timber and

bricks [6]. In clothing, drying is applied for production and maintenance processes [7]. In clothes production, the drying process is applied for raw material processing, dying, and maintenance of the products.

Many drying processes are based on heating the product and lowering the humidity of the circumstance. Solar drying is very popular due to its cost and simplicity. People do not need to pay fuel for it and it can be done without any special equipment to allow the process happens. Kiln is applicable for many drying processes and has wide range of temperature [8], [9], [10]. A kiln can be applied for food processing with temperature controlled to be less than 50oC to raw material drying such as cement production with temperature of 800oC. The other common drying methods are hot air drying [11], ultra-sound dryer [12], [13], refrigerated and freeze drying [14], [15], dehumidification drying [16] and any other methods. Generally, most of the drying process consists of application of low humidity air which has less moisture pressure than the water pressure of the material surface. This basic principle allows the water vaporized easily.

Dehumidification is a potential method for clothes drying due to its low energy cost. Purwadianta and Sugiharto [7] reported performance of the dehumidification drying for clothes with variation of clothes number and type of flowing air. With 200 W R134a heat pump of 7.94 COP for drying room of 1.39 m3, 15 – 45 cotton clothes of 2.55 – 6.51 kg need drying time of 210 – 450 minutes. However, a deeper analysis concerning about the drying effectivity and psychrometric of the drying performance was still out of the discussion. The gap will be the main topic of this work. The report will also include effect of IR additional heat comparing to the absence of the equipment for clothes drying.

To show the psychrometric drying performance, the rest of the article is composed of methodology presenting theory of dehumidifying drying, analysis of the psychrometric, vapor compression heat pump, experiment setup, and the proposed performance analysis. The third section is about the data of the experiment and its discussion. Final part of the presentation is the conclusion.

2 Material and Methods

The drying effectivity consists of parameters regarding the process. It considers time for drying, used energy for drying, human resource necessity, and product quality. Those parameters co-exist and are intertwined. In small scale clothes drying, the aspects of human necessity, product quality, and time can be neglected. Household drying can be done by a single worker with equal product quality. Therefore, energy analysis becomes the focus of the discussion with energy effectivity for drying as the main parameter.

The method of the work consists principle of dehumidifying drying theory, psychrometer analysis, experiment setup, and parameters of the drying effectivity. The dehumidifying theory shows the theory of convective drying applied in clothes. The psychrometer analysis focuses on theory of the humidity relation to the air condition. The experiment setup mentions about the equipment where the experiment was conducted and it's the variation of the conditions. The parameter explains relation of energy and drying load.

A. Dehumidification drying

Dehumidifying drying is a method for removing water from the solid called moisture content using reduction of the vapor pressure reduction. This vapor pressure decrease can be made using some methods. To reduce the vapor pressure, desiccant and heat pump approaches can be applied. Desiccant can be used to be adsorbent, and the moist becomes the adsorbate. While the moist of the air is adsorbed into the desiccant, the vapor pressure of air decreases. This decrease allows the moist on the surface of the adsorbate releases the moist content easily. The desiccant method has drawback of releasing the water content from the adsorbent which need special treatment. The heat pump uses the psychrometric principle for reducing the moisture pressure of the air. To reduce the vapor pressure, the evaporator of the heat pump reduces the air temperature beyond its saturated temperature. The condensed water is collected and the air is recirculated. The drawback of the method is energy need during the cycle. The cycle of condensation means latent energy of the water released.

The dehumidifying drying principle is shown in Figure 1. The Fig. 1 (a) and Fig. 1(b) are the desiccant dehumidifier drying and the heat pump dehumidifier drying, respectively. Fig. 1 (a) shows that ambient air is transformed into hot dry air as the air supply for drying room. The desiccant is used to adsorb the moist of the air. The heater is applied for increasing the temperature. The Fig. 1 (b) mentions that air is circulated through heat pump element and drying room. The air from drying room (return air) is dehumidified using evaporator to be dry cool air. Then its temperature is increased through condenser and supplied to drying room as hot dry air.

B. Psychrometric process of closed loop heat pump dehumidification drying

The drying process of dehumidification drying consists of supplying hot dry air, removing water from the load, and removing water from the air. In closed loop heat pump dehumidifying drying process, the evaporator is applied to reduce the moist of the air. It provides dry cool air as consequences of the condensation process in evaporator. Then the condenser increases its temperature to provide hot dry air as the supply air for drying room. In drying room, the hot dry air absorbs the moist from the object. General psychrometric process of closed loop dehumidifying drying process is shown in Fig. 2.

The Fig. 2 shows that cool dry air, hot dry air, and the return air are numbered (1), (2), and (3) respectively. The process of (1) to (2) happens by condenser.

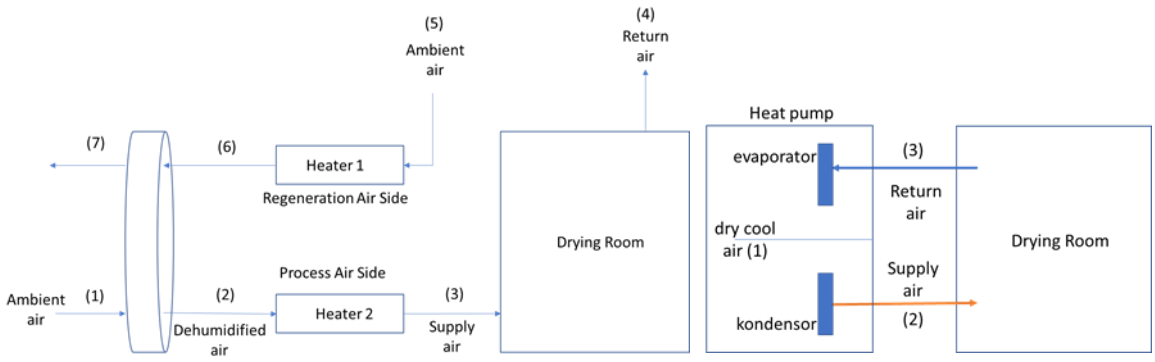

Figure 1. (a) Schematic desiccant dehumidifying drying process.[17], [18]; (b) Schematic closed loop heat pump dehumidifying drying process.

The process of (2) to (3) takes place in drying room as the drying process. Accordingly, the process of (3) to (1) is located at the evaporator. At this point, temperature is decreased to (3a) where some of the moist the condensed through decreasing temperature to be point (1). The condensed moist is equal to enthalpy difference of the point (3a) and (1).

C. The experiment setup.

To earn the psychrometric performance of the humidifying drying for clothes, the equipment is setup as shown in Fig. 3. A built-up dehumidifier with capacity of 30 l/day is applied instead of customized vapor compression machine. The machine uses R290 refrigerant with operating pressure of 2.6 MPa and 1.0 MPa for the high and low pressures, respectively. The compressor rate is 715 W with the current of 3.2 A. The inlet of the wet air flow is on the back part of the apparatus.

The experiment was conducted for 25 and 35 cotton clothes. The dry weight of the clothes were 4.78 kg and 6.76 kg, for 25 and 35 clothes, respectively. Meanwhile, the weight of 25 clothes was 7.07 and the weight of 35 wet clothes was 9.90. The wet clothes were put into the drying room and the machine was started.

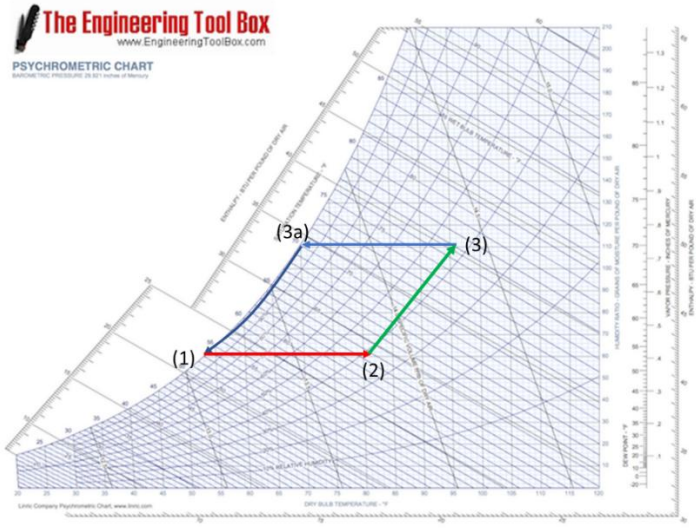

Figure 2. The psychrometric process of closed loop heat pump dehumidifying drying regarding the air as shown in Figure 1(b).

Every 30 minutes, the measured weight of the clothes was recorded in addition to wet bulb and dry bulb temperatures of drying room and the environment. The condensed water was collected and its volume was measured at the same time. The temperature of inlet air and the outlet air were also recorded. The experiments were stopped after the targeted dry clothes weight reached.

In addition to the dehumidification drying process, IR light was applied for every condition to inject additional heat to the room. The IR light was provided by an IR lamp located above the clothes. The light had rate of 375 W. Therefore, variation of the experiment can be seen in Table 1.

D. Performance Measurement

The drying performance was measured as ratio of drying capacity and energy rate injected to the drying system. The drying efficiency is defined as ratio of energy for evaporating the water from the clothes to energy supplied for the system. The total energy for evaporating is calculated from the water latent proportional to amount of energy as

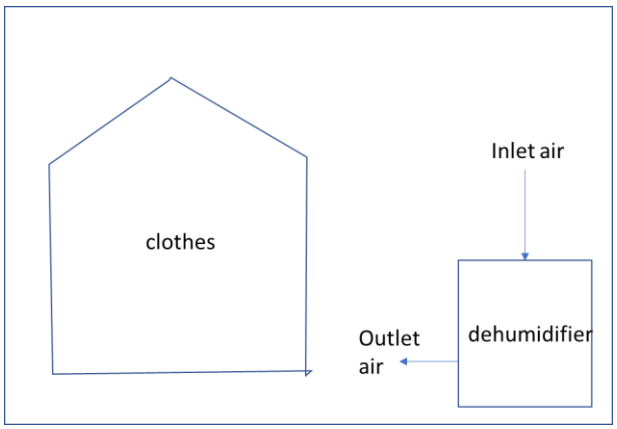

Figure 3. The apparatus setup of the experiment.

Table 1. Experiment condition setup

Load Variation	Dryer Variation
25 clothes, 4.78 kg dry	715 W dehumidifier
35 clothes, 6.76 kg dry	715 W dehumidifier
25 clothes, 4.78 kg dry	715 W dehumidifier + 375 W IR
35 clothes, 6.76 kg dry	715 W dehumidifier + 375 W IR

shown in equation (1), with E, m_v, and L_v as the energy of vaporization, vapor mass, and vaporization latent, respectively. The vapor mass is assumed as amount of water loss from the clothes.

$$E_v = m_v * L_v \tag{1}$$

Then, the efficiency of drying is calculated using equation (2), with E_s as the energy supplied to the system for operation.

$$\eta = \frac{E_v}{E_s} * 100\% \tag{2}$$

The energy supplied to the system for operation is calculated according to equation (3), with P_d, and P_{iR} are the power of dehumidifier, and IR lamp, respectively.

$$E_s = \sum_{i=1}^{n} \left(P_d + P_{iR} \right) \Delta t \tag{3}$$

The Δt is time scale measurement (30 minutes) and n as the amount of measuring time until the dry weight clothes reached.

3 Results and Discussions

The temperatures of the dehumidifier rooms, temperature of the environment, and the condensed water collected in every 30 minutes for 4.78 kg, and 6.76kg clothes are presented in Table 2, and Table 3 below, respectively. The tables reveal that more clothes need more time to finish for drying. It is confirmed that more clothes related to more water to dry up. The dry bulb drying room temperatures tend to increase as time going up. It also takes place for the wet bulb. The environment temperature affects the drying room temperature. If the environment temperature increase, the drying room temperature will increase as well. It shows that heat release from drying room to the environment affects the drying temperature.

The accumulative water condensed during drying process for 4.78 kg, and 6.76 kg clothes are shown in Fig. 4. The table mentions that condensed water capacity decreases

as time going up. The water content of the clothes was 2.29 and 3.29 litres for 4.78 and 3.14 for 4,78 kg and 6.76 clothes. Among the evaporated water, 1.96 and 2.62 litres were condensed. It was 85% and 83% of the water evaporated in drying process. Results and discussions are written with times new roman 12 pt, 1 (one) column, 1.5 space density one space density, on A4 paper with a top-left margin of 3 cm and bottom-right 3.5 cm.

Table 2. Drying condition of 4.78 kg clothes

Time (min)	Drying Room Temperature (C)		Environment Temperature (C)		Water Condensed (kg)
	Tdb	Twb	Tdb	Twb	
0	36.4	29.9	26.5	25.5	0.000
30	42.4	34.9	27.0	25.0	0.545
60	45.4	36.4	27.5	25.0	0.545
90	45.4	36.4	27.5	24.5	0.405
120	47.4	34.9	27.5	24.5	0.330

Table 3. Drying condition of 6.76 kg clothes

Time (min)	Drying Room Temperature (C)		Environment Temperature (C)		Water Condensed (kg)
	Tdb	Twb	Tdb	Twb	
0	33.0	40.5	27.0	24.0	0,000
30	39.0	46.0	27.0	24.0	0,555
60	39.5	47.0	28.0	24.0	0,535
90	42.0	51.0	28.0	24.0	0,540
120	46.5	59.0	27.5	24.5	0,470
150	43.0	55.0	25.0	25.0	0,335
180	45.5	55.5	25.5	25.0	0,185

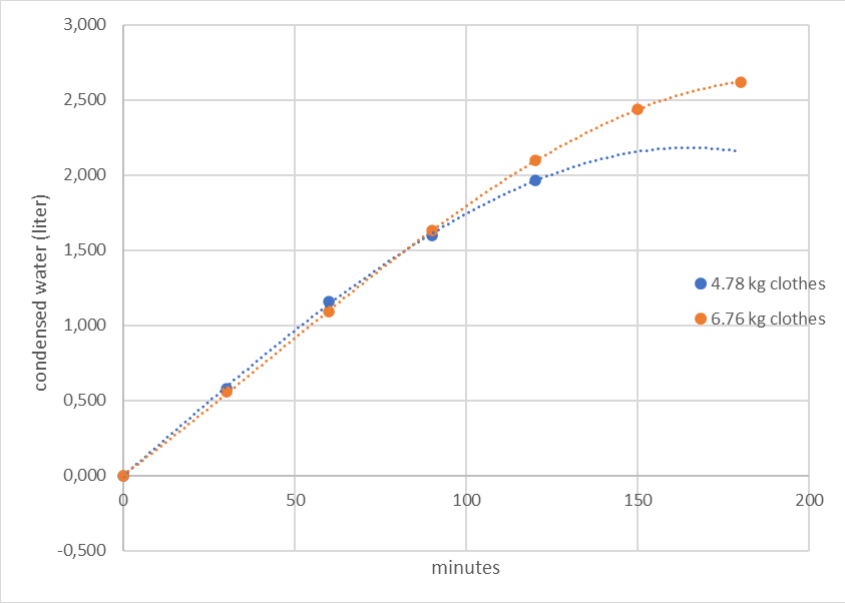

Figure 4. Water condensed during the drying process.

Additional IR Light of 375 W reduced time of drying by 30 minutes. The drying time of 4.78 kg clothes became 120 minutes using additional 375 W IR light. Without IR light, the drying time was 150 minutes. The similar pattern happens to 6.76 kg clothes. Time for drying with 375 W IR light got less to be 150 minutes from 180 minutes without IR. The cumulative condensed water according time for drying using 715 W dehumidifier with additional 375 IR Light is shown in Fig. 5.

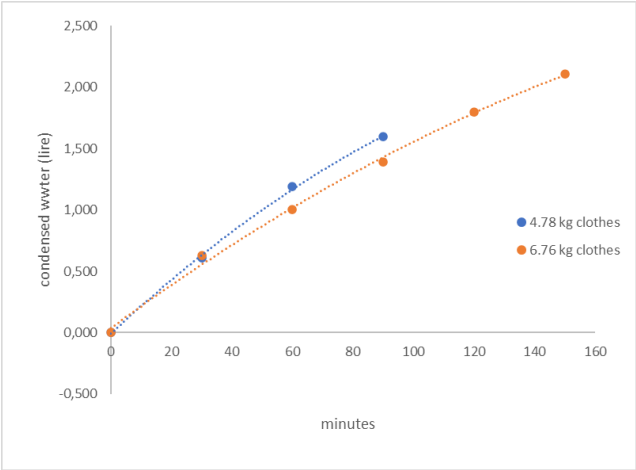

Figure 5. The condensed water accumulation during drying using dehumidifier and additional 375 W IR light.

Considering energy of drying as the main parameter for performance, it can be said that drying using 715 W dehumidifier without additional 375 W IR light is more efficient than drying the same clothes using dehumidifier with additional 375 W IR light. The comparison of the energy efficiency as proposed in equation (2) is shown in Table 4. The 100% or more mentioned that there is regenerative process which mentions that the condensation taking place at the evaporator increase effectivity of drying process. In term of effectivity, the drying energy as evaporative energy needed for 4.78 kg clothes are 2248 kJ/kg and 2570 kJ/kg water for 715 W dehumidifier and 715 W dehumidifier + 375 W IR light, respectively. Accordingly, the 6.76 kg clothes need 2455 kJ/kg and 3119 kJ/kg drying energy for 715 W dehumidifier and 715 W dehumidifier + 375 W IR light drying respectively. It shows that 715 W dehumidifier with additional 375 W IR light needs more energy to evaporate every kg water from the wet clothes than 715 W dehumidifier only.

Table 4. Drying condition and energy efficiency

Drying equipment	4.78 kg clothes	6.76 clothes
715 W dehumidifier	109%	100%
715 W dehumidifier + 375 W IR light	96%	79%

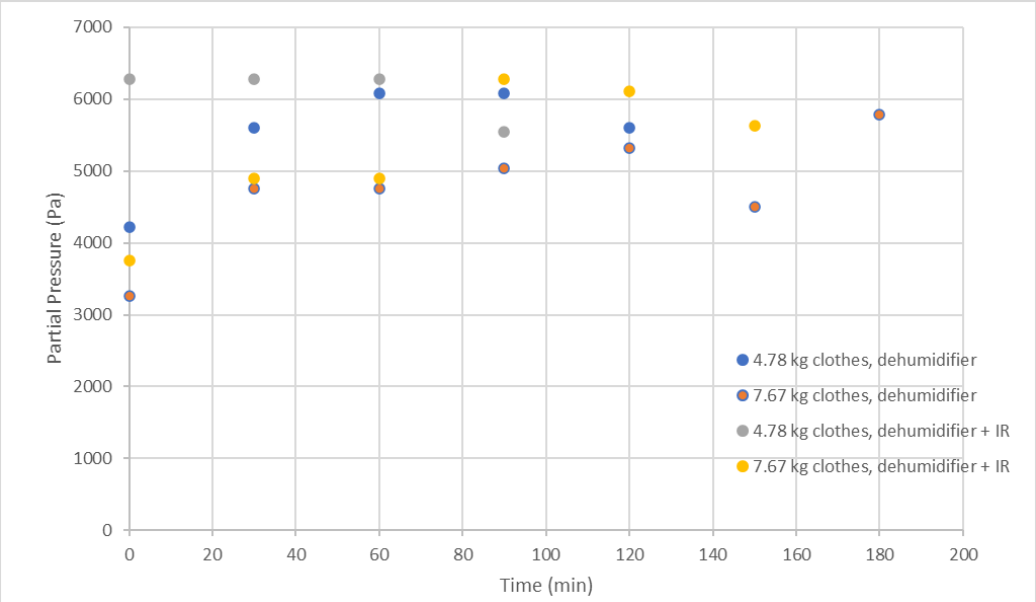

Figure 6. Partial Pressure of the moist in the drying room.

Fig. 6 explains the reason of energy effectivity of the equipment. The drying system with additional IR makes more moist content in the air of the drying room. In average, partial pressures of the moist in drying process of 4.78 kg are 5515 Pa and 6096 Pa of respective dehumidifier and dehumidifier + IR. Accordingly, the 7.67 kg clothes have 4775 Pa and 5262 Pa partial moist pressure in drying room with dehumidifier and dehumidifier + IR, respectively. Even the 7.67 kg clothes have less partial moist pressure, they attribute higher relative humidity than clothes of 4.78 kg. The partial humidity in average for the systems are 60.2%, 58.4%, 56.8%, and 48.9% in drying 4.78 kg clothes with dehumidifier only, 7.67 kg clothes with dehumidifier only, 4.78 kg clothes with dehumidifier + IR, and 7.67 kg clothes with dehumidifier + IR, respectively. It exposes the reason dehumidifier + IR needs less time than dehumidifier only even the absolute partial pressure is higher than drying with the dehumidifier only.

Air dehumidifier is a common machine for controlling air humidity in a room. It is a kind of heat pump using vapor compression machine working with the inlet air flowing through the evaporator for reducing air humidity and followed by heating up using condenser. The method implying COP of the drying approach as ratio of the combination of evaporator and condenser heat rate over the compressor inlet power. Higher COP means higher effectivity of energy usage during cooling process of air. At the same time, the cooling process implying reducing temperature of the wet air and condensation to the psychrometric system. Accordingly, the condenser releases heat to the air circulated in the drying room. It implies that both cooling process and heating process contribute into drying process. The cooling with absolute moist content reduction, while the heating reduces relative humidity of the circulated air. It is in accordance with the work of Purwadi and Prasetyadi [5].

4 Conclusions

The research mentions that dehumidification work well in drying the clothes with various weight. Generally, the drying time depends on weight of clothes. The efficiency of the energy for drying as ratio of the evaporative drying over supplied energy mentions a tricky condition as more clothes related to less partial pressure but the relative humidity

implying drying time. The efficiencies of drying 4.78 kg clothes with dehumidifier, 4.78 kg clothes with dehumidifier + IR, 7.67 kg clothes with dehumidifier, and 7.67 kg clothes with dehumidifier + IR are 109%, 96%, 100%, and 79%, respectively. The efficiency which is higher than 100% revealed the condensation role for reducing the absolute humidity in dehumidification drying process using heat pump. The results suggest accommodation of heat pump drying process as ratio of cooling and heating energy over the supplied energy plus one.

Acknowledgements

The authors would like to thank Sanata Dharma University for its support in conducting this research

References

[1] S. Salve, A. M. Fulambarkar, and M. Arici, "Experimental studies on drying characteristics of green chilies in a solar dryer," J Ther Eng, vol. 8, no. 5, pp. 1–8, 2022, doi: 10.14744/jten.2022.0000.

[2] G. Dadaev, S. Sultanova, J. Safarov, and Q. Mukhiddinov, "Calculation of the drying process of dietary materials in solar dryers," in E3S Web of Conferences, EDP Sciences, Oct. 2023. doi: 10.1051/e3sconf/202343401035.

[3] N. Ahmed, J. Singh, H. Chauhan, P. Gupta, A. Anjum, and H. Kour, "Different Drying Methods: Their Applications and Recent Advances International Journal of Food Nutrition and Safety, 2013, 4(1): 34-42 International Journal of Food Nutrition and Safety Different Drying Methods: Their Applications and Recent Advances," 2013. [Online]. Available: https://www.researchgate.net/publication/275650176

[4] Y. Çelik and B. B. Kenanoğlu, "The Effect of Different Drying Processes on the Quality of Pepper Seeds Harvested in Uşak Conditions," 2022, [Online]. Available: https://creativecommons.org/licenses/bync/4.0/Availableonlinehttps://dergipark.org.tr/ijafls

[5] P. Kanisius Purwadi and A. Prasetyadi, “Characteristics of Wooden Furniture Drying Machine,” International Journal of Applied Sciences and Smart Technologies, vol. 4, no. 1, pp. 75–88, 2022.

[6] P. Kanisius Purwadi and A. Prasetyadi, “Air Circulation Types on Albizia Chinensis Refrigerated Drying.”

[7] D. Purwadianto and B. Sugiharto, “Performance of Low Power Electric Energy Clothes Dryers for Households,” International Journal of Applied Sciences and Smart Technologies, vol. 5, no. 1, pp. 39–54.

[8] A. S. Mujumdar, “Handbook of Industrial Drying.”

[9] S. K. Amponsah, H. Asare, H. Okyere, J. O. Owusu-Asante, E. Minkah, and H. K. Ketemepi, “Performance Characterization of a Locally Developed Fish Smoke-Drying Kiln for Charcoal and Briquette,” Journal of Agricultural Science, vol. 14, no. 11, p. 43, Oct. 2022, doi: 10.5539/jas.v14n11p43.

[10] H. S. Lee et al., “Design of a modified charcoal production kiln for thermal therapy and evaluation of the charcoal characteristics from this kiln,” Bioresources, vol. 14, no. 3, pp. 7275–7284, Aug. 2019, doi: 10.15376/biores.14.3.7275-7284.

[11] X. Song et al., “Effect of Hot-Air Drying Conditions on the Drying Efficiency and Performance of a Waterborne Coating on Pine Wood,” Forests, vol. 14, no. 9, Sep. 2023, doi: 10.3390/f14091752.

[12] S. Tüfekçi and S. G. Özkal, “Application of Ultrasound in Food Drying,” Pamukkale University Journal of Engineering Sciences, vol. 21, no. 9, pp. 408–413, 2015, doi: 10.5505/pajes.2015.05902.

[13] F. Salehi, "Effects of ultrasonic pretreatment and drying approaches on the drying kinetics and rehydration of sprouted mung beans," Legume Science, 2023, doi: 10.1002/leg3.211.

[14] A. M. N. Lal et al., "A comparison of the Refrigerated Adsorption Drying of Daucus carota with fluidized bed drying," Lwt, vol. 154, p. 112749, 2022, doi: 10.1016/j.lwt.2021.112749.

[15] J. Garcia-Noguera, F. I. P. Oliveira, C. L. Weller, S. Rodrigues, and F. A. N. Fernandes, "Effect of ultrasonic and osmotic dehydration pre-treatments on the colour of freeze dried strawberries," J Food Sci Technol, vol. 51, no. 9, pp. 2222–2227, 2014, doi: 10.1007/s13197-012-0724-x.

[16] A. Prasetyadi, R. Sambada, and P. K. Purwadi, "Development of a new fast drying determinant method using resistivity for the industry of coconut shell charcoal briquettes," Eastern-European Journal of Enterprise Technologies, vol. 1, no. 8 (127), pp. 58–66, Feb. 2024, doi: 10.15587/1729-4061.2024.297541.

[17] S. Hanif, M. Sultan, T. Miyazaki, and S. Koyama, "Investigation of energy-efficient solid desiccant system for the drying of wheat grains," International Journal of Agricultural and Biological Engineering, vol. 12, no. 1, pp. 221–228, 2019, doi: 10.25165/j.ijabe.20191201.3854.

[18] M. Sultan, S. Hanif, T. Miyazaki, S. Koyama, and B. Road, "Evaluation of Solid Desiccant based Drying System for Energy-Efficient Drying of Agricultural Products," 2018, doi: 10.11322/tjsrae.18-40AC_OA.

IJASST International Journal of Applied Sciences and Smart Technologies
Volume 08
Issue 01
p-ISSN 2655-8564, e-ISSN 2685-943, pp. 183-202, 2026

Principal Component Analysis-Driven Feature Reduction for Predicting Coffee Quality Using a Machine Learning Approach

Siti Yuliyanti[1 *], Heni Sulastri [2], Sakifah [3]

[1]*Department of Informatics, Faculty of Engineering, Siliwangi University, Tasikmalaya, West Java, Indonesia*
[2]*Department of System Information, Faculty of Engineering, Siliwangi University, Tasikmalaya, West Java, Indonesia*
[3]*Department of Digital Banking and Finance, Faculty of Economics and Business, Siliwangi University, Tasikmalaya, West Java, Indonesia*
[*]*Corresponding Author: sitiyuliyanti@unsil.id*

(Received 29-09-2025; Revised 13-01-2026; Accepted 09-04-2026)

Abstract

Coffee quality assessment using a machine learning approach faces major challenges, including high data dimensionality and redundancy between features. Therefore, PCA is proposed as a feature reduction technique to improve the efficiency and accuracy of coffee quality prediction models. The research phase began with data acquisition, data cleaning, feature engineering, explanatory data analysis, testing the normalization of coffee parameter profiles, implementing PCA on Random Forest and XGBoost models, and then evaluating model performance. Model evaluation using MAE and MAPE showed that Random Forest provided more precise predictions than XGBoost, particularly when applying PCA. This resulted in a 39% performance increase for Random Forest from 0.11903 to 0.08542 and an 8% increase for XGBoost, shifting the score from 0.12511 to 0.11570. Prediction visualization reinforced the consistency and precision of the Random Forest model, regardless of whether PCA was used. The findings of this study highlight the importance of feature cleaning and engineering, and the role of PCA in improving the precision of coffee quality predictions. The use of the Random Forest model with PCA is recommended as an efficient method for modeling the quality of Arabica coffee, taking into account sensory and environmental factors.

Keywords: Coffee Quality, Feature Reduction, Pearson Correlation, PCA, Principal Component

1 Introduction

Arabica coffee (Coffea arabica) is the most highly valued coffee variety globally, accounting for over 60% of global coffee production. It possesses high economic value, with a complex flavor and distinctive aroma influenced by environmental, genetic, and post-harvest factors. Traditionally, coffee quality evaluation is conducted through a

cupping process by trained panelists, but this method is subjective, time-consuming, and inconsistent across evaluators[1], [2]. Therefore, a data-driven approach using artificial intelligence is increasingly needed to improve efficiency and objectivity in coffee quality analysis. One challenge in coffee quality data analysis is the high dimensionality of the data, encompassing sensory, chemical, and physical features. To address this, Principal Component Analysis (PCA) is used as a dimensionality reduction technique to remove redundancy and retain the most significant information in the form of principal components [3]. PCA can help simplify input data while improving the performance of classification models.

Machine learning approaches have been widely used to automatically classify coffee quality based on sensory, physical, or chemical data[4], [5]. Support Vector Machines and Random Forests are capable of classifying coffee based on geographic origin with high accuracy. However, one of the main challenges in coffee data processing is the large number of features, which can lead to overfitting and decreased predictive performance[6]. The Random Forest and Extreme Gradient Boosting (XGBoost) algorithms have proven effective for classifying complex and heterogeneous data, including in the agriculture and food sectors. Random Forest is a decision tree-based ensemble algorithm that works by randomly constructing multiple trees and combining their results through voting. Its advantages lie in its resistance to overfitting and its ability to handle nonlinear data[7], [8]. Meanwhile, XGBoost is one of the most advanced and efficient boosting algorithms designed for high performance, large scalability, and high accuracy. Compared to traditional boosting algorithms, XGBoost offers optimizations in terms of regularization, execution speed, and overfitting control[9], [10]. In previous studies, XGBoost demonstrated superiority in the quality classification of agricultural products, including coffee, with higher accuracy than other models[11], [12].

Previous studies have only used coffee datasets from a single country or region [13], [14], so the prediction models have not been tested on global Arabica coffee data, which has high genetic, environmental, and post-harvest diversity. Previous studies have rarely conducted direct comparisons between the Random Forest and XGBoost algorithms in the context of sensory data-based coffee quality prediction, especially after dimensionality reduction using PCA[3], [15], [16]. Most studies focus solely on

prediction accuracy, without considering model efficiency and its potential application in automated quality assessment systems in the coffee industry. No research has yet tested the combination of PCA as the primary feature extraction with Random Forest and XGBoost, and applied it to global Arabica data from various countries (with differences in flavor, aroma, and body).

This study aims to develop a quality classification model for Arabica coffee from various countries by applying PCA as a feature extraction stage, which is then used as input to the Random Forest and XGBoost models. The global dataset used includes sensory data from cupping results such as aroma, flavor, acidity, body, and aftertaste. Evaluation was conducted to measure the performance of both models in predicting coffee quality based on the results of dimensionality reduction. This approach is expected to produce an accurate, efficient, and reliable coffee quality evaluation system, as well as serve as a basis for the development of an automated coffee grading system on a global industrial scale.

2 Material and Methods

This research methodology outlines the research stages, into several parts as illustrated in Fig. 1.

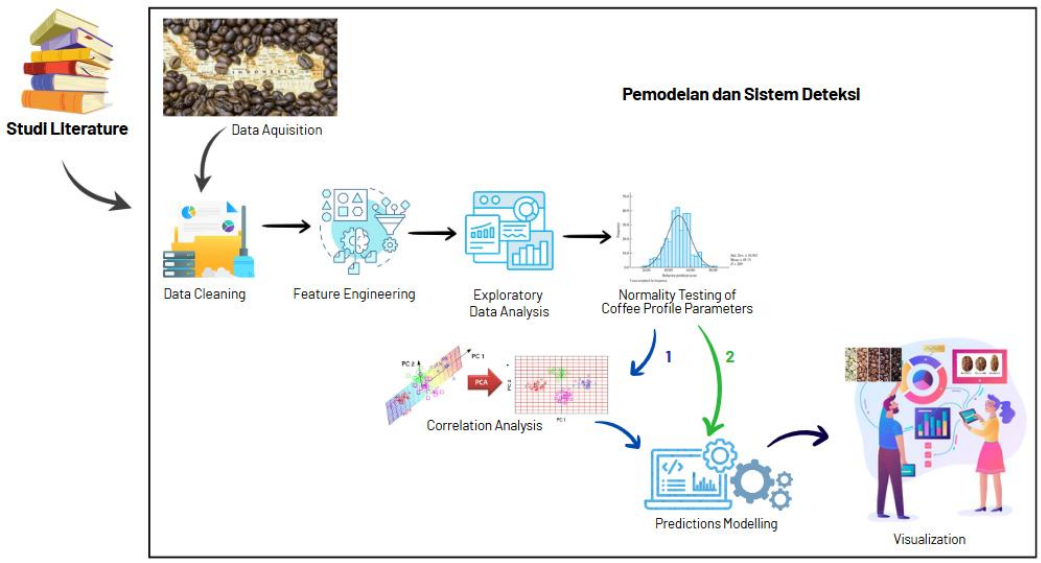

Figure 1. Framework Research

Data Acquisition

The dataset used in this study was obtained from the Coffee Quality Institute (CQI), which provides publicly accessible Arabica coffee cupping data collected under standardized evaluation protocols. The dataset is available for academic research purposes under open access terms. After data cleaning and filtering, the final dataset consisted of 207 samples with 41 original features, including sensory attributes (e.g., aroma, flavor, aftertaste), environmental factors (e.g., altitude), and processing information. PCA was applied only at the modeling stage, reducing the feature space to 2–3 principal components while preserving the original dataset dimensionality for exploratory and correlation analysis.

A limitation of this dataset is its moderate sample size relative to the number of sensory features, which motivates the use of dimensionality reduction to prevent overfitting.

Data Cleansing

Data cleansing is essential for accurate statistical calculations and machine learning models. The steps include:

1. Feature scaling and feature selection: filling all empty cells with mode data, standardizing the scale for a value, and eliminating redundant columns to speed up the data analysis process[17], [18].
2. Altitude: cleaning numeric data defined as strings. The altitude feature is used in models to predict flavor profiles or quality scores. For example, coffee from Garut, at an altitude of 1,400 m above sea level, likely has higher acidity and aroma than coffee from lower areas. Based on the values listed in all cells in the "Altitude" column, we can see that the values are a minimum value. This is not good for data analysis and model building. The middle value of the range is used to replace it.

Feature Engineering

This research adds new features that may be useful for the model creation process, based on existing data. For the harvest year data, we will use the first year[19], [20]. This is so that when calculating the coffee bean age, we can consider the possibility of rotting beans first. The data does not specify the harvest date; therefore, we will assume that all

harvests occurred simultaneously on January 1, 2021, or 2022 and 2023. This simplifies the calculation of coffee age. Next, perform the calculation as below. Next, process the coffee plantation height data, categorizing the height of the farm based on the dataset. After the data cleaning and feature engineering process, the dataset, consisting of 270 rows and 41 columns, became 207 rows and 2 columns.

Exploratory Data Analysis

Well-organized data makes the EDA process more effective. Initially, summary statistics are shown for the complete dataset, indicating the type of data and the quantity of missing (null) entries in the dataframe. The examination proceeds with visual representations of coffee variety information from each nation to identify which country boasts the highest diversity of coffee varieties.

Normality Test for Coffee Profile Parameters

Normality assessments are conducted on each coffee profile characteristic, including acidity, sweetness, balance, and so forth. This step is vital for every data point, confirming a suitable distribution with the help of the Shapiro-Wilk normality test, especially since a vast amount of data is sourced from worldwide datasets[4], [12].

Correlation Analysis of Factors Influencing Coffee Quality

A Pearson correlation analysis was carried out to assess how strongly the sensory attributes observed during cupping are related to the overall coffee quality rating (Total Cup Points)[21]. The Pearson correlation coefficient (r) for every combination of parameters was determined using Equation 1. Visualization is done using heatmaps to facilitate identification of relationship patterns between features.

$$r_{xy} = \frac{\sum_{i=0}^{n}(x_i-\bar{x})(y_i-\bar{y})}{\sqrt{\sum_{i=1}^{n}(x_i-\bar{x})}.\sqrt{\sum_{i=1}^{n}(x_i-\bar{y})^2}.} \quad (1)$$

r_{xy} : correlation coefficient between variables x and y

$\bar{x}, \bar{y}$: average of each variable

n : number of data, the r value ranges from −1 to +1

Principal Component Analysis (PCA)

Principal Component Analysis (PCA) is applied as a key dimensionality reduction technique to extract the most informative components from high-dimensional coffee sensory data[3], [15]. The original dataset consists of several correlated sensory attributes—such as aroma, flavor, aftertaste, acidity, body, balance, and overall score—which, while individually informative, tend to exhibit multicollinearity and redundancy when used collectively as input to a machine learning model. PCA transforms these original variables into a new set of uncorrelated variables known as principal components (PCs), which are ordered by the amount of variance they capture from the original data. The first step is to standardize the data so that all features have the same scale (mean = 0, std = 1) using Equation 1.

$$Z_{ij} = \frac{Xij - \mu j}{\sigma_j} \quad (1)$$

X_{ij} : value of the j-th feature from the i-th observation

μ_j : mean of the j-th feature

σ_j : sigma_j

σj : standard deviation of the j-th feature

Next, determine the Covariance matrix using Equation 2, in which z represents the normalized data matrix (mean = 0), C denotes the covariance matrix, n indicates the number of samples, and p refers to the number of features.

$$C = \frac{1}{n-1} Z^T Z \quad (2)$$

After obtaining the covariance value, calculate the eigenvalues (λ) and eigenvectors (*e*) using Equation 3. Then, project the principal component data using the projection matrix or principal components using Equation 4. Where Z is the standardized data matrix, E_k: the p × k eigenvector matrix, and PCS is the result of transforming the data into a new *k*-dimensional space.

$$C_e = \lambda_e \quad (3)$$

$$PCS = Z.E_k \quad (4)$$

Random Forest (RF) Modeling

Random Forest is a group learning method that creates several decision trees during the training phase, producing class predictions for classification purposes. This approach enhances prediction accuracy by combining the outcomes of numerous weak learners, each trained on a randomly selected subset of the data and characteristics (bagging)[8]. The RF model utilizes principal components derived from PCA as input variables, which helps minimize redundancy and boosts computational effectiveness[22]. Tuning of hyperparameters is conducted to refine key settings, including the number of trees (n_estimators), maximum allowable depth (max_depth), and the number of features evaluated at each split (max_features). This model showcases strong generalization skills and is less likely to face overfitting due to its smoothing properties.

Extreme Gradient Boosting (XGBoost) Modeling

XGBoost is a sophisticated version of gradient boosting that constructs trees one after another, with each new tree focusing on correcting the mistakes of the preceding one. This model incorporates a regularized learning approach to limit overfitting and supports parallel processing along with effective management of missing data[22]. The features transformed by PCA were employed to train the XGBoost model, and a grid search was carried out to fine-tune important parameters like the learning rate (eta), maximum depth of the trees (max_depth), and the number of boosting iterations (n_estimators). XGBoost showed remarkable performance in both training and validation phases, excelling in recognizing intricate feature interactions and non-linearities in the dataset.

Model Evaluation

Performance assessment in this research aims to analyze the use of Random Forest and XGBoost, both with and without PCA, utilizing MAE to quantify the average absolute deviation between actual and predicted figures, and MAPE (Mean Absolute Percentage Error) serves as a measure of the average absolute error expressed as a percentage of the actual value[23], [24].

3 Results and Discussions

The process of cleaning data involves an altitude characteristic that is utilized in the model to forecast taste characteristics or quality ratings. For instance, coffee sourced from Garut, situated at 1,400 meters above sea level, typically possesses greater acidity and fragrance compared to coffee harvested from lower altitudes. By examining the figures in the "Altitude" column, we can observe a variation of values present. Such discrepancies are not optimal for analysis and model creation. Therefore, we will replace the varied values with the middle value of the range. Additionally, due to the lengthy nature of the task, we will eliminate certain columns deemed unnecessary and subsequently review for any parameters that contain null values or vacant cells. The empty entries will be filled using the mode of the data. For instance, in this analysis, the "Processing Method" column contains missing entries. We will use mode imputation to address these gaps. At this stage, the aim is to display the unique values, maximum values, and minimum values from the "Altitude" column. To facilitate this, we assign each altitude a category, namely Highlands, Mid-Altitude, and Lowland, as shown in Table 1.

Exploratory data analysis in this study visualizes how many coffee varieties there are in each country, as shown in Fig. 2. Fig. 2 (a) shows the number of coffee varieties in each country, and (b) displays a bar graph illustrating the variety of coffee types found across three elevation groups: lowland, mid-altitude, and highland.

Table 1. Altitude category labeling table

ID	Altitude	Altitude_Category
0	1815	Highlands
1	1200	Mid-Altitude
2	1300	Highlands
...	...	...
206	1300	Highlands
207	1200	Mid-Altitude

The horizontal axis (X) denotes the elevation groups, while the vertical axis (Y) indicates how many coffee varieties have been documented within each group. The depicted data suggests that the total number of coffee varieties tends to rise as altitude increases. The lowland group contains the fewest varieties, approximately 5. In the mid-altitude range, this amount jumps significantly to around 18 varieties. The highland group shows the greatest diversity, with about 35 varieties recorded. This observation implies that regions with higher altitudes tend to exhibit a richer diversity of coffee types. This trend can be linked to the more advantageous agroclimatic conditions found in highland areas, such as cooler temperatures, reduced temperature variations, and improved drainage in the soil. These factors may create a more consistent and suitable environment for a variety of coffee plants, especially the Coffea arabica species, which is recognized for its ability to thrive at specific elevations. Overall, this chart provides evidence supporting the idea that altitude is a significant ecological element affecting the distribution and variety of coffee species within a particular area. These findings hold valuable significance for strategies aimed at conserving coffee genetic resources and for the planning of cultivation practices that foster the growth of elite varieties suited to particular geographic conditions.

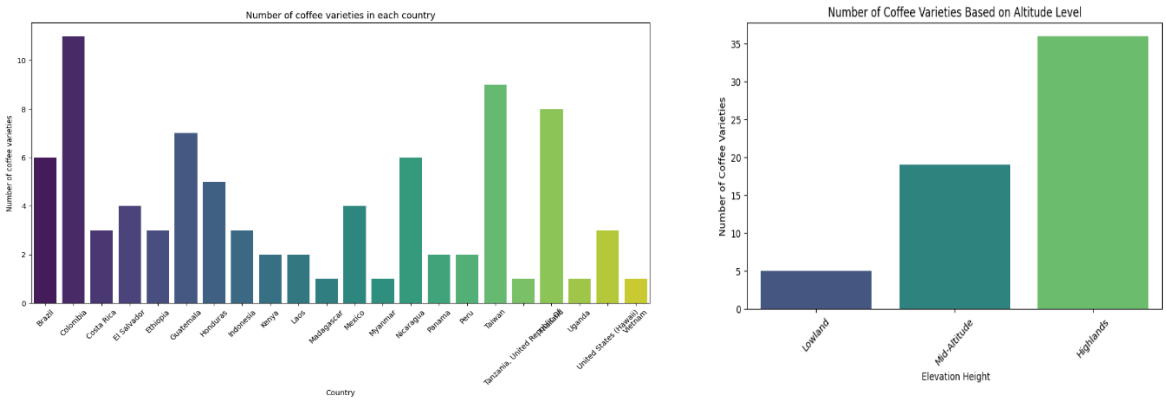

(b)

Figure 2. Visualisasi exploratory data analysis: (a) Number of coffee varieties in each country (b) Number of coffee varieties based on altitude level

The stages of the coffee profile parameter normality test using the Kolmogorov-Smirnov test are to check whether each column in the dataset is normally distributed or not. Then, a correlation analysis is performed on the numerical parameters and total cup points (coffee value), consisting of sweetness, acidity, aroma, flavor, aftertaste, body, balance, uniformity, and total cup points. The Pearson correlation is then calculated and visualized in a heatmap in Fig. 3.

Fig. 3 displays a heatmap that illustrates the correlations among various coffee quality evaluation factors, which consist of sweetness, acidity, aroma, flavor, aftertaste, body, balance, uniformity, and total cup points. The correlation coefficients were derived using the Pearson correlation technique, with values ranging from -1 to 1, signifying both the intensity and direction of the linear relationships among the factors. The findings reveal that flavor has the strongest correlation with total cup points, scoring 0.93, closely followed by aftertaste (0.92), balance (0.92), acidity (0.89), and sweetness (0.89). This suggests that flavor, aftertaste, and balance are key elements in assessing the overall quality of coffee flavor. Additionally, uniformity demonstrated a very weak correlation with total cup points (0.00) as well as with other factors, implying that it has little impact on the overall cup rating.

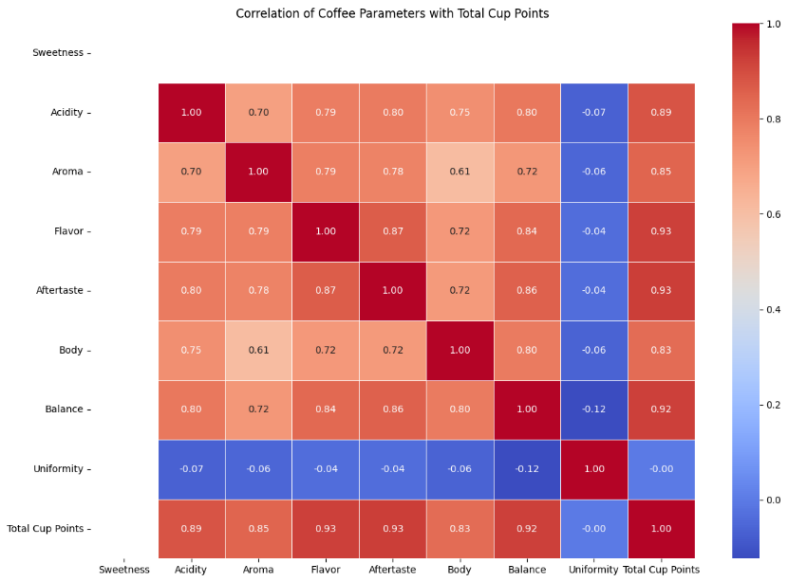

Figure 3. Correlation of coffee parameters with total cup points

At the same time, a reasonably strong positive correlation was observed between flavor and aftertaste (0.87), along with a notable correlation between balance and aftertaste (0.86), underscoring the interconnections in sensory attributes related to flavor and balance during coffee assessment.

Cumulative Variance Analysis Based on Principal Component Analysis (PCA) in Fig. 4 presents a plot of the cumulative variance explained by each principal component based on the results of a PCA analysis of coffee quality feature data.

The purpose of this visualization is to determine the optimal number of principal components capable of representing the information in the initial data with minimal information loss. The analysis results show that the first principal component explains approximately 74% of the total variance in the dataset. The addition of the second component increases the cumulative explained variance to 87%, while the first three components account for over 90% of the total variance. Furthermore, six principal components successfully explain almost all of the variance in the data (approaching 100%). The curve shown shows a decreasing pattern in the rate of variance increase, with an elbow visible at the third to fourth components. This indicates that most of the information in the dataset can be effectively represented using only three to four principal components without significant information loss.

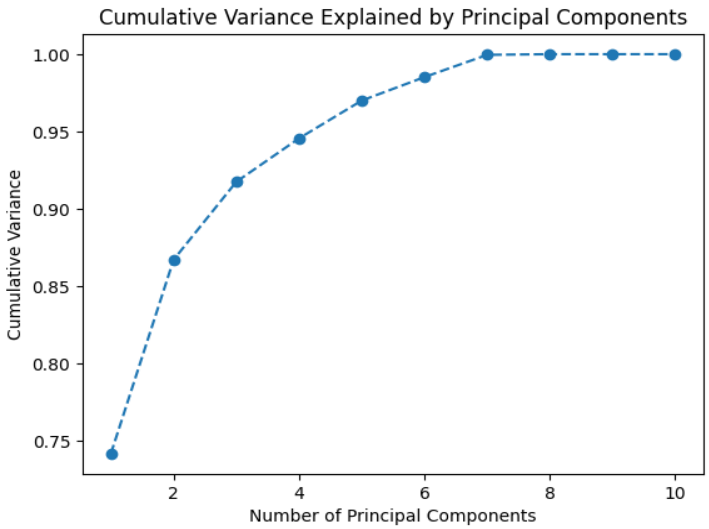

Figure 4. Result: cumulative variance explained by PCA

Thus, these results can be used as a basis in the dimensionality reduction process to simplify data, speed up the computational process, and reduce the risk of overfitting in subsequent modeling, such as classification or regression using machine learning algorithms.

The following step involves choosing the number of components for PCA. In this research, two primary components were utilized since the cumulative variance chart indicates that the initial two components account for roughly 87% of the total variance, whereas including the first three components surpasses 90%. As a result, opting for three components is deemed better to preserve adequate information from the original dataset, particularly when using the Random Forest and XGBoost methods. The PCA results for the explained variance ratio reveal that PC1, PC2, and PC3 have values of 0.741, 0. 26, and 0.050, respectively. Explained Variance Ratio is used in dimensional analysis in Principal Component Analysis (PCA).

Based on Table 2, the PCA analysis results show that the first principal component (PC1) explains 74.1% of the total variance in the data, while the second component (PC2) accounts for 26.0%. The combination of these two components accounts for approximately 100% of the information in the dataset. The third component (PC3) only explains an additional 5.0% of the variance and is therefore considered less significant. Therefore, the first two principal components are considered representative enough for use in further analysis and dimensionality reduction. The modeling phase begins with dividing the training and test data and scaling based on the PCA-reduced dataset.

Principal Component Analysis (PCA) is theoretically justified in this study due to the strong multicollinearity observed among sensory attributes such as flavor, aftertaste, balance, and acidity, as evidenced by Pearson correlation coefficients exceeding 0.85. High feature correlation can degrade the performance of tree-based ensemble models by introducing redundant splits and unstable decision boundaries.

PCA addresses this issue by projecting the original correlated feature space into a lower-dimensional orthogonal space defined by eigenvectors of the covariance matrix. Each principal component corresponds to an eigenvector associated with an eigenvalue that quantifies the amount of variance captured. According to Kaiser’s criterion,

components with eigenvalues greater than 1 should be retained, while the scree plot elbow method helps identify the point of diminishing returns in variance contribution. Based on both the scree plot elbow observed between PC2 and PC3 and the Kaiser criterion, retaining two principal components is statistically sufficient, capturing over 87% of the total variance without introducing noise from lower-variance components.

X is the principal feature, and y is the target prediction, which is then evaluated using MAE and MAPE for both the Random Forest and XGBoost models. The Random Forest model uses n_estimators = 300 and random_state = 42, where n_estimators is the number of decision trees in the Random Forest. The more trees, the more stable and accurate the prediction results, up to a certain point. The optimal random_state in previous machine learning research approaches averages 42. At the same time, the settings implemented in XGBoost include learning_rate set at 0.1, n_estimators at 300, random_state as 42, reg_lambda valued at 2, and verbosity level of 2.

Table 3 displays model performance using MAPE and MAE, which aim to assess, compare, and communicate the accuracy of regression models quantitatively and interpretably. The combination of the two provides a comprehensive picture of how well the model performs in a real-world context.

Table 2. Eigenvalues and Cumulative Explained Variance

PC	Eigenvalue	Explained Variance (%)	Cumulative (%)
PC1	5.93	74.1	74.1
PC2	2.08	26.0	100
PC3	0.41	5.0	105

Table 3. Evaluation of model performance

Evaluation	non-PCA		PCA	
	Random Forest	XGBoost	Random Forest	XGBoost
MAPE	0.11903	0.12511	0.08542	0.11570
MAE	0.09974	0.10464	0.07186	0.09735

Based on the findings under conditions without PCA, the Random Forest model exhibited a MAPE of 0. 11903 and an MAE of 0. 09974, while XGBoost had a MAPE of 0. 12511 and an MAE of 0. 10464. This suggests that, when dimensionality reduction isn't applied, Random Forest outperforms XGBoost in both absolute and relative error metrics. After implementing PCA, there was a noticeable enhancement in the performance of both models, especially for Random Forest. The Random Forest model utilizing PCA achieved the lowest MAPE of 0. 08542 and an MAE of 0. 07186, demonstrating a substantial improvement in accuracy compared to its performance without PCA. On the other hand, the XGBoost model also showed a minor improvement in accuracy with PCA, as reflected by a drop in MAPE to 0. 11570 and a decrease in MAE to 0. 09735, although it remained less accurate than Random Forest in both scenarios. In summary, these outcomes suggest that employing PCA as a method for dimensionality reduction enhances the performance of the Random Forest model by 39% and the XGBoost model by 8%. Additionally, Random Forest consistently achieves better results than XGBoost across all evaluation metrics in every scenario. These results indicate that, for the dataset evaluated, Random Forest demonstrates greater adaptability to the data structure both prior to and following the PCA transformation, making it a more dependable option for the predicted task at hand.

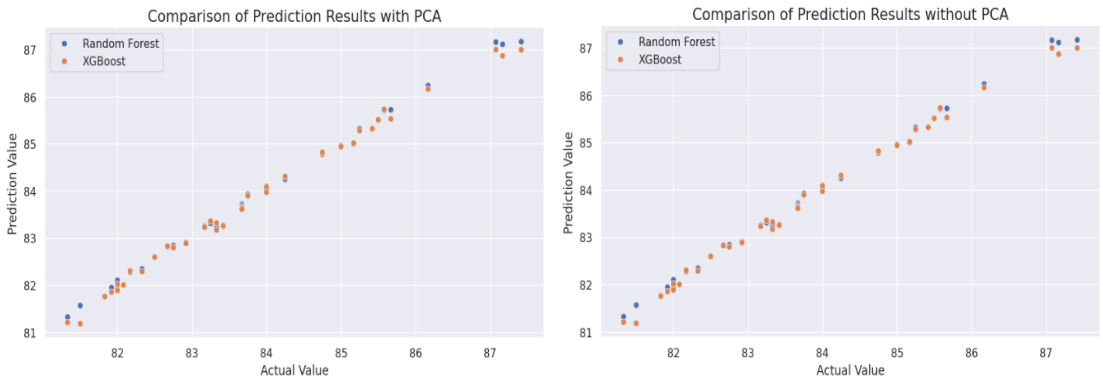

Figure 5. Visualisasi comparison of prediction: (a) model using PCA (b) model without PCA

Fig. 5 (a) illustrates a comparison of the results obtained from two regression techniques, Random Forest and XGBoost, about the real values after utilizing Principal Component Analysis (PCA) for reducing dimensions. The graph shows the correspondence between the actual values on the X-axis and the predicted values on the Y-axis, with each dot representing an individual observation. The blue dots signify the forecasts made by the Random Forest model, whereas the orange dots indicate predictions from XGBoost. Overall, both models display a linear pattern and move closer to the identity line (which signifies a perfect fit), suggesting that their predictions tend to be fairly accurate when compared to the actual data. Nonetheless, it appears that the forecasting points from the Random Forest model generally fall nearer to the real values than those from XGBoost, which sometimes shows slightly greater discrepancies. This graph reinforces prior quantitative results shown in Table 3, which indicated that Random Forest yielded lower MAE and MAPE figures after PCA was applied. Consequently, it can be deduced that the Random Forest model not only has superior numerical effectiveness but also offers greater consistency in prediction stability against the real values represented in this graph. Additionally, this visualization verifies that implementing PCA does not significantly weaken the model's predictive power; rather, it enhances prediction accuracy, particularly for the Random Forest model.

Fig. 5(b) presents a visualization of the comparison of the prediction results between the Random Forest and XGBoost models against the actual values, without Principal Component Analysis (PCA). This graph displays the relationship between the actual values (X-axis) and the predicted values generated by both models (Y-axis), where each point represents a prediction from a single observation. The blue color represents the prediction results from the Random Forest model, while the orange color represents the prediction results from XGBoost. In general, both models show a fairly accurate and linear trend in their predictions relative to the actual values. Most data points are quite close to the diagonal line (an imaginary line representing perfect prediction), indicating that both Random Forest and XGBoost have good predictive capabilities without dimensionality reduction. However, a visual comparison shows that Random Forest slightly outperforms in terms of prediction consistency, especially in the mid-to-high range. This aligns with the quantitative evaluation results in Table 3, where Random

Forest recorded lower MAPE (0.11903) and MAE (0.09974) values compared to XGBoost (MAPE 0.12511, MAE 0.10464) in the scenario without PCA. This visualization reinforces the interpretation that although both models perform reasonably well without feature transformation, Random Forest provides more stable and accurate performance than XGBoost in representing the relationship between input features and target outputs.

4 Conclusions

The data cleaning phase of this research incorporated altitude features that affect the flavor characteristics and quality of coffee. Variations in altitude measurements that were inconsistent were substituted with the median of their respective altitude groups to assist in analysis. Furthermore, irrelevant columns were eliminated, and any gaps in the data were filled in using the most frequent value to ensure uniformity in the dataset. The preliminary data analysis indicated that as elevation increased, there was a rise in the variety of coffee types, with the highest diversity found in elevated areas. This trend likely stems from the favorable climate and agricultural conditions in highlands, which promote the cultivation of high-quality Coffea arabica types. Normality assessments and Pearson correlation analyses revealed a strong positive relationship between flavor characteristics such as taste, aftertaste, and balance with total cup points, underscoring the significance of these factors in assessing overall coffee quality. The Principal Component Analysis (PCA) demonstrated that three primary components accounted for more than 90% of the data's variance, showing that PCA is effective for reducing the complexity of the data without significant information loss. During the modeling phase, both Random Forest and XGBoost regression models were evaluated, with and without PCA.

The performance analysis using MAPE and MAE indicated that Random Forest consistently performed better than XGBoost. The introduction of PCA enhanced the accuracy of the Random Forest model by 39%, while XGBoost's accuracy increased by 8%. Visual representations of the predictions affirmed that the Random Forest model offered more precise and reliable forecasts compared to XGBoost, whether PCA was applied or not. These results suggest that Random Forest is a more trustworthy method

for forecasting coffee quality in this dataset, with PCA proving to be an effective approach for enhancing model accuracy and computational speed.

Acknowledgements

The research team would like to express its gratitude to LPPM Siliwangi University for the assistance and funding for the 2025 budget year so that this research can be completed and published.

References

[1] V. Sari, F. Firdausi, and Y. Azhar, "Perbandingan Prediksi Kualitas Kopi Arabika dengan Menggunakan Algoritma SGD, Random Forest dan Naive Bayes," *Edumatic J. Pendidik. Inform.*, vol. 4, no. 2, pp. 1–9, 2020, doi: 10.29408/edumatic.v4i2.2202.

[2] R. Rusinek *et al.*, "How to Identify Roast Defects in Coffee Beans Based on the Volatile Compound Profile," *Molecules*, vol. 27, no. 23, pp. 1–13, 2022, doi: 10.3390/molecules27238530.

[3] F. H. Alkallas, A. M. Mostafa, E. A. Rashed, A. B. G. Trabelsi, M. A. I. Essawy, and R. A. Rezk, "Authentication of Roasted Coffee Beans via LIBS: Statistical Principal Component Analysis," *Coatings*, vol. 13, no. 10, 2023, doi: 10.3390/coatings13101790.

[4] Kamil Fadli, "Pengolahan Citra Digital Menggunakan Metode Yolo Untuk Mendeteksi Kualitas Dari Biji Kopi Berbasis Android," *J. Artif. Intel. dan Sist. Penunjang Keputusan*, vol. 1, no. 1, pp. 120–125, 2023, [Online]. Available: https://jurnalmahasiswa.com/index.php/aidanspk

[5] S. Asghar, J. Choi, D. Yoon, and J. Byun, "Spatial pseudo-labeling for semi-supervised facies classification," *J. Pet. Sci. Eng.*, vol. 195, Dec. 2020, doi:

10.1016/j.petrol.2020.107834.

[6] V. No, D. Gusmaliza, and S. Aminah, "Edumatic : Jurnal Pendidikan Informatika Sistem Identifikasi Kualitas Biji Kopi Robusta berbasis Image Processing dengan Support Vector Machine," vol. 8, no. 2, pp. 744–753, 2024, doi: 10.29408/edumatic.v8i2.28008.

[7] Rizkya Nur Amalda, "Decision Tree: Algoritma C5.0." [Online]. Available: https://rizkyanuramalda.medium.com/decision-tree-algoritma-c5-0-52e76661a31d

[8] K. Ciptady, M. Harahap, J. Jonvin, Y. Ndruru, and I. Ibadurrahman, "Prediksi Kualitas Kopi Dengan Algoritma Random Forest Melalui Pendekatan Data Science," *Data Sci. Indones.*, vol. 2, no. 1, 2022, doi: 10.47709/dsi.v2i1.1708.

[9] G. Idoje, C. Mouroutoglou, T. Dagiuklas, A. Kotsiras, I. Muddesar, and P. Alefragkis, "Comparative analysis of data using machine learning algorithms: A hydroponics system use case," *Smart Agric. Technol.*, vol. 4, Aug. 2023, doi: 10.1016/j.atech.2023.100207.

[10] T. Firmansyah, R. Kurniawan, and A. T. Hidayat, "Klasfikasi Tingkat Kematangan Roasting Biji Kopi Berbasis Deep Learning dengan Arsitektur MobileNet," vol. 6, no. 2, pp. 1432–1442, 2025, doi: 10.47065/josh.v6i2.6811.

[11] D. Herdhiansyah, S. Sudarmi, S. Sakir, and A. Asriani, "Analisis Faktor Prioritas Pengembangan Komoditas Perkebunan Unggulan Dengan Metode Ahp (Analtycal Hierarchy Process," *J. Tek. Pertan. Lampung (Journal Agric. Eng.*, vol. 10, no. 2, p. 239, 2021, doi: 10.23960/jtep-l.v10i2.239-251.

[12] S. Wahyudi, "Aplikasi Deteksi Kualitas Biji Kopi Menggunakan Metode Histogram Equalization Berbasis Android," vol. 2, no. 1, pp. 50–56, 2018.

[13] K. Przybył *et al.*, "Application of Machine Learning to Assess the Quality of Food Products—Case Study: Coffee Bean," *Appl. Sci.*, vol. 13, no. 19, 2023, doi: 10.3390/app131910786.

[14] J. A. Suarez-Peña, H. F. Lobaton-García, J. I. Rodríguez-Molano, and W. C. Rodriguez-Vazquez, *Machine Learning for Cup Coffee Quality Prediction from Green and Roasted Coffee Beans Features*, vol. 1274 CCIS, no. October. Springer International Publishing, 2020. doi: 10.1007/978-3-030-61834-6_5.

[15] N. Neighbor *et al.*, "Jurnal Darma Agung Implementasi Algoritma Principal Component Analysis (PCA) dan K -," pp. 1–10, 2023.

[16] R. P. Tanjung and D. W. Utomo, "Implementasi Principal Component Analysis (PCA) pada Pengenalan Wajah Resolusi Rendah," vol. 15, no. 01, pp. 109–116, 2024, doi: 10.35970/infotekmesin.v15i1.2148.

[17] A. Z. Putra, C. Chalvin, A. Nurhadi, A. E. Tambun, and S. Defha, "Coffee Quality Prediction with Light Gradient Boosting Machine Algorithm Through Data Science Approach," *Sinkron*, vol. 8, no. 1, pp. 563–573, 2023, doi: 10.33395/sinkron.v8i1.12169.

[18] A. Astaraja, B. S. Syamsudin, M. Diaz, and M. Dhafin, "Optimizing Coffee Ripeness Classification Using Yolov5 for Automated Detection and Sorting," vol. 4, 2025.

[19] A. E. Minarno, M. Fadhlan, Y. Munarko, and R. Chandranegara, "International Journal On Informatics Visualization journal homepage : www.joiv.org/index.php/joiv International Journal On Informatics Visualization Classification of Dermoscopic Images Using CNN-SVM." [Online]. Available: www.joiv.org/index.php/joiv

[20] X. Mu, L. He, P. Heinemann, J. Schupp, and M. Karkee, "Mask R-CNN based apple flower detection and king flower identification for precision pollination," *Smart Agric. Technol.*, vol. 4, Aug. 2023, doi: 10.1016/j.atech.2022.100151.

[21] "Non-destructive method for identification and classific.pdf."

[22] C. H. de Freitas, R. D. Coelho, J. de O. Costa, and P. C. Sentelhas, "Smart Coffee: Machine Learning Techniques for Estimating Arabica Coffee Yield," *AgriEngineering*, vol. 6, no. 4, pp. 4925–4942, 2024, doi: 10.3390/agriengineering6040281.

[23] U. P. Ganesha, "Klasifikasi Kualitas Biji Kopi Robusta Dengan Metode Naive Bayes," vol. 10, pp. 280–289, 2023.

[24] E. Aghdamifar, V. Rasooli Sharabiani, E. Taghinezhad, A. Rezvanivand Fanaei, and M. Szymanek, "Non-destructive method for identification and classification of varieties and quality of coffee beans based on soft computing models using VIS/NIR spectroscopy," *Eur. Food Res. Technol.*, vol. 249, no. 6, pp. 1599–1612, 2023, doi: 10.1007/s00217-023-04240-x.

IJASST
International Journal of
Applied Sciences and Smart Technologies
p-ISSN 2655-8564, e-ISSN 2685-943, pp. 203-238, 2026

Volume 08
Issue 01

A Sub-Saharan African Airport Mechanical Equipment Failure Assessment Using Joint FMECA-GRA Method Based on Technical Process Efficiency

Olanrewaju Samson Omisakin[1], Sunday Ayoola Oke[1*], Adeyinka Oluwo[1], John Rajan[2], Swaminathan Jose[3]

[1]*Department of Mechanical Engineering, University of Lagos, Akoka-Yaba, Lagos, Nigeria*
[2]*School of Mechanical Engineering, Vellore Institute of Technology, Chennai Campus, Chennai, India*
[3]*School of Mechanical Engineering, Vellore Institute of Technology, Vellore Campus, Vellore, India*
[*]*Corresponding author's address: sa_oke@yahoo.com*

(Received 16-10-2025; Revised 26-03-2026; Accepted 09-04-2026)

Abstract

This article establishes how airport ground equipment fails in operations to enhance failure prediction, reduce maintenance and costs. Airports are essential to enhance the economy of a developing country and these failures affect the efficiency of the airport system. Consequently, this paper deals with utilising the risk priority number of equipment failures to create ranks for selected airport ground equipment and study the performance of this equipment using the grey relational analysis. Three methods were established to evaluate the failures of five selected major equipment (elevators, travellator, escalator, baggage handling equipment and air-conditioners): the risk priority number (RPN), RPN with same weights and RPN with different weights for the risk factors. All the methods approved elevator 8, travellator 6, escalator 11, baggage handler 3 and air conditioner 9 as the best, indicating reduced risk factors from the equipment. The worst equipment approved by all the methods are elevator 2, baggage handler 6 and air-conditioner 7. However, while the RPN, and RPN (with an equal weight of risk factors) approve travellator 3 and escalator 9 as the worst equipment, a divergent choice of travellator 1 and escalator 5 is mapped RPN method with different weights for the risk factors as the worst equipment. This work contributes to the airport maintenance literature by applying three models to evaluate the failure of ground equipment in airports to identify equipment that should be given the utmost priority and those that warrant the least attention of the airport maintenance management.

Keywords: Prioritisation, mechanical equipment, airport, aerospace industry, customer service

1 Introduction

Airports in sub-Saharan African countries prioritise excellence in customer service to sustain their continued operations in the face of dwindling economic fortunes in the aerospace industries [1-3]. Traditionally, safety and maintenance of ground equipment which services customers on arrival and departure locations, in the airport, have been the backbone of excellent customer service in the airport [4, 5]. However, the presence of hazards and equipment downtime has constrained the capacity of airports to offer adequate and excellent ground mechanical equipment service to passengers [6, 7]. Consequently, the management of airports and researchers are increasingly promoting safety and effective maintenance of ground mechanical equipment [8, 9]. These activities communicate and support the improvement of safety performance and avoid disrupting service [8, 9].

Moreover, flight passengers in airports are expected to experience superior flight customer service and this experience begins and ends at the airports [3, 6]. While awaiting flights or on arrival from a flight, passengers spend enormous time in the airport and some comfort is expected from the available ground equipment as passengers move through the airport and at the terminal hall [6]. Unfortunately, many airports have poorly implemented maintenance schedules, opening up costly damages to the ground equipment and exposing both passengers and staff of the airport to hazards, which may cause accidents. Therefore, the identification of key failures and trends of ground equipment is crucial for effective maintenance [8]. Consequently, understanding and assessing when the ground equipment would fail is an important issue which should be given utmost attention for improved operational efficiency in airports [8, 10, 11-20]. Currently, in airport maintenance management, enough ground equipment failure information is not frequently available to the maintenance managers and this issue continues to expand with an increase in demand for airport services.

Ground equipment such as air conditioners, baggage handling equipment, vary in age, capacity, usage levels, and the number of maintenance tasks carried out on them. There are no scientific means of even deciding their failure performance; how much time the machine must fail despite the utmost maintenance attention is not known. This

research gap motivates the present investigation to pursue an assessment of the failure behaviour of ground equipment in a case airport. Consequently, the purpose of this paper is to analyse the failure performance of major airport ground equipment using the failure modes effects analysis (FMEA) [21-25] with the grey relational analysis. To achieve this, three methods were developed and used to analyzed the airport ground equipment, namely the risk priority number (RPN) method [8, 10], the grey-RPN with equal weights of the risk factors and the grey-RPN with unequal weights of the risk factors. Five major pieces of equipment were used in the study, namely the elevator, escalator, travellator, baggage handling equipment and air conditioners. For each piece of equipment, the total number in varying capacities and locations within the airport was considered in the analysis. The failure modes of each piece of equipment were assessed based on expert's opinion, handbooks and manuals on these pieces of equipment from the manufacturers.

The application of the three methods yielded ranks, RPN, and grey-RPN values. Ranks provided the most important to the least important failure of the machine and these are varied for each piece of equipment. To evaluate the maximum possible failure of the equipment, the top three failures were identified and matched to the three methods in an eigenvalue determination approach using the matrix method. The determinant of the difference between the three by three matrix containing the topmost failures and the corresponding values of the methods was noted against the product of the lambda and the identity matrix to yield a polynomial of the maximum power of three. The final values were however obtained from these. The eigenvalues of this linear operator on a linear space were determined. The eigenvalues are the highest possible failure level. The principal advantages of the methods include assured effective preventive maintenance planning, minimization of cost, enhanced throughout and minimized equipment downtime.

Briefly mentioned, the survey of airport maintenance literature reveals a prospect to develop a study involving the following scope:

1. An airport field study that exposes ground equipment failures in the developing country context.

2. The choice of ground equipment has limits to escalators, elevators, travellators, baggage handling equipment and air conditioners
3. Failure modes effects and criticality analysis and grey relational analysis are employed as tools for failure assessment.

2 Material and Methods

2.1 Justification for the choice of equipment

In the airport system, there are several categories of ground support equipment. Some of these are luggage trolleys, airport passenger boarding bridges, runway, sweeper, automated aircraft washing, robots, towing tractors, ground power units, elevators, escalators, travelators, air-conditioners and baggage handling equipment (Fig. 1).

However, a problem confronted in this study is to choose the most important equipment with which efforts can be concentrated to reduce failures and enhance their service performance customers. This section provides the essential details to justify the choice of the equipment analyzed in this study. In an airport, the failure of air-conditioners, for example, in the waiting hall is a leading passenger discomfort criterion. Airport air-conditioning system failure in airport terminal buildings may cause major discomfort to passengers. This prompts the maintenance crew and contractors to work in mitigating the effects and repair the cooling system failure. This failure may be due to chiller motors having stopped operating. With failures, temperatures in the building become high and immediate efforts by airport staff may be the use of fans and dehumidifiers to make the airport terminal more comfortable to passengers. To strengthen the choice of the air conditioner as important in the air transport system, looking beyond the terminal one may consider a planes air-conditioner not working. This failure makes breathing difficult for passengers and the pilot may be constrained to ground the plane for passenger safety.

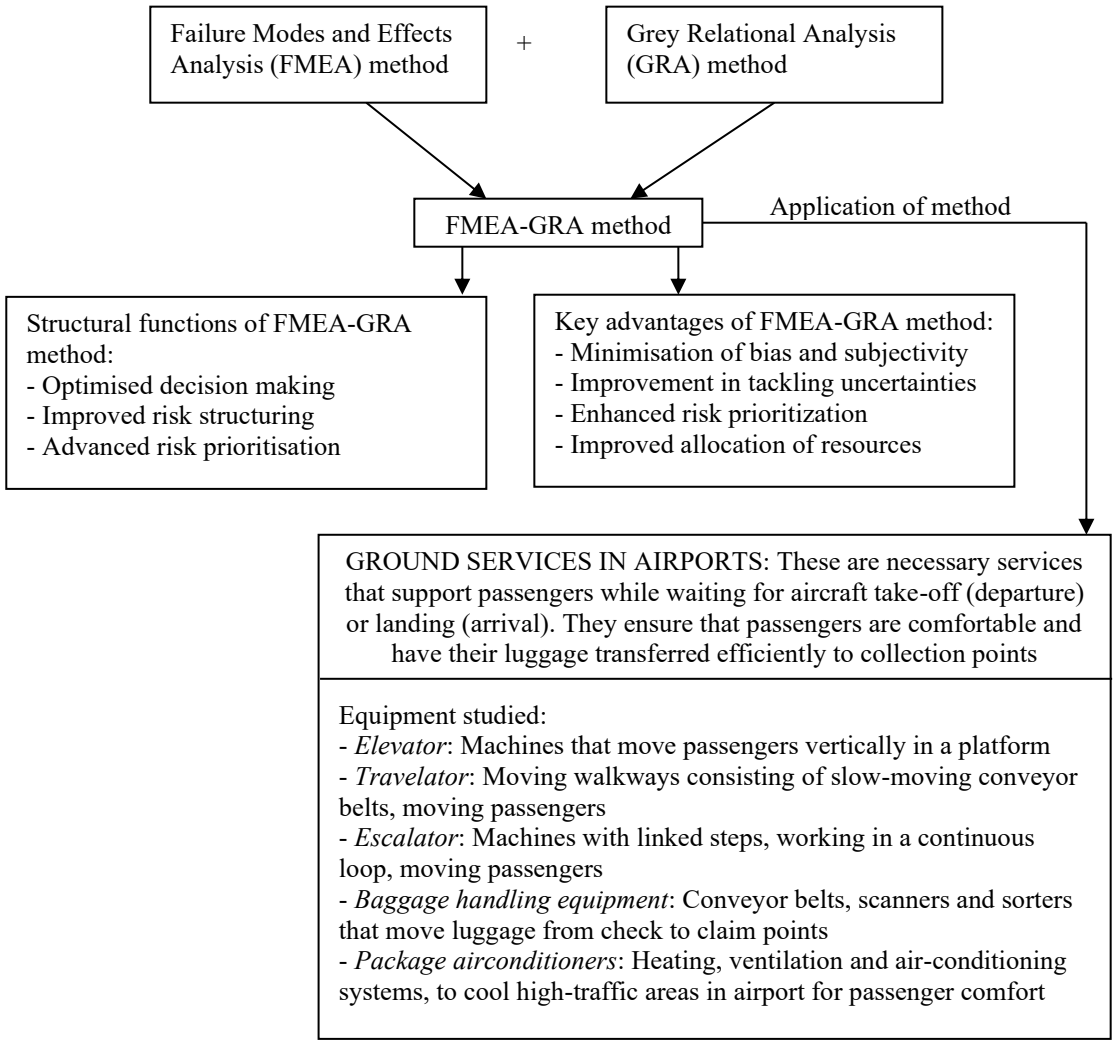

Figure 1. The FMEA-GRA method and its application to ground services in airports

2.1.1 Air-conditioner

While establishing a portfolio of essential equipment for an airport's ground equipment, the choice of the air-conditioner is a substantial decision. In this instance, important issues such as the following should be considered; the size of the room/hall to be cooled, capacity and physical size of the air-conditioner, the type of air-conditioner, (maybe split, floor standing or others), power requirements, condensate channelling control, location of outdoor unit/cross ventilation, spare parts availability, protection system/phase failure and sequence control, number of air-conditioners required, hours of operation per day, equipment/persons to serve, estimated years of use, location of the emergency control system, cooling coil make, (copper or aluminium for split air-

conditioners), blowers and quantity as well as compressors and quantity while considering bigger units. The choice of air-conditioner as key ground equipment is important because it offers uncompromising service quality levels to passengers awaiting departure to destinations or arriving from a place. Terminal halls require strong air conditioners to ascertain superior comfort to passengers' all-the-year-round. Air-conditioners are key equipment responsible for controlling the energy efficiency of the airport and the use of drillers and heat pumps with energy-efficiency designs guarantees the attainment of energy efficiency in airports. With today's technology, it is possible to use air-conditioners attached with an integrated heat recovery system to minimize waste energy consumption.

2.1.2 Baggage handling equipment

This is a kind of conveyor arrangement at an airport that serves three principal functions. First, it moves travellers' bags from the inspection area to the exit area. Second, it runs the travellers' bags from gates to gates while transferring loads. Third, it runs the travellers' bags from the entrance gate to the baggage receiving area. Consequently, understanding the failure attributes of the baggage handling equipment is a crucial factor while deciding on the failure assessment of critical airport ground equipment. The reason is that a properly functioning baggage handling equipment has a direct effect in maintaining the happiness of customers. It is influential in attracting travellers to an airport, maintaining the main airline hub where a focal linkage point from which several flights regarding a specific airline may be routed. The baggage handling equipment is often assessed on the movement of bags from one point to another at the speed of the travellers. Slow-moving bags keep travellers frustrated as they want for their bags at each point; bags may fail to make the linking flights on if too slow. Also when the bags are too fast in movement, they may make the linking flights which passenger misses. However, with a failed baggage handling system, its unavailability many warrant the airport using less effective carriage systems, leaving the customers frustrated.

2.1.3 Elevator

The elevator in an airport is a piece of substantial equipment for ground movements which should be considered while analysing equipment failures of critical ground equipment in airports. The reason is that it makes it practical for travellers to move about at the airport terminal, making travels by air accessible and comfortable to handicapped people. The failure of the control system, which determines the direction of the movement of the elevator and the safety systems for the prevention of catastrophes may leave the travellers unhappy particularly those with disabilities. Thus, failure analysis phenomenon such as the failure modes effects and criticality analysis may be important to understand the failures of the elevators and improve their service qualities.

2.1.4 Escalator

In the scheme to choose key ground equipment in the airport for analysis there is scope to include the escalator. It is largely expensive ground equipment in the airport, a variation of the conveyor belt. It works as a pair of moving chain loops draws a set of stairs regularly, thereby moving many travellers for a short distance at a relatively acceptable speed. However, a deep knowledge of the failure mechanism for escalators is required in a drive for lean maintenance where many failures are predicted before occurrence and maintenance cost minimum. Including escalator in the equipment list to analyse for failures brings maintenance of the airport cheaper in the long run as escalators hold a major investment and repair cost in airports.

2.1.5 Travellators

Travellators are imperative ground equipment, which should be included in choosing the key ground equipment whose failures are to be analysed in an airport. The airport maintenance manager often displays eagerness on when a failed travellator will be working “as-good-as-new” after repairs to make travellers happy in their travelling experience. Travellators, also known as moving-walkways, is essential as the traveller moves around the airport. Persistent movement interruptions of the traveller by the travellator influences the average downtime cost of maintaining the travellators and their manning staff lifespan in service and the overall facility condition.

Moreover, the risk priority evaluation through application of FMECA combined with grey relational analysis was intended for analysis of performance of select mechanical equipment within the airport setting of a developing country. However, the majority of malfunction assessment was controlled by the need to have improved as well as significant accessibility and dependability of components in order to guarantee effective sustenance processes. In achieving the above, a mathematical technique in support of recognizing and analyzing probable malfunctions was employed by utilizing failure mode effects and criticality analysis (FMECA) and grey relational analysis. The FMECA method integrated with the Grey Relational Analysis is executed by the following algorithms:

Step 1: Determination of standard (reference) series: target series, known as the standard series, of length R is as follows [10]:

$$Y_o = \{Y_o(1), Y_o(2), ..., Y_o(R)\} \quad (1)$$

Standard series are determined by taking the smallest value of all risk factors, since small values denote smaller risk

$$Y_o = \{Y_o(1), Y_o(2), ..., Y_o(R)\} = \{1, 1, ..., 1\} \quad (2)$$

Step 2: Determination of comparative series – h information series related to the occurrence, severity and detectability of failure is stated thus [10]:

$$Y_i = \{Y_i(1), Y_i(2), ..., Y_i(R)\} \quad i = 1, 2, ..., h \quad (3)$$

$Y_i(R)$ represents the R^{th} factor of Y_i.

To compare all information series, g information series is defined as in the following matrix

$$Y = \begin{bmatrix} Y_1 \\ Y_2 \\ \vdots \\ Y_g \end{bmatrix} = \begin{bmatrix} Y_1(1) & Y_1(2) & \cdots & Y_1(R) \\ Y_2(1) & Y_2(2) & \cdots & Y_2(R) \\ \vdots & \iddots & \ddots & \vdots \\ Y_g(1) & Y_g(2) & \cdots & Y_g(R) \end{bmatrix} \quad (4)$$

Step 3: Obtaining the distance between standard series and comparative series and calculating the coefficient value. All the three risk parameters are compared with the standard series for each failure series, and the relation coefficient is given by the following equation [10]:

$$\beta\left(Y_o(R), Y_j(R)\right) = \frac{\Omega_{\min} + \left(\theta\Omega_{\max}\right)}{\Omega_{oj}(R) + \left(\theta\Omega_{\max}\right)} \quad (5)$$

Where $j = 1,2,...,h$ and $R = 1,2,...,g$

$Y_o(R)$ is the standard series and $Y_j(R)$ is the comparative series.

$$\Omega_{\min} = \min_{\forall j \in i} \min_{\forall R} \left\| Y_o(R) - Y_j(R) \right\| \quad (6)$$

$$\Omega_{\max} = \max_{\forall j \in i} \max_{\forall R} \left\| Y_o(R) - Y_j(R) \right\| \quad (7)$$

θ is defined as a coefficient between $(0,1)$ but in order to reduce the effect of the maximum value on the relationship coefficient, θ is usually taken as 0.5. The aim of introducing this coefficient is to adjust the difference between $\Omega_{oj}(R) and \Omega_{\max}$.

Step 4: Determination of the grey relationship degree – This is measure of the geometric relationship between standard series and comparative series. If the two series are compared to be the same, then the grey relationship degree is equal to 1. The grey relationship degree indicates the degree of relationship between compared and standard series [10].

$$\lambda\left(Y_o, Y_j\right) = \frac{1}{g}\sum_{R=1}^{g} \beta\left(Y_o(R), Y_j(R)\right) \quad (8)$$

g = decision factor number

If the weights of each criterion are given, the grey relationship degree can be calculated by multiplying the grey relationship coefficient of the criterion and weight values of the degree magnitude of the criterion.

$$\lambda\left(Y_o, Y_j\right) = \sum_{R=1}^{g} \beta\left(Y_o(R), Y_j(R)\right) F_R \quad (9)$$

F_R is the weighting coefficient of the factors.

$$\sum_{R=1}^{g} F_R = 1 \quad (10)$$

Step 5: Rating the risk priorities – The factor series with the highest grey relationship degree denote the best alternative in decision making problems. This is to say that if

$\beta(Y_o, Y_i) \geq \beta(Y_o, Y_j)$, then the relationship between $Y_i \, and \, Y_o$ is greater than the relationship between $Y_j \, and \, Y_o$.

3 Results and Discussions

In section 2, the methodology of the grey relational analysis was defined in mathematical terms was observed as a complementary method for the failure modes effects and criticality analysis and has the potential of providing substantial information about the equipment failures and at the same time capable of performing in a situation where incomplete information surrounds the problem to solve. Data was collected from the records of the airport used for the study, located in a major city of a sub-Saharan African country. The declaration of the source of data is not made since the arrangement for the release of the data was based on the researcher maintaining confidentiality of the data. The airport ground service is maintained by an indigenous ground handling contractor servicing the airport. The company provided the essential data for this analysis. The collected data are on passenger handling services, ramp handling services, cargo handling services and baggage handling services. In this paper, the authors have streamlined choice to five pieces of equipment. Scoring of the RPN parameters was done by one of the authors, an expert in maintenance. The researcher who serves as the expert that provided scores for the present study has a bachelor's and master's degrees in mechanical engineering and is currently pursuing a doctoral degree in a Nigerian University in the area of maintenance engineering. Coupled with more than 5 years of experience in maintenance planning and execution in an airport, the researcher has valuable experience to assess the handling facilities of the ground services in the airport.

3.1 Scoring criteria

The scoring criteria adopted in this study are derived from the FMEA method and are referred to as the risk priority number (RPN) for ground service handling equipment. The RPN quantitatively assesses the risk involved in managing the ground support equipment. A risk number is assigned to the service function of the handling equipment, which is a part of a failure modes and effects analysis. In this paper, one of the authors is a senior maintenance personnel member at the studied airport, whose principal

function includes the maintenance of handling equipment, the scope of which is covered in the present study. The long-term experience of the author as maintenance personnel has been deployed to assign the RPN based on an established criterion of evaluating the severity of impact, S, frequency of occurrence, O, and likelihood of detection, D. Severity rates how critical the passenger to an airport will perceive the effect of a failed handling equipment. Passengers are concerned with their time wasted, risks to their belongings and inconvenience caused to them by a failed handling equipment. Severity may be heightened when the broken-down handling equipment causes broken or damaged belongings, lost luggage or mistracked belongings. Eventually, anxiety and stress develop for the passenger whose travel plans may be disrupted. Occurrence is another critical issue, which estimates the likelihood that the cause of a particular failure will occur. For example, a flaw in the design of the handling door for an elevator, which could cause failure, could be assigned a high occurrence based on past issues. However, a new landing door that has not yet tested in operation might show a low occurrence. The occurrence rating is often evaluated at the designed life of the landing door, for example. Detection estimates how effective control acts to detect or prevent failure modes before the passenger experiences them. The scoring criteria for the baggage handling activities place personal injury as overriding and focus on the maintenance effectiveness of the ground service equipment. In general, all three risk priority factors, S, O and D were measured based on a scale of 1 to 10. These factors have their scoring criteria discussed as follows:

1. Severity: Severity is represented by the letter S, and evaluates the failure impact on passengers. The following are the appropriate scores under severity:
10 (Mishap): Equipment malfunctions, causes equipment damage, injure workers, and result in costly delays.
7-8 (Excessive): Major service disruptions, handling equipment out-of-service.
4-6 (Moderate): Moderate disruption of handling services, 2-3 (Low): Minor inconvenience to passengers.
1 (Negligible): No noticeable influence on handling activities.

2. Occurrence: Occurrence is represented as O, states the failure frequency, commonly oriented towards preventive maintenance data. The following are the appropriate scores under occurrence:

9-10 (Profound): Repeated, exceeds once in 20 cycles.

7-8 (Excessive): Failure occurring, once in 20 to 100 cycles

4-6 (Moderate): Periodic failures, once in 100 to 1000 cycles

2-3 (Low): Infrequent failures

1: (Remote): Unlikely failures, less than once in 10,000 cycles.

3. Detection: Detection is represented as letter D, declares the ability of installed equipment controls, such as electronic sensors or even physical inspections, to establish the faults before being activated. The following are the appropriate scores under detection:

9-10 (Very low): No installed control or experienced maintenance team members to detect failure before it occurs.

7-8 (Low): The possibility of detecting failure before starting the handling equipment is low.

4-6 (Moderate): The faults can be detected on a moderate chance, such as when daily pre-operational checks on handling equipment are made.

2-3 (Excessive): The likelihood of detecting failure through the installed maintenance system is high.

1 (Expected): Installed preventive controls will certainly detect possible failure.

3.2 RPN calculations and interpretation of results

RPN can range from 1 to 1,000, where 1 indicates the lowest risk, and 1,000 indicates the highest risk. A higher risk priority number signifies a higher priority risk that needs immediate attention. Applying the RPN philosophy in airport ground service in failure mode is a numerical approach to focus scarce maintenance resources on the most critical risks. This prioritisation supports handling quality control in airports, passenger satisfaction and handling operational efficiency of passenger luggage. In

between these two extreme values of 1 and 1000 are four broad classifications, stated as follows:

- Critical Risk (RPN > 500): The system manager needs to take immediate mandatory steps to mitigate the operation.
- High Risk (RPN 300 – 500): Prioritise activities and engage in prompt action to stop failure.
- Moderate Risk (RPN 100 -300): It is essential to act within a reasonable time frame.
- Low Risk (RPN 1- 100): Need to monitor the service process but may not require immediate action.

From the computations of the RPN score, the researcher implements corrective actions targeting the highest RPN first. The higher the RPN, the more serious the handling equipment failures and the easier it is to detect such failures. Improvement efforts are directed at places where they are needed most.

3.3 The raw values for RPN components

The raw values for RPN components are shown in Table 1A and Table 1B in the Appendix. Consider the raw values of the elevator in Table 1A. In this section, the researcher wants to calculate the risk priority number for 10 potential failures of the elevator at the airport. The researcher, an experienced maintenance professional, assigns ratings of 1 to 10 based on the scoring criteria discussed in this paper, for each of the 3 categories of probability of occurrence, severity of failure and probability of an escape from being detected. The aim is to determine which of the 10 failure scores has the highest RPN. For the first failure, "Elevator Car", the product of O, S and D is 16. Other failure modes in the elevator are computed (Table A), and the observed highest value is 729. The same procedure was followed for other equipment, and the detailed calculations are shown in Tables 1A and 1B. It is shown that travellator, escalator, baggage handling equipment and package air conditioners have the highest values of 648 (controller), 648 (controller), 135 (controller), and 280 (power circuit board), respectively. These are the most important components of all the systems, which should be given the topmost attention. However, this analysis uses the traditional RPN scale,

which is a benchmark to compare the novel methods proposed in this work. The novel method integrates the grey relational analysis with the RPN, giving it unique and robust results shown in the other points of this work.

The information series matrix below is obtained by utilizing the RPN values (Risk Ranking Table for Elevator) so as to evaluate the comparative series.

$$\begin{bmatrix} Y_1(1) & Y_1(2) & Y_1(3) \\ Y_2(1) & Y_2(2) & Y_2(3) \\ Y_3(1) & Y_3(2) & Y_3(3) \\ Y_4(1) & Y_4(2) & Y_4(3) \\ Y_5(1) & Y_5(2) & Y_5(3) \\ Y_6(1) & Y_6(2) & Y_6(3) \\ Y_7(1) & Y_7(2) & Y_7(3) \\ Y_8(1) & Y_8(2) & Y_8(3) \\ Y_9(1) & Y_9(2) & Y_9(3) \\ Y_{10}(1) & Y_{10}(2) & Y_{10}(3) \end{bmatrix} = \begin{bmatrix} 1 & 8 & 2 \\ 1 & 8 & 1 \\ 1 & 8 & 1 \\ 8 & 7 & 1 \\ 3 & 7 & 2 \\ 3 & 7 & 2 \\ 2 & 8 & 2 \\ 9 & 9 & 9 \\ 2 & 7 & 2 \\ 2 & 7 & 2 \end{bmatrix}$$

The difference matrix is given below:

$$\begin{bmatrix} \Omega_1(1) & \Omega_1(2) & \Omega_1(3) \\ \Omega_2(1) & \Omega_2(2) & \Omega_2(3) \\ \Omega_3(1) & \Omega_3(2) & \Omega_3(3) \\ \Omega_4(1) & \Omega_4(2) & \Omega_4(3) \\ \Omega_5(1) & \Omega_5(2) & \Omega_5(3) \\ \Omega_6(1) & \Omega_6(2) & \Omega_6(3) \\ \Omega_7(1) & \Omega_7(2) & \Omega_7(3) \\ \Omega_8(1) & \Omega_8(2) & \Omega_8(3) \\ \Omega_9(1) & \Omega_9(2) & \Omega_9(3) \\ \Omega_{10}(1) & \Omega_{10}(2) & \Omega_{10}(3) \end{bmatrix} = \begin{bmatrix} 0 & 7 & 1 \\ 0 & 7 & 0 \\ 0 & 7 & 0 \\ 7 & 6 & 0 \\ 2 & 6 & 1 \\ 2 & 6 & 1 \\ 1 & 7 & 1 \\ 8 & 8 & 8 \\ 1 & 6 & 1 \\ 1 & 6 & 1 \end{bmatrix}$$

From the difference matrix, $\Omega_{\min} = 0, \Omega_{\max} = 8$

$$\beta\left(Y_o(R), Y_j(R)\right) = \frac{\Omega_{\min} + \left(\theta\Omega_{\max}\right)}{\Omega_{o1}(1) + \left(\theta\Omega_{\max}\right)} = \frac{0 + \left(0.5 \times 8\right)}{0 + \left(0.5 \times 8\right)} = 1$$

For $\Omega_1(2)$,

$$\beta\left(Y_o(R), Y_j(R)\right) = \frac{\Omega_{\min} + (\theta\Omega_{\max})}{\Omega_{o1}(2) + (\theta\Omega_{\max})} = \frac{0 + (0.5 \times 8)}{7 + (0.5 \times 8)} = 0.36$$

In like manner, for $\Omega_1(3)$ $\beta_1(3) = \frac{0 + (0.5 \times 8)}{1 + (0.5 \times 8)} = 0.8$

$\beta_2(1) = 1,$ $\beta_2(2) = 0.364,$ $\beta_2(3) = 1$

$\beta_3(1) = 1,$ $\beta_3(2) = 0.364,$ $\beta_3(3) = 1$

$\beta_4(1) = 0.364,$ $\beta_4(2) = 0.4,$ $\beta_4(3) = 1$

$\beta_5(1) = 0.667,$ $\beta_5(2) = 0.4,$ $\beta_5(3) = 0.8$

$\beta_6(1) = 0.667,$ $\beta_6(2) = 0.4,$ $\beta_6(3) = 0.8$

$\beta_7(1) = 0.8,$ $\beta_7(2) = 0.364,$ $\beta_7(3) = 0.8$

$\beta_8(1) = 0.333,$ $\beta_8(2) = 0.333,$ $\beta_8(3) = 0.333$

$\beta_9(1) = 0.8,$ $\beta_9(2) = 0.4,$ $\beta_9(3) = 0.8$

$\beta_{10}(1) = 0.8,$ $\beta_{10}(2) = 0.4,$ $\beta_{10}(3) = 0.8$

$$\begin{bmatrix} \beta_1(1) & \beta_1(2) & \beta_1(3) \\ \beta_2(1) & \beta_2(2) & \beta_2(3) \\ \beta_3(1) & \beta_3(2) & \beta_3(3) \\ \beta_4(1) & \beta_4(2) & \beta_4(3) \\ \beta_5(1) & \beta_5(2) & \beta_5(3) \\ \beta_6(1) & \beta_6(2) & \beta_6(3) \\ \beta_7(1) & \beta_7(2) & \beta_7(3) \\ \beta_8(1) & \beta_8(2) & \beta_8(3) \\ \beta_9(1) & \beta_9(2) & \beta_9(3) \\ \beta_{10}(1) & \beta_{10}(2) & \beta_{10}(3) \end{bmatrix} = \begin{bmatrix} 1 & 0.364 & 0.8 \\ 1 & 0.364 & 1 \\ 1 & 0.364 & 1 \\ 0.364 & 0.4 & 1 \\ 0.667 & 0.4 & 0.8 \\ 0.667 & 0.4 & 0.8 \\ 0.8 & 0.364 & 0.8 \\ 0.333 & 0.333 & 0.333 \\ 0.8 & 0.4 & 0.8 \\ 0.8 & 0.4 & 0.8 \end{bmatrix}$$

Grey relationship degree (Grey RPN) for each failure mode with assumption that all three risk factors have equal weights is calculated thus from Equation (8):

$$\lambda(Y_1, Y_3) = \frac{1}{3}(1 + 0.364 + 0.8) = 0.721$$

With the same process applied to other failure mode:

$$Grey\ RPN = \begin{bmatrix} 0.721 \\ 0.788 \\ 0.788 \\ 0.588 \\ 0.622 \\ 0.622 \\ 0.655 \\ 0.333 \\ 0.667 \\ 0.667 \end{bmatrix}$$

Calculation of Grey relationship degree (Grey RPN) with the assumption that the risk factors have different weights using Equation (9):

Taking $\sum_{R=1}^{g} F_R = 1$, the weight coefficients for the occurrence, severity and detectability of the failure were taken as $F_O = 0.4,\ F_S = 0.4,\ F_D = 0.2$ respectively.

$$\lambda(Y_1, Y_3) = \{(1 \times 0.4) + (0.364 \times 0.4) + (0.8 \times 0.2)\} = 0.706$$

With the same process applied to other failure modes

$$Grey\ RPN = \begin{bmatrix} 0.706 \\ 0.746 \\ 0.746 \\ 0.506 \\ 0.587 \\ 0.587 \\ 0.626 \\ 0.333 \\ 0.640 \\ 0.640 \end{bmatrix}$$

Table 1. RPN Values for Elevator

Elevator No.	Failure modes	RPN	Ranking	Grey RPN* weight	Ranking	Grey RPN** weight	Ranking
1	8	16	8	0.721	8	0.706	8
2	10	8	10	0.788	10	0.746	10
3	9	8	9	0.788	9	0.746	9
4	2	56	2	0.588	2	0.506	2
5	4	42	4	0.622	4	0.587	4
6	3	42	3	0.622	3	0.587	3
7	5	32	5	0.655	5	0.626	5
8	1	729	1	0.333	1	0.333	1
9	6	28	6	0.667	6	0.64	6
10	7	28	7	0.667	7	0.64	7

Note: *Risk factors have equal weights, ***Risk factors have equal different weights

Table 1 shows the results of three methods, namely the RPN, grey RPN with risk factor having equal weights and grey RPN with risk factors having different weights. For the first method, RPN, the highest and the least values are 729 and 8, correspondingly. The meaning is that keeping equipment 8 in service demand substantial risk values and if captured the whole system would run smoothly. Corresponding to elevator equipment 8 is the first rank for the RPN method. By tracing it to the other two methods, elevator 8 maintains the first position in both the grey RPN with equal risk factor weights, sharing grey values of 0.333 for each of these two methods. Table 1 also reveals the worst values for the three methods. It was elevator 2 for the three methods having the RPN of 8, grey RPN with an equal risk factor of 0.788 and grey RPN with an unequal risk factor of 0.746. Having done this analysis, the authors are interested in what causes the poor performance. It was observed that several causes may be responsible for the faults but some faults keep occurring all the time. This is referred to as the significant faults for the elevator. Four key faults were identified, namely the controller, landing door, car buffer and counterweight tension pulley arranged in order of importance. Consequently, efforts to reduce these faults will lead to the enhanced productivity of the equipment and the overall quality of service of all elevators in the system.

Table 2. RPN Values for Travelator

Travelator No.	Failure modes	RPN	Ranking	Grey RPN* weight	Ranking	Grey RPN** weight	Ranking
1	8	48	8	0.603	8	0.650	11
2	4	112	4	0.521	4	0.466	4
3	11	28	11	0.667	11	0.640	10
4	7	56	7	0.588	7	0.633	8
5	3	512	3	0.364	3	0.364	3
6	1	648	1	0.343	1	0.345	1
7	10	28	10	0.667	10	0.640	9
8	6	72	6	0.566	6	0.546	5
9	9	30	9	0.656	9	0.627	7
10	5	112	5	0.521	5	0.553	6
11	2	576	2	0.354	2	0.358	2

Note: *Risk factors have equal weights, ***Risk factors have equal different weights

By following through the same steps from the establishment of the information series index to the summary of results from the elevator to obtain Table 1, Table 2 is obtained for travelator. Table 2 shows the result using the three methods of RPN, grey RPN with equal risk factor weights and grey RPN with unequal risk factor weights when travellator is considered. For the first method, RPN, the highest and the least values are 648 and 28, respectively. This means that keeping the travellator 6 in service demands substantial risk value and efforts to capture it should be topmost for this travellator 6. By tracing the positions for the other two methods, travellator 6 still retain the best values, with the grey RPN of 0.343 and 0.345, respectively, for grey RPN with an equal weight of cycle factor and grey RPN with an unequal weight of risk factors, respectively. Benchmarked against the elevator, for the RPN method, the performance of the best travellator is worse than the best of the elevator by 11.1%. For the grey RPN with an equal weight of risk factors, the best travellator is better than the equivalent best elevator by 1%. For the grey RPN with an unequal weight of risk factors, best travellator is better than the best elevator by 3.6% for the worst cares, for the RPN methods, the best performance of the travellator exceeds the performance of the best elevator by 250%. The grey RPN with an equal weight of risk factor and grey RPN with an unequal weight of risk factor were used to select the best values for the travellator and compared with the best values of the elevator, it was known that they were worse

by 15.36% and 14.21%, respectively. A similar procedure conducted for elevator is extended to escalator, Table 3.

Table 3 shows the results of the three methods, for the first method, RPN, the highest and the least values are 648 and 28, correspondingly for the escalators 11 and 9. By tracing the position for the other two methods, escalator 11 retains the first position for the grey RPN with an equal weight of risk factors having a value of 0.343 and for the same method, the worst values have retained an elevator 9 with a value of 0.667. For the third methods, the best escalator is escalator 11, having a value of 0.345 while the worst escalator is escalator 5 having a value of 0.650.

3.4 Benchmarked against the performance of elevators having the best and worst performance

We consider the first method, the RPN. The performance grew by 11.1% when the best escalator was compared with the best elevator. However, when the best escalator was compared with the best elevator using the grey RPN_E, the performance dropped by 3%. When the best escalator was compared with the best elevator using RPN (with an equal weight of risk factors), the performance dropped by 3.6%.

Table 3. RPN Values for Escalators

Escalator No.	Failure modes	RPN	Ranking	Grey RPN* weight	Ranking	Grey RPN** weight	Ranking
1	4	128	4	0.509	4	0.451	4
2	6	64	6	0.576	6	0.618	7
3	8	48	8	0.610	8	0.572	6
4	5	126	5	0.511	5	0.547	5
5	7	48	7	0.603	7	0.650	11
6	9	30	9	0.656	9	0.627	8
7	3	512	3	0.364	3	0.364	3
8	10	28	10	0.667	10	0.640	9
9	11	28	11	0.667	11	0.640	10
10	2	567	2	0.355	2	0.360	2
11	1	648	1	0.343	1	0.345	1

Note: *Risk factors have equal weights, ***Risk factors have equal different weights

Table 4. RPN values for baggage handling equipment

Baggage equipment No.	Failure modes	RPN	Ranking	Grey RPN* weight	Ranking	Grey RPN** weight	Ranking
1	8	24	8	0.677	8	0.612	7
2	10	14	10	0.733	10	0.720	10
3	1	135	1	0.426	1	0.422	1
4	5	48	5	0.610	5	0.599	5
5	6	42	6	0.622	6	0.613	8
6	11	6	11	0.815	11	0.778	11
7	7	36	7	0.637	7	0.604	6
8	4	54	4	0.600	4	0.560	4
9	9	24	9	0.681	9	0.658	9
10	3	96	3	0.536	3	0.483	3
11	2	108	2	0.526	2	0.471	2

Note: *Risk factors have equal weights, ***Risk factors have equal different weights

For the worst performance, when the worst performance of elevator was compared with the worst performance of the elevator, the performance dropped by 250%. For the second method, grey RPN with equal weight improved by 15.4%. For the third method, grey RPN with an unequal weight of the risk factors, the performance improved by 12.9. Table 4 shows the result of the three methods when the baggage handling equipment is considered. Again, the procedure used to obtain summarized results for the elevator in Table 1 is applied to obtain Table 4. The best baggage handling equipment was equipment 3 when the RPN method is considered. It displays a value of 135 as the RPN while the worst equipment was identified as equipment 6 with a value of 6. Using the grey RPN with equal risk weights factors, the best equipment was chosen as equipment 3 with a value of 0.425. However, for the worst equipment, equipment 6 was identified with a grey value of 0.815. Furthermore, using the grey RPN with unequal weight of the risk factors, baggage handling equipment 3 was chosen as the best with a grey value of 04.22. However, the worst performance was attributed to equipment 6

with a grey value of 0.778. By comparing the results of the best and worst-performing equipment of the benchmark of the best and worst-performing elevators, the following may be discussed for the RPN method, the best performing equipment improved by 81.5%. however, for the grey RPN with equal risk factor weights and grey RPN with unequal risk factor or weights, the performance of the best performing equipment dropped by 27.9% and 26.7%, respectively. For the worst values, there is an enhance mention performance when the RPN method is used, obtained as 25%. However, for the grey-RPN_E and grey-RPN_D, the worst values declined respectively by 3.4% and 4.3%. Also, following the steps taken to obtain Table 1, Table 5 was obtained.

Table 5 shows the result of the three methods. For the first method, RPN, the highest and least values are 280 (air conditioner 9) and 3 (air conditioner 3). For the grey RPN with equal weights, the best and then worst equipment are air-conditioner 9 (0.421) and air-conditioner 7 (0.889), respectively. for the grey RPN with unequal weights, the best and the worst equipment are air conditioner 9(0.426) and air conditioner 7 (0.867), respectively. By comparing the results of the best and worst-performing equipment of the air conditioner and the benchmark of the best and worst-performing elevators, the following may be established. For the RPN method, the best performing equipment improved by 61.6%. nonetheless, for the grey RPN with equal risk factor weights and grey RPN with unequal risk factor weights, the performance concerning the best performing equipment reduced by 26.4% and 27.9%, respectively. For the worst values, there is an enhancement in performance when the RPN method is used, obtained as 62.5%. Nonetheless, for the grey RPN with equal weights of risk factors, the worst values declined respectively by 12.8% and 16.2%.

Table 5. RPN values for air conditioners

Air conditioner No.	Failure modes	RPN	Ranking	Grey RPN* weight	Ranking	Grey RPN** weight	Ranking
1	4	108	4	0.526	4	0.542	4
2	5	70	5	0.567	5	0.580	5

3	8	40	8	0.621	8	0.646	8
4	7	40	7	0.621	7	0.646	7
5	9	40	9	0.621	9	0.646	9
6	3	120	3	0.505	3	0.506	3
7	12	3	12	0.889	12	0.867	12
8	2	144	2	0.492	2	0.501	2
9	1	280	1	0.421	1	0.426	1
10	10	28	10	0.633	10	0.660	10
11	6	48	6	0.603	6	0.634	6
12	11	25	11	0.667	11	0.700	11

Note: *Risk factors have equal weights, ***Risk factors have equal different weights

3.5 Benchmarked with travellator as the base performance equipment

For a comprehensive evaluation of the performance of the best equipment, the performance obtained for each of the pieces of equipment was compared with the travellator. The following results were obtained. For the RPN method, the comparative best performance of the elevator, escalator, baggage handling equipment and air-conditioners to travellator is 112.5%, 100%, 20.8% and 43.2%, respectively. For the grey RPN with equal weight for the risk factors, concerning elevator, escalator, baggage handling equipment and air-conditioners relative to travellator, the best performance is 97.1%, 100%, 124.2% and 122.7%, respectively. For the grey-RPN with an unequal weight of the risk factor, the elevator, escalator, baggage handling equipment and air-conditioner relative to the best performing travellator are 96.5%, 100%, 22.3%, 123.5%, respectively.

Concerning the worst performance, for the RPN method, concerning the elevator, escalator, baggage handling equipment, and air-conditioner, relative to the travellator, the worst performance is 28.6%, 100%, 21.4% and 10.7% correspondingly. For the grey RPN with an equal weight of the risk factor, the elevator, escalator, baggage handling equipment and air-conditioner, relative to the worst-performing travellator are 118.1%, 100%, 122.2% and 133.3%, respectively. For the grey RPN with an unequal weight of

the risk factor, the elevator, escalator, baggage handling equipment and air-conditioner, relative to the worst-performing travellator, the performance travellator, the performance are 114.8%, 100%, 119.7% and 133.4%, respectively.

3.6 Benchmarking with an escalator as the base performance equipment

To evaluate the performance of the equipment broadly, the performance obtained for each of the pieces of equipment was compared with the escalator. The following results were obtained. For the RPN approach, the relative performance of the elevator, baggage handling equipment, travellator and air-conditioner in their best performance is 112.5%, 20.8%, 100% and 43.2%, respectively. For the grey RPN with equal weight for the risk factors, concerning elevator, baggage handling equipment, travellator and air-conditioner in their best performance, the results are 97.1%, 124.2%,100% and 122.7%, respectively. For the grey RPN with unequal weights of risk factors, elevator, baggage handling equipment, travellator and air-conditioner, relative to the best performing escalator, the performance and 96.5%, 122.3%, 100% and 123.5%, respectively.

Concerning the worst performance, for the RPN approach, concerning the elevator, baggage handling equipment, travellator and air-conditioner, relative to the escalator, the worst performance is 28.6%, 21.4%, 100% and 10:7%, respectively. For the grey RPN with equal weights of the risk factors, the elevator, baggage handling equipment, travellator and air-conditioner, relative to escalator with the worst performance, the relative performance of the mentioned equipment are 118.1%, 122.2%, 100% and 133.3%, respectively. For the grey RPN with an unequal weight of risk factor, concerning elevator, baggage handling equipment, travellator and air-conditioner, in association with the escalator of the worst performance, the performance is 114.8%, 119.7%, 100% and 133.4% respectively.

3.7 Benchmarking with baggage handling equipment as the base performance measuring equipment

An attempt to appraise the performance of the equipment from a wide perspective leads the investigator to consider each other piece of equipment with the baggage handling equipment. The following results are obtained. For the RPN

approach, the comparative performance of the elevator, escalator, travellator and air conditioner in their best performance is 540%, 480%, 490% and 208.4%, respectively. For the grey RPN with equal weight for the risk factors; regarding elevator, escalator, travelator and air conditioner in their best performance, the results are 78.2%, 80.5%, 80.5% and 98.8%, respectively. For the grey RPN with unequal weights of risk factors, elevator, escalator, travellator and air-conditioner, relative to the baggage handling equipment, the best performance is 78.9%, 81.8%, 81.8% and 100.9%, receptively. Concerning the worst performance, considering the RPN technique and taking note of the elevator, escalator, travellator and the air-conditioner, relative to the baggage handling equipment, the worst performance is 133.3%, 466.7%, 466.7% and 50%, respectively. By attempting to evaluate using the second technique, which is the grey RPN with an equal weight of the risk factors, the elevator, escalator, travellator and air-conditioner, relative to the baggage handling equipment whose worst performance is evaluated, the comparative performance of the defined equipment are 96.7%, 81.8% 81.8% and 109.1%, respectively. For the grey RPN with unequal weights of the risk factors, the elevator, escalator, travellator and air conditioner, relation to escalator with the worst performance, the relative performance of the mentioned equipment are 95.9%,83.5%, 83.5% and 11.4%, respectively. Benchmarking with the air conditioner as the base performance measuring equipment to evaluate the performance of a set of ground equipment that is key to the airport, a wide range of perspective is adopted. This idea leads to an enquiry of the performance of each piece of equipment against the air-conditioner.

The following results were obtained from the analysis first, the RPN method is considered in which the best performance of the air-conditioner is compared with the best performance of each of the following equipment: elevator, escalator, travellator and baggage handling equipment. The performance set is 260.4%, 231.4%, 231.4% and 48.2%, respectively. For the grey RPN method where the weights of risk factors are equal, the best performance of the air-conditioner is compared with the best performance of each of the following equipment: elevator, escalator, travellator and baggage handling equipment. The performance set is 78.2%, 81%, 81% and 99.1%, respectively. Considering the worst performance, the first method, RPN, is analyzed on

the equipment. The worst performance of the air-conditioner is compared with the worst performance of each of the following equipment; elevator, escalator, travellator and baggage handling equipment, the performance is 88.6%, 75%, 75% and 91.7%, respectively. For the third method, grey RPN with an unequal weight of the risk factors, when the worst performance of the air-conditioner is matched against each of the following: elevator, escalator, travellator and baggage handling equipment, the performance is 86%, 75%, 75% and 89.7%, respectively.

3.8 Optimal failure computation using polynomial

To determine the optimal failure for each of the piece of equipment, the determining matrix, Fop, is first established. This as a three-by-three matrix that was created based on the top three best values of the performance evaluation given in Tables 1 to 5. To illustrate this choice, consider the first equipment, elevator. Information from the columns representing the RPN, grey-RPN_E and grey-RPN_D are extracted concerning the values attached to the ranks in each of the following columns. For RPN, the first three values are 729, 56 and 42. This is the first column of the optional failure matrix created. Consider the first three positions in grey-RPN_E, we have 0.333, 0.588 and 0.622, respectively. This represents the second column of the optimal failure matrix. The third column is obtained as 0.333, 0.506 and 0.587, respectively, by tracing the best three values under the grey-RPN_D column. To obtain the optimal failure value, the difference between the F_{op} and I is obtained, where I is the identity matrix. Thus, for the elevator, the following solution is true (Equation (11)):

$$\begin{bmatrix} 729 & 0.333 & 0.333 \\ 56 & 0.588 & 0.506 \\ 42 & 0.622 & 0.587 \end{bmatrix} - \begin{bmatrix} \lambda & 0 & 0 \\ 0 & \lambda & 0 \\ 0 & 0 & \lambda \end{bmatrix} = \begin{bmatrix} 729-\lambda & 0.333 & 0.333 \\ 56 & 0.588-\lambda & 0.506 \\ 42 & 0.622 & 0.587-\lambda \end{bmatrix} = 0 \qquad (11)$$

By carrying out the analysis, the final equation is obtained as (Equation (12)):

$$-\lambda^3 + 729\lambda^2 - 850.768\lambda + 21.376 = 0 \qquad (12)$$

The solution to $\lambda = 0.03$, 1.14 and 727.83

The same approach is used for other pieces of equipment. Thus, for the travellator, the following solution is true (Equation (13)):

$$\begin{bmatrix} 648 & 0.343 & 0.345 \\ 576 & 0.354 & 0.358 \\ 512 & 0.364 & 0.364 \end{bmatrix} - \begin{bmatrix} \lambda & 0 & 0 \\ 0 & \lambda & 0 \\ 0 & 0 & \lambda \end{bmatrix} = \begin{bmatrix} 648-\lambda & 0.343 & 0.345 \\ 576 & 0.354-\lambda & 0.358 \\ 512 & 0.364 & 0.364-\lambda \end{bmatrix} = 0 \quad (13)$$

By carrying out the analysis, the final equation is obtained as (Equation (14)):

$$-\lambda^3 + 648.718\lambda^2 - 465.523\lambda + 167.832 = 0 \quad (14)$$

The solution to $\lambda = 648$

3.9 Novelty the article

The key thrust of this article is to evaluate failures of selected airport ground equipment, which includes the elevator, escalator, travellator, baggage handling equipment and the air-conditional. These pieces of equipment are critical in the definition of customer service quality to passengers awaiting flights in airports or those on arrival from a flight. Although the literature has expressed concern on flight quality and customer service of passengers in airports, a major part of the literature focuses on the ride quality of passengers after securing a place in the aircraft. Extremely little attention was paid to passengers' comfort while awaiting flights, in moving to have a seat in the plane or arriving from a flight, which requires some rest periods before leaving the airport. In all these situations, both the luggage of the passengers and the passenger requires comfort. These are in luggage flow and the cooling comfort while awaiting the next action at the terminal hall. A new approach is presented to evaluate the failure of the equipment using the failure modes effects and criticality analysis and the grey relational analysis. Three novel methods were proposed for the first time, in the perspective of failure modelling of airports ground equipment. These are the RPN method, the grey RPN with equal weights of risk factors and the grey RPN with different weights of risk factors. The best and worst performances of each of the selected equipment were measured. Benchmarking of all other equipment relative to each of the selected equipment was done along with the directions of the best and worst

performance. The final ranks were made after considering all equipment in each particular class.

Furthermore, while it is acknowledged that several researchers have involved can customer satisfaction models in airports, details on failure concerning the key equipment's and particularly the minimum possible failure control threshold of the key equipment such as elevators, escalators, baggage handling equipment and air conditioners have not been tracked. But knowledge of the least possible failure could help the maintenance manager to deploy manpower and resources to control such failures. A novel feature of the current work is the introduction of a polynomial for calculating the least possible failure for any ground equipment based on a matrix generated from the best performance values on each piece of equipment whose number is equivalent to the number of methods considered in the evaluation of the performance of the equipment. The RPN, grey-RPN_E, grey-RPN_D is correspondingly mapped to the best, next best and the third-best entries from the failure evaluated to form the matrix, whose results are transformed to a polynomial.

3.10 Uncertainty measurement

To establish the reliability of the findings, random uncertainty analysis was conducted on the RPN values for all the equipment analyzed. Random uncertainty, the ratio of the difference between the maximum value and the minimum value of the RPN to the number of values considered under each equipment, was observed. Moreover, percentage uncertainty, which is the product of absolute uncertainty and 100 units divided by the measurement, was considered for the analysis. The summary of the results is given in Table 6.

Table 6. Absolute and percentage uncertainty for the RPN values of all equipment.

Equipment	Absolute Uncertainty	% Uncertainty
Elevator	98.90 ± 72.10	72.90
Travelator	202.00 ± 56.36	27.90
Escalator	202.45 ± 56.36	27.84
Baggage handling equipment	53.35 ± 9.27	14. 38
Package air conditioner	78.83 ± 23.08	29. 28

Table 6 reveals the highest and lowest % uncertainty with the elevator and the baggage handling equipment, respectively. These are 72.90 and 17.38, respectively. The high value of 72.90 as a percentage uncertainty does not mean low data reliability but high variability in the opinion of the expert who conducted the assessment. This is understandable as the expert opinion differentiates the elevator as the most critical equipment in the system that needs the greatest attention. Also, the baggage handling equipment is observed to be the one that requires the least attention in service.

3.11 Limitations, practical uses of the findings and contributions

The conducted equipment failure assessment has certain limitations resulting from the challenges with complex interactions. The FMEA-GRA method hardly considers the multi-failure situations and the complexity of the ground handling equipment. This weakness can be corrected in the future by considering the infusion of the Markov chain methodology into the proposed framework to mitigate interaction capability deficiencies. Moreover, there is another limitation of the FMEA-GRA method termed the static analysis. This refers to the consideration of the method on a one–time basis and fails to consider real-time changes. Interestingly, the Markov chains mentioned earlier could serve this second purpose of analyzing when the period of analysis changes. Also, the FMEA-GRA method is historical data-dependent, which may not work well for a new airport whose ground service handling equipment is being planned. To overcome this limitation, data could be imported from an existing airport base to the new one, complemented with simulation data.

In this paper, the FMEA-GRA method has been applied to an airport with findings which appear to have practical use from various dimensions. First, the grey relational analysis aspect of the combined FMEA-GRA method has the potential to support sound decisions where limited maintenance data and poor maintenance information are available. Thus, in the joint FMEA – GRA method, the maintenance manager can improve decision-making where uncertainty prevails, leading to more assured results from risk assessments. Secondly, understanding and establishing potential failure modes in baggage handling equipment reveals how to eliminate non-value adding activities with significant downtime reduction. Therefore, there is an improvement in ground

service operational efficiency through this route. Third, maintenance schedules could be updated and improved using the findings of the FMEA-GRA method's application to airport ground services. Since this helps the plant to transform reactive to proactive maintenance, the optimization of maintenance strategies is aided by the results obtainable from the application.

Moreover, the application of the FMEA-GRA method to airport ground services delivers results that align with the broader reliability engineering practices. It achieves this through the provision of a data-oriented method, which priorities risks within a complex airport working environment. The combined FMEA-GRA method offers results that provide actionable improvements to reliability. Furthermore, the integrated FMEA-GRA method offers substantial theoretical advancements, changing the assessment platform from a subjective, multiplication-oriented perspective to a mathematically rigorous, objective decision structure. It contributes the following benefits to the literature: First, the proposed method permits managing uncertainty, promoting more objective results. Second, the ambiguity concerning the RPN is resolved as the grey relational analysis focuses on distance measurement instead of just multiplication alone.

3.12 Maintenance recommendations

Arising from the application of the FMEA-GRA method for the ground services in the airport, the following actionable maintenance recommendations are provided:

1. High-risk equipment components should be prioritized: The results obtained from the FMEA-GRA methodical application show that the following components have the highest risk priority numbers in each piece of equipment: controller (elevator), controller (travelator), drive system (escalator), controller (baggage handling equipment), and power aircraft board (package air conditioners). These are highly crucial components that require urgent maintenance intervention. The principal intervention that could be done to controllers in elevators, travelators and baggage handling equipment typically includes the following. First, a smart sensor upgrade could be pursued to aid improved load sensing, door operation and accurate smoothing. Moreover, introducing the variable frequency drives as upgrades of

older drives prevents excessive energy consumption and reduces noise since torque and motor speeds are adjusted dynamically. Furthermore, regeneration drives could be introduced that aid in the recycling of excessive energy produced as the elevator descends. This promotes a reduction of energy costs.

2. Establish spare parts strategy: With the established failure modes, the maintenance of high-risk spare parts should be available on request during corrective maintenance sessions. This will eventually lower downtime significantly. Critical spare parts for controllers in elevators that should be stocked include inverter drives, relays and contractors. For power circuit boards in package air conditioners, power transistors, relays, capacitors and fuses could be stocked.

The maintenance recommendations suggested earlier have the potential to improve ground service efficiency in airports if addressed.

4 Conclusions

In this paper, a novel approach to establishing the failures of key ground equipment, which involves elevator, escalator, travellator, baggage handling equipment and the air conditioner was discussed and implemented in an airport operating in a developing country. Three methods namely the RPN, grey RPN_E and grey RPN_D were developed and the failures of equipment determined based on the failure modes effects and atonality analysis and the grey relational analysis. The conclusions based on the study are as follows:

1. The three models, the RPN, grey-RPN_E and grey-RPN_D are effective methods in determining the failures of the ground equipment in an airport.
2. The eigenvalue method by which polynomial equations are developed and solved is a component approach to establishing the failure of the ground equipment of the airport.
3. The best values for the equipment performance through the three methods of RPN, grey- RPN_E and grey- RPN_D are respectively as follows: (729,0.333 and 0.333) for elevation, (648,0.343 and 0.345) for travellator, (648,0.343 and 0.345) for the escalator, (135, 0.426 and 0.422) for baggage handling equipment, and (280, 0.421 and 0.426) for air conditioning.

In the future contributions in the area of optimization of the process using the Taguchi method, genetic algorithm and combined Taguchi and genetic method may profit from the work.

4.1 Appendix

Table 7. Risk ranking for all equipment

Component Name	Occurrence (O)	Severity (S)	Detectability (D)	RPN = O x S x D
Elevator				
Elevator Car	1	8	2	16
Machine Drive	1	8	1	8
Brake System	1	8	1	8
Landing Door	8	7	1	56
Counterweight Tension Pulley	3	7	2	42
Car Buffer	3	7	2	42
Over-speed Governor	2	8	2	32
Controller	9	9	9	729
Counterweight Frame	2	7	2	28
Car Guide Rail	2	7	2	28
Travelator				
Handrail	1	6	8	48
Landing Plate	7	8	2	112
Braking System	2		2	28
Truss	1	7	8	56
Drive System	8	8	8	512
Controller	9	8	9	648
Lubrication System	2	7	2	28
Tracks	3	8	3	72
Balustrade Panels	3	5	2	30
Comb Plates	2	7	8	112
Safety Devices	8	8	9	576
Escalator				
Landing Platform	8	8	2	128
Truss	1	8	8	64
Tracks	3	8	2	48
Steps	2	7	9	126
Handrail	1	6	8	48
Escalator Exterior	3	5	2	30
Drive System	8	8	8	512
Lubrication System	2	7	2	28
Braking System	2	7	2	28
Safety Devices	9	7	9	567
Controller	9	8	9	648

Table 8. Risk ranking for all equipment

Component Name	Occurrence (O)	Severity (S)	Detectability (D)	RPN = O x S x D
Baggage Handling Equipment				
Belt	3	8	1	24
Truss	1	7	2	14
Controller	5	9	6	135
Drive System	2	8	3	48
Drum Roller	2	7	3	42
Bumper	6	1	1	6
Carrier	3	6	2	36
Chain	3	9	2	54
Slat	6	2	2	24
Lubrication System	6	8	2	96
Motor/Gear	6	9	2	108
Package Airconditioner				
Compressor	2	9	6	108
Condensing Fan	2	7	5	70
Evaporator Fan/Blower	1	8	5	40
Condenser Coil	1	8	5	40
Evaporator Coil	1	8	5	40
Refrigerant	4	6	5	120
Air Filter	1	3	1	3
Electrical Control System	3	8	6	144
Power Circuit Board	5	8	7	280
Piping System	1	7	4	28
Expansion Valve	1	8	6	48
Thermostat	1	5	5	25

References

[1] K. Button, G. Martini, D. Scotti, N. Volta, "Airline regulation and common markets in Sub-Saharan Africa," *Transportation Research Part E: Logistics and Transportation Review*, vol. 129, pp. 81-91, 2019. https://doi.org/10.1016/j.tre.2019.07.007

[2] O.S. Al-Kwifi, G.L. Frankwick, Z.U. Ahmed, "Achieving rapid internationalization of sub-Saharan African firms: Ethiopian Airlines' operations under challenging conditions," *Journal of Business Research,* vol.119, pp. 663-673, 2020. https://doi.org/10.1016/j.jbusres.2019.02.027

[3] M. Arif, R.Singh, A. Williams, "Customer service in the aviation industry - An exploratory analysis of UAE airports," *Journal of Air Transport Management*, vol. 32, no. 7, pp. 1-7, 2013. DOI: 10.1016/j.jairtraman.2013.05.001

[4] H.N.P. Tucci, F. Facchini, "Ground support equipment and flight delays: a multivariate analysis in different locations," *CEAS Aeronautical Journal*, 2025. https://doi.org/10.1007/s13272-025-00891-6

[5] K. Timmermans, P. Roling, G.R.C. Mouli, B. Atasoy, "The impact of transitioning to electric Ground Support Equipment on the fleet capacity and energy demand at airports," *Case Studies on Transport Policy,* vol. 21, 2025, 101498. https://doi.org/10.1016/j.cstp.2025.101498

[6] L. Al-Qatawneh, M. Arafeh, M. Barghash, F. Shihabeddin, S. Mahmoud, A. Odeh, "Improving baggage handling time at an international airport using Six Sigma methodology: A case study in the Middle East region," *International Journal of Engineering Business Management*, vol. 14, no. 1, 2025. https://doi.org/10.1177/18479790251322345

[7] J. Evler, E. Asadi, H. Preis, H. Fricke, "Airline ground operations: Schedule recovery optimization approach with constrained resources," *Transportation Research Part C: Emerging Technologies,* vol. 128, 2021, 103129. https://doi.org/10.1016/j.trc.2021.103129

[8] B. Puthillath, R. Sasikumar, "Selection of maintenance strategy using failure mode effect and criticality analysis," *International Journal of Engineering and Innovative Technology* vol. 1, no. 6, pp. 73-79, 2012.

[9] C. Potente, A.Ragnoli, G. Tamasi, R. Vergari, P.D. Mascio "Quantitative risk

assessment of temporary hazards and maintenance worksites in the airport safety areas: A case study", *Transportation Research Procedia*, vol. 35, pp. 166-175, 2018. DOI: 10.1016/j.trpro.2018.12.031

[10] B. Kursun, U. Kurt, S. Guvercin, K. Okten, S. Akgul, A. Yildiz, "An application for the failure mode and effects analysis integrated with the grey relational analysis," *Trakya University Journal of Engineering Sciences,* vol. 17, no. 2, pp. 1-10, 2016.

[11] M. ElMansouri, H. Sekkat, M. Talbi, Tahiri Z., and Nhila O., "FMECA process analysis for managing the failures of 16-Slice CT scanner," *Journal of Failure Analysis and Prevention*, vol.24, pp.436-442, 2025, https://doi.org/10.1007/s11668-023-01853-y

[12] A. Gula, M. Bujna, C.K. Lee, R. Drlicka, "Proposal for use of DEMATEL in combination with FMEA and FMECA method, *Acta Technology*, pp.149-158, 2025, https://doi.org/10.2478/ata-2025-0019

[13] M.P. Kumar, N.V.S. Raju, M.V.S. Kumar, and G. Gupta, "Risk assessment and prioritization using fuzzy FMECA: a case study of dumper breakdowns," *International Journal of System Assurance and Management*, 2025, https://doi.org/10.1007/s1398-024-02506-5

[14] S. Elbarmile, J. Gharib, and Y. Gahi, "Risk assessment of integration in cybersecurity: A systematic approach with FMECA and ISO31000," *Proceeding of the 4th Conference on Advances in Communication Technology and Computer Engineering*, pp.257-272, 2025, https://doi.org/10.1007/978-3-031-94620-2_23

[15] A.A. Zuniga, J.A. Fernandes, P.J.C. Branco, "Comparisons between quantitative

FMECA methods: A case study on power transformer risk assessments," *Advances in Reliability Engineering for Complex Systems*, vol.13, Article 50, 2025, https://doi.org/10.3390/systems13060450

[16] N.H. Elkasrawy, H. Farouk, and Y.M. Youssef, "Maintenance optimization based on modified FMECA: a case study applied to a spinning factory," *International Journal of System Assurance Engineering*, vol.16, pp.73-88, 2025, https://doi.org/10.1007/s13198-024-02617-z

[17] C. Liu, C. Zhou, L. Tan, J. Cui, W. Xiao, J. Liu, H. Wang, and T. Wang, "Reliability analysis of subsea manifold system using FMECA and FFTA," *Scientific Reports*, vol.14, 2025, 22873, https://doi.org/10.1038/s41598-024-73410-y

[18] H. Tian, Y. Sun, C. Chen, Z. Zhang, T. Liu, T. Zhang, J. He, and L. Yu, "A novel FMECA method for CNC machine tools based on D-GRA and data envelopment analysis," *Scientific Reports*, Vol.14, 2024, Article 26596, https://doi.org/10.1038/s41598-024-77920-7

[19] M. Chennoufi, and A. Chakhrit, "An extended FMECA approach using new risk assessment and prioritization based approach," *International Journal of Information Technology*, vol.16, pp.1595-1604, 2023, https://doi.org/10.1007/s41870-023-01455-9

[20] A. Bouzidi, I.M. Bedaida, W. Belimane, "Risk management applying FMECA in pharmaceutical packaging production: implementation of ISO15378:2017 - Case study," *Timisoara Journal of Economics and Business*, vol.18, no. 1, pp. 95-112, 2025, https://doi.org/10.2478/tjeb-2025-0005

[21] A. Wiangkham, R. Vongvit 2026, "Integrating machine learning with FMEA for

failure prioritization and process risk analysis in manufacturing", *Results in Engineering*, vol. 29, Article 109128. https://doi.org/10.1016/j.rineng.2026.109128

[22] E. Akdamar, G. Elidolu, M. Gögebakan, B.O. Ceylan, 2026, "Entropy-based borda extended weighted expert FMEA approach: Comparison with classical and fuzzy FMEA on a ship system", *Applied Soft Computing*, vol. 188, Article 114424. https://doi.org/10.1016/j.asoc.2025.114424

[23] Y. Liu, X. Wu, "An asymmetric Choquet integral-based TODIM linguistic FMEA method with interacting risk factors and incomplete weight information", *Applied Soft Computing*, vol. 187, 2026, Article 114275. https://doi.org/10.1016/j.asoc.2025.114275

[24] W. Jin, T. Gai, J. Fang, H. Fujita, J. Wu 2026, "A group experts–LLMs collaborative decision making method to improve reliability in FMEA risk evaluation", *Advanced Engineering Informatics*, vol. 71, Article 104304. https://doi.org/10.1016/j.aei.2025.104304

[25] N. Shojaei, N. Moradi, A. Sharifi, E. Yasari 2026, "Heavy metal and microplastic contamination in amphibian breeding marshes deep within the Hyrcanian Forests: A screening-level ecological risk assessment using FMEA framework", *Environmental Development*, vol. 57, Article 101393. https://doi.org/10.1016/j.envdev.2025.101393

IJASST International Journal of Applied Sciences and Smart Technologies
Volume 08
Issue 01
p-ISSN 2655-8564, e-ISSN 2685-943, pp. 239-260, 2025

Development of an Arduino-Based Water Rocket Launcher in Physics Experiments

Larasati Rizky Putri[1*], Fakhrizal Arsi[2], Kiar Vansa Febrianti[3], Sentot Novianto[1], Ika Wahyu Utami[1], Muhammad Najih[1] Sofia Debi Puspa[1], Amrullah Gilang Ibrahim[1], Harry Munandar[1]

[1]*Faculty of Industrial Technology, Universitas Trisakti, Grogol West Jakarta, 11440, Indonesia*
[2]*Physics of High School, State Senior High School 8 Jakarta, Tebet South Jakarta, 12840, Indonesia*
[3]*Physics of Middle School and High School, Cita Buana School, Jagakarsa South Jakarta, 12620, Indonesia*
[*]*Corresponding Author: larasati.rizki@trisakti.ac.id*

(Received 18-09-2025; Revised 02-12-2025; Accepted 09-04-2026)

Abstract
The effective science education requires practical methods that allow students to explore complex physics concepts. One promising approach is the use of physics experiment as an interactive media. This research focuses on the development of water rocket launcher using an Arduino as an innovative physics experiment. Arduino in water rocket launcher is used for making the precise control and relevant measurement of variables, such as angle of projection, speed of launch, maximum altitude of launch, and air pressure. The research process followed the ADDIE instructional design model and involved hardware, software prototyping, work testing, and user instruction. The launcher's performance was tested with 33 engineering students and assessed by 5 experts. Expert evaluations rated the relevance, design, and usability of the kit highly (3.4–4.0 on a 4-point Likert scale). User responses from 33 students indicated strong agreement on ease of use and engagement (mean scores 3.79–3.91), with a high reliability (Cronbach's alpha = .964). Experimental launches, using three and four finned rockets, showed maximum height percentage differences between theoretical and observed values ranging from 0.0%–52.6% (three fins) and 1.2%–51.8% (four fins); range errors were 3.4%–36.8% (three fins) and 2.1%–42.7% (four fins). The findings confirm that the Arduino-based water rocket launcher provides effective, interactive learning, though further refinement in data accuracy and instructional materials is recommended to maximize its classroom impact and is needed for improved accuracy.

Keywords: Arduino, Experiment, Launcher, Water Rocket.

1 Introduction

Science, Technology, Engineering, and Mathematics (STEM) education is widely recognized as a key driver for developing problem-solving ability, creativity, and 21st-

century skills among students [1], [2], [3]. Project-based and hands-on learning, especially in physics, has been found to increase student engagement, conceptual understanding, and scientific interest [3], [4]. However, in many educational settings, barriers such as limited resources and teacher readiness can restrict the adoption of innovative practical activities [5].

Integrating microcontroller platforms, such as Arduino, into physics classrooms enables students to automate experiments, collect real-time data, and connect abstract concepts with tangible projects [6]. Reviews and systematic studies confirm that Arduino-based activities help bridge theory with practice, enhance computational thinking, and support the development of engineering skills [1], [6]. Water rocket experiments, in particular, are effective for teaching core topics like Newton's laws, the action-reaction principle, air pressure [7], momentum, and projectile motion, all while enhancing motivation and inquiry-based learning [3], [4].

Despite these benefits, implementing Arduino-enhanced practical physics projects on a broad scale requires consideration of curriculum integration, teacher training, and equitable access to technology [5]. To answer that problem, the research needs to consider the technical aspects of developing a water rocket launcher, including optimal hardware and software design. In addition, the research should also determine whether the water rocket launcher is properly made by comparing the launch data with theoretical data. Thus, this study aims to design, build, and evaluate an Arduino-based water rocket launcher as an engaging physics teaching tool, assessing its impact on student understanding and motivation in physics learning.

1.1 Principles of STEM and Project-Based Learning

STEM education is grounded in the integration of science, technology, engineering, and mathematics, aiming to equip students with skills for problem-solving, inquiry, and innovation [1], [2]. Project-based learning (PBL), a cornerstone of effective STEM teaching, encourages students to engage deeply with content by designing, constructing, and evaluating tangible products or solutions [4]. Research shows that PBL promotes higher-order thinking and increases students' motivation for learning science concepts [3].

The successful implementation of technological tools like Arduino within STEM education demands not only adequate resources but also teacher readiness and effective curriculum integration [5]. Professional development and support help educators design learning experiences where technology is not an add-on but an essential part of the investigation and discovery process.

1.2 Physics of Water Rocket

Water rocket experiments are an accessible means to teach principles of mechanics, specifically Newton's laws of motion, conservation of momentum, and projectile motion. When the rocket is launched, expelling water downwards due to the pressurized air creates an upward thrust as described by Newton's third law. The motion of the rocket after launch demonstrates projectile motion, where the range and maximum height can be mathematically described using classical equations:

$$R = \frac{v_0^2 \sin 2\theta}{g} \tag{1}$$

where R is the range, v_0 is the initial velocity, θ is the launch angle, and g is the acceleration due to gravity [4].

1.3 Water Rocket Launcher

Project-based physics learning allows students to research, plan, design and reflect on the creation of their technology projects. This type of learning not only stimulates student creativity but also requires different assessments. Projects will provide information about students' understanding and knowledge of the learning process, their ability to apply knowledge, and their ability to communicate information. Recent research in this field has shown that the use of Arduino-based water rocket launchers can improve students' understanding of physics concepts. In addition, the use of this technology also stimulates students' interest in science and technology. This is particularly relevant in the face of modern educational challenges where students often struggle to understand abstract physics concepts [22].

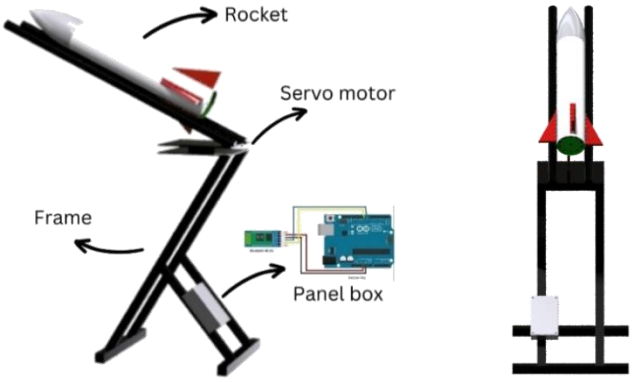

Figure 1. Development of water rocket launcher: (a) Parts of Arduino-based water rocket launcher and (b) Back view of the launcher.

The components of the launcher are shown in Fig. 1. The main raw material of the kit is hollow aluminum pipe and 3 mm iron plates. Hollow pipe was cut into several pieces, then iron plates were cut into 20 × 20 cm size. Researcher also welded the hollow pipes into L-shape. After that researcher drills some hole for motor servo installation later, then welded iron plates to the hollow pipes and installed ball bearings between the plates. After the frame is fixed, researcher installed servo motors and the Arduino. The installation documentation is shown in Fig. 2.

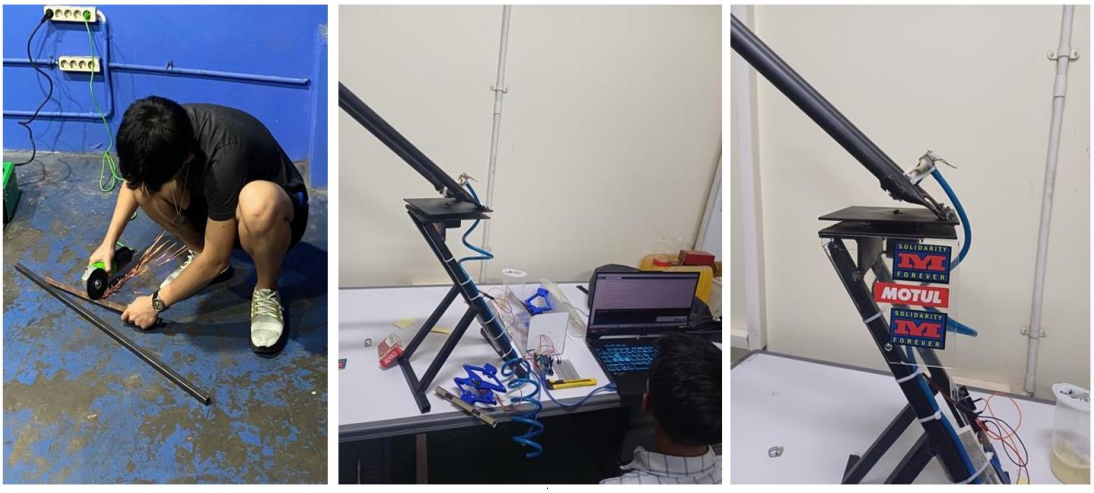

Figure 2. Frame assembly and installation

1.4 Arduino Installation and Coding

Arduino is an open-source microcontroller platform, widely adopted for introducing automation, programming, and sensor data acquisition in classroom environments. Systematic reviews of classroom Arduino use show that it fosters the development of computational thinking, problem-solving, and scientific inquiry [6]. In STEM projects, Arduino provides a bridge between theoretical physics and practical application by allowing real-time measurement, control of system variables (such as launch angle or timing), and digital data logging [6].

As technology advances, the use of Arduino in the development of water rocket launchers has become increasingly popular. Arduino is an affordable and programmable hardware platform that can be used to control a wide variety of experimental tools, including water rocket launchers. With Arduino, teachers can program the device to measure physics parameters during the rocket launch, such as angular projection, velocity, altitude, and air pressure, so that students can see and analyze the experimental results directly [8].

The servo motor is controlled via Arduino Uno and Bluetooth module HC-05 (Fig. 3). Researcher used Bluetooth HC-05 module, male to male cable, Arduino Uno, and a breadboard. The pins of HC-05 module are connected to the Arduino with the following configuration.

- VCC : 5V
- GND : GND
- TXD : RXD
- RXD : TX

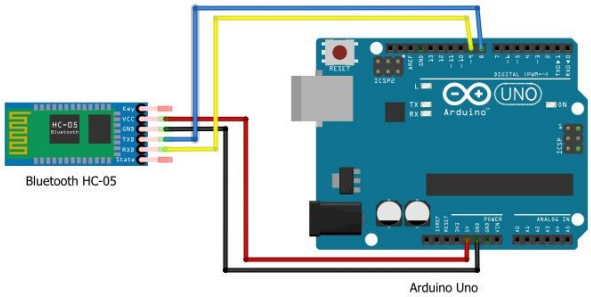

Figure 3. Arduino schemes

Then, researcher installed Arduino IDE from https://www.arduino.cc/en/software, connected Arduino cable to a laptop, and run the software. The following code is written to control the servo motor (Fig. 4).

After the code is installed, researcher connected their phones to HC-05 module via Bluetooth, and control the Arduino using Arduino Controller apps. The rocket launcher then tested with two types of rockets, 3-fins rocket and 4-fins rocket as shown in Fig.5.

```
#include <Servo.h>
Servo servoAxis1;  // Create servo object for first axis
Servo servoAxis2;  // Create servo object for second axis
int posAxis1 = 90;  // Initial value for first axis (90°)
int posAxis2 = 90;  // Initial value for second axis (90°)
char receivedChar;  // Variabel to receive data from Bluetooth
void setup() {
  servoAxis1.attach(9);  // Attach servo motor for first axis to pin no.
9
  servoAxis2.attach(10); // Attach servo motor for first axis to pin no.
10
  Serial.begin(9600);  // Initialize serial communication
  Serial.println("Kendalikan servo dengan tombol 'u', 'd', 'l', 'r' di
ponsel Anda melalui Bluetooth."); // Print servo motor instruction in
Indonesian
}
void loop() {
  if (Serial.available() > 0) {
    receivedChar = Serial.read();
    if (receivedChar == 'u') {
      // Up botton pressed
      posAxis1 = 120;  // Adjust position increment as needed
    } else if (receivedChar == 'd') {
      // Down botton pressed
      posAxis1 = 60;  // Adjust position decrement as needed
    } else if (receivedChar == 'l') {
      // Left button pressed
      posAxis2 = 120;  // Adjust position increment as needed
    } else if (receivedChar == 'r') {
      // Right button pressed
    // Limit servo motor range
    posAxis1 = constrain(posAxis1, 0, 180);
    posAxis2 = constrain(posAxis2, 0, 180);

    // Adjust servo motor position
    servoAxis1.write(posAxis1);
    servoAxis2.write(posAxis2);
  }
}
```

Figure 4. Arduino codes

Figure 5. Three-fins rocket and four-fins rocket

Researchers compile the launch data in Table 1.

Table 1. Experimental data

Number of fins	Launch Angle (º)	T (s)	Powered flight time (s)	Projectile flight time (s)	Total distance/ x total (m)	Air pressure (kPa)	Nozzle diameter (m)	Initial mass (kg)	Final mass (kg)	Ejected water mass (kg)	Max height (m)
3	15	0.82	0.01	0.82	7.4	250	0.012	0.52117	0.20777	0.3134	0.3
3	30	0.92	0.02	0.9	14.35	300	0.014	0.52117	0.18443	0.33674	1.33
3	45	1.24	0.04	1.2	20.86	250	0.016	0.52117	0.17131	0.34986	2.35
3	60	1.5	0.05	1.45	13.51	210	0.018	0.52117	0.16988	0.35129	5.23
3	75	1.69	0.07	1.62	10.34	200	0.02	0.52117	0.15933	0.36184	6.01
3	90	1.87	0.09	1.78	2.52	150	0.024	0.52117	0.15142	0.36975	9.41
4	15	0.68	0.01	0.67	10.15	350	0.012	1.00479	0.30036	0.70443	1.67
4	30	0.77	0.02	0.75	18.13	300	0.014	1.00479	0.34658	0.65821	2.92
4	45	1.15	0.04	1.11	23.1	250	0.016	1.00479	0.35958	0.64521	4.14
4	60	1.44	0.06	1.38	15.58	210	0.018	1.00479	0.23772	0.76707	5.84
4	75	1.66	0.08	1.58	12.96	200	0.02	1.00479	0.20513	0.79966	8.67
4	90	1.95	0.12	1.83	3.79	150	0.024	1.00479	0.18248	0.82231	10.4

2 Material and Methods

This research utilized the Research and Development (R&D) approach, adopting the ADDIE instructional design model, Analysis, Design, Development, Implementation, and Evaluation, as proposed by Dick and Carey in 1996 [9] and adapted widely in educational technology development [10], [11]. The ADDIE model provides a systematic and iterative process well-suited to producing effective educational materials and STEM kits [11].

To begin, the researchers conducted open-ended interviews with physics teachers to identify challenges and needs in conducting water rocket activities. The feedback highlighted practical difficulties in assembling launchers and the need for better alignment with learning objectives. As suggested by prior studies, gathering user input in the early stages supports relevant and effective instructional design [12]. Consequently, this research was undertaken to create an Arduino-based water rocket launcher so that teachers can focus more in the physical concepts rather than the launcher assembly itself.

During the Design stage, the water rocket launcher was designed using 3D modelling software. Particular attention was paid to selecting low-cost, locally available components, ensuring affordability and ease of replication, an important consideration in educational kit design [13]. All parts were chosen based on quality, durability, and their suitability for educational use. Then in the Develop stage, a prototype of the kit was assembled.

During the Implement stage, the prototype was pilot tested with 30 engineering students at Universitas Trisakti, Jakarta, Indonesia. Data collected for each launch angle (repeated 10 times) included air time, maximum distance, maximum height, air pressure, rocket nozzle diameter, initial rocket mass, and final rocket mass. Experiments were conducted using both three- and four-finned rockets to examine stability and performance, consistent with methodologies used in practical physics research [4].

In the final evaluation stage, experimental results were compared with theoretical calculations to assess the kit's effectiveness in demonstrating physics concepts and to identify discrepancies for further improvement. Iterative evaluation and refinement are

essential aspects of the ADDIE approach and are supported by best practices in instructional design [11], [12].

2.1 Development of Research Instrument

Two self-developed questionnaires were used as primary research instruments. The first questionnaire was designed for expert assessment, aiming to evaluate the content accuracy, clarity, and alignment of the Arduino-based water rocket launcher with educational objectives. The second questionnaire targeted end-users (students), focusing on their attitudes and satisfaction with the kit's usability and learning value. Both questionnaires employed twelve statements rated on a four-point Likert scale, ranging from "strongly disagree" to "strongly agree," allowing participants to express their level of agreement with each item [14].

2.2 Validity and Reliability

Content validity was established through expert review: two lecturers in science education and two experienced physics teachers examined the questionnaire drafts for completeness, accuracy, and item clarity. Their feedback was used to revise ambiguous or redundant items, following established guidance for instrument validation [15].

Cronbach’s alpha was utilized to assess internal consistency as a measure of reliability. The experts’ questionnaire yielded a Cronbach’s alpha of .513, indicating weak internal consistency and suggesting that items may assess somewhat different constructs or lack coherence [16]. This result should be interpreted with caution; further item refinement or expansion may be warranted. In contrast, the user attitude questionnaire demonstrated excellent reliability with a Cronbach’s alpha of .964, well above the commonly accepted threshold of .7, indicating strong internal consistency and repeatability among items. Together, these steps help ensure that the research instruments are credible for evaluating both expert perspectives and end-user experiences in the context of educational kit development.

2.3 Data Collection Procedure

2.3.1 Target Respondents

To ensure participants were appropriately qualified to address the research objectives, the expert questionnaire was distributed to university lecturers in Indonesia

who specialize in fundamental physics and mechanical engineering, particularly those involved with experimental topics such as water rocket investigations. These experts were selected from departments known to support and engage with the Arduino-based water rocket launcher, ensuring the feedback was grounded in relevant technical and pedagogical experience [17]. The user questionnaire was administered to students enrolled in fundamental physics courses within the mechanical engineering department at the same university. These students had recent hands-on experience with the Arduino-based water rocket launcher developed for this research.

2.3.2 Instrument Delivery and Collection

For the user survey, the procedure was as follows: Researchers collaborated with faculty within the engineering faculty to identify relevant departments and courses where fundamental physics experiments are taught. Course lecturers were briefed about the developed water rocket launcher and its intended educational use. The demonstration of the tool was conducted as part of a laboratory experiment. After participating in the experiment, students were invited to complete the user questionnaire. For the expert evaluation, five lecturers across different subject areas relating to tool development and mechanical engineering were individually contacted and invited to review and test the educational kit. They then completed the expert questionnaire provided by the research team.

2.3.3 Responding Rate

A total of 5 expert questionnaires and 35 user questionnaires were distributed. All 5 experts responded (100% response rate), and 33 out of 35 students completed the user questionnaire, resulting in a response rate of approximately 94%. These response rates are considered high and support the credibility of the dataset [18].

2.3.4 Respondents' Professional Background

The five expert respondents were experienced lecturers teaching subjects associated with industrial automation, materials engineering, machine construction, applied physics, and fluid mechanics. The 33 student participants were undergraduates enrolled in a fundamental physics course within the mechanical engineering department, ensuring familiarity with both the subject matter and the experimental apparatus.

2.3.5 Statistical Analysis

All responses were analyzed using IBM SPSS Statistics version 22.0. Cronbach's alpha was first calculated to assess the internal consistency of the instruments. Descriptive statistics (means and standard deviations) were then computed to summarize participant perceptions of the Arduino-based water rocket launcher and to identify strengths and areas for improvement. Where appropriate, inferential tests such as independent-samples t-tests were used to examine group differences in perception or satisfaction, following standard practice in educational evaluation research [19].

3 Results and Discussions

Expert Evaluation of Arduino-based Water Rocket Launcher

Experts provided high ratings for the launcher kit across multiple dimensions, with mean scores ranging from 3.80 to 4.00 out of 4.00 (Table 2). All respondents agreed that the kit aligns well with key physics concepts, supports project-based learning, and can be safely and effectively utilized in the classroom with minimal teacher supervision.
Each item was rated by experts on a four-point Likert scale:
4 = Strongly agree, 3 = Agree, 2 = Disagree, 1 = Strongly disagree.

Table 2. Expert evaluation of arduino-based water rocket launcher

No	Factors	Mean Score
1	The launcher kit aligns well with physics concepts (e.g., Newton's Laws, projectile motion).	4.00
2	The launcher kit content is appropriate for the intended educational level.	3.80
3	The experiment reflects real-world physics principles accurately.	3.80
4	The design and materials of the launcher are appropriate for school use.	4.00
5	The Arduino programming is relevant and effectively supports the experiment.	4.00

No	Factors	Mean Score
6	The Bluetooth control system operates reliably and enhances interactivity.	4.00
7	The launcher kit helps students understand complex concepts in a simple and engaging way.	4.00
8	The launcher kit supports student-centered, project-based learning methods.	3.80
9	The launcher kit encourages students' curiosity and scientific thinking.	4.00
10	The launcher kit is safe for classroom/laboratory use with minimal risk.	3.40
11	Instructions for assembling and operating the launcher kit are clear and easy to follow.	4.00
12	The launcher kit can be used with minimal teacher supervision.	4.00

User Evaluation on Arduino-based Water Rocket Launcher

As shown in Table 3, user ratings for the Arduino-based water rocket launcher were consistently high across all measured factors, with mean scores generally above 3.8 (on a 4-point Likert scale). Respondents agreed that the kit was easy to use, enhanced engagement through Bluetooth control, and helped clarify important physics concepts such as the relationship between launch angle, pressure, and projectile motion. Most participants indicated that the activity fostered critical thinking, made lessons feel more "real" and hands-on, and increased their interest in physics and technology.

Each item was rated by experts on a four-point Likert scale:
4 = Strongly agree, 3 = Agree, 2 = Disagree, 1 = Strongly disagree.

Table 3. User evaluation on arduino-based water rocket launcher

No.	Factors	Mean Score
1	The launcher kit is easy to set up and operate.	3.85
2	The Bluetooth control makes launching the rocket more engaging.	3.85
3	I am able to control the launcher's angle and timing easily.	3.79
4	The instructions are easy to understand.	3.85
5	The activity helps me understand physics concepts better.	3.91
6	Using the launcher kit makes the physics lesson more enjoyable.	3.91
7	I now have a better understanding of how angle and pressure affect projectile motion.	3.79
8	This activity encourages me to think critically and experiment more.	3.82
9	I enjoy learning physics using this launcher kit.	3.85
10	I would recommend this activity to others learning physics.	3.82
11	This experiment makes me more interested in physics and technology.	3.85
12	The launcher kit makes the lesson feel more real and hands-on.	3.88

3.1 Discussions

Experts Recommendations

Expert evaluations highlighted that the utilization of Arduino as the primary controller was appropriate for facilitating interactive physics experiments, as it simplifies measurement and allows for reproducible trials, an advantage well documented in literature on technology-enhanced science learning [6]. However, experts emphasized the need to further enhance data accuracy through well-defined sensor calibration procedures, particularly for the pressure and angle sensors. Incorporating calibration steps and validating measurements against standardized reference instruments, such as a certified manometer, are essential to ensuring the reliability of experimental data [20].

In addition, experts recommended explicit documentation of safety operating procedures (SOP), including the use of personal protective equipment (PPE), maintaining

a safe distance, and installing protective barriers during launches. Refining the launcher's structural stability, through a stronger support base or reinforced framework, was also suggested to improve operational safety and consistency.

Enhancements in user experience and data management were among the suggestions, specifically the development of a simple graphical user interface (GUI) using platforms such as Processing or web-based dashboards to monitor real-time parameters like pressure and angle. Automated data storage to SD cards or cloud-based systems was recommended to facilitate subsequent data analysis and reporting.

Documentation emerged as a priority; experts urged the inclusion of comprehensive Arduino schematic diagrams, complete source code, and a detailed component list in supplemental materials. Providing an accessible user manual would also allow for the tool's replication and wider adoption in other educational settings [13].

To further strengthen the instructional value, experts recommended a more rigorous theoretical framework, utilizing equations of projectile motion and fluid dynamics to model the rocket's behavior. Direct comparison of experimental outcomes with theoretical predictions would offer students deeper insight into the physical principles at play and promote higher-order analytical skills.

User Feedback

User responses were overwhelmingly positive. Students consistently reported that the Arduino-based water rocket launcher was engaging, easy to operate, and effective in clarifying physics concepts through hands-on investigation. Many respondents expressed increased motivation and interest in physics and technology and viewed the tool as highly beneficial for active learning in engineering education. Several users suggested maintaining or expanding the deployment of this tool, with some proposing commercial development for broader educational access.

Direct comments highlighted that the activity made abstract physics concepts feel more tangible and enjoyable, and that the launcher contributed positively to both their learning and classroom experience. No significant negative feedback or suggestions for major improvements were recorded, indicating a strong alignment of the tool with student expectations and educational needs.

Launch Result and Comparison with Theoretical Value

To evaluate the performance of the Arduino-based launcher and analyze its educational effectiveness, researchers compared empirical launch data with theoretical predictions. Due to the brevity of the rocket's powered flight phase, a simplified model was employed: the mass flow rate ($\dot{m}$) was first calculated using the nozzle area, the water density, and the internal bottle pressure, following Sutton & Biblarz [20]:

$$\dot{m} = C_d A\sqrt{2\rho P} \tag{2}$$

where:

$\dot{m}$ is the mass flow rate (kg/s)

C_d is the discharge coefficient (average is 0.7)

A is the cross-sectional area of the nozzle (m^2)

ρ is the density of water (approximately 1000 kg/m^3)

P is the pressure inside the bottle (Pa)

The exhaust velocity of the water leaving the rocket nozzle was approximated using Bernoulli's equation:

$$v_e = \sqrt{\frac{2(P_{in} \times P_{out})}{\rho}} \tag{3}$$

where:

P_{in} is the pressure inside the bottle

P_{out} is the pressure of air outside the bottle

ρ is the density of water.

Total thrust (T) is then calculated as:

$$T = \dot{m}v_e \tag{4}$$

where:

$\dot{m}$ is the mass flow rate.

v_e is the exhaust velocity.

The initial velocity v_0 is derived using the thrust and the duration of the powered flight.

$$v_0 = \frac{T \times t_{powered}}{m_i} \tag{5}$$

where:

T is the thrust.

$t_{powered}$ is the powered flight time

m_i is the initial mass of the rocket.

For the ballistic (unpowered) phase, standard projectile motion equations give maximum height (hmax) and range (R) [21]:

$$H_{max} = H_{powered} + \frac{v_0^2 \sin^2(\theta)}{2g} \quad (6)$$

$$R = D_{powered} + \frac{v_0^2 \sin(2\theta)}{g} \quad (7)$$

Given the short-powered flight time, the rocket's initial velocity and subsequent projectile motion can be approximated without detailed integration. According to the mentioned equations, the theoretical value compared to the experimental value of maximum height and total distance are as following.

For maximum height, the percentage difference between experimental and theoretical values for the three-finned rocket ranged from 0.0% to 52.6%, whereas for the four-finned rocket, it ranged from 1.2% to 51.8%. In terms of total distance (range), the percentage differences for the three-finned rocket ranged from 3.4% to 36.8%, and for the four-finned rocket from 2.1% to 42.7%, excluding cases where the theoretical value was zero (vertical launches at 90°, for which the theoretical range is always zero and the percentage difference is undefined).

These variations can be attributed to multiple factors, including experimental limitations, air resistance, minor inconsistencies in rocket construction, or deviations in the discharge coefficient from assumed values. Researchers use the average value 0.7 for discharge coefficient due to the limitations of apparatus, while the actual number may vary from 3-fins rocket to 4-fins rockets (Table 4). Another possible cause that causes the difference is the flaw in the rocket design itself, with flaws which make it not following projectile trajectory.

Larger discrepancies, exceeding 50% in some height comparisons, often occurred at lower or intermediate launch angles, which may reflect measurement errors, environmental influences, or instability during flight. Nonetheless, the data generally demonstrate reasonable agreement between theoretical models and empirical outcomes,

underscoring the kit's value as a practical, inquiry-based learning tool. The inclusion of quantitative error analysis not only deepens students' understanding of the underlying physics but also highlights the importance of critical thinking and iterative improvement in experimental science [4], [20].

Table 4. Comparison between experimental and theoretical data

Number of Fins	Launch Angle (°)	Experimental		Theoretical	
		Maximum Height (m)	Total Distance (m)	Maximum Height (m)	Total Distance (m)
3	15	0.30	7.40	0.30	5.63
3	30	1.33	14.35	2.70	22.39
3	45	2.35	20.86	4.96	23.39
3	60	5.23	13.51	6.65	17.19
3	75	6.01	10.34	8.58	10.08
3	90	9.41	2.52	8.30	0.00
4	15	1.67	10.15	1.10	17.71
4	30	2.92	18.13	2.46	23.01
4	45	4.14	23.10	4.46	21.42
4	60	5.84	15.56	7.72	22.08
4	75	8.67	12.96	10.25	13.24
4	90	10.40	3.79	10.53	0.00

4 Conclusions

The development and evaluation of an Arduino-based water rocket launcher demonstrated both strong feasibility and educational value. Quantitative comparisons showed that, while some measurement discrepancies exist due to real-world factors, the experimental results broadly align with theoretical predictions, providing a sound basis for experiential physics education. Expert assessments confirmed that the tool is pedagogically effective, technologically robust, and safe for classroom and laboratory

use, while user feedback underscored its positive impact on student engagement, motivation, and conceptual understanding.

In summary, the Arduino-based water rocket launcher offers a replicable, scalable, and impactful solution for introducing project-based STEM learning. Continued development should focus on enhancing data accuracy, safety, and supporting materials to maximize its educational potential. Broader implementation may contribute to improved science learning outcomes and increased student interest in physics and engineering disciplines.

Acknowledgements

We would like to express my sincere gratitude to Universitas Trisakti for providing the facilities and resources. Our appreciation goes to all participants and colleagues who contributed to this study. Finally, we are deeply grateful to my family and friends for their encouragement throughout this journey.

References

[1] L. D. English, "STEM education K-12: Perspectives on integration," *International Journal of STEM Education*, vol. 3, no. 1, pp. 1–8, March 2016. https://doi.org/10.1186/s40594-016-0036-1

[2] T. Kennedy & M. Odell, "Engaging students in STEM education". *Science Education International*, vol. 25, no. 3, pp. 246–258, Available: https://files.eric.ed.gov/fulltext/EJ1044508.pdf

[3] Z. Abidi, R. A. Annisa, A. R. Arianti, & Y. H. Anggriawan, "Integrating STEM and Environmental Education: Effects On Student Attitudes and Knowledge", *International Journal of Mathematics and Science Education*, vol. 1, no. 1, pp. 48–54. https://doi.org/10.62951/ijmse.v1i1.80

[4] R. J. Beichner, "Instructional technology research and development in a US physics education group," *European Journal of Engineering Education*, vol. 31, no. 4, pp. 383–393, August 2006, https://doi.org/10.1080/03043790600676125

[5] D. Herro & C. Quigley, "Exploring teachers' perceptions of STEAM teaching through professional development: implications for teacher educators," *Professional Development in Education*, vol. 43, no. 3, pp. 416–438, Jul. 2016, https://doi.org/10.1080/19415257.2016.1205507

[6] García-Tudela, Pedro & Marín-Marín, José-Antonio. (2023). Use of Arduino in Primary Education: A Systematic Review. Education Sciences. 13. 134. https://doi.org/10.3390/educsci13020134

[7] Box, S., Bishop, C. M., & Hunt, H. (2014). *Stochastic six-degree-of-freedom flight simulator for passively controlled high-power rockets*. Journal of Aerospace Engineering, 24(1), 31-45. https://doi.org/10.1061/(ASCE)AS.1943-5525.0000252

[8] Muslow, M. (2011). *Modelling and optimization of multi-stage water rockets* (Bachelor's thesis). Ernst-Moritz-Arndt-Universität Greifswald. Retrieved from https://physik.uni-greifswald.de/storages/uni-greifswald/fakultaet/mnf/physik/ag_schneider/Arbeiten/matthiasBA.pdf

[9] Dick, W., & Carey, L. 1996. *The systematic design of instruction 4th ed*. New York, NY: HarperCollins College Publishers.

[10] Molenda, M. (2003). *In search of the elusive ADDIE model.* Performance Improvement, 42(5), 34–36. https://doi.org/10.1002/pfi.4930420508

[11] Branch, R. M. (2009). Instructional design: The ADDIE approach. Springer. https://doi.org/10.1007/978-0-387-09506-6

[12] Gagné, R. M., Wager, W. W., Golas, K. C., & Keller, J. M. (2005). Principles of instructional design (5th ed.). Wadsworth/Thomson Learning.

[13] Mills, Julie & Treagust, David. (2003). *Engineering Education, Is Problem-Based or Project-Based Learning the Answer.* Aust J Eng Educ. 3.

[14] DeVellis, R. F. (2017). *Scale development: Theory and applications* (4th ed.). Sage Publications.

[15] Boateng, G. O., Neilands, T. B., Frongillo, E. A., Melgar-Quiñonez, H. R., & Young, S. L. (2018). *Best practices for developing and validating scales for health, social, and behavioral research: A primer*. Frontiers in Public Health, 6, 149. https://doi.org/10.3389/fpubh.2018.00149

[16] Tavakol, M., & Dennick, R. (2011). *Making sense of Cronbach's alpha.* International Journal of Medical Education, 2, 53–55.

[17] Creswell, J. W., & Creswell, J. D. (2018). *Research design: Qualitative, quantitative, and mixed methods approaches* (5th ed.). Sage.

[18] Fowler, F. J. (2014). Survey research methods (5th ed.). Sage.Box, S., Bishop, C. M., & Hunt, H. (2014). Stochastic six-degree-of-freedom flight simulator for passively controlled high-power rockets. *Journal of Aerospace Engineering, 24*(1), 31-45. https://doi.org/10.1061/(ASCE)AS.1943-5525.0000252

[19] Field, A. (2013). *Discovering statistics using IBM SPSS Statistics* (4th ed.). Sage.

[20] Sutton, G. P., & Biblarz, O. (2016). *Rocket propulsion elements* (9th ed.). John Wiley & Sons.

[21] Serway, R. A., & Jewett, J. W. (2014). *Physics for scientists and engineers with modern physics* (9th ed.). Cengage Learning.

[22] Irawati, I. (2016). *Water rocket competition: Application of project-based physics learning.* Proceedings of the National Seminar on Physics (E-Journal) SNF2016, 5, 29-34. https://doi.org/10.21009/0305010207

This page intentionally left

IJASST
International Journal of
Applied Sciences and Smart Technologies
p-ISSN 2655-8564, e-ISSN 2685-943, pp. 261-278, 2026

Volume 08
Issue 01

Analysis of Key Features in PCOS Diagnosis Using Random Forest and XGBoost with SMOTE and SHAP

Aulia Firdatunnisa[1], Eka Wahyu Hidayat[1*], Siti Yuliyanti[1]

[1]*Department of Informatics, Faculty of Engineering,*
Siliwangi University, Indonesia
[*]*Corresponding Author: ekawahyu@unsil.ac.id*

(Received 18-07-2025; Revised 02-09-2025; Accepted 9-04-2026)

Abstract
Polycystic Ovary Syndrome (PCOS) is a hormonal disorder in women of reproductive age characterized by irregular cycles, hyperandrogenism, and polycystic ovarian morphology. Diagnosis is challenging because symptoms overlap with other endocrine disorders. This study proposes an interpretable machine learning approach for PCOS diagnosis using Random Forest and XGBoost. The Synthetic Minority Oversampling Technique (SMOTE) was applied to handle class imbalance, while Shapley Additive Explanations (SHAP) enhanced model interpretability. The dataset included 541 samples with 45 clinical and hormonal features, processed through preprocessing and hyperparameter tuning with GridSearchCV. XGBoost with SMOTE and GridSearchCV achieved the best performance, with 93% accuracy, 92% precision, 89% recall, and 90% F1-score. Random Forest obtained comparable results with 93% accuracy, 94% precision, 87% recall, and 90% F1-score. SHAP analysis highlighted key features such as follicle count, Anti-Müllerian Hormone (AMH), skin darkening, weight gain, and irregular cycles. Global SHAP interpretation identified the most influential predictors, while local SHAP provided patient-specific explanations that improved transparency. The consistency of SHAP results with the Rotterdam criteria supports the model's clinical validity and strengthens trust in AI-assisted tools. Overall, combining SMOTE, GridSearchCV, and SHAP not only improved predictive performance but also ensured transparent outcomes, indicating potential use for early PCOS screening.

Keywords: Machine Learning, PCOS, SHAP, SMOTE, XGBoost

1 Introduction

Polycystic Ovary Syndrome is a hormonal disorder that affects women childbearing age [1]. This hormonal disorder is characterized by symptoms of irregular menstrual cycles, abnormal hair growth, excess androgen hormones and ovarian cysts [2]. PCOS symptoms like irregular cycles, acne, and hirsutism often overlap with other hormonal

disorders such as hypothyroidism, hyperprolactinemia, and adrenal disorders, making diagnosis challenging. For instance, hypothyroidism causes irregular periods, weight gain, and fatigue, while congenital adrenal hyperplasia leads to hirsutism and elevated androgens [3]. Hyperprolactinemia, characterized by high prolactin levels, can also trigger menstrual disorders and infertility [4]. The similarity of these symptoms often leads to misdiagnosis if not accompanied by hormonal and ultrasound examinations.

Based on the Rotterdam Criteria (2003), the diagnosis of PCOS is established if the patient meets at least two of the three criteria: oligo/anovulation, hyperandrogenism, and polycystic ovarian morphology (PCOM) [5]. The prevalence of PCOS in Indonesia is increasing significantly, from 4-6% (1990) to 20% by 2023. If left untreated, PCOS can lead to insulin resistance, type 2 diabetes, and cardiovascular disease [6], [7]. Based on this, an accurate and interpretative diagnosis system is required.

Random Forest offers strong interpretability and stability with limited features, while XGBoost provides high accuracy and efficiency on large, complex data, effectively handling overfitting and high dimensionality [8] [9]. Both models have shown excellent performance in diagnosing diseases, including PCOS. However, class imbalance remains a key challenge in clinical datasets. SMOTE helps address this and has been shown to improve accuracy Random Forest achieved 93.26% [10] and XGBoost 96%[11]. For diagnostic clarity, Explainable AI methods like SHAP help reveal the most influential features, such as insulin, BMI, and LH/FSH ratio [12], [13], [14] .

There are not many studies that combine SMOTE and SHAP integrated in Random Forest and XGBoost respectively. This study aims to develop and evaluate the PCOS model. So that the model not only achieves high accuracy, but the model is also able to explain the diagnosis results.

2 Material and Methods

Research Data

This study uses the PCOS dataset from Kaggle uploaded by Prasoon Kottarathil, containing 541 female patients from a hospital in Kerala, India [15]. The patients' age range is 20–45 years old, with the majority in the 25–35 age group. Women of South

Asian ethnicity, including Indian, have a higher risk of PCOS (3.7–22.5%) [16]. This disorder can also be experienced by other ethnicities, especially those with unhealthy lifestyles. This demographic information is added so that readers can assess the extent to which the model can be generalized.

Data Preprocessing

Data preprocessing was performed by removing irrelevant columns and rows with missing values. During the preprocessing stage, irrelevant columns are removed because they do not contribute to the prediction and have the potential to cause noise, while missing values are removed to maintain input consistency [17]. This step is important because even though Random Forest is quite resistant to noise, irrelevant data still reduces stability, while XGBoost, which is more sensitive to missing values, actually improves performance when such data is removed [18], [19]. Missing values accounted for only about 0.18%, which did not have a significant effect and were removed to maintain data integrity [20]. In addition, imputation risks introducing bias in sensitive medical data. For future research, the use of more sophisticated imputation techniques such as model-based or regression-based imputation is recommended.

Exploratory Data Analysis

The Exploratory Data Analysis stage in this research is carried out to find out the relationship patterns between data. In addition, to find out the initial insight of the data before interpretation is carried out.

Model Implementation

This study uses Random Forest and XGBoost models, with SMOTE applied to prevent data leakage and GridSearchCV for optimal parameter tuning. Three schemes are tested: (1) baseline, (2) with SMOTE, and (3) with SMOTE + GridSearch. The complete methodology is data collection, preprocessing, modeling, evaluation, and SHAP-based interpretation shown in Fig. 1.

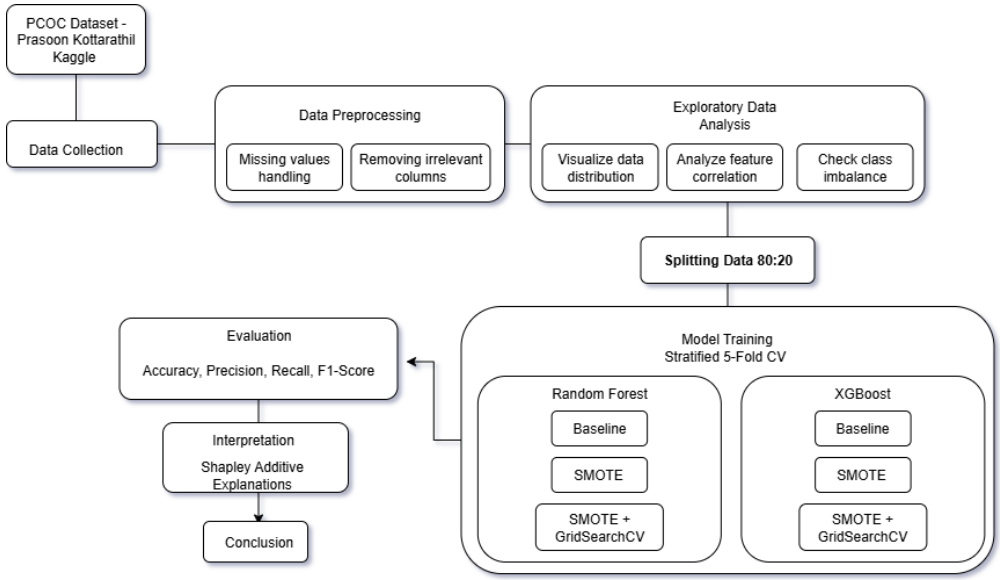

Figure 1. Research flow

Interpretability with SHAP

The SHAP approach was used to interpret the trained model, identifying key features contributing to the diagnosis. Interpretation was conducted at both global (entire dataset) and local (individual patient) levels.

3 Results and Discussions

Exploratory Data Analysis

The Exploratory Data Analysis stage was conducted to understand the distribution of data, the relationship between features, and see the differences in characteristics between PCOS and non-PCOS patients. The dataset used in this study consists of 541 patient data samples with 45 features containing physical, hormonal indicators, and clinical symptoms.

Based on EDA, it is found that the class distribution on the target label shows data imbalance. There are more non-PCOS patients than PCOS patients. The unbalanced class distribution is shown in Fig. 2.

Based on descriptive analysis, it was found that PCOS patients were generally between 25-30 years old and had higher BMI values compared to non-PCOS patients. The correlation heatmap illustrates the relationship between features and the PCOS label.

Features like follicle count (right and left), skin darkening, hair growth, and weight gain show strong correlations. Meanwhile, hormonal features such as AMH and LH/FSH ratio have lower linear correlations but may influence outcomes through non-linear relationships not captured by Pearson correlation. A visualization of the correlation heatmap is shown in Fig. 3.

Model Evaluation

Model evaluation was conducted with 3 schemes, including: (1) baseline, (2) model with SMOTE, (3) model with SMOTE and GridSearchCV as tuning parameter. The algorithms used are Random Forest and XGBoost. Table 1 presents the model evaluation results.

Based on the evaluation results in Table 1, applying SMOTE significantly improved model accuracy. GridSeacrhCV on XGBoost provided better metric balance for minority classes compared to Random Forest. In disease diagnosis like PCOS, recall is crucial as it reflects the model's ability to identify actual patients and reduce false negatives. SMOTE increased recall in both models, but XGBoost with SMOTE and GridSearchCV achieve stable recall (0.80), high precision (0.91), and F1-Score of 0.85 indicated a balanced and accurate detection of positive cases.

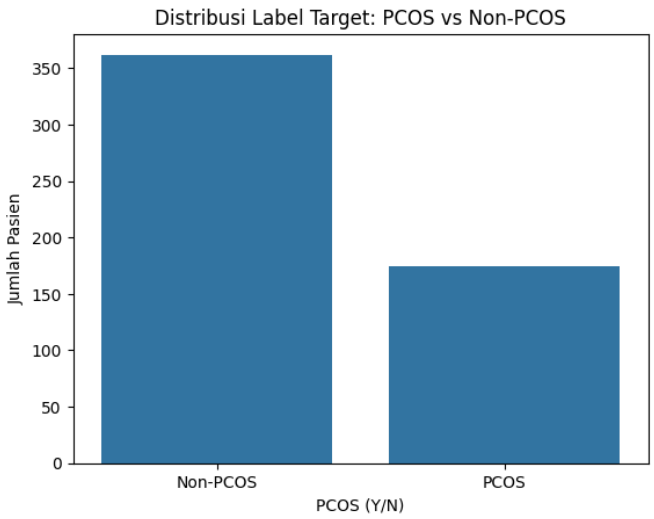

Figure 2. Label distribution

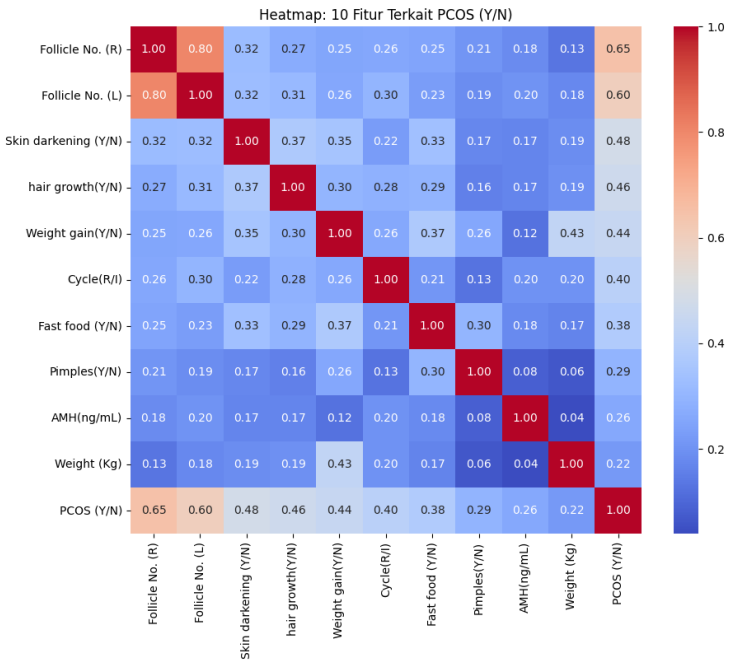

Figure 3. Heatmap correlation

Table 1. Evaluation results of Random Forest and XGBoost

Model	Schema	Accuracy
Random Forest	Baseline	0.89
Random Forest	SMOTE	0.95
Random Forest	SMOTE + GridSeacrhCV	0.93
XGBoost	Baseline	0.89
XGBoost	SMOTE	0.91
XGBoost	SMOTE + GridSearchCV	0.93

Model Interpretation with SHAP

The interpretation stage is carried out on both models with the aim of finding out which features are most influential on the model diagnosis results. Interpretation is done in two stages between global interpretation and local interpretation.

Random Forest Model

Global interpretation is done to determine the most influential features in general or overall, in the model. Follicle No. (R) and Follicle No. (L) are two main features in the

diagnosis, in line with the Rotterdam Criteria which mention PCOM as the main indicator of PCOS [5]. The third feature is the skin darkening, a common symptom in PCOS patients with insulin resistance [21] Fig. 4 shows the 10 most contributing features in the Random Forest model.

Based on the interpretation results presented in Fig. 4. Hirsutism or excessive hair growth occupies the fourth position. In a clinical context, this is a clinical manifestation of hyperandrogenism which is included in one of the Rotterdam Criteria [22]. Weight gain and Fast food (Y/N) are interrelated features that contribute significantly to the diagnosis. Both reflect an unhealthy lifestyle that triggers obesity and metabolic disorders, including insulin resistance [23][24]. AMH (ng/mL) also supports the diagnosis ah high AMH levels indicated an increased number of follicles, in accordance with the PCOM criteria in Rotterdam Criteria [25].Irregular menstrual cycle and cycle length features showed significant influence on diagnosis, in line with oligo/anovulation in Rotterdam Criteria [26]. Pimples (Y/N) reflecst acne symptons due to androgen excess, also part of the criteria [27].

Local interpretation is also performed on the Random Forest model, similar to the global interpretation, this interpretation is done to find out which features are most influential on the diagnosis results, but more specifically for one patient diagnosed with PCOS. Local interpretation on PCOS patients is presented in Fig. 5.

Based on Fig. 5, the patient was predicted to have PCOS with a probability of 92.3% (f(x) = 0.923), an increase from the model average prediction of 35.8% (F[f(x)] = 0.358).

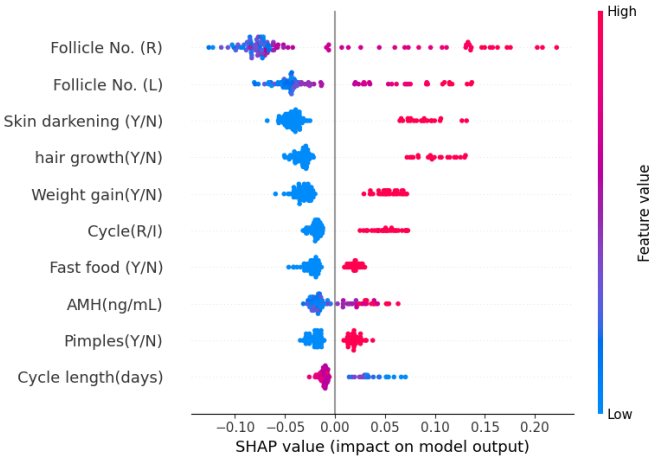

Figure 4. Global Random Forest interpretation results with SHAP

The Follicle No. (R) feature contributed the most (+0.15), indicating a high number of follicles. Other features that contributed positively included Hair Growth (+0.08), Skin Darkening (+0.08), Weight Gain (+0.05), and Follicle No. (L) (+0.05), all supporting the diagnosis of PCOS according to Rotterdam criteria [22][28].

Irregular menstrual cycle (Cycle (R/I) = 4, +0.05) and cycle duration (+0.03) reflected oligo/anovulation. The features Pimples (+0.04) and Fast-Food consumption (+small value) also strengthened the prediction of PCOS although their contribution was lower. These features cumulatively increased the predictive value towards a positive diagnosis.

XGBoost Model

The model not only evaluated in terms of performance, this study emphasized the importance of model interpretability in medical diagnosis, given that PCOS symptoms are similar to other hormonal diseases. Interpretation is necessary to reduce the risk of misdiagnosis and ensure the prediction results can be understood logically an clinically. The results of SHAP interpretation on the XGBoost model are presented in Fig. 6.

Based on Fig. 6, Follicle No. (R) is the most influential feature in the interpretation of the XGBoost model, with consistently high SHAP values increasing the prediction of PCOS, in accordance with the PCOM criteria in the Rotterdam Criteria [28].

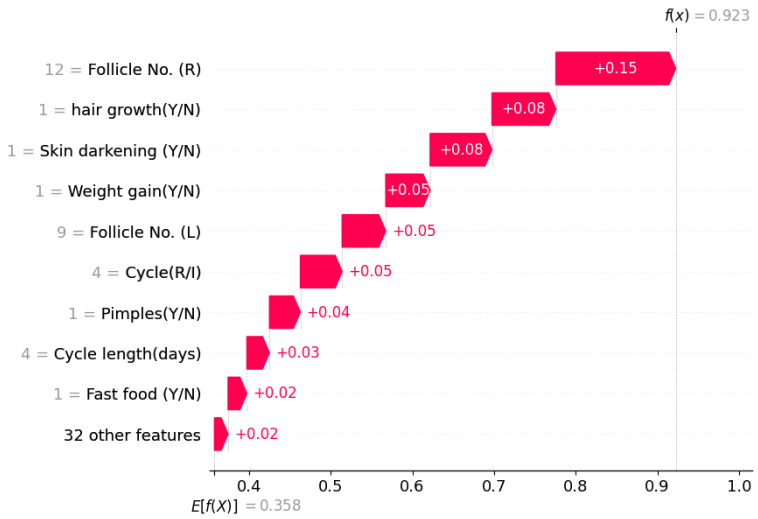

Figure 5. Local interpretation results of Random Forest model with SHAP

Hair growth (Y/N) feature followed as a major contributor, reflecting symptoms of hyperandrogenism [22].

Skin Darkening, Weight Gain, and AMH features also made significant contributions. Skin Darkening is related to insulin resistance and obesity [21]. Weight gain (Y/N) reflects obesity which exacerbates metabolic disorders [6], and AMH indicates a high follicle count [29], [30]. Other features such as Pimples (acne), Cycle (R/I) (menstrual cycle disorder), and Waist:Hip Ratio (central obesity) also contribute, all associated with PCOS symptoms [6][31]. PRL (ng/mL) is also considered although not the main criterion, as abnormal prolactin levels can cause menstrual cycle disorders and need to be differentiated from other hormonal disorders [32]. Follicle No. (L) also contributes, although smaller than the right side, it still supports the identification of PCOM [5].

Local interpretation of the XGBoost model using SHAP was performed to see the effect of each feature on the diagnosis result for one patient. The result shown in Fig. 7. Based on the local interpretation results shown in Fig. 7, the final prediction value of the model reaches ($f(x) = 8.63$), well above the model average ($E[f(x)] = -0.641$). Follicle No. (R) was the main contributor (+3.07), reflecting the number of excess follicles that fit the PCOM criteria [28]. The Skin Darkening (+0.98), Weight Gain (+0.85), Cycle (R/I) (+0.70), and AMH (+0.65) features also contributed greatly to the positive classification, as they are associated with insulin resistance, obesity, menstrual cycle disorders, and high follicle count [21].

The Pimples feature (+0.65) reflected symptoms of hyperandrogenism, while Hair Growth (-0.51) did not contribute significantly as it was 0. High Waist:Hip Ratio (+0.51) indicating central obesity, and PRL (+0.39), although within normal limits, was still considered relevant as it could affect the menstrual cycle. Overall, the model judged the features to be clinically relevant and strengthened the positive prediction of PCOS.

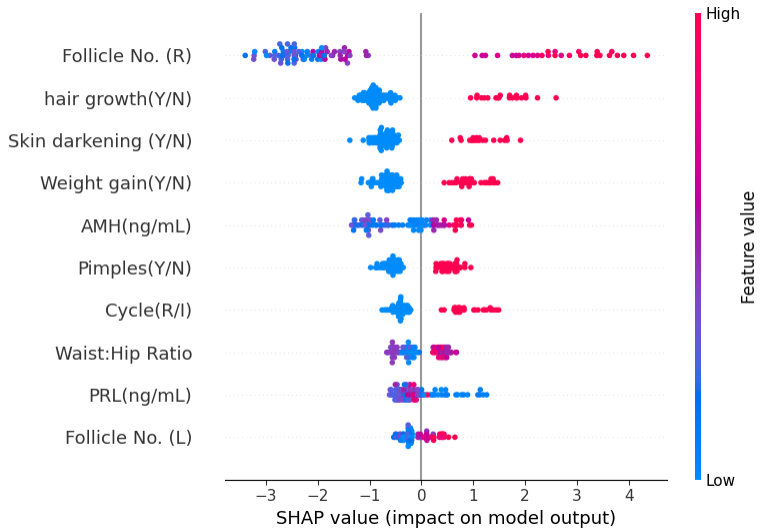

Figure 6. Global interpretation with SHAP on the XGBoost model

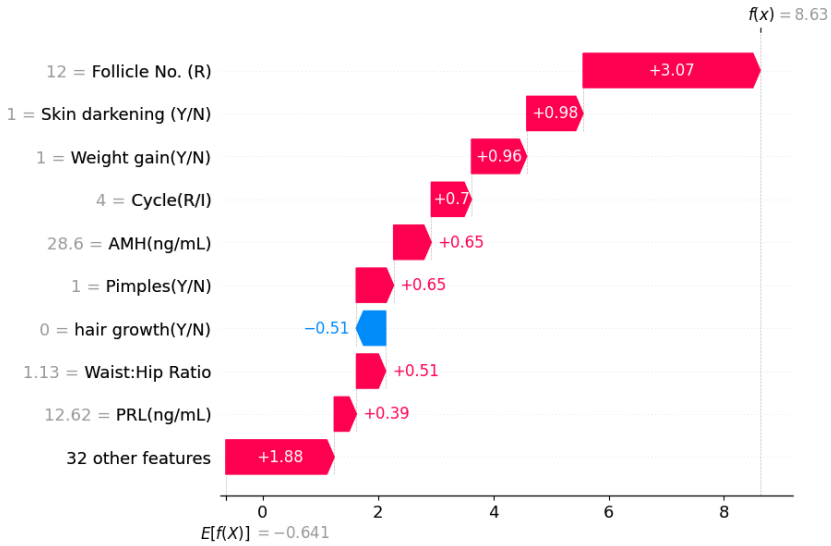

Figure 7. Local interpretation on XGBoost model with SHAP

Comparison of SHAP and Feature Importance

Feature importance and SHAP are model interpretation methods that differ in approach. Feature importance calculates feature contributions globally based on impurity or gain, without considering interactions or direction of influence. In contrast, SHAP uses game theory to calculate the contribution of individual features, both globally and locally,

and shows the direction and magnitude of influence, making it more transparent and in line with the principles of XAI. Fig. 8 shows a Venn diagram comparing features identified by SHAP and feature importance in both models.

Based on Fig. 8. Follicle No. (R) consistently appears as the most influential feature in both SHAP and feature importance, alongside clinical features like Hair Growth, Skin Darkening, Weight Gain, and Cycle (R/I). However, SHAP uniquely identifies features such as Pimples and Cycle Length, while feature importance highlights Blood Group and BP Systolic. This difference reflects SHAP's advantage in capturing local and non-linear interactions, offering more comprehensive and clinically relevant interpretations, especially in PCOS diagnosis.

Comparison of Models with Other Studies

The results of this study were compared with several previous studies that also examined PCOS diagnosis using machine learning. This was done to provide a more comprehensive context. Table 2 shows the results of this study and comparisons with other studies.

Table 2 shows that previous studies produced higher accuracy. However, most of them only emphasized predictive performance without considering clinical interpretability. Meanwhile, this study focuses on the balance between model performance and the transparency of model prediction results with the application of SHAP, so that it can provide added value in the context of medical decision systems.

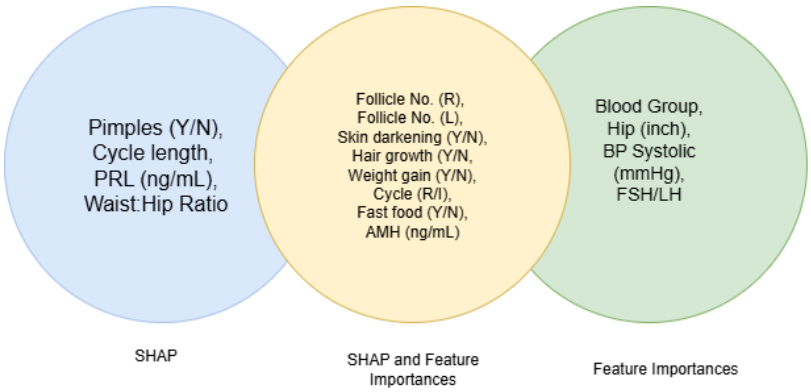

Figure 8. Comparison of SHAP and feature importance

Table 2. Evaluation results of Random Forest and XGBoost

Study	Method	Accuracy
[33]	Random Forest	0.91
[12]	XGBoost	0.90
Our Research	Random Forest + SMOTE + GridSeacrhCV	0.93
Our Research	XGBoost+ SMOTE + GridSeacrhCV	0.93

4 Conclusions

This study shows that the integration of Random Forest and XGBoost with SMOTE and SHAP interpretation produces an accurate and explainable PCOS diagnosis model. The best model was obtained from XGBoost with SMOTE and GridSearchCV, which provided balanced accuracy and recall. SHAP analysis highlighted important features such as follicle count, AMH, menstrual cycle, skin darkening, and weight gain. The interpretation is aligned with the Rotterdam criteria, which are widely recognized by the medical community, thus providing a strong basis for interpretation. However, further validation by medical experts is still needed to improve interpretability in clinical practice

This study is based on a collection of secondary clinical data obtained from hospitals, not from direct clinical examinations in laboratories or medical imaging. Therefore, the validity of the results is still limited to the available data patterns. Further research is recommended using real clinical data and integration with medical examinations such as ultrasound or laboratory tests. It should be emphasized that the main purpose of this study is as an initial screening tool or decision support system, not a substitute for medical diagnosis, so that it can help health workers identify cases that require further examination.

The limitation of this study lies in its predictive, rather than causal, model can only predict without definitively explaining the cause-and-effect relationship. If future studies use large datasets with high missing values, the application of modern imputation techniques such as regression-based imputation is recommended.

Acknowledgements

The author would like to thank the Department of Informatics, Faculty of Engineering, Universitas Siliwangi, for the support provided in completing this research.

References

[1] I. A. Begum, A. S. M. S. Hosen, D. Ghimire, and M. J. Park, "Association of Polycystic Ovary Syndrome with Clinical, Physical, and Reproductive Factors: A Data-Driven Analysis," *Diagnostics*, vol. 15, no. 6, Mar. 2025, doi: 10.3390/diagnostics15060711.

[2] C. Johnson, G. Garipoğlu, Y. Jeanes, G. Frontino, and A. Costabile, "The Role of Diet, Glycaemic Index and Glucose Control in Polycystic Ovary Syndrome (PCOS) Management and Mechanisms of Progression," Dec. 01, 2025, *Springer*. doi: 10.1007/s13668-024-00601-4.

[3] M. Yesiladali, M. G. K. Yazici, E. Attar, and F. Kelestimur, "Differentiating Polycystic Ovary Syndrome from Adrenal Disorders," Sep. 01, 2022, *Multidisciplinary Digital Publishing Institute (MDPI)*. doi: 10.3390/diagnostics12092045.

[4] K. van der Ham *et al.*, "The prevalence of thyroid dysfunction and hyperprolactinemia in women with PCOS," *Front Endocrinol (Lausanne)*, vol. 14, 2023, doi: 10.3389/fendo.2023.1245106.

[5] J. J. Kim, K. R. Hwang, D. Lee, S. Kim, and Y. M. Choi, "Adolescents diagnosed with polycystic ovary syndrome under the Rotterdam criteria but not meeting the diagnosis under the updated guideline," *Human Reproduction*, vol. 39, no. 5, pp. 1072–1077, May 2024, doi: 10.1093/humrep/deae042.

[6] X. Zeng, Y. jie Xie, Y. ting Liu, S. lian Long, and Z. cheng Mo, "Polycystic ovarian syndrome: Correlation between hyperandrogenism, insulin resistance and obesity," Mar. 01, 2020, *Elsevier B.V.* doi: 10.1016/j.cca.2019.11.003.

[7] Muna Dinur Rafifah, RB. Soeherman Herdiningrat, and Rizki Perdana, "Hubungan Obesitas dengan Polycystic Ovarian Syndrome (PCOS) di RSUD Al-Ihsan Provinsi Jawa Barat," *Bandung Conference Series: Medical Science*, vol. 5, no. 1, pp. 135–140, Jan. 2025, doi: 10.29313/bcsms.v5i1.16251.

[8] M. Song, H. Jung, S. Lee, D. Kim, and M. Ahn, "Diagnostic classification and biomarker identification of alzheimer's disease with random forest algorithm," *Brain Sci*, vol. 11, no. 4, Apr. 2021, doi: 10.3390/brainsci11040453.

[9] R. Chen *et al.*, "A study on predicting the length of hospital stay for Chinese patients with ischemic stroke based on the XGBoost algorithm," *BMC Med Inform Decis Mak*, vol. 23, no. 1, Dec. 2023, doi: 10.1186/s12911-023-02140-4.

[10] P. Chauhan, P. Patil, N. Rane, P. Raundale, and H. Kanakia, "Comparative Analysis of Machine Learning Algorithms for Prediction of PCOS," Institute of Electrical and Electronics Engineers (IEEE), Aug. 2021, pp. 1–7. doi: 10.1109/iccict50803.2021.9510128.

[11] M. S. Khan Inan, R. E. Ulfath, F. I. Alam, F. K. Bappee, and R. Hasan, "Improved Sampling and Feature Selection to Support Extreme Gradient Boosting for PCOS Diagnosis," in *2021 IEEE 11th Annual Computing and Communication Workshop and Conference, CCWC 2021*, Institute of Electrical and Electronics Engineers Inc., Jan. 2021, pp. 1046–1050. doi: 10.1109/CCWC51732.2021.9375994.

[12] B. J. Chelliah, S. K. Gahra, and A. Senthilselvi, "Enhancing PCOS Prediction Using Machine Learning and Explainable AI," in *2024 International Conference*

on Intelligent Computing and Sustainable Innovations in Technology (IC-SIT), IEEE, Nov. 2024, pp. 1–5. doi: 10.1109/IC-SIT63503.2024.10862800.

[13] B. V. Madhavi, A. Firdouse, and A. Kodipalli, "Detection of PCOS Leveraging Machine Learning and Interpretation Using Explainable AI," in *2024 1st International Conference for Women in Computing, InCoWoCo 2024 - Proceedings*, Institute of Electrical and Electronics Engineers Inc., 2024. doi: 10.1109/InCoWoCo64194.2024.10863596.

[14] P. Gethsia, J. Anitha, and S. Juliet, "Interpreting PCOS Risk Factors Using Explainable AI and Ensemble Modeling Techniques," in *Proceedings of the 4th International Conference on Ubiquitous Computing and Intelligent Information Systems, ICUIS 2024*, Institute of Electrical and Electronics Engineers Inc., 2024, pp. 33–38. doi: 10.1109/ICUIS64676.2024.10867148.

[15] P. Kottarathil, "Polycystic Ovary Syndrome (PCOS) Dataset," Kaggle Dataset.

[16] M. A. Ganie *et al.*, "Prevalence, Phenotypes, and Comorbidities of Polycystic Ovary Syndrome Among Indian Women," *JAMA Netw Open*, vol. 7, no. 10, p. e2440583, Oct. 2024, doi: 10.1001/jamanetworkopen.2024.40583.

[17] T. Shadbahr *et al.*, "The impact of imputation quality on machine learning classifiers for datasets with missing values," *Communications Medicine*, vol. 3, no. 1, Dec. 2023, doi: 10.1038/s43856-023-00356-z.

[18] Y. Akhiat, Y. Manzali, M. Chahhou, and A. Zinedine, "A New Noisy Random Forest Based Method for Feature Selection," *Cybernetics and Information Technologies*, vol. 21, no. 2, pp. 10–28, Jun. 2021, doi: 10.2478/cait-2021-0016.

[19] N. Shi, Y. Li, L. Wen, and Y. Zhang, "Rapid prediction of landslide dam stability considering the missing data using XGBoost algorithm," *Landslides*, vol. 19, no. 12, pp. 2951–2963, Dec. 2022, doi: 10.1007/s10346-022-01947-y.

[20] A. Arora *et al.*, "The value of standards for health datasets in artificial intelligence-based applications," *Nat Med*, vol. 29, no. 11, pp. 2929–2938, Nov. 2023, doi: 10.1038/s41591-023-02608-w.

[21] B. Khan and R. Basu, "Acanthosis nigricans in adolescents with polycystic ovary syndrome," *Int J Reprod Contracept Obstet Gynecol*, vol. 11, no. 3, p. 765, Feb. 2022, doi: 10.18203/2320-1770.ijrcog20220553.

[22] P. M. Spritzer, L. B. Marchesan, B. R. Santos, and T. M. Fighera, "Hirsutism, Normal Androgens and Diagnosis of PCOS," Aug. 01, 2022, *Multidisciplinary Digital Publishing Institute (MDPI)*. doi: 10.3390/diagnostics12081922.

[23] R. Heidari, F. Eftekhari, and M. Koushkie Jahromi, "Association of physical activity and nutrition-related knowledge, attitudes and practices with obesity indices in college-aged females with polycystic ovary syndrome in Shiraz, Iran: A cross-sectional study," *BMJ Open* , vol. 15, no. 5, May 2025, doi: 10.1136/bmjopen-2025-099260.

[24] E. J. Houston and N. M. Templeman, "Reappraising the relationship between hyperinsulinemia and insulin resistance in PCOS," May 01, 2025, *BioScientifica Ltd.* doi: 10.1530/JOE-24-0269.

[25] K. van der Ham, J. S. E. Laven, C. T. Tay, A. Mousa, H. Teede, and Y. V. Louwers, "Anti-müllerian hormone as a diagnostic biomarker for polycystic ovary syndrome and polycystic ovarian morphology: a systematic review and meta-analysis," Oct. 01, 2024, *Elsevier Inc.* doi: 10.1016/j.fertnstert.2024.05.163.

[26] S. Syamsiah, C. Adelin, and R. Kundaryanti, "THE RELATIONSHIP BETWEEN OBESITY, MENSTRUAL CYCLE, AND POLYCYSTIC OVARY SYNDROME CASES," *Jurnal Kebidanan Malahayati)*, vol. 10, no. 9, pp. 929–934, 2024, doi: 10.33024.

[27] S. A. Kanbour and A. S. Dobs, "Hyperandrogenism in Women with Polycystic Ovarian Syndrome: Pathophysiology and Controversies," *Androgens*, vol. 3, no. 1, pp. 22–30, Mar. 2022, doi: 10.1089/andro.2021.0020.

[28] R. Yang *et al.*, "Enhancing repeatability of follicle counting with deep learning reconstruction high-resolution MRI in PCOS patients," *Sci Rep*, vol. 15, no. 1, Dec. 2025, doi: 10.1038/s41598-024-84812-3.

[29] M. I. Cedars, "Evaluation of Female Fertility - AMH and Ovarian Reserve Testing," Jun. 01, 2022, *Endocrine Society*. doi: 10.1210/clinem/dgac039.

[30] L. Melanie and E. Moolhuijsen, *Polycystic Ovary Syndrome and anti-Müllerian Hormone Integrating Genetics in Etiology and Diagnosis*. 2025. [Online]. Available: www.ridderprint.nl

[31] B. Keyif and A. Yavuzcan, "Visceral and Dysfunctional Adiposity Indices as Predictors of Insulin Resistance and Metabolic Syndrome in Women with Polycystic Ovary Syndrome: A Cross-Sectional Study," *Medicina (Lithuania)*, vol. 61, no. 3, Mar. 2025, doi: 10.3390/medicina61030424.

[32] Z. Davoudi, F. Araghi, M. Vahedi, N. Mokhtari, and M. Gheisari, "Prolactin level in polycystic ovary syndrome (Pcos): An approach to the diagnosis and management," *Acta Biomedica*, vol. 92, no. 5, Nov. 2021, doi: 10.23750/abm.v92i5.9866.

[33] S. Majumdar, S. K. Biswas, and B. Purkayastha, "Effectiveness of Class Imbalance Treatment for Diagnosis of PCOS Using Machine Learning Models: A

Comparative Study," in *10th International Conference on Advanced Computing and Communication Systems, ICACCS 2024*, Institute of Electrical and Electronics Engineers Inc., 2024, pp. 1346–1351. doi: 10.1109/ICACCS60874.2024.10717284.

IJASST
International Journal of
Applied Sciences and Smart Technologies
p-ISSN 2655-8564, e-ISSN 2685-943, pp. 279-292, 2026

Volume 08

Issue 01

Durability of Silica Sand-Based Self-Compacting Mortar: A Study on Sorptivity and Chemical Attack

Toluwalope Dominion Zubair [1*], Mutiu Abiodun Kareem [1], Abibat Oyindamola Usman [1], Divine Favour Adejumo [1], Glory Olajide Ponnle [1], David Adeyemi Adeyeye [1], Ojo Adeleye Akinbade[1]

[1]*Civil Engineering Department, Osun State University, Osogbo, Osun State, 230284, Nigeria*

**Corresponding Author: toluwalope.zubair@cset.uniosun.edu.ng*

(Received 11-09-2025; Revised 12-03-2026; Accepted 09-04-2026)

Abstract

Cement is an essential construction material which serves as the binder in the production of concrete, mortar and bricks production. The production of cement poses a serious issue as it results in the emission of greenhouse gases directly responsible for climate change. In this study, Self-Compacting Mortar (SCM) mixes were developed by incorporating Ground Silica Sand (GSS) of 0 - 10% at a step of 2.5% and Raw Ground Silica Sand (RSS) of 0 - 100% at a step of 25% as replacement for cement and fine aggregate, respectively. The sorptivity and chemical attack via the use of Sodium Chloride (NaCl) on SCM specimens produced from different mixes were determined after 28 and 56 days of curing. The sorptivity of SCM specimens increased at all levels compared to the control when RSS is used as replacement for fine aggregate while the same was experienced when GSS was used as replacement for cement except at the 5% replacement level. All specimens fell under the ASTM standard for sorptivity states that all construction materials must have a water absorption value within 20%. When exposed to chemical attacks, there was an increase in weight loss and compressive strength loss with every increase in percentage replacement while the SCM does not deteriorate rapidly after exposure to NaCl. It can be concluded that GSS and RSS exhibited the potential for application as binder and sand contents in SCM production.

Keywords: Cement, Chemical Attack, Self-Compacting Mortar, Silica sand, Sorptivity

1 Introduction

The mixture of cement, sand, and water known as cement mortar is frequently used in construction to lay bricks and blocks, plaster walls and ceilings, and for other

purposes [1]. Mortar is produced extensively worldwide and its use is strongly related to the global construction sector [2]. It is composite material which is produced from the mixture of cement, fine aggregate and water. The characteristics that distinguish Self-Compacting Concrete (SCC) from regular concrete can be attributed largely to those exhibited by the mortar it contains, while the presence of aggregate in it contributes less.

Self-Compacting Mortar (SCM) is a mortar type that incorporates chemical admixtures in addition to other constituents used in the production of normal mortar and acts exactly like the mortar presence in SCC. SCC is a type of concrete that can flow under its own weight and be placed in formwork with congested reinforcement without requiring vibration while maintaining uniformity. Among the benefits of SCC are quicker construction, reduced site manpower, better surface finishing, relatively simple placement, and enhanced durability [3]. Developing SCM with improved characteristics is critical in the production of SCC that meet the relevant standard requirements [4].

Both SCM and SCC employed high cement contents to achieve the desired self-consolidation characteristics, giving them an advantage over normal concrete. However, cement has great impact on the environment as it is a major source of carbon dioxide emission which contributes to climate change [5]. The activities related to extraction of non-renewable resources such as natural sand creates negative environmental impacts with increasing risk of ecological imbalance such habitat destruction, flooding, erosion. In addition, the priceless resources run the risk of running out if they are continuously harvested.

Consideration of alternative materials as alternative to cement and fine aggregate in mortar and concrete production is gaining popularity because of the needs to conserve resources as well as reduce the negative impacts of cement production and these factors have influenced numerous studies on the utilization of alternative materials which production techniques make use of renewable energy sources and emit fewer emissions in SCM and SCC. Over the years, experimental studies have been conducted by replacing some of the components (cement or fine aggregate) of mortar and concrete

with materials such as seashells, metakaolin, recycled glass, red wood, recycled aggregate concrete, waste plastics, silica sand [6].

Previous studies have in the past applied silica sand as constituents of mortar and concrete. [7] established that silica sand is appropriate for usage as replacement for fine aggregate with improved the mechanical characteristics. [8] used silica sand as partial replacement of fine aggregate in concrete. It was found that the maximum compressive strength was achieved at 15% of fine aggregate replacement with sand in concrete. [9] explored the possibility of replacing cement with silica sand in concrete. The study revealed that silica sand (up to 12%) can effectively serve as partial replacement of cement in concrete without compromising the strength of concrete. [10] investigated the influence of nano silica sand addition as cement replacement in cement mortar and found that the mortar workability decreased while the compressive and flexural strength was increased with the addition of nano silica sand. The reported studies have shown that silica served have found applications in normal cement mortar and concrete. However, its application in SCM is not yet documented. This study evaluates the durability properties of SCM incorporating Silica Sand as Binder and Fine Aggregate Contents.

2 Material and Methods

2.1 Materials

In this study, sharp sand served as fine aggregate and was collected from riverbanks within Osogbo, Nigeria. Dangote 3X Portland Limestone Cement, CEM II 42.5N (A-L) was used as binding material. It was obtained from a retail store within Osogbo, Osun State, Nigeria. The locally available silica sand free from clayey matters was sourced from Owo Eba, Osogbo, Nigeria (Lat: 7° 43’ 44.83” N, Long: 4° 34’ 49.30” E) and the chemical composition of silica sand is shown in Table 1. The silica sand was used as supplementary cementitious material and fine aggregate contents in this study. Conplast SP 430 was used as chemical admixture (Superplasticizer) to achieve the workability recommended by [3] for fresh self-compacting mortar (SCM). It was

sourced from a retailing store within Osogbo, Osun State. Potable water was employed in mixing and curing of all materials which conforms to [11]. The water was collected from the laboratory at Osun State University. The particle size distribution of our materials is shown in Fig 1.

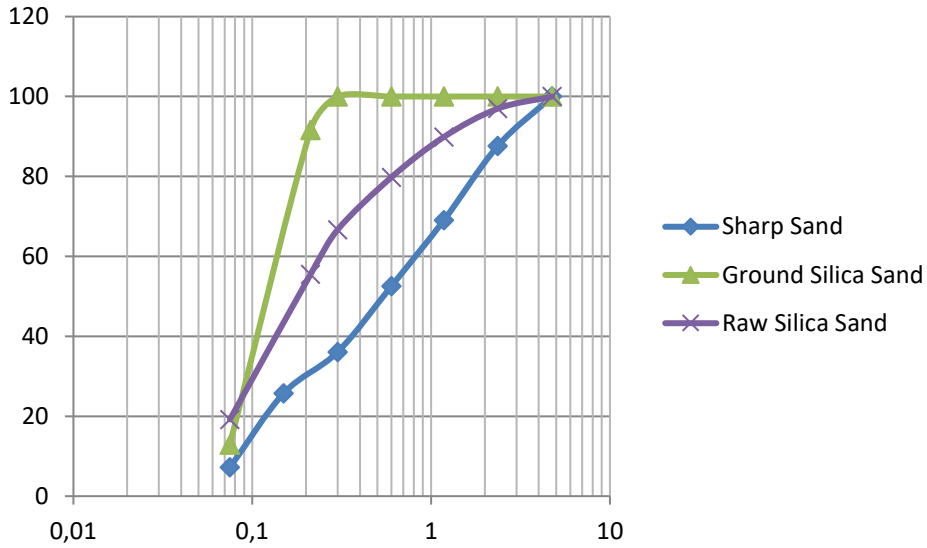

Figure 1. Particle size distribution for materials

Table 1. Chemical Composition of Silica Sand

Chemical Constituents	Compositions (%)
SiO_2	95.39
Al_2O_3	2.13
Fe_2O_3	1.87
CaO	0.20
SO_3	0.01
Mg_2O	0.02
MgO	1.53
K_2O	0.36
TiO_2	0.89
$SiO_2 + Al_2O_3 + Fe_2O_3$	99.39

2.2 Chemical Composition

The summary of the detailed chemical composition of silica sand is presented in Table 2. The main compounds present in RSS and GSS are Silica (SiO2), iron oxide (Fe2O3) and alumina (Al2O3) with the values of 95.39, 1.87 and 2.13 for RSS and 68.82, 18.461, and 4.337 for GSS. The addition of these three compounds is 99.39% for RSS and 91.622% of GSS. In [12], the minimum value for the sum of these three oxides is specified as 70%. Although both RSS and GSS are found to be enriched in silicates, they contain limited amounts of lime, sulphate, magnesia, sodium oxide, potassium oxide and titanium dioxide. The main compositional difference between RSS and GSS is in terms of the RSS having a higher content of SiO2 but lower Al2O3, Fe2O3 and Na2O + 0.659 K2O than GSS while GSS have no composition of sodium oxide (Na2O) and sulfur trioxide (SO3).

Table 2. Chemical Composition of Silica Sand

Chemical Constituents	Compositions (%)	
	RSS	GSS
SiO_2	95.39	68.82
Al_2O_3	2.13	18.461
Fe_2O_3	1.87	4.337
CaO	0.20	0.722
SO_3	0.01	-
Na_2O	0.02	-
MgO	1.53	0.219
K_2O	0.36	3.410
TiO_2	0.89	1.591

$Na_2O + 0.659\ K_2O$	0.38	3.410
$SiO_2 + Al_2O_3 + Fe_2O_3$	99.39	91.622

2.3 SCM mix proportion and specimens preparation

Mix proportion of 1:2.2 (cement: sand) with fixed water/cement ratio of 0.50, total binder content 676 kg/m^3, Conplast SP 430 of 8.11 kg/m^3 were used to prepare the mortar mixes. The first five SCM batches were prepared using ground silica sand to replace cement at five different replacement levels (0, 2.5%, 5%, 7.5% and 10%) by weight. The second five SCM batches were prepared by replacing sharp sand using silica sand at five different percentage replacements (0, 25%, 50%, 75% and 100%) by weight. The mixture proportions of the various mortar mixes for the replacement of fine aggregate and cement are summarized in Tables 3(a-b)

Table 3a. Mix design for mortar with GSS as substitute for cement (1 kg/m^3)

Mix ID	GSS (%)	Cement (kg)	GSS (kg)	Sand (kg)	Water (kg)
1	0	676	0	1487	338
2	2.5	659.1	16.9	1487	338
3	5.0	642.2	33.8	1487	338
4	7.5	625.3	50.7	1487	338
5	10.0	608.4	67.6	1487	338

Table 3b. Mix design for mortar with RSS as substitute for sharp sand (1 kg/m^3)

Mix ID	RSS (%)	Cement (kg/m^3)	RSS (kg)	Sand (kg)	Water (kg)
1	0	676	0	1487	338
2	25	676	371.75	1115.25	338
3	50	676	743.5	743.5	338
4	75	676	1115.25	371.75	338
5	100	676	1487	0	338

2.4 Testing Methods

The workability of the fresh mortar mixes was studied by measuring the slump values of fresh mortar, with the temperature being monitored with the use of a thermometer before pouring the steel molds. The mini-slump flow test was used for determining the workability and consistency of fresh SCM as stated in the [3]EFNARC (2005) and the V-funnel flow test was used to assess the workability and consistency of fresh SCM. The sorptivity coefficient of specimens was obtained by capillary water absorption test carried out according to [13]. The chemical attack to observe the specimens resistance to sodium chloride were carried out according to [14].

3 Results and Discussions

3.1 Durability properties of SCMs

The durability properties of the hardened mortar were examined through carrying out the sorptivity tests alongside the chemical attack tests aged 28 and 56 days.

3.1.1 Sorptivity Test

The sorptiivity coefficient results are shown in Fig. 2(a-b). ASTM standard for sorptivity states that all construction materials must have a water absorption value within 20% and all our replacement levels fall within that standard. The results show that the sorptivity values ranged from 1.65 to 4 mm/h$^{1/2}$ for SCM with 0 to 10% GSS and ranged from 1.85 to 7 mm/h$^{1/2}$ for SCM with 0 to 100% RSS, respectively. The sorptivity results increases by percentage replacement with both GSS and RSS experiencing a slight drop at 2.5% and 5% GSS content, with effects more prominent with RSS replacement. The 10% GSS replacement mix shows the highest sorptivity observed with 5% recording the lowest but close to the control mix and the 100% RSS replacement mix recorded the highest sorptivity with 25% recording the lowest sorptivity but closest to the control mix. Tables 4(a-b) shows the soprtivity value compared with standard deviation.

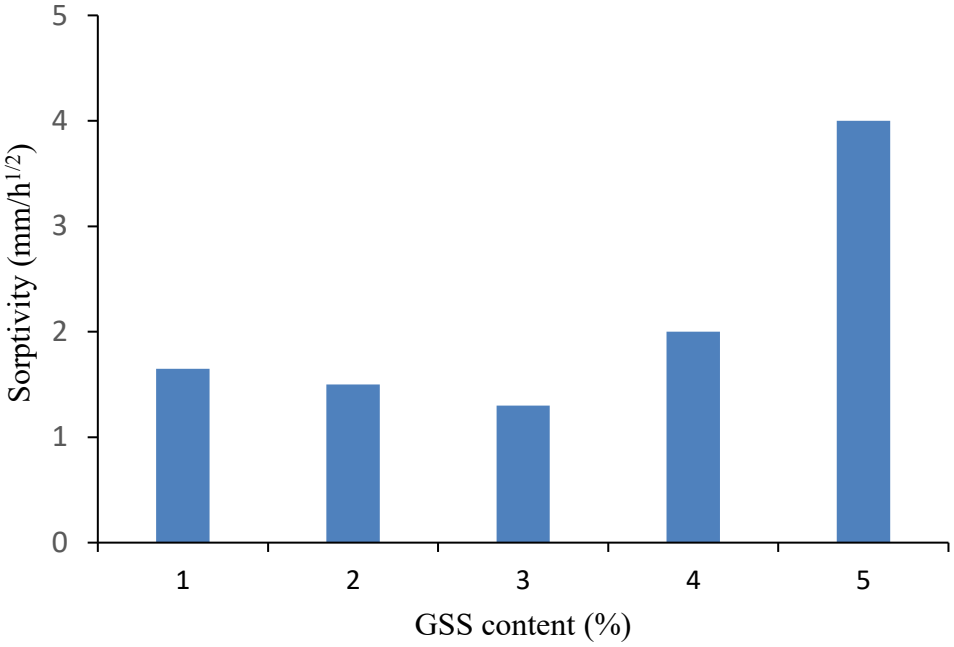

Figure 2a. Sorptivity of SCM with GSS as replacement for cement

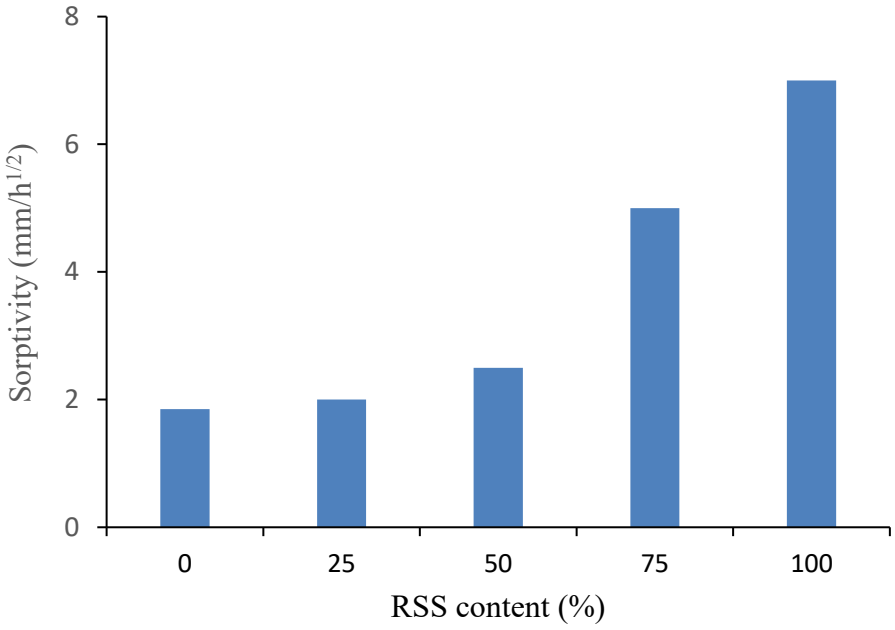

Figure 2b. Sorptivity of SCM with RSS as replacement for fine aggregate

Table 4a. Chemical Attack with NaCl on SCM with GSS

Sample Mix ID (%)	Sorptivity ($mm/h^{1/2}$)	Sorptivity ($mm/h^{1/2}$) mean ± SD
0	1.65	1.65 ± 0.18
2.5	1.80	1.80 ± 0.15
5.0	1.78	1.78 ± 0.16
7.5	2.59	2.59 ± 0.22
10	4.00	4.00 ± 0.19

Table 4b. Chemical Attack with NaCl on SCM with GSS

Sample Mix ID (%)	Sorptivity ($mm/h^{1/2}$)	Sorptivity ($mm/h^{1/2}$) mean ± SD
0	1.85	1.85 ± 0.17
25	2.75	2.75 ± 0.15
50	4.20	4.20 ± 0.19
75	5.30	5.30 ± 0.20
100	7.00	7.00 ± 0.21

3.1.2 Chemical Attack

The weight loss and compressive strength loss results of hardened SCM due to chemical attack using NaCl are indicated in Table 4(a-b). The test follows [15] which provides standard test methods for chemical resistance of mortar. The results showed that the weight loss for GSS ranged from 0.96 to 2.14% while also experiencing a compressive strength loss ranging from 4.67 to 9.25% and the weight loss for RSS ranged from 1.25 to 2.11% while also experiencing a compressive strength loss for RSS ranging from 3.81 to 9.68%. The weight loss experienced a gradual increase as GSS replacement increased and the same was experienced with the RSS replacement. The compressive strength loss also experienced a gradual increase with both GSS and RSS replacement. The SCM does not deteriorate rapidly when exposed to NaCl.

Table 5a. Chemical Attack with NaCl on SCM with GSS

Sample Mix ID (%)	Weight Loss (%)	Compressive Strength Loss (%)	Compressive Strength Loss (%) mean ± SD
0	0.96	4.37	4.37 ± 0.30
2.5	1.38	3.03	3.03 ± 0.25
5.0	1.69	3.05	3.05 ± 0.27
7.5	1.98	5.46	5.46 ± 0.33
10	2.14	9.25	9.25 ± 0.35

Table 5b. Chemical Attack with NaCl on SCM with RSS

Sample Mix ID (%)	Weight Loss (%)	Compressive Strength Loss (%)	Compressive Strength Loss (%) mean ± SD
0	1.25	3.81	3.81 ± 0.27
25	1.74	4.76	4.76 ± 0.40
50	1.98	7.98	7.98 ± 0.45
75	1.90	6.54	6.54 ± 0.33
100	2.11	9.68	9.68 ± 0.38

3.2 Comparison with other SCM modifiers

Table 6 shows the comparison between SCM made with silica sand as a modifier compared to other modifiers, it compares their durability results (sorptiity and chemical attack). Ground silica sand mortars (1.65–4.00 mm/h$^{(1/2)}$ sorptivity, 0.96–2.14% weight loss, 4.37–9.25% strength loss) match or surpass other SCMs while fly ash, metakaolin, and silica fume offer sorptivity ranges between 3.5–6.5 mm/h$^{\{1/2\}}$ and chemical attack weight losses between 1.0–2.2%, with silica fume exhibiting the lowest strength loss at 2.5–5.0%. The modified self-compacting mortars modified with silica sand, fly ash, and metakaolin all exhibit increased durability through significantly reduced sorptivity and resistance to chemical attack.

Table 6. SCM Modifiers and Durability Comparisons

SCM Modifier	Sorptivity ($mm/h^{1/2}$)	Weight loss (%)	Strength loss (%)	Source
Silica Sand (GSS and RSS)	1.65–7.00	0.96–2.14	3.81–9.68	
Fly Ash	3.8–6.5	<2.0	<6.0	[16]
Metakaolin	3.5–4.2	1.4–2.2	3.5–6.5	[17]
Silica fume	3.5–4.1	1.0–2.0	2.5–5.0	[16]

4 Conclusion

Based on the findings from the study, a conclusion can be drawn. GSS and RSS exhibited the potential for application as binder and sand contents in SCM production. The weight loss for GSS ranged from 0.96 to 2.14% while also experiencing a compressive strength loss ranging from 4.67 to 9.25% and the weight loss for RSS ranged from 1.25 to 2.11% while also experiencing a compressive strength loss for RSS ranging from 3.81 to 9.68%. The sorptivity values ranged from 1.65 to 4 $mm/h^{1/2}$ for SCM with 0 to 10% GSS and ranged from 1.85 to 7 $mm/h^{1/2}$ for SCM with 0 to 100% RSS, respectively. GSS replacement 10% for cement and 25% RSS replacement for sharp sand are adequate for the production of SCM. GSS and RSS also exhibited the potential for binder and fine aggregate content in SCM production.

Acknowledgments

The author would like to thank his supervisor, co-authors and the departmental staff of the Civil Engineering department, Osun State University for their support so that this research can be completed.

References

[1] M. S. Nasr, A. A. Shubbar, Z. A.-A. R. Abed, and M. S. Ibrahim, "Properties of eco-friendly cement mortar contained recycled materials from different sources," Journal of Building Engineering, vol. 31, p. 101444, Sep. 2020, doi: https://doi.org/10.1016/j.jobe.2020.101444.

[2] C. R. Gagg, "Cement and concrete as an engineering material: An historic appraisal and case study analysis," *Engineering Failure Analysis*, vol. 40, pp. 114–140, May 2014, doi: https://doi.org/10.1016/j.engfailanal.2014.02.004.

[3] EFNARC, "EFNARC PUBLICATIONS," *EFNARC*, 2019. https://efnarc.org/publications-form (accessed Oct. 11, 2025).

[4] A. Tuaum, S. Shitote, and W. Oyawa, "Experimental Study of Self-Compacting Mortar Incorporating Recycled Glass Aggregate," *Buildings*, vol. 8, no. 2, p. 15, Jan. 2018, doi: https://doi.org/10.3390/buildings8020015.

[5] S. A. Miller, G. Habert, R. J. Myers, and J. T. Harvey, "Achieving net zero greenhouse gas emissions in the cement industry via value chain mitigation strategies," *One Earth*, vol. 4, no. 10, pp. 1398–1411, Oct. 2021, doi: https://doi.org/10.1016/j.oneear.2021.09.011.

[6] J. Dang, J. Zhao, W. Hu, Z. Du, and D. Gao, "Properties of mortar with waste clay bricks as fine aggregate," *Construction and Building Materials*, vol. 166, pp. 898–907, Mar. 2018, doi: https://doi.org/10.1016/j.conbuildmat.2018.01.109.

[7] B. Durga and M. Indira, "Experimental Study on Various Effects of Partial Replacement of Fine Aggregate with Silica Sand in Cement Concrete and Cement Mortar," *International Journal of Engineering Trends and Technology*, vol. 33,

no. 5, pp. 252–256, Mar. 2016, doi: https://doi.org/10.14445/22315381/ijett-v33p250.

[8] R. Malathy et al., "Use of Industrial Silica Sand as a Fine Aggregate in Concrete—An Explorative Study," *Buildings*, vol. 12, no. 8, p. 1273, Aug. 2022, doi: https://doi.org/10.3390/buildings12081273.

[9] J. L. Chaudhary, A. Harison, and V. Srivastava, "USE OF SILICA SAND AS CEMENT REPLACEMENT IN PPC CONCRETE," *International Journal of Research in Engineering and Technology*, vol. 04, no. 11, pp. 55–58, Nov. 2015, doi: https://doi.org/10.15623/ijret.2015.0411010.

[10] Z. Najeeb and M. A. Mosaberpanah, "Mechanical and durability properties of modified High-Performance mortar by using cenospheres and Nano-Silica," *Construction and Building Materials*, vol. 362, p. 129782, Jan. 2023, doi: https://doi.org/10.1016/j.conbuildmat.2022.129782.

[11] BSI, *BS EN 1008:2002 Mixing Water for Concrete. Specification for Sampling, Testing and Assessing the Suitability of Water, Including Water Recovered from Processes in the Concrete Industry, As Mixing Water for Concrete*. BSI, 2002.

[12] ASTM C618-12, "Standard Specification for Coal Fly Ash and Raw or Calcined Natural Pozzolan for Use in Concrete".

[13] ASTM C618-12, "Standard Test Method for Measurement of Rate of Absorption of Water by Hydraulic-Cement Concretes".

[14] BS EN 1015-11:1999, "Methods of test for mortar for masonry - Determination of flexural and compressive strength of hardened mortar".

[15] ASTM C267-97, "Standard Test Methods for Chemical Resistance of Mortars, Grouts, and Monolithic Surfacings and Polymer Concretes".

[16] A. Benli, "Mechanical and durability properties of self-compacting mortars containing binary and ternary mixes of fly ash and silica fume," *Structural Concrete*, vol. 20, no. 3, Jan. 2019, doi: https://doi.org/10.1002/suco.201800302.

[17] E. Güneyisi and M. Gesoğlu, "Properties of self-compacting mortars with binary and ternary cementitious blends of fly ash and metakaolin," *Materials and Structures*, vol. 41, no. 9, pp. 1519–1531, Jan. 2008, doi: https://doi.org/10.1617/s11527-007-9345-7.

IJASST
International Journal of
Applied Sciences and Smart Technologies
p-ISSN 2655-8564, e-ISSN 2685-943, pp. 293-320, 2026

Volume 08
Issue 01

Grouping Weekly Weather Based on Weather Elements in Pagaralam by Using *K*-Means Clustering Analysis

Sri Indra Maiyanti[1], Irmeilyana[1*], Putri Nilam Cayo[1],
Dinny Indah Angelia, Angelina[1]

Faculty of Mathematics and Natural Sciences, University of Sriwijaya,
Jln. Lintas Timur Palembang-Prabumulih KM. 32,
Indralaya, 30129, Indonesia
[*]Corresponding Author: irmeilyana@unsri.ac.id

(Received 12-12-2025; Revised 01-02-2026; Accepted 02-03-2026)

Abstract

Weather is the result of the interaction and combination of various atmospheric elements that occurs in a relatively small place or region over a short period of time. This study aims to analyze weekly weather characteristics in Pagaralam using the *K*-Means Clustering method. The data used was weekly weather in 2022 and 2023 with 15 variables, namely Maximum temperature, Minimum temperature, Temperature, Dew, Humidity, Precipitation, Precipitation cover, Wind gust, Wind speed, Wind direction, Sea pressure, Cloud cover, Solar radiation, UV Index, and Moon phase. The analysis process began with data standardization, followed by clustering using *K*-Means Clustering with several *K* values to observe variations in cluster structure. The optimal number of clusters was determined using the elbow and silhouette methods. The best optimal *K* value for each of the 2022 and 2023 data was *K*=3. A small number of weeks in both years had high temperatures and solar radiation and accompanied by lower dew, humidity, precipitation, and cloud cover than other weeks. A small number of weeks in 2022 had low minimum temperature and were also accompanied by lower cloud cover, dew, and humidity, but they had higher wind gusts and wind speeds than other weeks. Meanwhile, a small number of weeks in 2023 had lower temperatures and accompanied by higher cloud cover, wind gusts, and wind speeds than other weeks.

Keywords: Elbow, *K*-Means Clustering, Pagaralam, Silhouette, Weather elements

1 Introduction

Weather is an atmospheric condition that occurs in a relatively small place or region over a short period of time. Weather is the result of the interaction and combination of various atmospheric elements such as temperature, rainfall, humidity, wind speed, and

duration of sunlight, where changes in one element will affect other elements [1]. Weather is a condition resulting from differences in temperature and humidity in various regions [2-3]. Changing weather patterns on a global scale, lasting for a very long time (slow pace) and progressing slowly (slow onset) indicate the phenomenon of climate change [4]. Weather changes are characterized by an increase in the Earth's surface temperature and an increase in extreme weather events such as extreme rainfall, which are the main cause of disasters [5]. Global warming arises from increasingly intensive human activities, such as the burning of fossil fuels, increased industrial production, and large-scale deforestation [6], which can disrupt the balance of the Earth's meteorological and geological cycles [3]. Global climate change is affecting the decline in coffee productivity [7-10], including in Indonesia.

The main elements that shape weather include temperature, air pressure, humidity, wind, and rainfall. Sunlight, clouds, lightning, and rainbows also influence the formation of weather in a region [11]. Weather changes also occur in tropical regions like Indonesia, which are highly sensitive to changes in weather elements. In recent years, Indonesia has been impacted by the La Nina phenomenon, which is known to increase rainfall and change wind direction. These changes will continue with varying intensity and affect seasonal patterns and weather stability in various regions [12]. Detailed weather information is highly beneficial because it impacts various sectors of life, such as agriculture, health, tourism, and the economy [13-14].

Pagaralam Municipality, South Sumatra, is one of the areas heavily affected by weather variability due to its location at an altitude of 500-3,000 meters above sea level and its unique microclimate. Weather instability in this region can hamper the coffee cultivation and post-harvest processes, while in the tourism sector [15-17], so understanding the weather characteristics in Pagaralam is important to maintain the sustainability of these sectors [18].

Assessment of the drought threat index in Dempo Tengah District, Pagaralam, using GIS shows that most areas are included in the high threat zone [19]. However, in this study, the weather element data used only rainfall within 1 month and is less visually descriptive. Based on interviews conducted in [20-26], coffee farmers in Pagaralam stated that the decline in coffee production was mostly due to the influence of weather.

Information on time groups dominated by high or low values of certain weather elements can represent the characteristics of general weather conditions for 1 harvest period. Based on the mean difference test in [27], the variables of temperature, maximum temperature, minimum temperature, dew point, rainfall coverage, and cloudiness in Dempo Tengah District in 2021 were significantly different than in 2022. Likewise, the test results for 2 time periods from 2022 to 2024 showed significant differences for temperature, dew, humidity, wind conditions, cloud cover, and sea level pressure [28].

Pagaralam's geographical conditions, which are sensitive to increasingly complex weather changes, require analytical methods capable of explaining the interrelationships between weather elements. Biplot analysis can map the interrelationships between weather elements, simplifying the interpretation of complex weather data into more concise and clear information [29]. Weather data in Pagaralam changes daily, necessitating analytical methods to simplify and display the main patterns. The simplification focuses on weekly weather patterns to make inter week variations more visible. Clustering, an unsupervised data mining method, is used to group data and consists of hierarchical and non-hierarchical clustering. Clustering is a data mining method that can be used to extract valuable information by grouping data into clusters with similar characteristics. Examples of non-hierarchical clustering methods are *K*-means clustering [30] and *K*-medoids clustering [31].

Combining data using *K*-Means Clustering can improve data quality [32]. An example of the application of *K*-Means Clustering was to assess the effectiveness of language learning techniques on students by grouping pre-test and post-test data [33], but the analysis results were not supported by cluster plot visualization. *K*-Means Clustering was also used to group commodity priorities for food policy [34]. However, the determination of *K* did not use statistical justification methods, such as the Elbow method or the Silhouette Index and DBI (Davies-Bouldin Index) value.

Applications of *K*-Means Clustering include Pramoedya, et al. [35] who grouped weather conditions in the Kediri region and obtained three optimal clusters based on the DBI value. Cahaya, et al. [36] grouped rice potential in 35 sub-districts in Pagaralam in 2020 to 2022 period into three rice potential clusters: low, medium, and high. Another study by Rahman, et al. [37] combined *K*-Means Clustering and Random Forest to group

and classify annual weather data in Cilacap City using the silhouette and elbow methods. However, in these studies, weather grouping generally still focuses on regions (spatially) or uses annual data. Even though changes in weather conditions often occur rapidly from week to week.

The purpose of this study is to analyze weekly weather clustering in Pagaralam Municipality 2022 and 2023 based on weather elements using the *K*-Means Clustering method. The results obtained by identifying the characteristics of each weather cluster can provide basic information that can be used in practical activity planning, such as developing agricultural cultivation calendars and other activities that depend on weather conditions.

2 Material and Methods

The data used in this study is secondary data obtained from the website visualcrossing.com. The data contains daily weather information for Pagaralam Municipality, South Sumatra, in 2022 and 2023. The objects in the data matrix are weekly periods, from January 1 to December 31 in a year, resulting in 53 weeks, with the 53rd week consisting of only one or two days. Variables and their notations and units include: Maximum Temperature (Tmax; X_1; in ^oC), Minimum Temperature (Tmin; X_2; in ^oC), Mean temperature (Temp; X_3; in ^oC), Dew point (Dew; X_4; in ^oC), Relative humidity (Hum; X_5; in %), Precipitation (Precip; X_6; in mm), Precipitation Cover (Pcover; X_7; in mm), Wind Gust (Wgust; X_8; in km/h), Wind Speed (WSpeed; X_9; in km/h), Wind Direction (WDir; X_{10}; in $degrees\ from\ North$), Sea level pressure (Seapress; X_{11}; in mb), Cloud cover (CCover; X_{12}; in %), Solar radiation (SolRad; X_{13}; in W/m^2), UV Index (UVI; X_{14}; $between\ 0\ and\ 10$), Moonphase (Moophase; X_{15}; $between\ 0\ and\ 10$). Two data matrices used were data on 15 weather elements in Pagaralam in 2022 and 2023.

The following were the steps taken in this research:

1. Describe the data for each variable.

2. Construct a data matrix for 2022 and 2023. For example, a data matrix consisting of n objects (i.e. the number of weeks) and p variables (i.e. the number of weather elements) is denoted as $\boldsymbol{X} = (x_{ij} *)$; where $i = 1, 2, \dots, n$ and $j = 1, 2, \dots, p$.
3. Standardize the data using Equations (1), (2), and (3):

$$z_{ij} = \frac{x_{ij} * - \bar{x}_j}{s_j} \tag{1}$$

$$\bar{x}_j = \frac{\sum_{i=1}^{n} x_{ij}}{n} \tag{2}$$

$$s_j = \sqrt{\frac{\sum_{i=1}^{n} (x_{ij} * - \bar{x}_j)^2}{n-1}} \tag{3}$$

where

z_{ij} : Standardized value of the $i-$th object on the $j-$th variable;

$i = 1, 2, \dots, n$; $j = 1, 2, \dots, p$

$x_{ij} *$: Initial value of the $i-$th on the $j-$th variable

$\bar{x}_j$: Average value of the $j-$th variable

s_j : Standard deviation value of the $j-$th variable

4. Perform *K*-Means Clustering analysis [38-40]
   a. Determine the number of initial clusters *K* to be used in the analysis process.
   b. Determine the initial centroid $\boldsymbol{c_k}$.
   c. Calculate the distance of each object i to centroid $\boldsymbol{c_k}$ using Equation (4):

$$d(\boldsymbol{x_i}, \boldsymbol{c_k}) = \sqrt{\sum_{j=1}^{p} (x_{ij} - c_{kj})^2} \tag{4}$$

where

$d(\boldsymbol{x_i}, \boldsymbol{c_k})$: Euclidean distance of the $i-$th object to the $k-$th cluster centroid;

$k = 1, 2, \dots, K$

x_{ij} : Standardized value of the $i-$th object to the $k-$th variable

c_{kj} : Centroid value of the $k-$th for $j-$th variable

   d. Group each object i into the $k-$th cluster with the closest distance.

e. Recalculate the centroid position $\boldsymbol{c_k}$ based on the average value of the members in cluster k using Equation (5).

$$c_{kj} = \frac{\sum_{i=1}^{n_k} x_{ij}}{n_k} \tag{5}$$

where

c_{kj} : Centroid value of the $k-$ th for the $j-$ th variable

x_{ij} : Standardized value for the $i-$ th object for the $j-$ th variable in the $k-$ th cluster; $i = 1, 2, 3, \ldots, n_k$

n_k : Number of objects in the $k-$ th cluster

f. Repeat the calculation steps until the centroid position $\boldsymbol{c_k}$ remains unchanged (converges).

5. Determine the optimal number of clusters, K, based on the SSE (Sum of Squared Errors in elbow method) and silhouette values. The elbow method is a method for determining the best number of clusters in a model by looking at the optimal point from the comparison between the number of clusters and the data variation value. The silhouette coefficient method combines two metrics, namely cohesion which assesses the proximity between objects within a cluster, and separation which measures the distance between one cluster and another [40]. The silhouette coefficient ranges from -1 to 1, with higher values indicating better cluster formation [41]. The SSE and silhouette values are calculated by using Equation (6) and Equation (7), respectively.

$$SSE = \sum_{k=1}^{K} \sum_{x_i \in c_k} \sum_{j=1}^{p} \left(x_{ij} - c_{kj}\right)^2 \tag{6}$$

$$s(i) = \frac{b(i) - a(i)}{\max\left(a(i) - b(i)\right)} \tag{7}$$

Where:

$s(i)$: Silhouette value for the $i-$ th object

$a(i)$: The average value of the distance between the $i-$ th object and all other objects in the same cluster

$b(i)$: The average value of the distance between the $i-$th object and objects in other nearby clusters

$\max(a(i)-b(i))$: Maximum value between $a(i)$ and $b(i)$, used as a divisor so that the result is in the range -1 to 1

6. Interpretation of results.

Data processing and analysis using software Minitab 19, SPSS 24, and R Studio version 4.3.1.

3 Results and Discussions

The data aggregation process was carried out to convert daily weather data into weekly data. Construct the 2022 and 2023 data matrices, respectively, as $\boldsymbol{X} = (x_{ij}*)$ with $i = 1, 2, \dots, 53$ and $j = 1, 2, \dots, 15$. The next step is to conduct a descriptive analysis to provide an initial overview of the data distribution. This analysis includes calculating the minimum, maximum, median, mean, and standard deviation values. Descriptive statistics for variables in 2022 as shown in Table 1.

Data standardization on Table 2 was performed using Equation (1) based on average and standard deviation values in Table 1. The standardized data used in a *K*-Means Clustering analysis to group weekly weather conditions based on their weather elements.

Table 1. Descriptive statistics for variables in 2022

Variable	Average	Minimum	Maximum	Median	Standard Deviation
X_1	78,8518	76.57	81.51	78.71	1.2118
X_2	66.1369	63.80	67.93	66.13	0.7801
X_3	71.3493	70.29	73.57	71.30	0.8060
X_4	66.9453	64.46	69.01	67.03	0.9845
X_5	86.8577	79.03	91.80	87.14	2.9053
X_6	0.3794	0.07	0.99	0.33	0.2206
X_7	51.5837	12.50	92.26	48.81	16.6234
X_8	18.5264	12.77	36.00	16.46	4.9401

Variable	Average	Minimum	Maximum	Median	Standard Deviation
X_9	4.1057	2.63	8.50	3.79	1.2158
X_{10}	210.3827	107.60	298.20	225.60	49.7460
X_{11}	1012.3191	1010.00	1015.00	1012.00	1.0222
X_{12}	90.9844	56.83	99.64	93.31	8.8680
X_{13}	197.9790	135.90	276.90	192.30	27.0349
X_{14}	7.5148	5.86	9.43	7.29	0.7597
X_{15}	0.4772	0.10	0.87	0.45	0.2202

Table 2. Standardized data in 2022

Week-*i*	X_1	X_2	X_3	X_4	...	X_{14}	X_{15}
1	0.3935	0.7218	0.5060	0.6940	...	-0.1135	-0.6620
2	-1.0094	0.5203	-1.0183	0.5344	...	-0.4896	-0.9020
3	-0.9386	-0.2854	-1.3196	-0.1766	...	0.4506	0.1361
4	0.7825	0.3189	0.4351	0.0556	...	0.4506	1.2522
⋮	⋮	⋮	⋮	⋮	⋮	⋮	⋮
53	-0.8679	-2.9955	-0.9297	-1.7727	...	0.6386	-0.9410

The number of clusters tested was $K = 2$. Some of the calculation examples were performed manually using Equation (4), while the overall clustering process was completed using RStudio software version 4.3.1. The steps of the *K*-Means Clustering analysis for the 2022 data matrix are explained below.

1. Determine the initial centroid by randomly selecting several data points in Table 3. The centroid for cluster 1 is denoted as $\boldsymbol{c_1}$, derived from the weather data from week 13. Similarly, the centroids for clusters 2 is denoted as $\boldsymbol{c_2}$ derived from weather data from week 45.
2. Perform iteration 1 by calculating the object's distance to the initial centroid using the Euclidean distance in Equation (4). For example, the distance from week 2 to the centroid in cluster 1 is

$$d(\boldsymbol{x_2}, \boldsymbol{c_1}) = \sqrt{(-1.0094 - 2.1971)^2 + (0.5203 + 0.2854)^2 + \cdots + \left(-0.9020 - (1.2262)\right)^2} = 9.8346$$

3. The results of the Euclidean distance calculation and cluster grouping are shown in Table 4.
4. Iteration 2

   The centroid is calculated by taking the average value of each variable in each cluster. Based on Table 4, the weekly weather for 2022 consists of 18 weeks in cluster 1 and 35 weeks in cluster 2. The new centroid coordinates c_{kj} are determined using the standardized initial data and Equation (5), with the number of cluster members being $n_1 = 18$ and $n_2 = 35$.

   For example, to calculate the new centroid for variable X_1 in cluster 1 is based on the X_1 values of 18 weeks in cluster 1. These values are based on Table 2.

$$c_{1,1} = \frac{0.7825 + 0.6882 + \cdots + (-1.0919) + (-0.8679)}{18} = 0.7759$$

   New centroid for variable X_1 in cluster 2 is

$$c_{2,1} = \frac{0.3935 + (-1.0094) + \cdots + (-0.9033) + (-0.7264)}{35} = -0.3991$$

5. By the same calculation, new centroid values for each cluster from the 2022 data are shown in Table 5. The Euclidean distance and clustering results from the second iteration can be seen in Table 6.

Table 3. Initial centroid values for 2022

Centroid	X_1	X_2	X_3	⋯	X_{14}	X_{15}
$\boldsymbol{c_1}$	2.1971	-0.2854	2.2784	⋯	2.5190	1.2262
$\boldsymbol{c_2}$	-1.8817	0.1358	-1.1601	⋯	-1.9939	0.0583

Table 4. Euclidean distance and clustering from iteration 1 on 2022 data

Week-i	$\boldsymbol{c_1}$	$\boldsymbol{c_2}$	Minimum distance	Cluster-k

1	7.8420	**5.4629**	5.4629	2
2	9.8346	**3.3025**	3.3025	2
3	8.5152	**5.2021**	5.2021	2
4	**6.4918**	6.8082	6.4918	1
⋮	⋮	⋮	⋮	⋮
53	**9.3431**	9.9322	9.3431	1

Note: Bold numbers indicate the minimum distance from week-i to the centroid $\boldsymbol{c_k}$

Table 5. New centroid values for the second iteration from the 2022 data

Centroid	X_1	X_2	X_3	⋯	X_{14}	X_{15}
$\boldsymbol{c_1}$	0.7759	-0.3556	0.6872	⋯	0.9833	-0.0005
$\boldsymbol{c_2}$	-0.3991	0.1829	-0.3534	⋯	-0.5057	0.0002

Table 6. Euclidean distance and clustering in the second iteration of 2022 data

Week-i	$\boldsymbol{c_1}$	$\boldsymbol{c_2}$	Minimum distance	Cluster-k
1	3.5435	**2.6195**	2.6195	2
2	5.3713	**2.3735**	2.3735	2
3	3.9657	**2.3234**	2.3234	2
4	**2.8835**	3.5707	2.8835	1
⋮	⋮	⋮	⋮	⋮
53	**6.8134**	7.9778	6.8134	1

Table 6 still shows differences in cluster members from the previous calculation. Therefore, the iteration continues using the same process until the cluster members are the same as those calculated in the previous iteration (convergence). In this case, the calculation for $K = 2$ on the 2022 data matrix reaches iteration 6. New centroid values for each cluster from the 2022 data are shown in Table 7. The Euclidean distance and clustering results from the second iteration can be seen in Table 8.

Table 7. New centroid values for the sixth iteration from the 2022 data

Centroid	X_1	X_2	X_3	⋯	X_{14}	X_{15}
$\boldsymbol{c_1}$	0.5167	-0.3978	0.4391	⋯	0.7925	-0.0851
$\boldsymbol{c_2}$	-0.3667	0.2823	-0.3116	⋯	-0.5624	0.0604

Table 8. Euclidean distance and clustering in the sixth iteration of 2022 data

Week-i	$\boldsymbol{c_1}$	$\boldsymbol{c_2}$	Minimum distance	Cluster-k
1	3.4187	**2.6863**	2.6863	2
2	5.0844	**2.2889**	2.2889	2
3	3.6431	**2.5060**	2.5060	2
4	**2.7653**	3.7774	2.7653	1
⋮	⋮	⋮	⋮	⋮
53	**6.3493**	8.4069	6.3493	1

Furthermore, the *K*-Means Clustering visualization for $K = 2$ on the 2022 and 2023 data matrices can be seen in Figs. 1 and 2. Based on Fig. 1, the *K*-Means clustering results show two clusters distributed in different positions, although some objects in both clusters are relatively close together. In general, the distribution of each cluster indicates that each group has distinct characteristics.

The number of clusters is evaluated to determine the optimal *K* value using the elbow and silhouette methods. The stage of evaluating the number of clusters using the elbow method is to determine the SSE value for week i in cluster k using Equation (6):

$$SSE_{k,i} = \sum_{k=1}^{K} \sum_{x_i \in c_k} \sum_{j=1}^{p} \left(x_{ij} - c_{kj}\right)^2$$

For example, to calculate the SSE value for week 4 in cluster 1 (notated as $SSE_{1,4}$) is based on data of week 4 in Table 2 and centroid of cluster 1 ($\boldsymbol{c_1}$) in Table 7.

$$SSE_{1,4} = \Big((0.7825 - 0.5167)^2 + \left(0.3189 - (-0.3978)\right)^2 + \cdots + (0.4506 - 0.7945)^2 + \left(1.2522 - (-0.0850)\right)^2\Big)$$

Calculation of the SSE value for week 53 in cluster 1 (notated as $SSE_{1,53}$) is based on data of week 53 in Table 2 and centroid of cluster 1 ($\boldsymbol{c_1}$) in Table 7.

$$SSE_{1,53} = \Big((-0.8679 - 0.5167)^2 + \big(-2.9955 - (0.3978)\big)^2 + \cdots + (0.6386 - 0.7945)^2 + \big(-0.9410 - (-0.0850)\big)^2\Big) = 40.3131$$

So, the SSE for cluster 1 is obtained as follows

$$SSE_1 = SSE_{1,4} + SSE_{1,6} + \cdots + SSE_{1,53}$$
$$= 7.6470 + 14.6696 + \cdots + 40.3131 = 308.0786$$

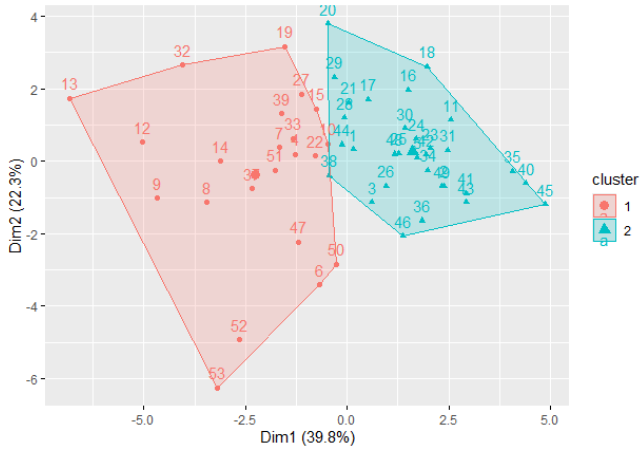

Figure 1. *K*-Means clustering for $K = 2$ in 2022

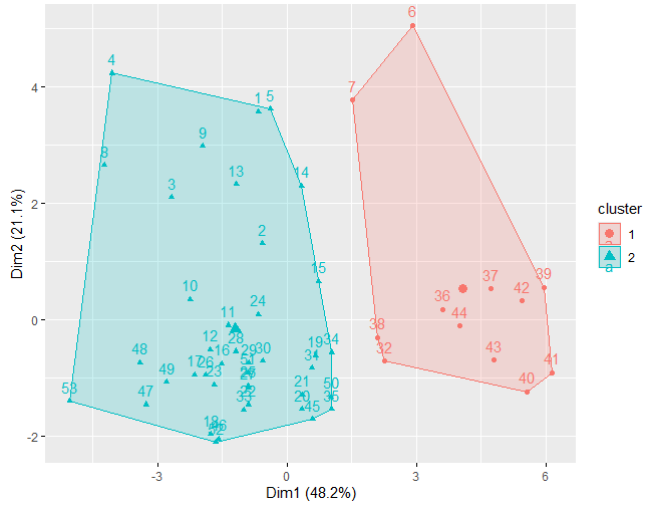

Figure 2. *K*-Means clustering for $K = 2$ in 2023

Based on manual calculations, the SSE value for cluster 1 was 308.0786. The calculation process was repeated until the optimal clustering result was achieved. For example, at K=2, the SSE value for cluster 1 was combined with the SSE value for cluster 2. Using the same steps, the SSE for cluster 2 was 270, resulting in a total SSE of 577.9574 at K=2. The overall SSE calculation results can be seen in Table 9.

Based on Table 9, the SSE value in the 2022 data matrix experienced a very sharp decline at $K = 4$. At $K > 4$, the percentage change in the SSE value was less than 22. This indicates that increasing the number of clusters at $K > 4$ did not provide optimal clustering. Thus, the elbow method resulted an optimal number of clusters of $K = 4$.

The SSE value in the 2023 data matrix shows the largest decreasing at $K = 3$. At $K > 3$, the percentage change in the SSE value becomes smaller than 23, so increasing the number of clusters to $K >3$ does not provide optimal results. Thus, the elbow method results the optimal number of clusters at $K = 3$.

Next, the silhouette method was used to measure the proximity between objects within a cluster. The calculation example was performed on objects in week 4 based on the initial data and using Equation (7).

Table 9. SSE calculation results for K-clusters in 2022 and 2023

Number of Clusters (K)	2022 Data Matrix			2023 Data Matrix		
	SSE Value	Change in SSE Value	%age Change	SSE Value	Change in SSE Value	%age Change
2	577.9574	0	0	513.6831	0	0
3	506.0911	71.8663	12	393.4374	**120.2457**	**23**
4	395.7869	**110.3042**	**22**	353.1861	40.2513	10
5	370.5297	25.2572	6	330.4316	22.7545	6
6	340.0241	30.5056	8	273.2691	57.1625	17
7	300.0259	39.9982	12	257.5825	15.6866	6
8	285.2293	14.7966	5	227.3601	30.2224	12
9	259.3365	25.8928	9	210.2731	17.0870	8
10	241.3491	17.9874	7	197.4074	12.8657	6

Note: Bold numbers indicate a significant decrease in SSE.

Based on the results of previous calculations, the week 4 is included in cluster 1. The first step taken is to calculate the distance between objects in the same cluster.

$$d(4,6) = \sqrt{\left(0.7825 - (-1.1626)\right)^2 + \cdots + \left(1.2522 - (-1.1291)\right)^2} = 5.0471$$

$$d(4,53) = \sqrt{\left(0.7825 - (-1.8679)\right)^2 + \cdots + \left(1.2522 - (-1.9410)\right)^2} = 7.6325$$

The average distance between the 4th week and all objects in the same cluster is

$$a(4) = \frac{5.0471 + 3.1511 + 3.1187 + \cdots + 6.4894 + 7.6325}{22} = 4.3903$$

The next step is to calculate the distance between week 4 and other objects in different clusters.

$$d(4,1) = \sqrt{\left(0.7825 - (0.3935)\right)^2 + \cdots + \left(1.2522 - (-0.6620)\right)^2} = 2.9701$$

$$d(4,49) = \sqrt{\left(0.7825 - (-0.9033)\right)^2 + \cdots + \left(1.2522 - (-0.2078)\right)^2} = 4.5553$$

The average distance between the 4th week and all objects in different clusters.

$$b(4) = \frac{2.9701 + 4.7830 + 4.2221 + \cdots + 3.9250 + 4.5553}{31} = 4.6742$$

The silhouette coefficient values for week 4 are as follows.

$$s(4) = \frac{4.6742 - 4.3903}{4.6742} = 0.0607$$

Based on manual calculations, the silhouette coefficient value for week 4 was 0.0607. The calculation process was repeated for all objects to obtain the average silhouette coefficient value at *K*=2. The overall calculation results are shown in Table 10.

According to Table 10, the highest silhouette coefficient value for the 2022 data matrix at *K*=3 was 0.2722. This value is the largest compared to other cluster size, indicating a good separation distance between clusters. Therefore, the silhouette method indicates *K*=3 as the optimal number of clusters.

Table 10. Silhouette coefficient calculation results in 2022 and 2023

Cluster (K)	Silhouette Coefficient Value (s_K)	
	2022 Data Matrix	2023 Data Matrix
2	0.2198	**0.3503**

3	**0.2722**	0.3101
4	0.2130	0.2957
5	0.1719	0.2425
6	0.1683	0.1797
7	0.1650	0.1843
8	0.1598	0.2193
9	0.1563	0.1735
10	0.1688	0.1663

The highest silhouette coefficient value for the 2023 data matrix was at K=2, namely 0.3503. This indicates the largest distance between clusters, so the silhouette method indicates K=2 as the optimal number of clusters. Next, a comparison was conducted to examine the characteristics of each cluster formed. The results of the comparison of cluster members in 2022 and 2023 can be seen in Table 11.

Table 11. Comparison of cluster members in 2022 and 2023

Month	Week	2022 Data Matrix		2023 Data Matrix	
		Silhouette 3 Clusters	Elbow 4 Clusters	Silhouette 2 Clusters	Elbow 3 Clusters
January	Week 1	2	2	2	3
	Week 2	2	4	2	3
	Week 3	2	4	2	3
	Week 4	2	2	2	3
January/February	Week 5	2	4	2	3
February	Week 6	1	3	1	3
	Week 7	2	2	1	3
	Week 8	3	1	2	3
February/March	Week 9	3	1	2	3
March	Week 10	2	2	2	2
	Week 11	2	4	2	2
	Week 12	3	1	2	2

Month	Week	2022 Data Matrix		2023 Data Matrix	
		Silhouette 3 Clusters	Elbow 4 Clusters	Silhouette 2 Clusters	Elbow 3 Clusters
	Week 13	3	1	2	3
March/April	Week 14	3	1	2	3
April	Week 15	2	2	2	2
	Week 16	2	2	2	2
	Week 17	2	2	2	2
April/May	Week 18	2	2	2	2
May	Week 19	2	2	2	2
	Week 20	2	2	2	2
	Week 21	2	2	2	2
May/Jun	Week 22	2	2	2	2
Jun	Week 23	2	4	2	2
	Week 24	2	4	2	2
	Week 25	2	4	2	2
	Week 26	2	4	2	2
Jun/July	Week 27	2	2	2	2
July	Week 28	2	2	2	2
	Week 29	2	2	2	2
	Week 30	2	4	2	2
July/August	Week 31	2	4	2	2
August	Week 32	3	1	1	1
	Week 33	2	2	2	2
	Week 34	2	4	2	2
	Week 35	2	4	2	2
August/Sept.	Week 36	2	4	1	1
September	Week 37	3	1	1	1
	Week 38	2	2	1	1

Month	Week	2022 Data Matrix		2023 Data Matrix	
		Silhouette 3 Clusters	Elbow 4 Clusters	Silhouette 2 Clusters	Elbow 3 Clusters
	Week 39	2	2	1	1
September/Oct.	Week 40	2	4	1	1
October	Week 41	2	4	1	1
	Week 42	2	4	1	1
	Week 43	2	4	1	1
October/Nov.	Week 44	2	2	1	1
November	Week 45	2	4	2	2
	Week 46	2	4	2	2
	Week 47	1	3	2	2
	Week 48	2	4	2	2
November/Dec.	Week 49	2	4	2	2
December	Week 50	1	3	2	2
	Week 51	2	2	2	2
	Week 52	1	3	2	2
	Week 53	1	3	2	2

Based on Table 11, the 2022 data matrix shows differences in cluster members between the elbow and silhouette methods, indicating that each cluster has a varied data pattern. At K =3, many weekly weather patterns cluster in the same group, so the variation pattern remains quite general. At K =4, the data is more clearly separated, but 2 of 4 clusters have same characteristics. Meanwhile, the other two clusters have the same members and characteristics as the 2 clusters in the $K = 3$ grouping results. This shows that the clustering for $K = 3$ is quite appropriate in distinguishing weekly weather characteristics more specifically. Comparison of cluster centroids can be seen in Table 12.

In Table 12, the results of the *K*=3 clustering of the 2022 show that each cluster has distinct weather characteristics, as follows:

(i) Cluster 1 consists of 5 weeks, predominantly characterized by Tmin, Dew, WGust, Wspeed, and WDir. This condition illustrates that these weeks have stronger winds, with minimum temperatures and dew points tending to be lower than other weeks.

(ii) Cluster 2 consists of 41 weeks, indicating that most weeks in 2022 tended to be less dominated by the more "extreme" weather elements.

(iii) Cluster 3 consists of 7 weeks, predominantly characterized by the Tmax, Temp, SolRad, and UVI variables, as well as the Dew, Hum, Precip, PCover, and CCover variables. This condition illustrates that these weeks experience warmer temperatures, but lower precipitation, dew, and humidity than other weeks.

Table 12. Comparison of cluster centroids in 2022 data

Variable	$K = 3$ Cluster Centroid			$K = 4$ Cluster Centroid			
	1	2	3	1	2	3	4
Tmax	-0.7547	-0.1310	**1.3063**	**1.3063**	0.5650	-0.7547	-0.7938
Tmin	**-0.9373**	0.2497	-0.7929	-0.7929	0.5075	**-0.9373**	0.0041
Temp	-0.6461	-0.0811	**0.9364**	**0.9364**	0.6850	-0.6461	-0.8107
Dew	**-1.4941**	0.3929	**-1.2338**	**-1.2338**	0.4691	**-1.4941**	0.3202
Hum	**-0.9511**	0.4095	**-1.7190**	**-1.7190**	-0.1034	**-0.9511**	0.8980
Precip	-0.6921	0.2607	**-1.0325**	**-1.0325**	-0.3843	-0.6921	0.8750
PCover	-0.4963	0.3030	**-1.4201**	**-1.4201**	-0.2958	-0.4963	0.8732
WGust	**2.4024**	-0.2918	-0.0066	-0.0066	-0.2592	**2.4024**	-0.3229
WSpeed	**2.4723**	-0.3311	0.1733	0.1733	-0.3883	**2.4723**	-0.2766
WDir	**1.0280**	-0.1863	0.3568	0.3568	-0.1618	**1.0280**	-0.2096
Seapress	0.5962	-0.1632	0.5303	0.5303	-0.4373	0.5962	0.0977
CCover	0.6790	0.1456	**-1.3376**	**-1.3376**	-0.1819	0.6790	0.4574
SolRad	0.2682	-0.3217	**1.6926**	**1.6926**	0.1978	0.2682	-0.8164
UVI	-0.0759	-0.2878	**1.7400**	**1.7400**	0.1403	-0.0759	-0.6956
MooPhase	-0.3933	-0.0091	0.3345	0.3345	0.0485	-0.3933	-0.0641

Number of objects	5	41	7	7	20	5	21

Note: Bold numbers indicate the dominant variables characterizing the cluster.

Furthermore, the results of the K=4 clustering of the 2022 show that:

(i) Cluster 1, consisting of 7 weeks, tends to have the same characteristics as cluster 3 at K=3, namely higher Tmax, Temp, SolRad, and UVI values, but lower Dew, Hum, Precip, PCover, and PCover values compared to other weeks.

(ii) Cluster 2, consisting of 20 weeks, and cluster 4 consisting of 21 weeks, each tend not to be dominated by more "extreme" weather elements. These two clusters represent a separation from cluster 2 at K=3.

(iii) Cluster 3, consisting of 5 weeks, has the same characteristics as cluster 1 at K=3, namely predominantly characterized by Tmin, Dew, WGust, Wspeed, and WDir.

Based on a comparison of the clustering results at the two K values in 2022 data, the optimal number of clusters was set at K =3. Although the elbow method results show the maximum SSE change at K=4, the resulting cluster characteristics tend to be similar to those obtained with K=3. The silhouette coefficient value suggests K=3 as the best choice. Based on the K=3 clustering results in Table 11, there are only 12 weeks with slightly more extreme weather than the others. These weeks, from late February to March, early August, and early September, are dominated by higher temperatures, solar radiation, and UVI, but those are as opposed with dew, humidity, and precipitation. Meanwhile, in early February, mid-November, and December, the weather is dominated by wind, dew and humidity.

Based on Table 11, the clustering results for the 2023 data matrix K=2 and K=3 do not result the same membership pattern. All members of one cluster at K=2 are separated into two clusters. Thus, the three resulting clusters have distinct characteristics. This indicates that some weeks exhibit inconsistent patterns that change as the number of clusters increases. Visualization for K = 2 on 2023 data matrix can be seen in Fig. 2.

Table 13 shows the results of clustering in the K=2, indicating that each cluster has distinct weather characteristics, as follows:

(i) Cluster 1, consisting of 12 weeks, tends to be characterized by the Tmax, Temp, WSpeed, SolRad, and UVI variables, as well as the Dew, Hum, Precip, PCover, and CCover variables. These two variable groups have opposite values. These conditions indicate that the weeks in this cluster are characterized by higher temperature, wind speed, solar radiation, and UVI, but also lower Dew, humidity, precipitation, and cover precipitation compared to other weeks.

(ii) Cluster 2 consists of 41 weeks, so that most of the weeks in 2023 are likely not to be dominated by more 'extreme' weather elements.

Table 13. Comparison of cluster centroids in 2023

Variable	$K = 2$		$K = 3$		
	Cluster Centroid		Cluster Centroid		
	1	2	1	2	3
Tmax	**1.2543**	-0.3671	**1.5238**	-0.1538	**-0.9378**
Tmin	-0.6742	0.1973	-0.5317	0.5291	**-1.0557**
Temp	**0.9317**	-0.2727	**1.2325**	0.0347	**-1.2214**
Dew	**-1.5566**	0.4556	**-1.6116**	0.6248	-0.3526
Hum	**-1.5863**	0.4643	**-1.7610**	0.4321	0.3438
Precip	**-0.8962**	0.2623	**-0.8739**	0.2439	0.0848
PCover	**-1.2357**	0.3617	**-1.2383**	0.3025	0.2458
WGust	0.6768	-0.1981	0.3088	-0.6008	**1.4672**
WSpeed	**1.0407**	-0.3046	0.6955	-0.6193	**1.1694**
WDir	-0.5482	0.1605	**-0.9465**	-0.1803	**1.3850**
Seapress	0.1622	-0.0475	0.4084	0.0006	-0.3729
CCover	**-1.0987**	0.3216	**-1.4463**	0.1049	**1.0096**
SolRad	**1.3950**	-0.4083	**1.5013**	-0.3635	-0.3073
UVI	**1.3662**	-0.3999	**1.4703**	-0.3901	-0.2017
MooPhase	0.3390	-0.0992	0.2151	-0.0180	-0.1431
Number of Objects	12	41	10	32	11

Based on Table 13, the results of the $K = 3$ clustering show that each cluster has distinct weather characteristics, as follows:

(i) Cluster 1 which consists of 10 weeks has the same characteristics as Cluster 1 at $K = 2$.

(ii) Cluster 2, consisting of 32 weeks, has the same characteristics as Cluster 2 at $K = 2$. Most weeks in 2023 tend not to be dominated by more extreme weather elements.

(iii) Cluster 3, consisting of 11 weeks, is predominantly characterized by the Tmax, Tmin, and Temp variables, as well as the Wgust, WSpeed, WDir, and CCover variables. These two groups of weather elements are inversely related. These two groups of weather elements are inversely related. It can be said that a small part of the weeks in 2023, low temperature conditions are characterized by high cloud cover, wind speed, and wind gust.

In cluster 1 and cluster 3, the wind direction is opposite to the North.

In the 2023 data, the optimal number of clusters using the silhouette coefficient method was $K = 2$, but the difference between $K = 2$ and $K = 3$ was not significant. Meanwhile, the optimal number of clusters using the elbow method was $K = 3$. Based on the $K = 3$ clustering results, the weeks between January and early March and from late March to early April were characterized by low temperatures accompanied by higher cloud cover, wind speed, and wind gusts than other weeks. Meanwhile, in early August, between September and early November, weather conditions tend to have characteristics of high temperature and solar radiation but accompanied by dew, humidity, precipitation, and cloud cover that tend to be lower than in other weeks.

The differences in weather elements that dominate a weekly time span within a 1-year period indicate weather variability in Pagaralam. Differences in weekly clustering results over two consecutive years also indicate changes in weather elements, which can affect the flowering process from cultivated plants to harvest, the harvest period, and crop production. Solar intensity, temperature, humidity, rainfall, and wind speed significantly influence fruit formation. If the weather changes are too extreme and the plants are vulnerable to the weather, then it can lead to pest and disease attacks, which can reduce fruit production and even crop failure.

For example, in Pagaralam's robusta coffee plants, the flowering process, which typically occurs throughout the year, can shift to specific months, thus altering the harvest period. The timing of plant maintenance strategies, such as weed control, pest and disease management, and pruning, can also shift and be adjusted to weather conditions. This agricultural calendar planning strategy represents an adaptive and mitigation management strategy to minimize the risk of climate impacts on crop production. Coffee farmers can also implement strategies such as creating rorak for drainage, proper pruning techniques, planting shade tree species that are more effective in controlling the microclimate, and also more intensively implementing GAP (Good Agricultural Practices) in sustainable agriculture.

4 Conclusions

For both 2022 and 2023 data, the elbow and silhouette methods resulted different optimal *K* values. However, considering the characteristics of each cluster generated at these two different *K* values, the best optimal *K* value for each of the 2022 and 2023 data was *K*=3. Most weeks in 2022 and 2023 in Pagaralam did not have dominant weather elements, especially from April to July. Furthermore, a small number of weeks in both years had high temperatures and solar radiation and they were accompanied by lower dew, humidity, precipitation, and cloud cover than other weeks.

A small number of weeks in 2022 had low minimum temperature and were also accompanied by lower cloud cover, dew, and humidity, but they had higher wind gusts and wind speeds than other weeks. Meanwhile, a small number of weeks in 2023 had lower temperatures and accompanied by higher cloud cover, wind gusts, and wind speeds than other weeks.

The average weekly weather conditions in Pagaralam during certain periods throughout 2022 and 2023 varied considerably. To overcome the impact of variability in weather elements on the harvest period of cultivated crops, especially coffee, farmers should implement a schedule planning strategy and also appropriate plant maintenance management, so that coffee production can be stable and even increase.

This study used a non-hierarchical clustering method, allowing for further comparison with other clustering methods to determine the optimal number of clusters on

a larger data range, such as hierarchical clustering, including single linkage, complete linkage, and average linkage methods. Another example of a clustering method used for further research is Density-Based Spatial Clustering with Noise (DBSCAN), a density-based clustering algorithm that groups adjacent data points (high density) and separates noise (sparse areas) to find irregularly shaped clusters. Gaussian Mixture Models (GMM), a probabilistic unsupervised learnng model, can also be used, assuming that the data is generated from a combination of several different Gaussian distributions.

Acknowledgements

The research of this article was funded Universitas Sriwijaya 2025, in accordance with the Rector's Decree Number: 0027/UN9/LPPM.PT/2025, on September 17, 2025.

References

[1] N. Sunarmi, E. N. Kumailia, N. Nurfaiza, A. K. Nikmah, H. N. Aisyah, I. Sriwahyuni, and S. N. Lailly, "Analisis Faktor Unsur Cuaca Terhadap Perubahan Iklim di Kabupaten Pasuruan pada Tahun 2021 dengan Metode Principal Component Analysis." *Newton-Maxwell Journal of Physics*, vol. 3, no. 2, pp. 56–64, 2022.

[2] S. Marlina, *Dampak Perubahan Iklim pada Kesehatan Masyarakat*. Palangka Raya: NEM, 2022.

[3] T. Mulyaningsih, Y. Purwaningsih, Barokatuminalloh, W. Perwithosuci, and I. A. Sasanti, *Adaptasi Perubahan Iklim dan Ketahanan Pangan*, 1st ed. Yogyakarta: Jejak Pustaka, 2022.

[4] E. Aldrian, M. Karmini, and Budiman, *Adaptasi dan Mitigasi Perubahan Iklim di Indonesia*. Jakarta Pusat: Pusat Perubahan Iklim dan Kualitas Udara BMKG, 2011.

[5] S. Y. Andarini and Sudarti. "Analisis Efek global warming terhadap perubahan iklim,". *Jurnal Phi*, vol. 4, no. 2, pp. 31–38, 2023.

[6] O. R. Pinontoan, O. J. Sumampouw, and J. E. Nelwan, *Perubahan Iklim dan Pemanasan Global*. Yogyakarta: Deepublish, 2022.

[7] S. G. Mbwambo, S. K. Mourice, and A. J. P. Tarimo, "The Impacts of Current Climate Variability on Coffee Production in the Northern and Southern Highlands of Tanzania," *J. Agric. Sci.*, vol. 14, no. 3, pp. 78–99, 2022.

[8] W. Merga and D. Alemayehu, "Effects of Climate Change on Global Arabica Coffee (Coffea arabica L) Production," *Greener J. Plant Breed. Crop Sci.*, vol. 7, no. 1, pp. 23–30, 2019, doi: https://doi.org/10.15580/GJPBCS.2019.1.072319143.

[9] E. Rahn, P. Vaastd, P. Läderachb, P. van Astenc, L. Jassognec, and J. Ghazoul, "Exploring adaptation strategies of coffee production to climate change using a process-based model," *Ecol. Modell.*, vol. 371, pp. 76–89, 2018.

[10] T. R. Moreira, S. F. da Silva, N. B. da Silva, G. M. A. D. A. dos Santos, and A. R. dos Santos, "Global warming and the effects of climate change on coffee production," in *Food Engineering Series: Quality Determinants In Coffee Production*, 1st ed., T. R. M. Lucas Louzada Pereira, Ed. Switzerland: Springer Cham, 2021, pp. 65–100.

[11] B. Susilo, *Mengenal Iklim dan Cuaca di Indonesia*. Yogyakarta: Diva Press, 2021.

[12] W. N. Harahap, B. Yuniasih, and S. Gunawan, "Dampak La Nina 2021-2022 terhadap Peningkatan Curah Hujan," *Jurnal Phi: Jurnal Pendidikan Fisika dan Fisika Terapan*, vol. 7, no. 1, pp. 26–32, 2023.

[13] A. A. Lestari, "Dampak Perubahan Iklim Terhadap Sistem Pertanian Berkelanjutan di Wilayah Tropis," *Literacy Notes*, vol. 2, no. 4, pp. 1–8, 2024.

[14] S. Febriosa, W. S. Pratama, Z. Mahdalena, and Ikhwan, "Analisis Dampak Perubahan Iklim Terhadap Kualitas Lingkungan Hidup dan Kehidupan Sosial Masyarakat," *J. MUDABBIR J. Res. Educ. Stud.*, vol. 5, no. 2, pp. 2211–2214, 2025.

[15] S. Maleachi and F. Christianus, "Analisis Pengelolaan Panen dan Pasca Panen Kopi Sebagai Faktor yang Mempengaruhi Kualitas Biji Kopi Robusta di Kota Pagar Alam," *J. Glob. Ilm.*, vol. 1, no. 7, pp. 482–488, 2024.

[16] D. Pratiyudha, M. Permatasari, and P. K. Karo, "Analisis Penataan Kamar Home Stay di Kota Pagar Alam, Sumatera Selatan," *J. Bisnis Hosp.*, vol. 12, no. 1, pp. 39–55, 2023.

[17] R. A. Qusyairi, M. T. Hendratono, and A. W. Sarwono, "Penerapan Konsep Pariwisata Hijau di Gunung Dempo Kota Pagar Alam Sumatera Selatan," *J-CEKI : Jurnal Cendekia Ilmiah*, vol. 2, no. 4, pp. 385–395, 2023.

[18] J. L. Rindika, S. Subiyanto, and F. J. Amarrohman, "Analisis Geospasial Perkembangan Nilai Ekonomi Kawasan Wisata Kota Pagar Alam Menggunakan Sistem Informasi Geografis," *Jurnal Geodesi Undip*, vol. 9, no. 4, pp. 22-31, Oct. 2020.

[19] K. Pasmah, F. Dhiniati, and B. Azizah, "Penilaian Indeks Ancaman Kekeringan di Kecamatan Dempo Tengah Kota Pagaralam Menggunakan Gis," *Bering's*, vol. 09, no. 01, pp. 23–30, Mar. 2022.

[20] Ngudiantoro, Irmeilyana, M. Nirwan Samsuri, "Binary Logistic Regression Modeling on Net Income of Pagar Alam Coffee Farmers," *International Journal of Applied Sciences and Smart Technologies*, vol. 2, no. 2, pp. 137–156, 2020.

[21] Irmeilyana, Ngudiantoro, M. N. Samsuri, and B. Suprihatin, "Logistic regression model on land productivity of Pagar Alam coffee farming," in *J. Phys.: Conf. Ser. 1943*, 2021, pp. 1–12, doi: 10.1088/1742-6596/1943/1/012135.

[22] Irmeilyana, N. Ngudiantoro, and D. Rodiah, "Correspondence Analysis pada Hubungan Faktor-faktor yang Mempengaruhi Pendapatan Petani Kopi Pagaralam," *BAREKENG: Jurnal Ilmu Matematika dan Terapan*, vol. 15, no. 1, pp. 179–192, Mar. 2021.

[23] Irmeilyana, Ngudiantoro, S. I. Maiyanti, and I. Febrianti, "Correspondence Analysis to Know Factors Related to the Use of Reducant Herbicide on Pagaralam Coffee Farmers," *Pattimura Int. J. Math.*, vol. 1, no. 2, pp. 69–80, 2022, doi: DOI https://doi.org/10.30598/pijmathvol1iss2pp69-80.

[24] Irmeilyana, N. Ngudiantoro, and S. I. Maiyanti, "Regression Model on Pagaralam Coffee Farmers' Income with the Influence of The Use of Herbicide Reductant Variable," *BAREKENG: Jurnal Ilmu Matematika dan Terapan*, vol. 16, no. 2, pp. 409–420, Jun. 2022, doi: 10.30598/barekengvol16iss2pp409-420.

[25] Irmeilyana, Ngudiantoro, and S. I. Maiyanti, "Hypothesis testing in the study of the characteristics of Pagaralam coffee farmers as herbicide reductant users," in *AIP Conf. Proc. 2913, 040005*, 2023, pp. 1–13, doi: https://doi.org/10.1063/5.0172023.

[26] Irmeilyana, B. Suprihatin, A. Desiani, O. Dwipurwani, and N. N. Aisyah, "Comparison of Graphical Representation of Simple and Multiple Correspondence Analysis Results on the Category of Factors Related to Farmers Status in Using Reductant Herbicide," in *Proceedings of the 3rd Sriwijaya International Conference on Basic and Applied Sciences, SICBAS 2023*, European Alliance for Innovation, Aug. 2024, pp. 1–12, doi: http://dx.doi.org/10.4108/eai.3-11-2023.2347775.

[27] Irmeilyana, Ngudiantoro, and S. I. Maiyanti, "Application of Two Groups Analysis and Cluster Analysis on comparison of Characteristics of Pagaralam Coffee Farmers Categories," *Barekeng*, vol. 17, no. 1, pp. 101–112, 2023, doi: https://doi.org/10.30598/barekengvol17iss1year2023.

[28] Irmeilyana, B. Suratama, S. I. Maiyanti, N. Ngudiantoro, B. Suprihatin, and A. Desiani, "Deskripsi dan uji hipotesis data elemen-elemen cuaca menggunakan uji selisih mean dan uji rasio variansi pada Tahun 2021-2022 di dua kecamatan penghasil kopi," *Jurnal Penelitian Sains*, vol. 27, no. 2, pp. 1–11, Jun. 2025.

[29] H. Venelia, K. Nisa, R. A. Wibowo, M. A. Muda, "Robust Biplot Analysis of Natural Disasters in Indonesia from 2019 to 2021". *Jurnal Aplikasi Statistika & Komputasi Statistik*, vol. 13, no. 2, pp. 61–68, 2021.

[30] R. Supardi and I. Kanedi, "Implementasi Metode Algoritma K-Means Clustering pada Toko Eidelweis," *J. Teknol. Inf.*, vol. 4, no. 2, pp. 270–277, 2020.

[31] E. H. S. Atmaja, "Implementation of k-Medoids Clustering Algorithm to Cluster Crime Patterns in Yogyakarta," *International Journal of Applied Sciences and Smart Technologies*, vol. 1, no. 1, pp. 33–44, 2019.

[32] I. A. Arshella, I W. Mustika, and P. Nugroho, "Improving the Accuracy of Prediction of Dissolved Oxygen and Nitrate Level Using LSTM with K-Means Clustering and Spearman Analysis," *International Journal of Applied Sciences and Smart Technologies*, vol. 7, no. 2, pp. 277-298, 2025.

[33] N. H. Wulandari and V. Purwayoga, "Cluster Change Analysis to Assess the Effectiveness of Speaking Skill Techniques Using Machine Learning," *International Journal of Applied Sciences and Smart Technologies*, vol. 7, no. 1, pp. 1–14, 2025.

[34] P. Pangestu, S. Maarip, Y. N. Addinsyah, and V. Purwayoga, "Clustering and Trend Analysis of Priority Commodities in The Archipelago Capital Region (IKN) Using A Data Mining Approach," *International Journal of Applied Sciences and Smart Technologies*, vol. 6, no. 1, pp. 169-182, 2024.

[35] M. F. Pramoedya, R. A. Ramadhani, and B. Setiawan, "Pemanfaatan K-Means Clustering dalam Pengelompokan Cuaca di Wilayah Kediri," *Inotek*, vol. 9, pp. 2155–2164, 2025.

[36] D. Tri Cahaya, D. Puspita, and R. Syahri, "Penerapan Metode K-Means Clustering untuk Pengelompokan Potensi Padi di Kota Pagar Alam," *JATI J. Mhs. Tek. Inform.*, vol. 8, no. 2, pp. 2187–2193, 2024.

[37] F. D. Rahman, M. I. Zulfa, and A. Taryana, "Clustering dan Klasifikasi Data Cuaca Kota Cilacap dengan Menggunakan Metode K-Means dan Random Forest," *J. SINTA Sist. Inf. dan Teknol. Komputasi*, vol. 1, no. 2, pp. 90–97, 2024.

[38] W. Härdle and L. Simar, *Applied Multivariate Statistical Analysis*. Hiedelberg: Springer-Verlag, 2015.

[39] R. A. Johnson and D. W. Wichern, *Applied Multivariate Statistical Analysis*, 6th ed. New Jersey: Prentice-Hall, Inc., 2007.

[40] M. Sholeh and K. Aeni, "Perbandingan Evaluasi Metode Davies Bouldin, Elbow dan Silhouette pada Model Clustering dengan Menggunakan Algoritma K-Means," *STRING Satuan Tulisan Ris. dan Inov. Teknol.*, vol. 8, no. 1, pp. 56–59, 2023.

[41] G. Andrian, D. Arisandi, and T. Handhayani, "Clustering Data Meteorologi Wilayah Indonesia Timur dengan Metode K-Means dan Fuzzy C-Means," *Inti Nusa Mandiri*, vol. 18, no. 2, pp. 100–106, 2024.

IJASST International Journal of Applied Sciences and Smart Technologies

Volume 08
Issue 01

p-ISSN 2655-8564, e-ISSN 2685-943, pp. 321-330,

Thermal Investigation of Changes in The Mass Flow Rate of The Lithium-Ion Battery Coolant

Stefan Mardikus[1*], Petrus Setyo Prabowo[2], Bernadeta Wuri Harini[2],
Budi Sugiharto[1], F.A. Rusdi Sambada[1],
Achilleus Hermawan Astyanto[1], I.M.W Ekaputra[1]

[1] Department of Mechanical Engineering, Faculty of Science and Technology, University of Sanata Dharma, Paingan, Maguwoharjo, Depok, Sleman, Yogyakarta, Indonesia
[2]Department of Electrical Engineering, Faculty of Science and Technology, University of Sanata Dharma, Paingan, Maguwoharjo, Depok, Sleman, Yogyakarta, Indonesia

**Corresponding E-mail: stefan@usd.ac.id*

(Received 31-05-2026; Revised 07-06-2026; Accepted 08-06-2026)

Abstract

An electric battery is an energy storage device that has a high energy density, a long lifetime and has a high rate of charging and discharging the battery. The performance of the Lithium-Ion battery greatly affects the temperature of charging and discharging, so a cooling method is needed that is able to maintain the working temperature of the battery at (25 – 50^{0}C) conditions. In this study, the Computational Fluid Dynamics method was used to investigate the effect of Depth of Discharge (DOD) on the cooling performance of BTMS (Battery Thermal Management System) Liquid Cooling using ethylene-glycol as the working fluid to be flowed on the curved cooling tube. The results of this study indicated that the maximum temperature and temperature difference of the battery module decreased as the mass flow rate of the cooling fluid increased, the lowest temperature value occurred at the mass flow rate of 18×10-4kg·s-1 with a temperature value of 303.6 K. The maximum temperature of the battery module fluctuated as the DOD value increased.

Keywords: Battery Thermal Management System, Depth of Discharged, Li-Ion Battery.

1 Introduction

In recent years, energy resources from fossil in the world are very difficult to find it is because demand in the transportation sector will increase each year [1]. Many

solutions that can overcome the demand for energy from fossil through government regulations, technology, and energy alternatives. One of the solutions to solve this problem is using electrical vehicle that is battery as its main energy source [2-4]. An electric vehicle is a modern transportation that can support conventional transportation, which is conducted by internal combustion engine. When use electrical vehicle, Lithium-ion is one of the types of electrical battery that has long durability of energy [5-6].

As a structure of lithium-ion battery, it consist of several parts of the propylene carbonate (PC) and spinal as electrolyte, cathode, and anode, which distribute Li ion and temperature exchange [7]. Thermal management as main issue nowadays that has repeatedly improved to control the temperature range at 20 ^{0}C - 40 ^{0}C [8]. Meanwhile, a uniform temperature of the battery is important to maintain durability, and it needs to keep the temperature at 5 K for each battery [8]. Zhang (2011) have investigated a cylindrical battery model using a Lithium-Ion battery on the behavior of heat generation. Based on his work, about 30% average of total heat generation, it is occurred because of the electrochemical reaction [7]. Bai (2017) has investigated battery thermal management system using PCM combined with liquid cooling. The experiment result showed that the mass flow rate of liquid cooling affects the temperature of battery module [9]. The previous study showed that it was still a lack of study to improve the cooling system of lithium-ion battery with a variety of BTMS (Battery Thermal Management System).

This study will offer a cooling system model using a cooling tube for a battery cooling system with ethylene glycol as a cooling fluid and the aim of study also will find the maximum temperature battery, temperature difference and contour of temperature distribution using computational fluid dynamic. Computational Fluid Dynamics (CFD) was employed to examine the influence of Depth of Discharge (DOD) on the cooling performance of a liquid-cooled Battery Thermal Management System (BTMS), where ethylene glycol served as the coolant circulating through a curved cooling tube.

2 Research Methods

This study focuses on a lithium-ion battery pack consisting of cylindrical 1650-type cells, as illustrated in Fig. 1. Cylindrical lithium-ion batteries are widely utilized in

electric vehicle applications due to their high energy density, reliability, and relatively stable thermal performance. In the present configuration, the center-to-center distance between adjacent battery cells is set at 23 mm to provide sufficient spacing for thermal management components. A curved cooling tube with a thickness of 2 mm is integrated into the battery module to facilitate heat dissipation during operation. The geometric arrangement is designed to investigate the interaction between battery heat generation and the cooling system under different operating conditions.

The thermal management system analyzed in this study employs a liquid-cooling configuration using a single curved cooling tube model. The model represents a simplified battery module consisting of five cylindrical battery cells, as shown in Fig. 2, which is intended to emulate the cooling arrangement commonly found in electric vehicle battery packs. The cooling tube is positioned strategically to maximize heat transfer from the battery surfaces to the circulating coolant. By focusing on a five-cell module, the computational model can effectively capture the thermal behavior of the battery pack while maintaining reasonable computational costs. This approach enables a detailed investigation of cooling performance and temperature distribution within the battery module.

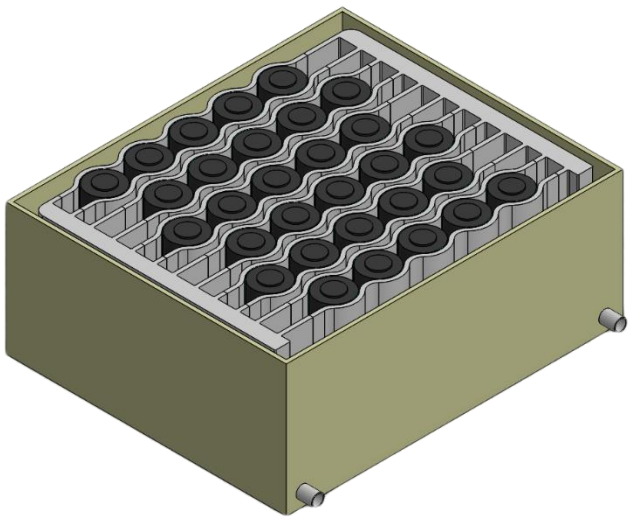

Figure 1. 3D visualization of cooling system for Lithium-Ion battery.

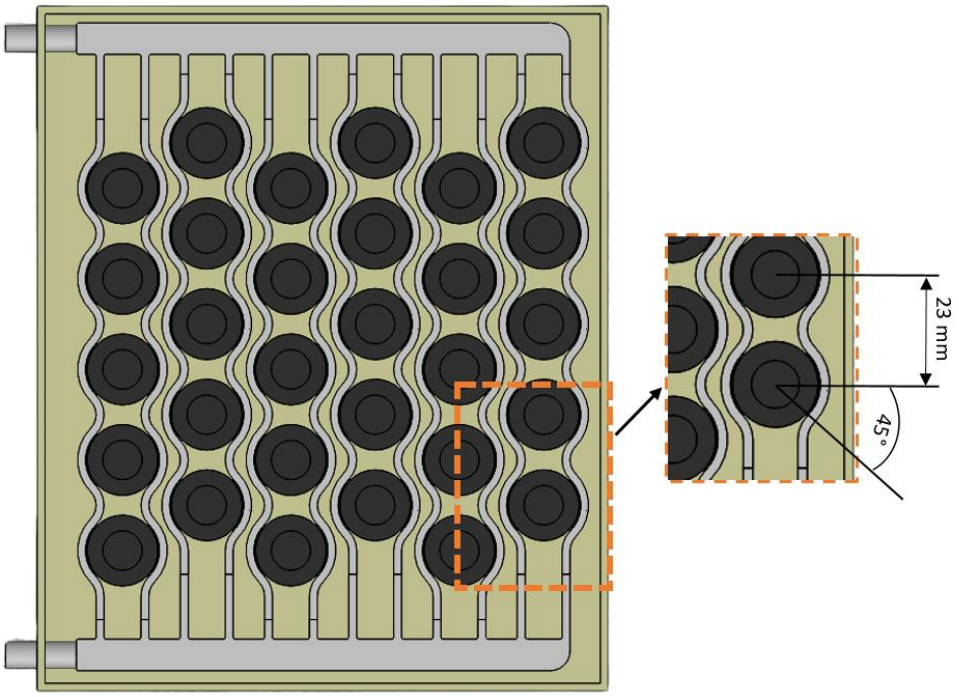

Figure 2. 3D visualization from top view for Lithium-Ion battery.

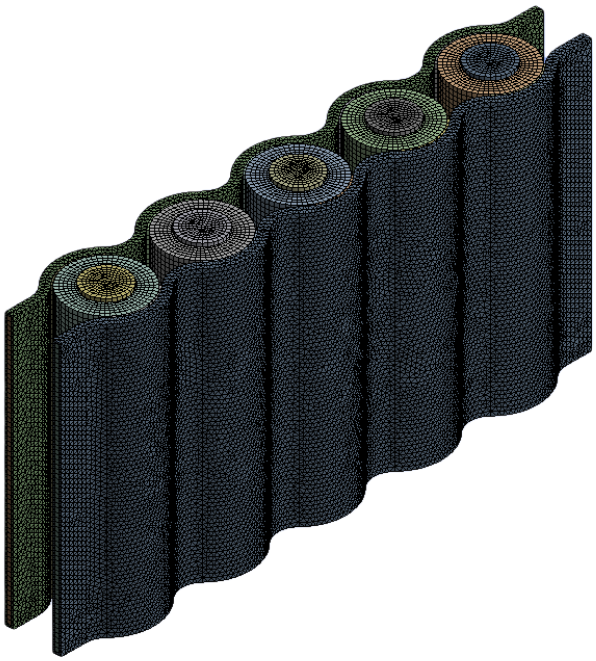

Figure 3. Meshing model for pack of lithium-ion battery.

To perform the numerical simulation, a three-dimensional mesh was generated using the mapped face meshing method with tetrahedral elements. An element size of 1 mm was selected to produce a structured and sufficiently refined mesh capable of accurately representing the complex geometry of both the battery cells and the curved cooling tube. The resulting mesh model is presented in Fig. 3. Furthermore, several boundary conditions were defined to accurately represent the physical system, including the battery cell, cooling pipe, positive tab zone, positive tab, negative tab zone, negative tab, fluid inlet, fluid outlet, and spacer components, as illustrated in Fig. 4. These boundary conditions were applied to ensure realistic simulation of heat generation, heat transfer, and coolant flow throughout the battery thermal management system.

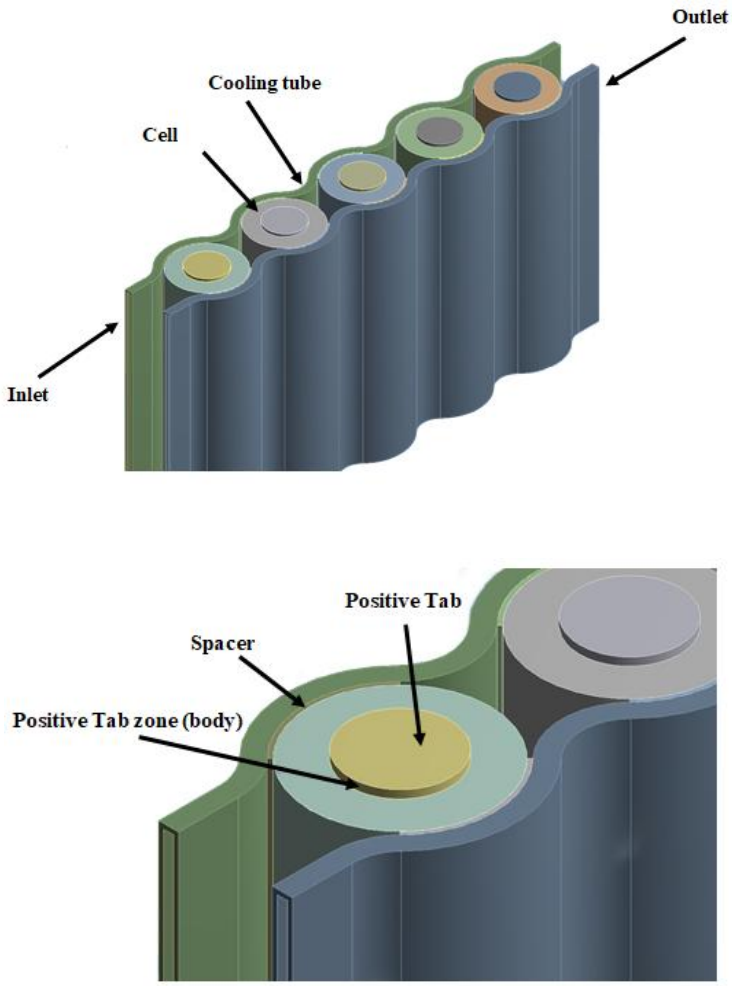

Figure 4. Boundary condition for Lithium-Ion battery.

3 Results and Discussion

Fig.5 shows that the maximum temperature of the battery module decreases as the Depth of Discharge (DOD) increases. However, at 90% DOD, a temperature rise occurs, followed by a decline again at 100% DOD. This behaviour is attributed to changes in the battery's entropy coefficient during the discharging process, which alternates between positive and negative values. As a result, both endothermic and exothermic reactions take place within the battery, causing the battery temperature to fluctuate[10]. Fig.5 further demonstrates that a higher coolant fluid mass flow rate leads to smaller temperature fluctuations in the battery module. This is because the mass flow rate has a direct influence on the heat transfer rate — the greater the mass flow rate of the fluid, the higher the rate of heat transfer that occurs [7].

Fig. 6 show that the temperature distribution for battery module with the varieties of mass flow rate of liquid cooling gradually increase as the coolant flow. In the fifth positive battery tab area, which is farthest from cooling tube inlet area and the lowest battery temperature located in the negative battery tab area, which is the nearest to the cooling tube inlet area.

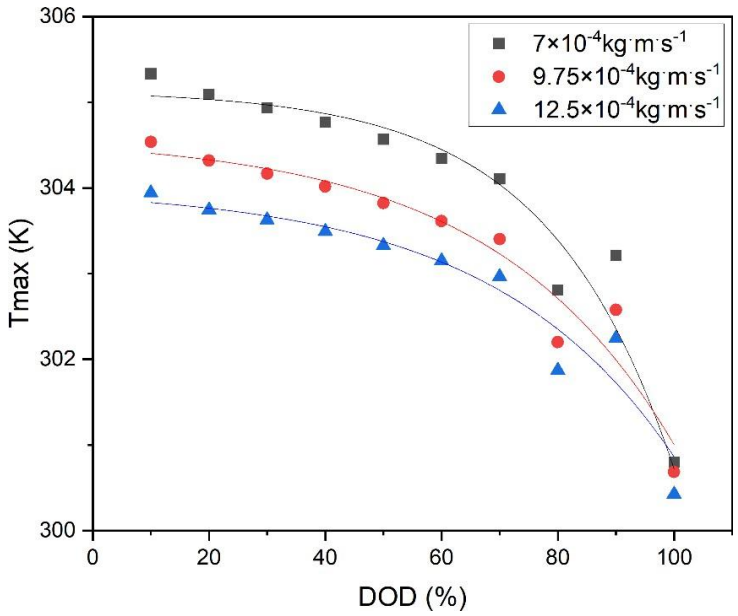

Figure 5. The correlation between Depth of Discharged versus Maximum Temperature on many differences of mass flow rates for the liquid cooling system

The uniform of temperature distribution is caused by the high thermal resistance of the battery cover and heat accumulation along the direction of the coolant stream of liquid cooling and the high temperature zone in the battery module shrinks as the mass flow rate of the coolant rises [2].

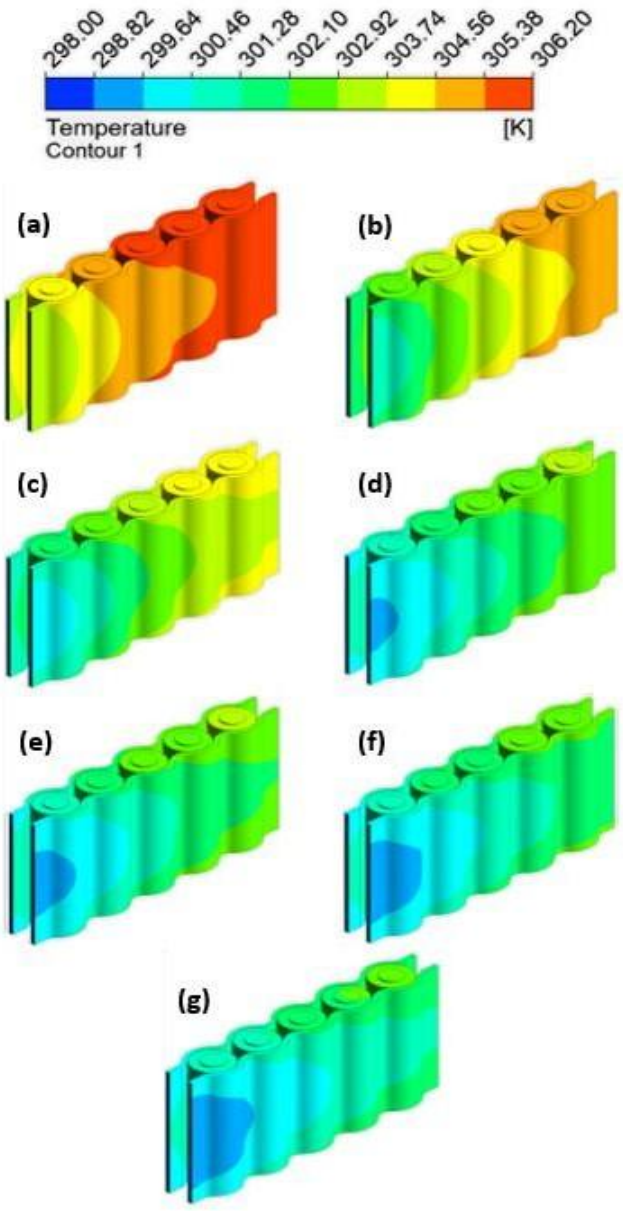

Figure 6. Isometric view of contour distribution temperature for the difference of mass flow rate liquid cooling for battery module

4 Conclusions

This study investigates the effect of mass flow rates for the liquid cooling system on battery module lithium-ion that the highest of mass flow rate able to keep battery temperature fixed at 20 ^{0}C – 40 ^{0}C where is at 300 K – 304 K. In addition, from the three-mass flow rate for liquid cooling that are different, it happened a uniform of temperature distribution for each lithium-ion battery.

References

[1] T. N. Zahari and B. C. McLellan, "Sustainability of Indonesia's transportation sector energy and resources demand under the low carbon transition strategies," *Energy*, vol. 311, p. 133385, doi: 10.1016/j.energy.2024.133385.

[2] A. G. Abdullah, S. Arif, M. K. Biddinika, R. Nugraha, and D. Mohamad, "Sustainable planning of EV charging infrastructure in urban regions: A hybrid GIS-MCDM approach for West Java, Indonesia," Green Technologies and Sustainability, vol. 4, no. 2, p. 100348, Jan. 2026, doi: 10.1016/j.grets.2026.100348.

[3] M. Waseem, M. Ahmad, A. Parveen, and M. Suhaib, "Battery technologies and functionality of battery management system for EVs: Current status, key challenges, and future prospectives," Journal of Power Sources, vol. 580, p. 233349, Jul. 2023, doi: 10.1016/j.jpowsour.2023.233349.

[4] A. A. Habib, M. K. Hasan, S. Islam, and K. A. A. Bakar, "Review on electric vehicles integration into smart grid cyber physical security system and performance analysis for smart city perspective," Global Energy Interconnection, Jun. 2026, doi: 10.1016/j.gloei.2026.01.011.

[5] J. Wang et al., "Evolution of electrical properties and thermal runaway characteristics in mechanically damaged lithium-ion batteries," Journal of Energy Storage, vol. 152, p. 120614, Jan. 2026, doi: 10.1016/j.est.2026.120614.

[6] P. N. Nowruzmahalle and M. M. Shokrieh, “Micromechanical modeling of the electrical conductivity in lithium-ion battery electrodes,” Journal of Energy Storage, vol. 167, p. 122429, May 2026, doi: 10.1016/j.est.2026.122429.

[7] X. Zhang, “Thermal analysis of a cylindrical lithium-ion battery,” Electrochimica Acta, vol. 56, no. 3, pp. 1246–1255, Oct. 2010, doi: 10.1016/j.electacta.2010.10.054.

[8] W. Yang, F. Zhou, H. Zhou, Q. Wang, and J. Kong, “Thermal performance of cylindrical lithium-ion battery thermal management system integrated with mini-channel liquid cooling and air cooling,” Applied Thermal Engineering, vol. 175, p. 115331, Apr. 2020, doi: 10.1016/j.applthermaleng.2020.115331.

[9] F. Bai, M. Chen, W. Song, Z. Feng, Y. Li, and Y. Ding, “Thermal management performances of PCM/water cooling-plate using for lithium-ion battery module based on non-uniform internal heat source,” Applied Thermal Engineering, vol. 126, pp. 17–27, Jul. 2017, doi: 10.1016/j.applthermaleng.2017.07.141.

[10] P.-L. Viollet, “From the water wheel to turbines and hydroelectricity. Technological evolution and revolutions,” Comptes Rendus Mécanique, vol. 345, no. 8, pp. 570–580, Jul. 2017, doi: 10.1016/j.crme.2017.05.016.

This page intentionally left

IJASST
International Journal of
Applied Sciences and Smart Technologies
p-ISSN 2655-8564, e-ISSN 2685-943

AUTHOR GUIDELINES

Author guidelines are available at the journal website:
http://e-journal.usd.ac.id/index.php/IJASST/about/submissions#authorGuidelines

IJASST
International Journal of
Applied Sciences and Smart Technologies
p-ISSN 2655-8564, e-ISSN 2685-943

This page intentionally left blank